NATIONAL AERONAUTICS AND SPACE ADMINISTRATION

Technical Memorandum 33-734

Volume I

Mariner Venus-Mercury 1973 Project Final Report

Venus and Mercury I Encounters

JET PROPULSION LABORATORY

CALIFORNIA INSTITUTE OF TECHNOLOGY

PASADENA, CALIFORNIA

September 15, 1976

PREFACE

The Mariner 10 spacecraft was launched from the Air Force Eastern Test Range (AFETR) at Cape Kennedy, Florida on November 3, 1973. Liftoff occurred at 05:45 GMT. The closest approach to Venus occurred at 17:01 GMT on February 5, 1974. The closest approach to Mercury occurred at 20:46 GMT March 29, 1974 at a distance of 704 km (437 miles) from the planet surface.

During the primary portion of the Mariner Venus/Mercury 1973 Project, Mariner 10 accomplishments were: (1) The first multi-planet gravity-assist mission, (2) the first spacecraft to photograph Venus, (3) the first spacecraft to approach and photograph Mercury, (4) the first Jet Propulsion Laboratory (JPL) spacecraft to transmit full resolution pictures, and (5) the first mission to use dual-frequency radio transmission.

The scientific (television and nonimaging science) information in this document was derived from status bulletins published during the mission under the direction of the Mariner Venus/Mercury 1973 Project. The data in these bulletins were obtained from the Principal Investigators in near-real time in relationship to the events discussed, and as such are to be interpreted as preliminary.

The work described in this report was performed by the Mariner Venus/ Mercury 1973 Primary Mission Project of the Jet Propulsion Laboratory whose membership was composed of personnel from the Jet Propulsion Laboratory and The Boeing Aerospace Company.

CONTENTS

TABLES

FIGURES

ABSTRACT

This document is Volume I of a two-volume report covering the Mariner
Venus/Mercury 1973 Project. Volume I covers that portion of the project
defined as the Primary Mission, which includes the Venus encounter and the
first Mercury encounter. The document describes the plans and activities
undertaken to successfully achieve the mission objectives. The operational
activities are identified by Mission Operation System (MOS) functions, pro-
viding a brief summary of each discipline. Spacecraft performance is sum-
marized by subsystems.

AC	Attitude control		FA	Flight acceptance
ACE	Attitude-control electronics		FCU	Flight command unit
ACE-1	Operational call designation for the on-duty ACMO		FDS	Flight data subsystem
			FDSC	Flight data subsystem count
ACMO	Assistant Chief of Mission Operations		FDR	Functional design review
AES	Auxiliary electronics subsystem		FE	Far encounter
AFETR	Air Force Eastern Test Range		FIP	Fixed instrument pointing (program)
AFPRO	Air Force Plant Representative Office		FMECA	Failure mode, effect, criticality analysis
AGC	Automatic gain control			
AOPT F	A optics front		FOPE	Facility operations project engineer
APA	Articulation and pointing actuator		FOV	Field of view
APS	Articulation and pointing subsystem		FPR	Flight project representative
AVID	A Vidicon		FY	Fiscal year
BER	Bit error rate		G&A	General and administrative
BET	Best estimate trajectory		GCA	Gyro control assembly
BOPT F	B optics front		GCP	Government furnished property
B/R	Booster regulator		GDS	Ground data system
BUTEC	Burn-time estimation calculator		GDSE	Ground data system engineer
BVID	B vidicon		GFE	Government furnished equipment
			GMT	Greenwich Mean Time
CA	Closest approach		GSFC	Goddard Space Flight Center
CBE	Current best estimate			
CC&S	Central computer and sequencer		HGA	High-gain antenna
CCW	Counter clockwise			
CMA	Command modulator assembly		IBM	International Business Machines
CMD	Command		IC	Integrated circuit
CMO	Chief of Mission Operations		IRR	Infrared radiometer
CMRS	Celestial mechanics and radio science		ISA	Incident surprise anomaly
COMGEN	Command generator		JPL	Jet Propulsion Laboratory
CPT	Charged particle telescope			
CST	Canopus star tracker		LCC	Limit cycle compensator
CTA 21	Compatibility test area		LGA	Low-gain antenna
CW	Clockwise		LIBPOG	Library POGASIS
CY	Calendar year		LV	Launch vehicle
DC	Direct command		MAG	Magnetometer
DCAA	Defense Contract Audit Agency		MARK1A	Mark 1A ranging
DCMO	Deputy Chief of Mission Operations		MCCC	Mission Control and Computing Center
DDA	Data decoder assembly			
DDR	Detailed design review		MCT	Mission Control Team
DIS	Digital Instrumentation subsystem		MDS	Modulation/Demodulation Subsystem
DN	Data number		MJS	Mariner Jupiter Saturn
DPTRAJ	Double Precision Trajectory Program		MM'71	Mariner Mars 1971
DSIF	Deep Space Instrumentation Facility		MOAT	Mission operations analysis team
DSN	Deep Space Network		MOS	Mission operation system
DSS	Data storage subsystem		MOSDT	Mission operation system design team
DSS 12	Echo Deep Space Station, Goldstone DSCC, Calif.		MSA	Mission support area
DSS 14	Mars Deep Space Station, Goldstone DSCC, Calif.		MSWG	Mission sequence working group
			MTC	Mission and test computer
DSS 42	Weemala Deep Space Station, Tidbinbilla DSCC, Australia		MVM'73	Mariner Venus/Mercury 1973
DSS 43	Ballima Deep Space Station, Tidbinbilla DSCC, Australia		NASA	National Aeronautics and Space Administration
DSS 62	Cebreros Deep Space Station, Madrid DSCC, Spain		NIS	Non-imaging science
			NAT	Network analysis team
DSS 63	Robledo Deep Space Station, Madrid DSCC, Spain		NOPE	Network operations project engineer
			NSP	NASA Support Plan
EDR	Experimentor data record		OD	Orbit determination
EDRGEN	Experimentor data record generator		ODR	Original data record
EDRVAL	Experimentor data record validation			
EOS	Electro Optical Systems		PAFUVS	Particles and Fields Ultraviolet spectrometer
EPIM	Magnetometer EDR Program		PFR	Problem failure report
ET	Ephemeris Time		PI	Principal investigator
ETE	Environmental Test Equipment		PMS	Performance measurement system
ETR	Eastern test range			

POGASIS	Planetary observation geometry and science instrument sequence		TA	Type approval
POR	Power on reset		TBC	The Boeing Company
PSE	Plasma science experiment		T/C	Temperature Control
PS&L	Power switching and logic		TCD	Telemetry and Command Data Subsystem
			TDH	Tracking Data Handling
QA	Quality assurance		TCM 1	First trajectory correction maneuver
			TCM 2	Second trajectory correction maneuver
RCA	Reaction Control Assembly			
RCM	Roll control maneuver		TCM 3	Third trajectory correction maneuver
RFMT	Reformat program		TI	Texas Instruments
RFP	Request for proposal		TLC	Tender loving care
RFS	Radio frequency subsystem		TLM	Telemetry
			TSOST	Television subsystem operational sequence table
SCE	Spacecraft event			
SCI	Science		TVCA	Thrust vector control assembly
SEA	Scanning electrostatic analyzer		TVS	Television subsystem
SEDR	Supplementary experiment data record		TWT	Traveling wave tube
SEG	Sequence of events generator		UTC	Universal Time Code
SES	Scanning electronic spectrometer		UVS	Ultraviolet spectrometer
SITT	Simultaneous interference tracking technique		UVSA	Ultraviolet spectrometer - airglow
SNR	Signal-to-noise ratio		UVSO	Ultraviolet spectrometer - occultation
SP	Solar panel			
SPEEA	Seattle Professional Engineer Employee Association		VCO	Voltage-controlled oscillator
			VE	Venus encounter
SPOP	Scan Platform Operations Program			
SPT	Scan platform telemetry		W	Watt
SRM	System for resource management		WUE	Work unit engineer
STRU	Structure Subsystem		WUM	Work unit manager
STV	Spacecraft thermal vacuum			
SXA	S/X-band antenna		XTX	X-band transmitter

I. INTRODUCTION

This is Volume I of a two-volume report on the Mariner Venus/Mercury 1973 Project primary mission. Preparation of this document is in accordance with a Mariner Venus/Mercury 1973 Project Office directive.

A. PURPOSE

The purpose of this document is to provide a historical summary record of the mission from design and fabrication of the spacecraft to the end of the primary mission, describe the philosophy of concepts used in key areas, identify techniques used that contributed to the success of the mission, and to point out those areas where improvements can be made to benefit future programs.

B. BACKGROUND

The unusual relative positions of the planets Earth, Venus, and Mercury in the 1973 time period provided a unique scientific opportunity for a Venus/Mercury mission. Use of the Venus gravitational pull on a spacecraft would allow scientific exploration of the planet Mercury using a relatively inexpensive Atlas Centaur launch vehicle. Presented with the relative merits of such a mission, the Space Science Board of the National Academy of Science endorsed the program as a low-cost/high scientific return project.

The Mariner Venus/Mercury 1973 (MVM'73) program was first introduced by the National Aeronautics and Space Administration in the FY1970 budget. From its inception and throughout the mission, a low-cost attitude was emphasized.

In December 1969, the Jet Propulsion Laboratory proposed to undertake this ambitious program for a cost not to exceed 98 million dollars.

The primary objectives of the mission were to conduct exploratory investigations of the planet Mercury by obtaining measurements of its environment, atmosphere, surface and body characteristics, and to conduct similar investigations of the planet Venus during its flyby. First priority was assigned to the Mercury investigation. Secondary mission objectives were to perform experiments in the interplanetary medium and obtain experience with a dual-planet gravity-assist mission. Figure 1 illustrates the Mariner 10 trajectory in relation to planet orbital characteristics.

The Request for Proposals (RFPs) for the spacecraft system was released in December 1970. It stressed incentive proposals with emphasis on low cost, award fee, overhead cost ceilings, and minimum documentation for the program. The contract effort was divided into work packages made up of specific tasks. The overall scope of the RFP included design, fabrication, assembly, and test of one flight spacecraft, one test spacecraft, necessary test models and support equipment, and required spares. It also included a Level of Effort technical support for systems, subsystems, and mission operations.

The Boeing Aerospace Company was selected on a competitive basis from four proposals received by the Jet Propulsion Laboratory for a cost plus award fee contract. The contract became effective on June 17, 1971.

C. SCOPE

This document provides a summary of the mission, including brief descriptions of the scientific results. Chronologically it covers the mission from the prelaunch phase through a short post-Mercury encounter period.
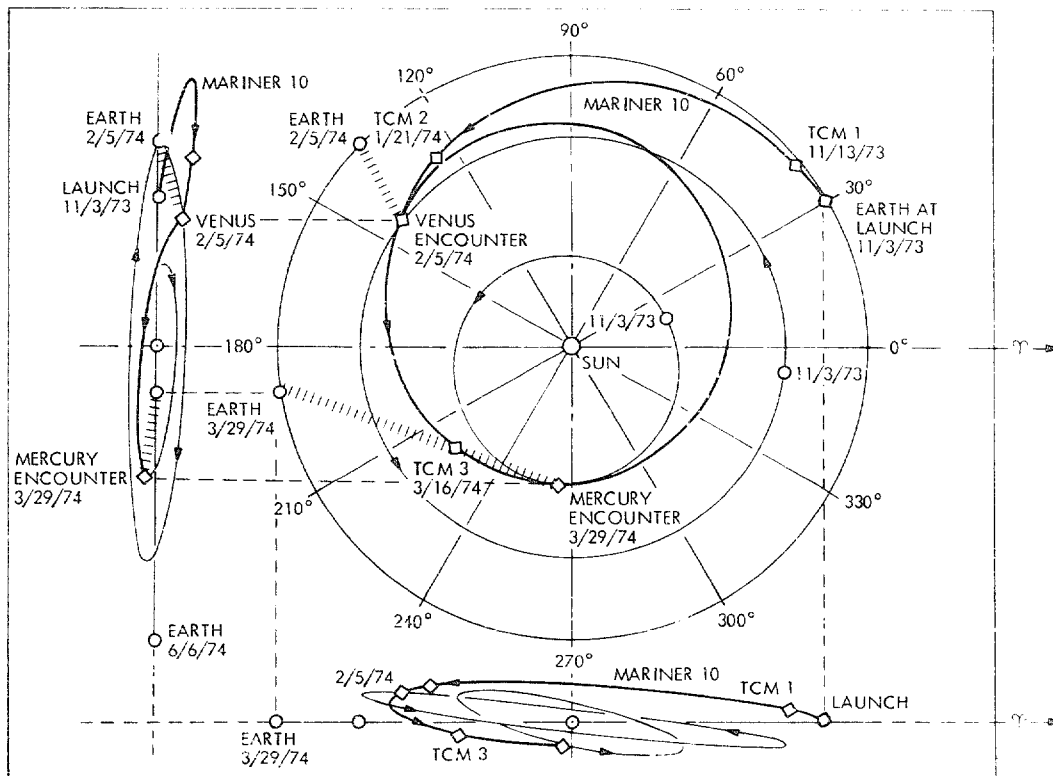
Fig. 1. Mariner 10 trajectory viewed from above and edge-on. Relative inclinations are 3 deg for Venus and 7 deg for Mercury

The most significant achievement, excluding that of a successful mission, was the performance of the System Contracting Mode. The Boeing Aerospace Company and the Jet Propulsion Laboratory worked together to produce a spacecraft with capabilities significantly beyond those originally anticipated for the 98 million dollar program.

This section has made no attempt to cover the spacecraft design, fabrication, and testing. The detail coverage of these areas can be found in the Mariner Venus/Mercury 1973 Spacecraft Program Final Report published by the Boeing Aerospace Company in July 1974.

A.   SYSTEM CONTRACTOR MODE

The System Contract was established on the basis of a work package concept which corresponds to the matrix organization of the Laboratory. The work package was used to scope and monitor the contractor activities.

The system contract was managed by the Project Office using the Spacecraft System Manager, Flight Project Representatives (FPRs), and Work Unit Managers (WUMs). The contractor organization mirrored the Project Office with the Program Manager, Activity and Area Managers, and Work Unit Engineers (WUEs) corresponding to the stated JPL positions.

B.   WORK UNIT MANAGERS AND WORK UNIT ENGINEERS

The Work Unit Managers and the Work Unit Engineers were key interfaces between the Project Office and the Boeing Aerospace Company. It was at this level that implementation plans were reviewed, technology transfer was accomplished, progress was monitored, and award evaluation of the contractor performance was initiated.

Activity Managers and Flight Project Representatives were responsible to their respective management for resolving problems within and between work units and for appraising Project Management of work unit activities and problems.

The implementation plan was responsive to the contract work definition and included manpower and dollar estimates, task definition, delivery dates, milestones, and schedules. Weekly meetings were held between the WUMs and the WUEs. Monthly meetings were conducted to review the Boeing Aerospace Company technical progress status, problem areas, and financial status. The monthly technical and financial status was used as an input for each work unit, and was integrated into the system to arrive at an overall evaluation of contractor technical and financial performance.

C.   AWARD EVALUATION

Award evaluations were conducted on a quarterly basis to evaluate The Boeing Aerospace Company progress. The spacecraft performance during the flight operations portion of the mission was used to modulate the performance or award fee earned during buildup, test, and launch of the spacecraft.

Technical reviews or milestone reviews were held as required and were identified as gates which the Boeing Aerospace Company could not proceed beyond without satisfying all action items established by the Review Board. The Review Board was chaired by the Project Manager and structured of individuals from the Project and non-Project personnel from both the Jet Propulsion Laboratory and the Boeing Aerospace Company.

D.   SCIENCE INSTRUMENTS

The science instruments were supplied to the Boeing Aerospace Company as government furnished equipment because of the difficulty of contracting for instruments because of the Jet Propulsion Laboratory experience in this area.

Interface between the instruments and the spacecraft was controlled using the spacecraft functional requirements, interface control drawings, and circuit data sheets, all of which were approved and signed off by the Boeing Aerospace Company, a JPL Representative, and the appropriate Principal Investigator.

E.   MISSION OPERATION SYSTEM SUPPORT

The Spacecraft Flight Support Work Units, which were level of effort technical support, were written in the same manner as the System Design Work Units except that instead of completing certain tasks, the contractor provided specific talent for flight operations.

1.   Spacecraft/DSN/MOS Compatibility Testing

Spacecraft/MOS compatibility tests were conducted with the spacecraft located in the space simulation chamber at the Jet Propulsion Laboratory. Four Spacecraft/MOS/DSN Compatibility sequences were conducted during two test periods. The first test was conducted on July 27, 1973 and covered the Venus and Mercury encounter phases. The second test was conducted on July 29, 1973 and covered the launch and trajectory correction maneuver (TCM) phases of the mission.

2.   Spacecraft/DSN Compatibility Testing

Final spacecraft/Deep Space Network (DSN) compatibility tests were performed at the Air Force Eastern Test Range (AFETR). Two of these tests were performed in Hanger AO and involved the 73-1 and 73-2 spacecraft. The other test was performed with the 73-2 spacecraft on the launch pad.

The purpose of these tests was to verify compatibility between the spacecraft and the DSN. The tests conducted in Hanger AO were under ambient temperature and pressure conditions. The first of these tests occurred on August 26, 1973. Test time was approximately 12 hours.

The second test was conducted on September 22 and 23, 1973. Test time was approximately 15 hours. Both tests were considered successful.

On October 23, 1973, during a 4.5 hour on-pad compatibility test, planetary ranging was successfully verified. The telemetry portion of the test was also successful.

F. SPACECRAFT MAGNETIC MAPPING

Magnetic mapping of Spacecraft 73-1 was accomplished at the Goddard Space Flight Center, Greenbelt, Maryland, on November 20 and 21, 1973. The mapping was accomplished by GSFC personnel on the unpowered spacecraft to determine the residual magnetic fields of the spacecraft to enhance the ability to interpret mission magnetometer data.

Meeting the primary scientific objectives of the mission included obtaining both television and nonimaging science data during Venus and Mercury encounter periods. The results of these objectives and the secondary cruise data objectives are discussed in this section.

A. TELEVISION SCIENCE

In preparation for the television sequences taken at Venus and Mercury, the TV cameras were calibrated by photographing the Earth and Moon shortly after Launch. The first Earth TV calibration occurred at 1:45 PM PST on Nov. 3, 1973. This was followed 1 hr, 15 min later by the second Earth TV calibration. The first Moon TV calibration occurred at 4:00 PM PST on Nov. 3, 1973. There were a total of five Earth TV calibrations and six Moon TV calibrations.

1. Venus Encounter

The Mariner 10 spacecraft encountered Venus on Feb. 5, 1974, at 10:01 PM Pacific Daylight Time. Venus encounter operations began on January 28 and continued through Feb. 13. As Mariner approached Venus, the Sun was in a direction nearly behind the planet as viewed from the spacecraft, with the result that photography of the illuminated disk (Fig. 2) began just minutes before closest approach. Mariner did not pass through the shadow of the Sun cast by the planet (solar occultation) but did fly behind the planet as viewed from Earth (Earth occultation). The 498.9 kg (1100 lb) spacecraft came within approximately 5631.5 km (3,500 miles) of the solid surface of the planet, at a speed of some 38,616 km/h (24,000 mph). Venus' gravity field slowed Mariner's velocity relative to the Sun by nearly 16,090 km/h (10,000 mph), deflecting its path toward the mission's primary target, Mercury. The scientific sequence planned for Venus long before launch was conducted, despite a number of spacecraft problems encountered earlier in the mission. During the encounter period, all but a few of the thousands of commands sent to the various subsystems of the spacecraft were executed by the on-board computer, which had been programmed to do so days before. Each of the seven experiments returned important new data on Venus, including observations of the body, atmosphere, and ionosphere of the planet and its interaction with the protons, electrons, and magnetic fields emanating from the Sun.

The Mariner 10 television cameras imaged the planet Venus in the visible and near ultraviolet for a period of eight days at resolutions ranging from 100 m to 130 km. The general pattern of the atmospheric circulation in the upper tropospheric/lower stratospheric region is displayed in the pictures. Atmospheric flow is symmetrical between the North and South Hemispheres. The equatorial motions are zonal (east-west) at approximately 100 m/s, consistent with the previously inferred four-day retrograde rotation. Angular velocity increases with latitude. The subsolar region, and the region downwind of it, show evidence of large-scale convection that persists in spite of the main zonal motion. Dynamical interaction between the zonal motion and the

relatively stationary region of convection is evidenced by bow-like waves. Various TV mosaics of Venus are shown in Figs. 3 to 9.

2. Mercury Encounter

Mariner 10 began taking TV pictures of Mercury on March 23, 1974 (near 240 deg on Fig. 10), a week after the third trajectory correction maneuver (TCM 3) from a distance of 5,310,000 km (3,300,000 miles). Photography was intermittent for the next four days, but became almost a continuous operation on March 28, taking one picture every 42 sec. However, Mariner 10 was unable to photograph Mercury during the half-hour around the time of its closest approach (0^m on Fig. 11) on March 29, because the flight path had been targeted to pass behind the planet on the night side. A further constraint was a mechanical stop on the Science scan platform, which prevented the TV cameras from pointing any closer than 58 deg from the sunline. While Mariner 10 was still in Earth's shadow (occultation), the cameras started taking TV frames of Mercury's far side from the closest possible altitude of about 3600 miles. Since the planet blocked radio communications at that time, the frames had to be tape recorded for later transmission to Earth. Periodic photographic operations continued for another five days until April 3 when the spacecraft was 2,200,000 miles past Mercury. More than 2000 TV frames were transmitted to the DSN 64-m tracking stations around the world, in California, Canberra, and Madrid.

The major landforms on Mercury observed by Mariner 10 are basins, craters, scarps, ridges, and plains (Fig. 12). Morphologically these features strongly resemble analogous landforms on the Moon. Where the plains are absent, overlapping craters and basins form rugged terrain. The plains materials have many of the characteristics of the lunar maria and have been cratered to approximately the same degree. This twofold division of the surface morphology of Mercury is strikingly similar to that on the Moon.

The largest basin observed so far on Mercury is centered at approximately 195°W, 30°N (Fig. 13) and has many of the characteristics of the lunar Imbrium basin. Numerous smaller basins also are evident, grading from sharply defined to barely discernible. Some have two concentric rings. Craters range in size downward from the dimensions of basins (Fig. 14) to the limits of detectability on the highest-resolution photographs (Fig. 14c). Extensive ray systems are present around some bright craters. The plains materials have filled and embayed the larger basins and adjacent lowlands (Fig. 13). Smooth material morphologically like lunar mare in some cases fills ancient craters without evidence of external origin. As on the Moon, a local source of volcanic material is suggested. Numerous wrinkle ridges similar to those on the lunar maria have formed within the plains (Figs. 13 and 14). A volcanic origin for much of this material is implied.
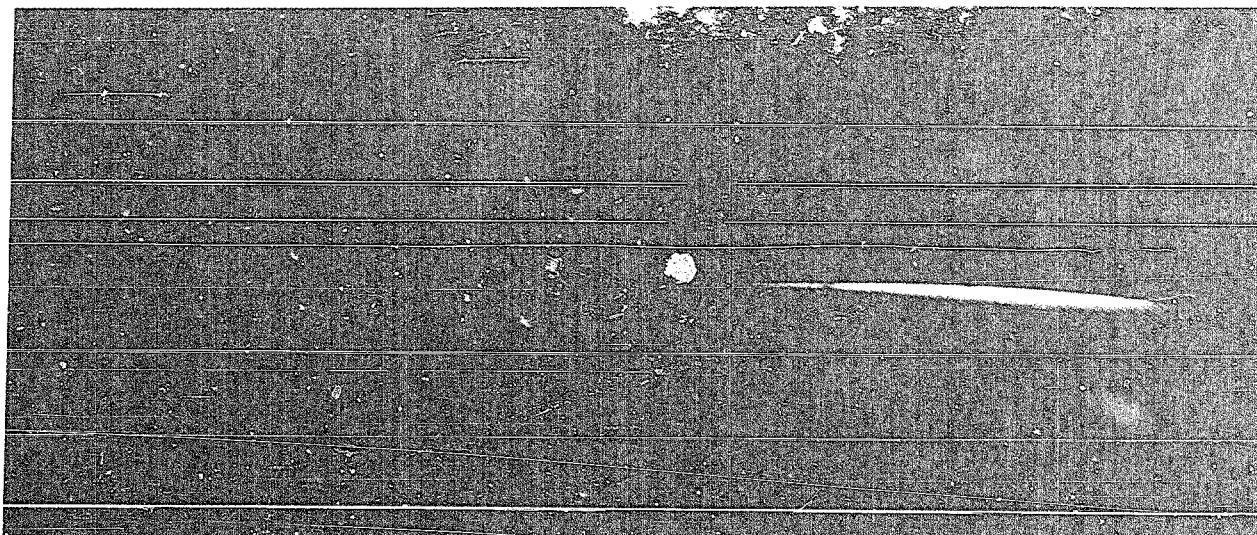
Fig. 2.   Wide-angle photograph of Venus, 17:49 GMT, Feb. 5, 1974
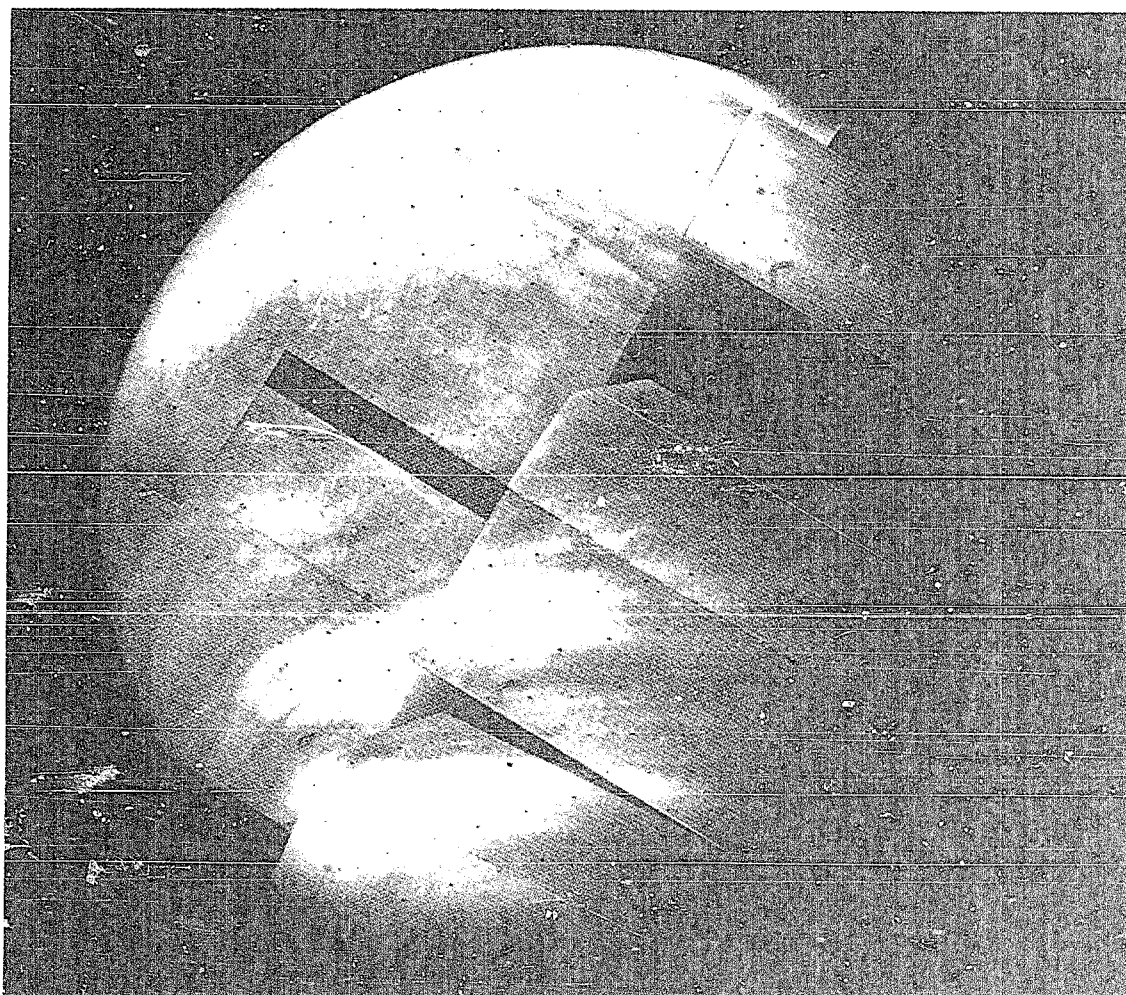
Fig. 3.   Venus mosaic from 70,790 km (440,000 miles)

Fig. 4.   Venus mosaic from 845,000 km (525,000)
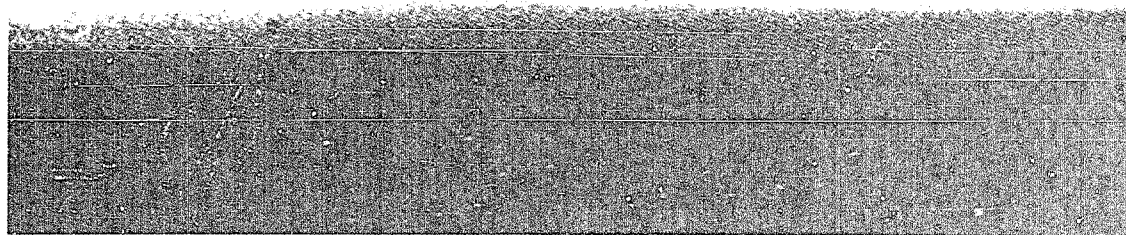
Fig. 5.   Photograph of haze layers on the limb of Venus
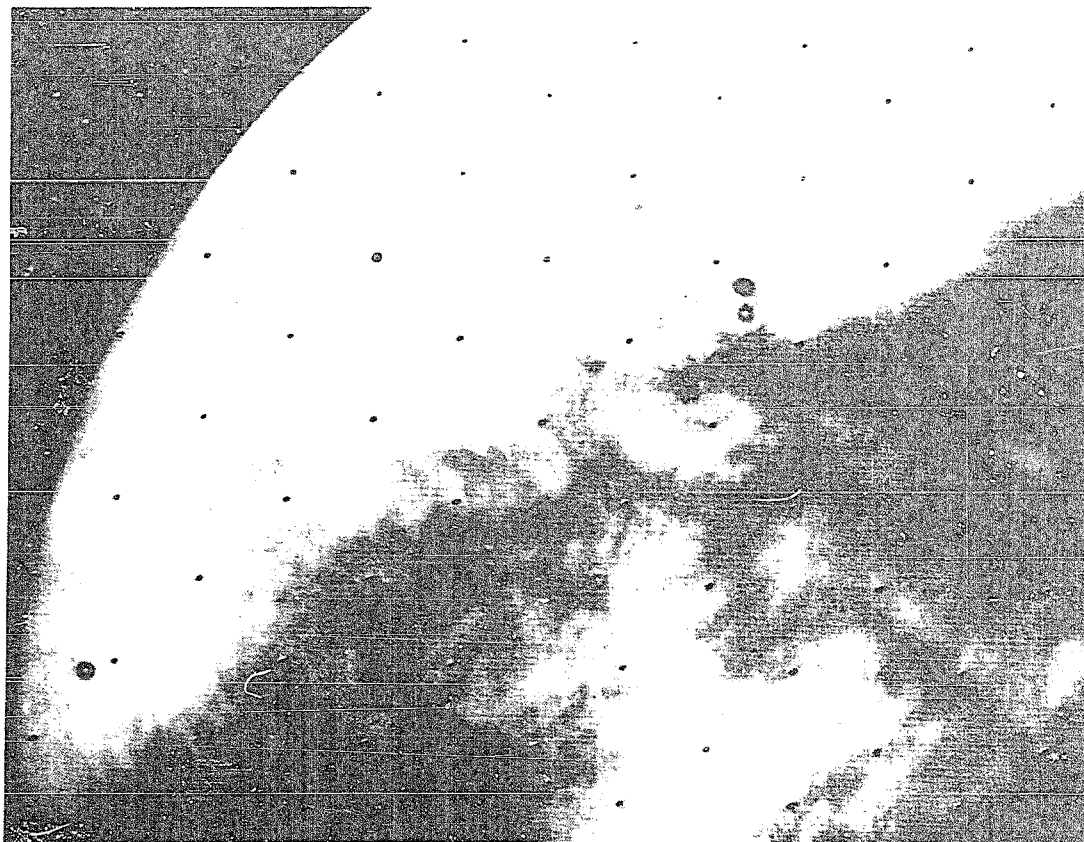
Fig. 6. Venus--Feb. 6, 1974
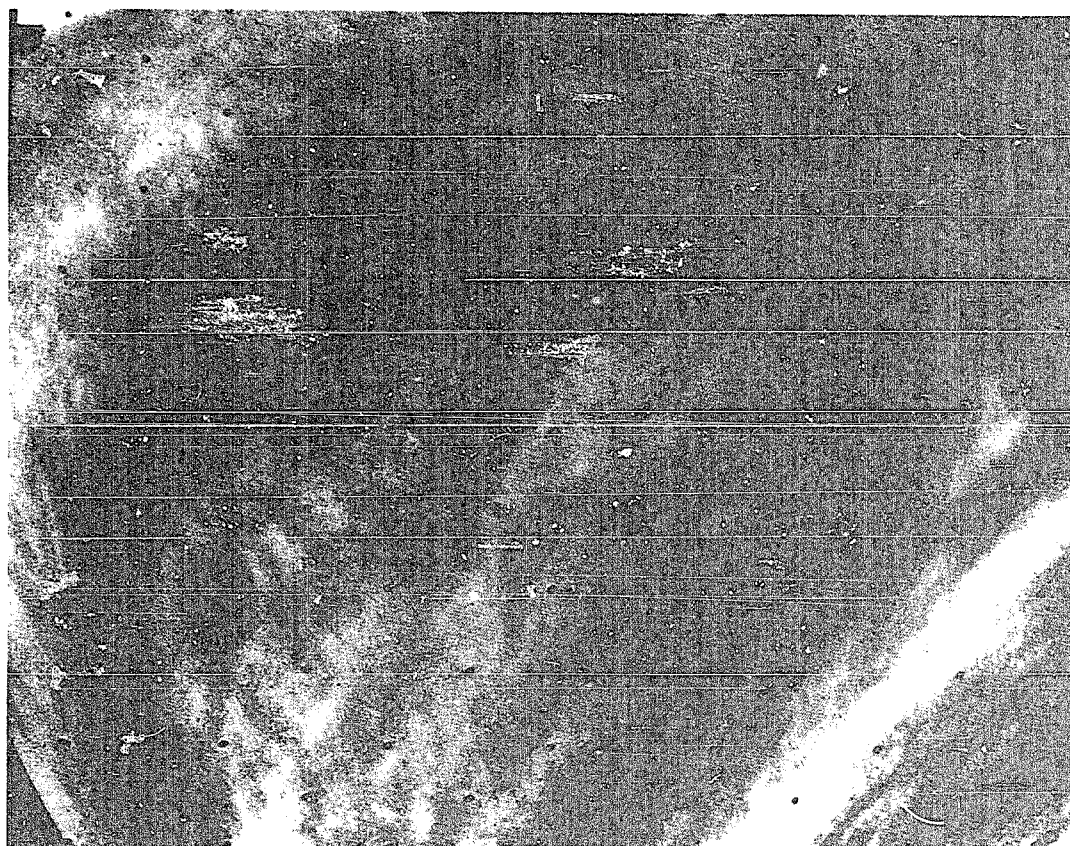
Fig. 7. Ultraviolet photograph of Venus--Feb. 6, 1974
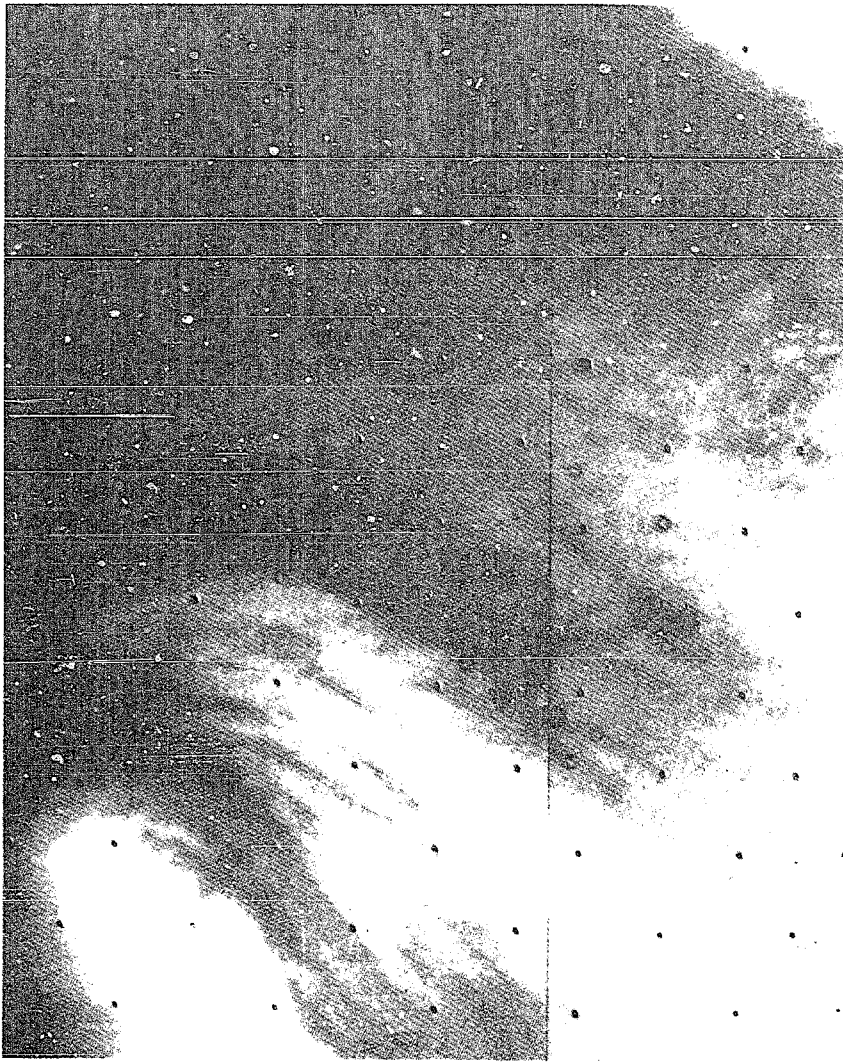
Fig. 8. Ultraviolet photograph of Venus' southern hemisphere

Fig. 9. Computer-enhanced
ultraviolet Venus mosaic
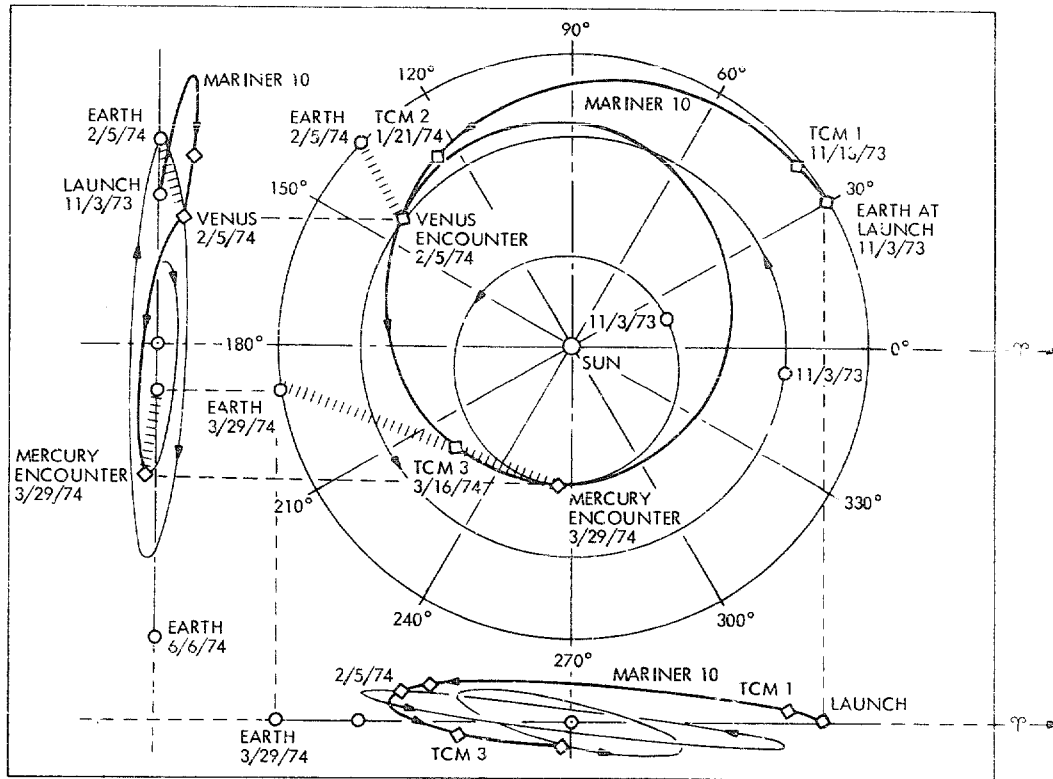
Fig. 10.   Mariner 10 trajectory
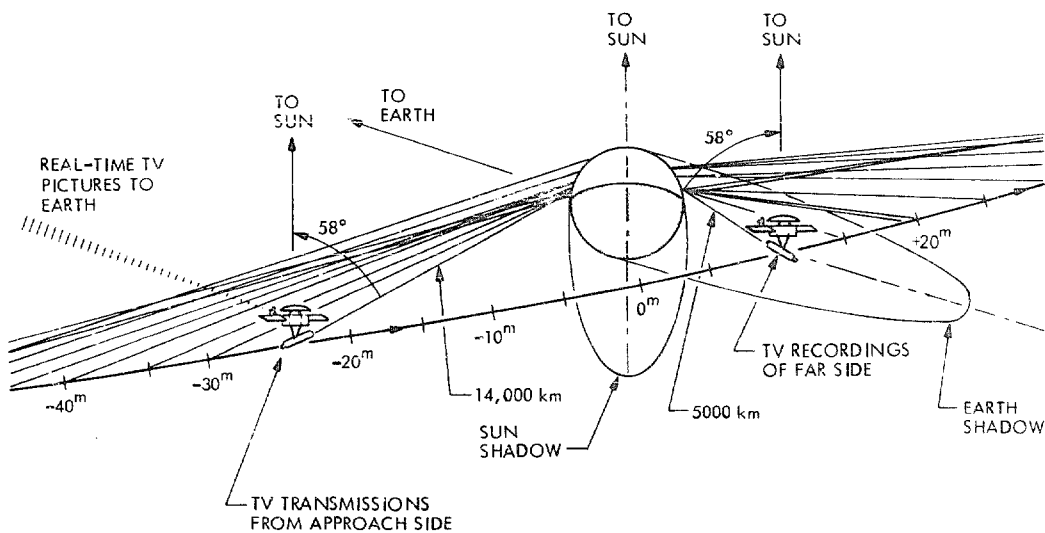
Fig. 11.   Mariner 10 Mercury encounter flight path and television camera sighting lines during the hour before and after closed approach
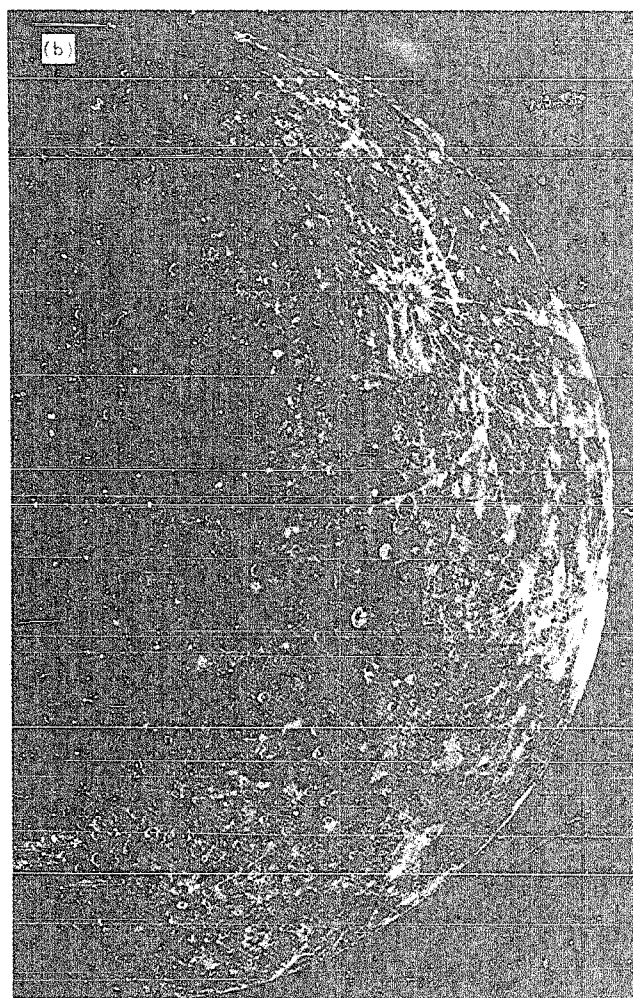
Fig. 12. Photomosaic of Mercury
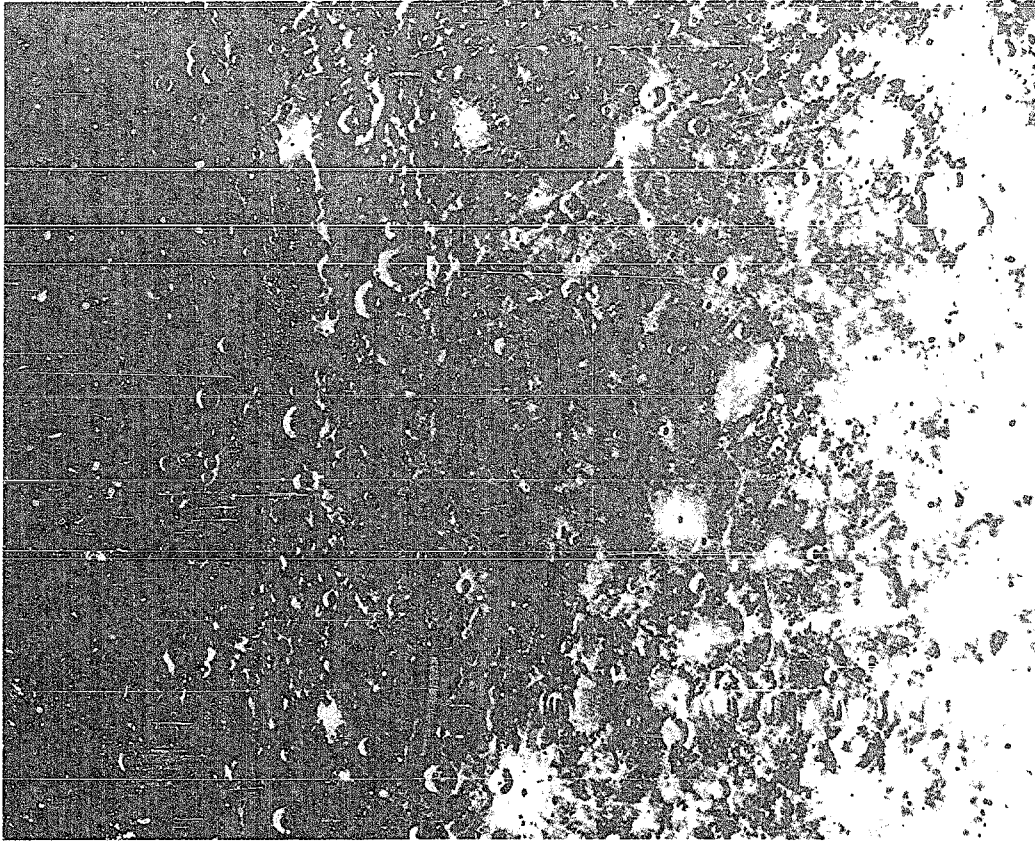
Fig. 13. Closeup view of Mercury
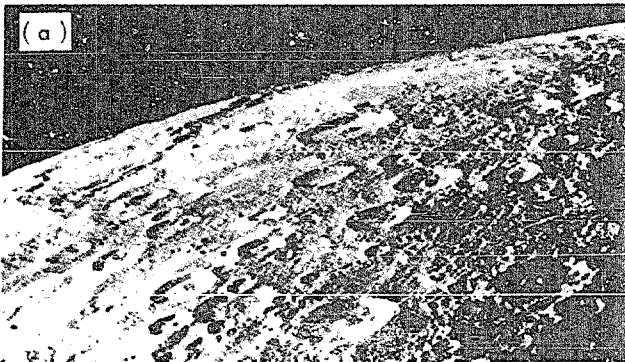
Fig. 14. Views of Mercury
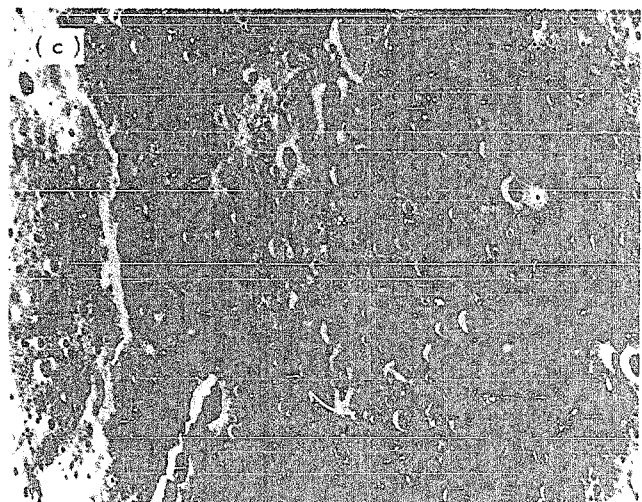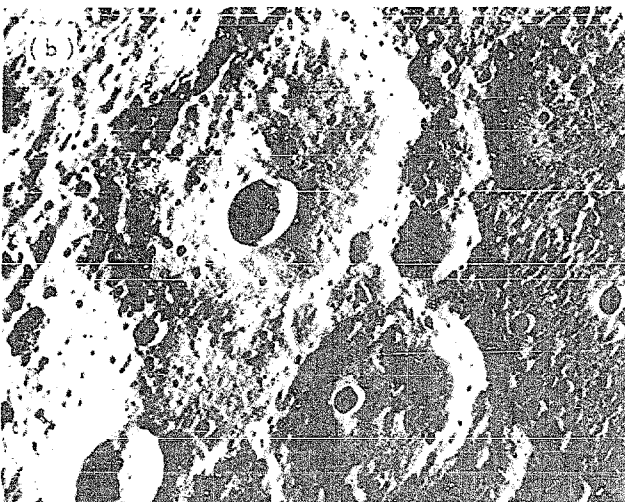
Prominent structural features on Mercury include irregular scarps which are up to 1 km high, extend for hundreds of kilometers, and cut across large craters and intercrater areas (Fig. 14a). Similar features are absent on the Moon. In addition, the paucity of straight rilles and graben on Mercury suggests a major difference in structural style between Mercury and the Moon. No features suggestive of either Earth-like plate tectonics or large-scale tensional faulting in the crust have been recognized so far.

The Mariner 10 photographs of Mercury, combined with previous studies of the terrestrial planets, suggest four preliminary conclusions.

(1) Extensive flooding by rock materials at least grossly similar to those of the lunar maria has occurred on Mercury. The large horizontal scale of such features implies a silicate composition (density approximately 3) for the entire outer regions of the planet, not just the upper centimeters or meters as is indicated directly by remote optical, infrared, and radio measurements. Yet the mean planetary density of 5.5 g/cm^3 requires that very much denser material must occur at depth, very probably in the form of a large iron core. Thus Mercury is a chemically differentiated planet.

(2) The heavily cratered surfaces on Mercury record the final periods of heavy impact bombardment at Mercury. We consider it likely that those landscapes include at least some topographic features which have survived from the end of tangible accretion. Since planetwide melting would have destroyed such topographic features, Mercury's major chemical differentiation must have taken place before the end of accretion there. Similarly, there can have been no tangible atmosphere, primitive or secondary, about Mercury since those topographic features formed, because eolian processes would have modified them, as on Mars. An early speculation by Kuiper that Mercury's high density might reflect an extraordinary erosion of surface material by anomalous solar activity likewise is not confirmed.

(3) In the half of the planet observed by Mariner 10, Mercury (like the Moon) seems to exhibit a hemispherically non-uniform distribution of flooded basins. If this impression is valid, previous explanations of the near-side/far-side dichotomy of the Moon which involve processes peculiar to the presence of the Earth may require re-evaluation.

(4) Mare-like surfaces now have been formed on the Moon, Mars, and Mercury which show a surprising similarity in accumulated impacts, although only those of the Moon have been dated radiometrically. The impacting objects traditionally have been regarded as asteroids or comets. A strong decrease in flux between Mars and Mercury had generally been expected. Yet, barring extraordinary coincidence

in both age and local fluxes, no strong dependence on heliocentric distance in post-accretion.

A selection of the Mercury encounter pictures are shown in Figs. 12 through 20.

B. MAGNETOMETER

The NASA Goddard Space Flight Center magnetic field instrument consists of two very sensitive magnetometers placed on a long boom. The purpose of the dual magnetometer system is to eliminate by appropriate mathematical analysis the contamination of measurement of the very weak magnetic field in space by the large and changing magnetic field of the spacecraft itself.

The boom deployment, electronics turn on and instrument conditioning was as planned. The temperature of the sensors after launch was approximately 20°F lower than expected; but this posed no significant problem. The magnetometer from spacecraft 73-1 was tested at Goddard Space Flight Center to better understand how it works at lower than prescribed temperatures. Early mission heater cycling was performed to evaluate current loop effects on the magnetic field.

Numerous attempts to flip the A&B instrument were only partially successful. PFR No. 5016 documents this anomaly. For the Venus encounter, the instrument did not respond to manual mode commands; upon the Principal Investigators' recommendation the instrument was successfully returned to the automatic mode and functioned properly.

During the Earth-Venus transit continuous and accurate measurements of the interplanetary magnetic field were performed with the highest sensitivity and most rapid sampling rates ever achieved in this region of space. While the interplanetary magnetic field ranged from 2 to 25 gammas (Earth's magnetic field at equator equals 30,000 gammas), it was usually between 5 to 10 gammas and in general agreement with earlier studies and theoretical expectations.

The trajectory of Mariner 10 is uniquely well suited for studying the interaction of the magnetized solar wind plasma with Venus. This is because the motion of the spacecraft places it along the dark side of Venus for a period of more than 10 days moving from great distances up to closest approach.

1. Venus Encounter

For more than 6 days preceding the Venus encounter, the magnetic field experiment observed distortion of the interplanetary magnetic field in which the direction was twisted so that the magnetic field appears to be pointing toward the planet Venus. This is interpreted to be associated with the interaction of the solar wind with the ionosphere of Venus, and thus there is a magnetic tail trailing behind Venus much like a comet's tail. During the 5 hours immediately preceding closest approach, the fluctuations of the magnetic field increased considerably, and just before radio occultation the magnetic field doubled in magnitude from approximately 10 to 20 gammas. The critical questions of whether or
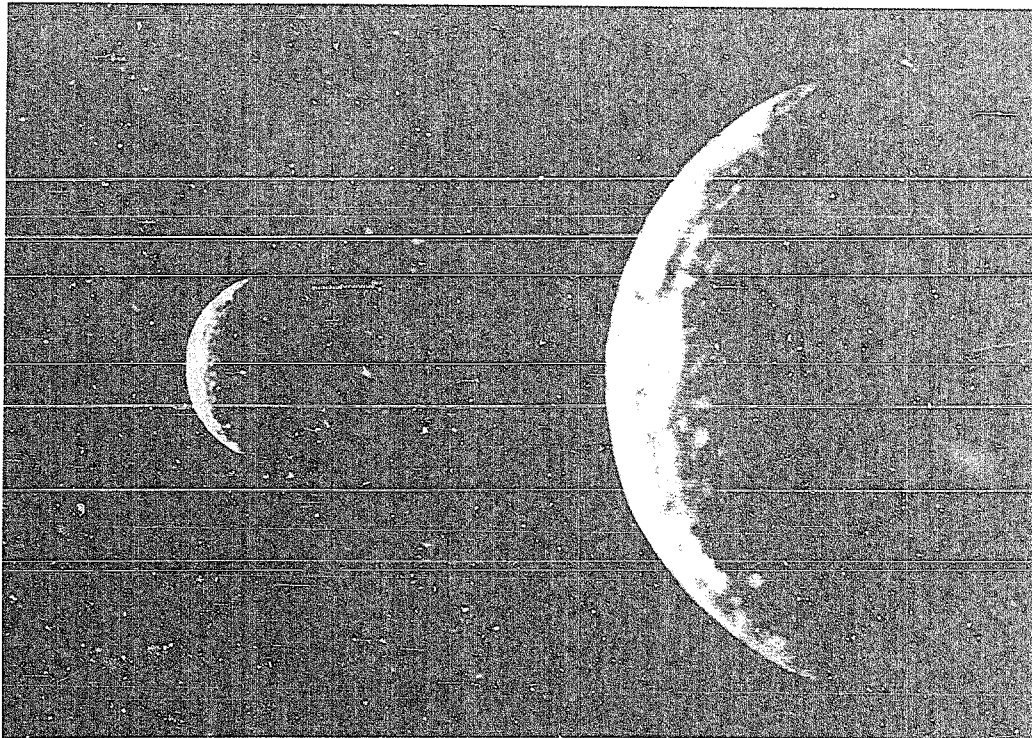
Fig. 15.   Real-time versus enlarged and enhanced photograph of
Mercury--March 26, 1974
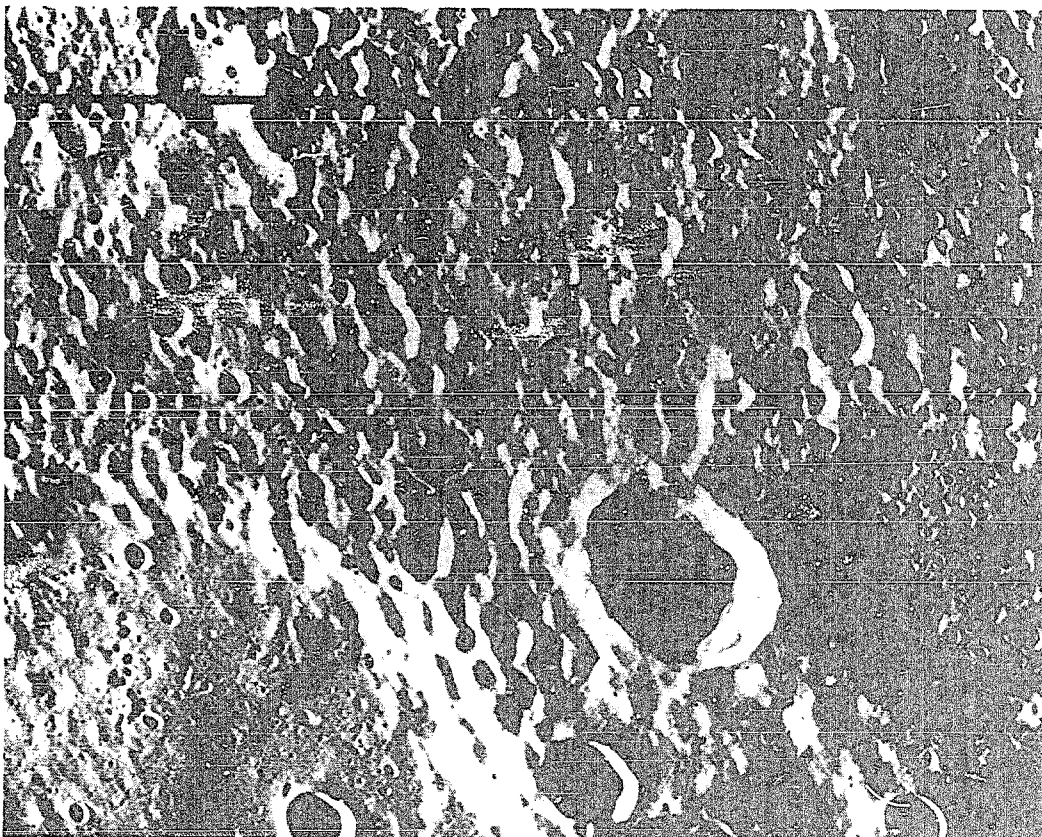
Fig. 16.   Densely cratered photograph of Mercury--March 29, 1974
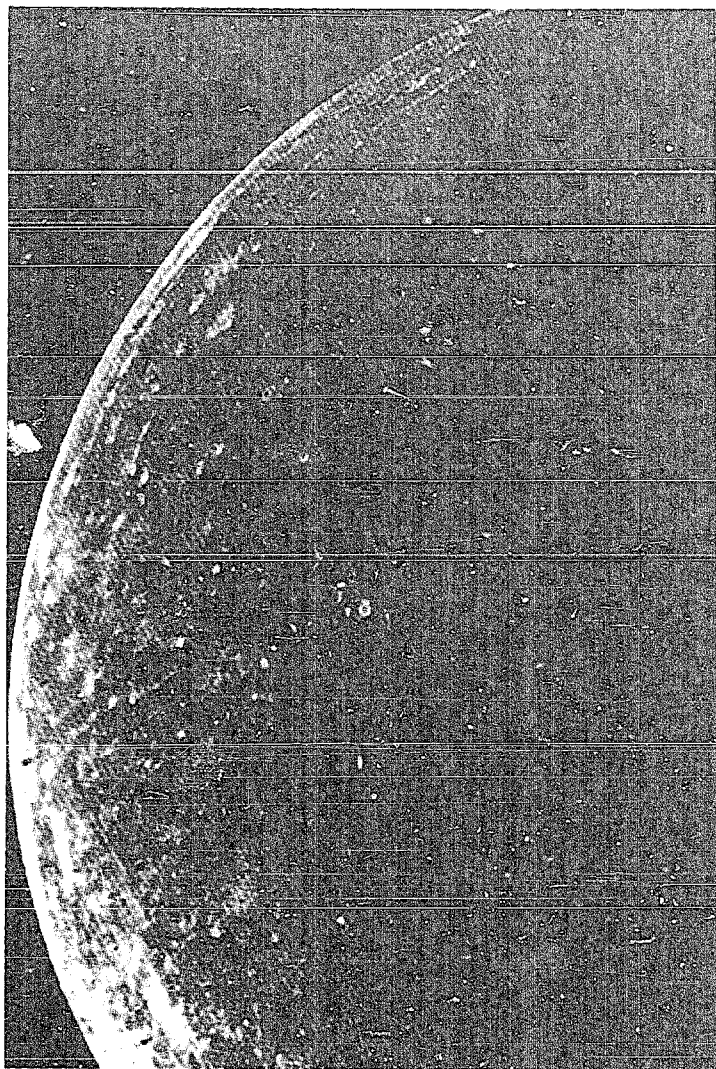
Fig. 17. Photograph of a heavily cratered
area of the planet Mercury--
10. 30 GMT, March 29, 1974
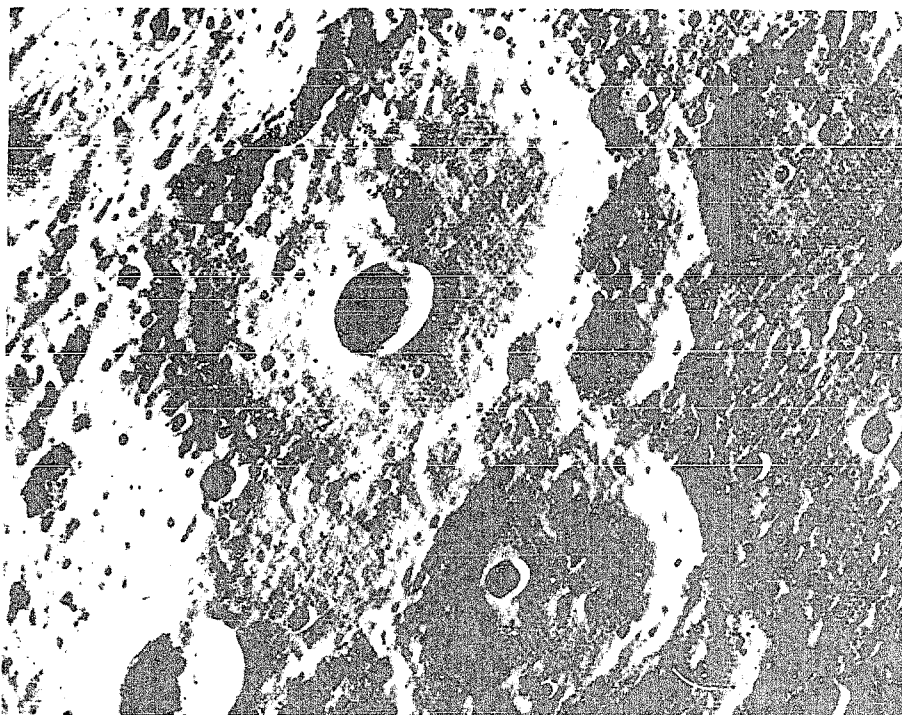
Fig. 18. Cratered photograph of Mercury--March 29, 1974
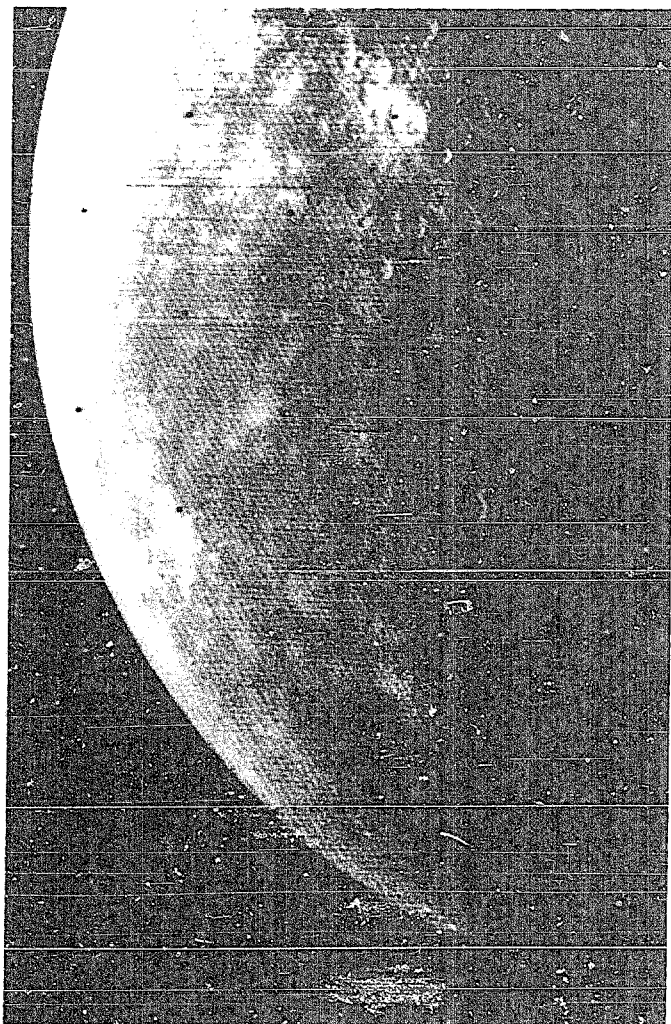
Fig. 19. Photograph of Mercury 13 hours prior to closest approach

Fig. 20. Computer-enhanced photograph of Mercury-- March 28, 1974

not a detached bow shock wave was crossed or not cannot be answered until the radio occultation data are available for analysis and a comparison is made with the plasma experiment data.

However, it is certain that Venus does not possess a magnetic field like the Earth, and indeed any such magnetic field must be less than one-twentieth of one percent of the Earth's magnetic field.

Four models of solar wind interaction with Venus are shown in Fig. 21. Venus, unlike the Earth, does not have a planetary magnetic field that is sufficiently strong to deflect the solar wind (model A). The other three models of the solar wind atmosphere interaction may explain the phenomenon of the detached bow shock wave. Model B corresponds to a direct ionosphere interaction, while model C is a more complex process with the solar wind digging very deep into the ionosphere. At the present time it would appear that model C, in which a magnetic field is induced in the planetary ionosphere leading to a pseudomagnetopause, is the most satisfactory explanation of our data. As the solar wind enters deeply into the atmosphere-ionosphere of Venus, it represents an additional energy source to be considered in the dynamics of the ionosphere and as a mass source to modify the chemical composition of the high atmosphere. Model D, proposed for comets, predicts only a weak shock, if indeed any is present. We do not believe that this mode of interaction is the type which has been observed.

2. Mercury Encounter

The results obtained at Mercury encounter have been startling. It was expected that the planet would not have a magnetic field because of its slow rotation, and because, unlike Jupiter, no radio emissions were observed from it. No radiation belts of charged particles would be expected if no magnetic field was present that could trap and contain the particles.

Thus, as the ionized gas from the Sun (the solar wind) flowed past the planet, it was anticipated that the results would be similar to those at the Moon (Fig. 22). There would be absorption of the solar wind by the planet and the creation of a void or cavity behind the planet, on the dark side. Only small and transient disturbances would result from the disturbance of plasma flow, and these would be located very close to the planet if a negligible atmosphere were assumed for Mercury.

However, very clear experimental evidence was obtained by the magnetic field experiment of the presence of a detached bow shock wave resulting from the deflection of solar wind flowing supersonically past the planet. The locations are shown in Fig. 22. Not all data have yet been analyzed to provide a complete interpretation of these results, but it is clear that the obstacle to solar wind flow is "global" in size, i.e., somewhat larger than the planet.

As Mariner 10 approached closer to the planet, the magnetic field increased very smoothly to a maximum of 90 to 100 gammas at closest approach (750 km from the surface). Preliminary analyses suggest by extrapolation that the

magnetic field on the surface is perhaps 100 to 200 gammas. This is more than sufficient to deflect the solar wind and create the observed bow shock.

The source of the magnetic field is not yet clear. It may be intrinsic to the planet and may represent the end result of an internal dynamo mechanism generating the field. As such it is about 100 to 1000 times smaller than the Earth's. The magnetic field may also be due to a complex mechanism associated with the solar wind interaction with the planet. In this model the sweeping of interplanetary field lines past the planet may generate an electrical current flow in the planet and/or a possible weak ionosphere which then generates the magnetic field observed.

The magnetic field experiment was conducted by a team of scientists from the NASA-GSFC Laboratory for Extraterrestrial Physics: Dr. Norman F. Ness, Principal Investigator; Co-Investigators are Drs. K. W. Behannon and R. P. Lepping, Dr. K. H. Schatten of Victoria University, New Zealand, and Y. C. Whang of Catholic University.

C. PLASMA SCIENCE EXPERIMENT

This system was turned on at 05:30 GMT on November 5, 1973. A DC 53 to unlatch and deploy the PSE boom was transmitted with proper response. The engineering data and scan data were good, although electrons were not being counted. Indications were that the scanning electrostatic analyzer (SEA) door was partially open. A special PSE troubleshooting sequence was run that consisted of cycling power on and off to the electronics in the scan package, looking for proton counts which should appear because of difference in the decay time constraints of the sweep, multiplier, and preamp voltages. No unambiguous indication of proton counting was obtained. PFR No. 5007 was established for the analysis and documentation of this anomaly. Numerous attempts to thermally shock the SEA door by pointing the instrument toward the Sun for several hours then placing it in the shade ($-70\,°F$) proved unsuccessful.

1. Venus Encounter

From the results of Plasma and Magnetic Field Experiments carried on the Mariner 5 Venus mission it is known that the solar wind flow near Venus is greatly modified by the presence of the planet. It is generally believed that the solar plasma interacts with the ionosphere of Venus so that a bow-shock is formed upstream from the planet (on the sunward side) and that a transition region of modified plasma flow exists between the bow shock and the ionosphere. In the transition region, the flow velocity of the plasma is lower and the particle density is higher than the corresponding values in the undisturbed plasma stream far away from Venus.

The trajectory of Mariner 10 during the near encounter period (out to 10 Venus radii) was expected to lie completely within the transition region. It was predicted that the plasma density should increase smoothly along the trajectory up to a maximum value at the point where Mariner 10
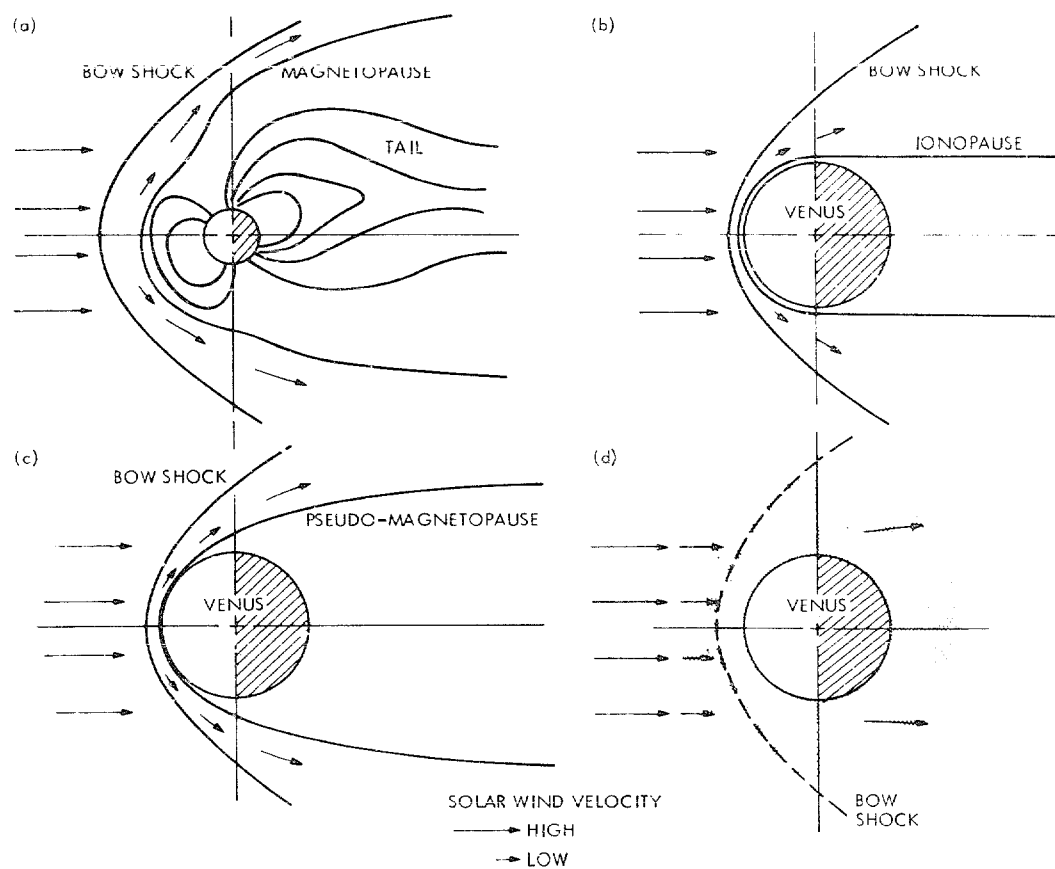
Fig. 21.   Solar wind velocity
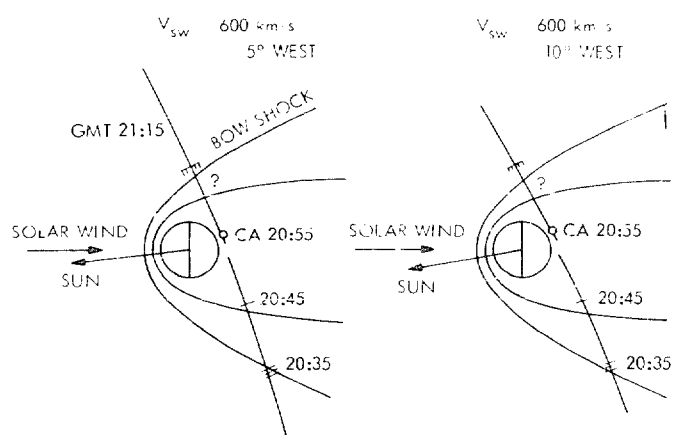
Fig. 22.   Bow shock at Mercury

passed through the bow shock. Just after the bow shock the density should drop sharply.

Values have been plotted of the plasma density observed by Mariner 10 near Venus encounter as a function of time and frame that they do increase as expected up to a maximum value at about the predicted position of the bow shock and then decrease abruptly. The position of maximum density occurs close to the time at which real-time data transmission ceased, and so a detailed analysis of the shock crossing must wait until the playback data has been received.

For several days prior to Venus encounter, the properties of the plasma observed by Mariner 10 are distinctly different from the properties of the undisturbed solar wind. The results show clearly that Venus has a long plasma wake or tail that extends roughly in the antisolar direction away from the planet. Mariner 10 is the first spacecraft to approach Venus from this direction; thus, this is the first time the "plasma tail" of Venus has been observed.

2. Mercury Encounter

Up to this time, there had been definitive information on the nature of the interaction between the solar wind and the Earth, the Moon, and Venus. All of these interactions are very different. It was generally believed, prior to the Mariner 10 encounter, that the interaction with Mercury would prove to be similar to that of the solar wind and the Moon. That is, it was expected that the plasma particles incident on the surface would be absorbed, and a cylindrical cavity or plasma shadow was expected to extend in roughly the antisolar direction. Instead, Mercury has a well-developed bow shock close to the planet, a region of transitional flow filled with hot shocked plasma, and instead of a plasma cavity a magnetosphere-like region in which plasma electrons are accelerated to energies above a kilovolt. These accelerated electrons provide a source for the night glow.

The properties of the planet which give rise to these effects are not yet understood. It is possible that Mercury has an intrinsic magnetic field, or it may be that an induced field is produced by the solar wind via "unipolar induction" in the ionosphere or, if the surface is a good electrical conductor, in the surface of the planet.

The Mariner 10 Plasma Science Experiment is a cooperative effort by several laboratories. The experiments include K. W. Ogilvie, R. E. Hartel, and J. D. Scudder (GSFC); J. R. Ashbridge, S. J. Bame, and W. C. Feldman, Los Alamos Scientific Laboratory; G. L. Siscoe (UCLA); and H. S. Bridge and A. J. Lazarus (MIT).

D. CHARGED PARTICLE TELESCOPE

1. Venus Encounter

The Charged Particle Telescope (CPT) Experiment on Mariner 10 spacecraft was designed by Professor John A. Simpson and the staff of the Laboratory for Astrophysics and Space Research to measure energetic particles, (electrons, protons, helium, and heavier nuclei),

in interplanetary space as well as to search for fluxes of such particles which might be accelerated as a result of the interaction of Venus with the solar wind. It is designed to detect electrons with energies above 0.2 MeV and protons at energies above 0.5 MeV. The existence of a bow shock at Venus as determined by previous spacecraft, as well as Mariner 10, suggests the possibility of local acceleration phenomena in analogy to the Earth, which had not as yet been detected in the vicinity of Venus.

For at least three days prior to and during the Venus encounter, the conditions in interplanetary space have been unusually quiet, thus providing the best possible conditions for the search for energetic particles associated with Venus. Sensitivity of the charged particle telescope to fluxes of energetic particles is 100 to 1000 times greater than instruments flown previously; however, no planet-associated fluxes were detected in the preliminary data received, thus indicating the absence of a magnetosphere and of particle acceleration by interaction with the bow shock.

Figure 23 shows the counting rates for the flux of electrons and protons in the more sensitive channels of the instrument during the encounter. These rates throughout the period are representative of quiet interplanetary levels.

Figure 24 shows the pulse height distribution for electrons and protons before, during and after closest approach to Venus. The shaded area represents a slight excess accumulation during the 30-min period around closest approach. However, this excess is not considered statistically significant and therefore does not indicate a planet-associated flux.

Table 1 is a table which compares results of the Mariner 10 measurements with those obtained during previous missions. It illustrates the establishment of a new set of upper limits for the interaction of Venus with the interplanetary environment.

2. Mercury Encounter

High-energy electron fluxes have been discovered in the magnetic field of Mercury. The electrons have an energy of approximately 1 MeV. They are distributed continuously from a distance of approximately 5000 km above the planetary surface (equivalent to 2 Mercury radii above the surface) to the closest approach of the spacecraft to the planet (approximately 700 km). The peak intensity was found near the closest approach. These electrons were energized in the external magnetic field of Mercury. However, from the preliminary data available at this time, it is not certain whether the electrons are accelerated at the planet and escape to space, or whether the electrons are from a trapped radiation region close to the planet. The electron intensities are below the level required to produce radio emissions that could be detected at Earth by radio telescopes.

Playback data returned from the interval when the spacecraft was occulted by Mercury, and only processed and analyzed in a preliminary way, show electron fluxes even greater, by a
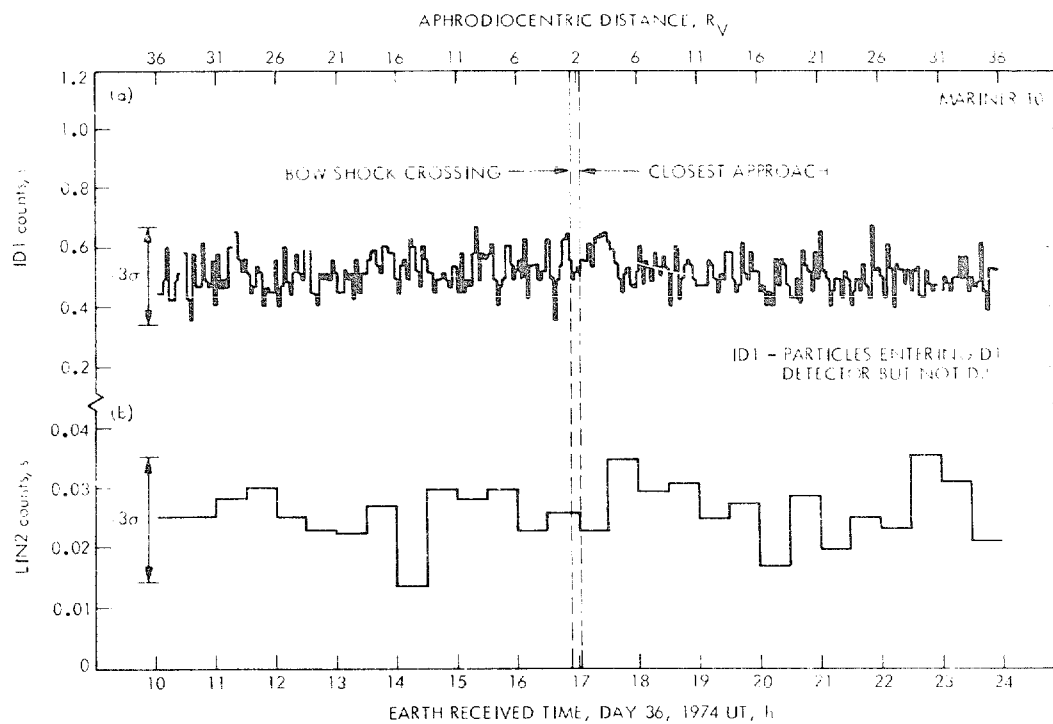
Fig. 23. CPT counting rates for the flux of electrons and protons--Venus encounter (University of Chicago)
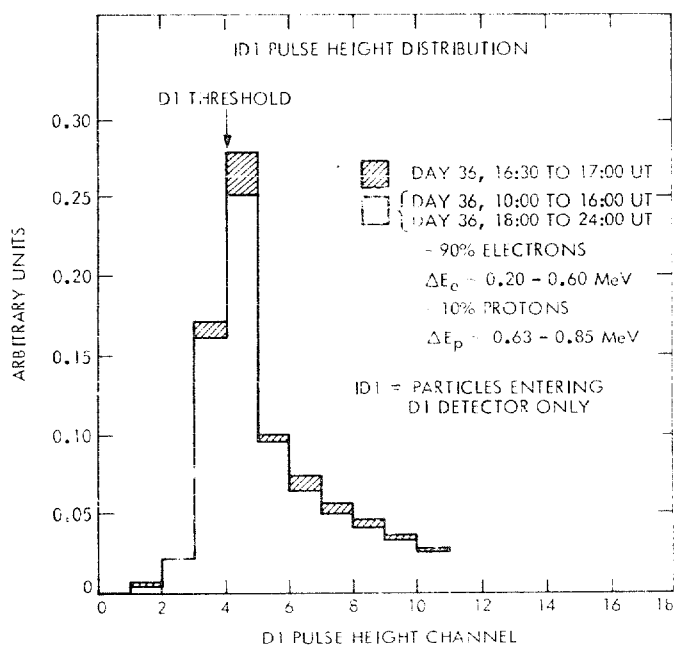
Fig. 24. CPT pulse height distribution for electrons and protons--Venus encounter (University of Chicago)
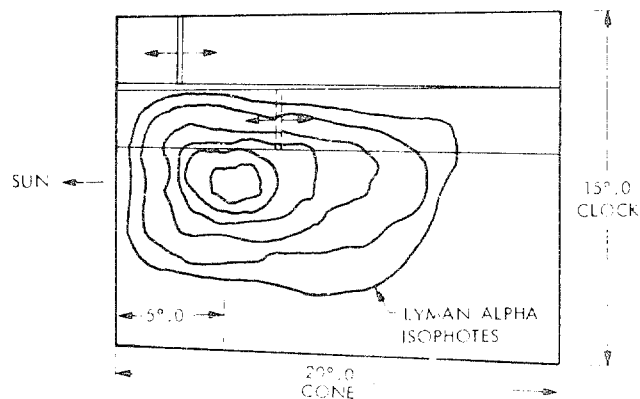
Fig. 25. Airglow ultraviolet spectrometer scan pattern of Kohoutek's hydrogen corona

Table 1. Comparison of charged particle and magnetic field experiments during Venus encounter

| Mission (Year of encounter) | Phase of solar cycle activity | Bow shock[a] plasma[b] | Search for Venus-associated charged particles | | | | M_V/M_E[c] | |
| | | | Electrons | | Protons | | Scaling of particle observations | Magnetometer |
			Minimum energy, keV	Minimum flux[b]	Minimum energy, keV	Minimum flux[b]		
Mariner 2 (1962)	Solar active	no	70	<5	500	<5	<9 × 10^{-2}	<5 × 10^{-2}
Mariner 5 (1967)	Near solar maximum	yes	45	<3	320	<1	<(1 × 10^{-3} - 1 × 10^{-2})$^{(2)}$	<2 × 10^{-3}
Venera 4 (1967)	Near solar maximum	yes						<3 × 10^{-4}
Venera 6 (1970)	Near solar maximum	yes						
Mariner 10 (1974)	Near solar minimum	yes	180	<5 × 10^{-3}	520	<1.4 × 10^{-2}	<1 × 10^{-3}	<5 × 10^{-4}

[a]Magnetic field and plasma identification.

[b]Equal to 3 σ fluctuations in the count rate (particles cm^{-2} sec^{-1} sr^{-1})

[c]M_V/M_E = ratio of magnetic moment of Venus to magnetic moment of Earth.

factor of more than 100, than the data provided in real-time before occultation. These fluxes and their distribution are quite inconsistent with the simple model of Mercury's interaction, which was generally believed before the Mariner 10 mission.

The measurements were made with charged particle telescopes in an instrument designed for this experiment and interplanetary studies by Professor J. A. Simpson and J. E. Lamport in the Laboratory for Astrophysics of the Enrico Fermi Institute at the University of Chicago.

E. ULTRAVIOLET SPECTROMETER

Following launch the instrument temperatures were as predicted. UVS airglow Earth scan, search for Mars (not attained), data obtained during the maneuvers, star and comet Kohoutek observations, yielded significant scientific results

The scan platform high cone angle restriction proved to be a nuisance during some of the scanning experiments.

From January 10 to 16, 1974 the Mariner 10 ultraviolet airglow spectrometer (UVSA) continued to observe Comet Kohoutek's tail in the extreme UV 30-166 nm wavelength range. On January 13, the hydrogen Lyman alpha (122 nm) intensity starting 20 deg from the comet's nucleus began to climb exponentially and then rose even more rapidly as the comet's nuclear region drifted toward the UVSA view field, as shown in Fig. 25. At about 7 p.m. PDT on January 16 the nucleus of Kohoutek was scanned. On January 19 the TV cameras attempted to take pictures of the comet (Fig. 26), but a preliminary examination of the frames indicated that Kohoutek was too dim to yield useful imaging data. The planned UVSA scans of the comet continued on January 22 and 24, even though no further attempts to obtain TV images were made.

Preliminary results of the UVSA scans of Comet Kohoutek have revealed a very large neutral hydrogen corona with a diameter of about 20 million kilometers. A very high peak intensity for hydrogen was measured at the nucleus. Evidence was also found for the presence of carbon in the nucleus. Further analysis of the data is

required to determine whether or not the signal in the argon channel was due to argon or some other source. On January 18, the occultation UVS was turned on for the first time. It functioned normally.

1. Venus Encounter

Hydrogen is an important element of Venus' atmosphere that can potentially shed light on the origin and evolution of the planet. The Earth's atmosphere evolved slowly over geologic time, leaking out of the crustal rock in hot springs and volcanoes. The major gases emitted by Earth were H_2O, CO_2 and N_2 with relative abundances given by the approximate ratios of 40:1:0.03. Terrestrial H_2O is found mainly in the oceans. CO_2 is precipitated as carbonates. N_2 remains in the atmosphere.

If the gases trapped by Venus were similar to those observed on Earth, we might expect that the primitive Venus should have had an exceedingly dense atmosphere, characterized by a surface pressure of about 1000 atm, with a CO_2 abundance comparable to that observed today — a partial pressure of about 90 atmospheres. The water would have been efficiently dissociated by ultraviolet sunlight, and its hydrogen could have escaped into interplanetary space, leaving oxygen to be absorbed by crustal rocks.

There are, however, other possible explanations for the present hydrogen abundance of Venus. Venus could have acquired its hydrogen in a chance impact with a large cometary nucleus — a celestial snowball. Alternatively, Venus could have built up its hydrogen inventory by steady accretion from the solar wind. Incident protons can transfer charge with constituents in the outer atmosphere of Venus, in the process becoming electrically neutral, and subsequently impacting the planet. The UVS experiment expects to clarify the relative roles of these various processes. The various sources provide characteristic records of their influence. Cometary nuclei are expected to be rich in heavy hydrogen (deuterium). If comets represent a major supply of hydrogen, Venus should be enriched in deuterium relative to hydrogen. Mariner 10, in contrast to data obtained in the earlier mission of Mariner 5, shows no evidence for deuterium on Venus. The Lyman alpha data are consistent, however, with a possible solar wind source for hydrogen. The Sun consumes deuterium in nuclear reactions which occur in the solar interior. Much of the Sun's original deuterium inventory has been depleted over 5 billion years, and the concentration of deuterium in today's solar wind is immeasurably small.

The study of Venus' hydrogen is important for several reasons: hydrogen, despite its low abundance, controls the chemistry of Venus' atmosphere. If Venus were to exhaust its present supply of hydrogen, we would expect atmospheric CO_2 to be rapidly converted to C_2 and CO. Hydrogen is thought to be a major element of the Venus' cloud deck, present in the droplets of H_2SO_4 as well as water vapor. The ultraviolet experiment will define and refine the processes which regulate Venus' hydrogen. The profile of Lyman alpha can be analyzed to give the temperature of the outer atmosphere. Preliminary analysis

suggests a temperature of about 600°F. The escape rate of hydrogen from Venus is smaller than measured Earth escape rates by more than a factor of 10.

Other major achievements of the Mariner 10 UV experiment can be summarized as follows: helium is an important trace element of the atmosphere. Its presence is clearly registered in the airglow emission observed at 548 Å. The upper atmosphere of Venus contains important quantities of atomic oxygen. The emission at 1304 Å is stronger by about a factor of 10 than that measured by Mariner 9 for Mars. The large concentration of oxygen in Venus' atmosphere may indicate a comparative absence of rapid vertical mixing in that planet's upper atmosphere and may shed light on the dynamical processes which influence the composition of all planetary atmospheres.

Atomic carbon is a significant trace element of Venus' atmosphere formed as a photochemical product of energetic processes involving CO_2.

2. Mercury Encounter

The ultraviolet experiment on Mariner 10 found definite evidence for helium in the atmosphere of Mercury. Its concentration is significantly higher than concentrations observed in the lunar atmosphere. If gas is formed primarily by radioactive decay of uranium and thorium, the observation can be interpreted to yield information on the concentrations of these elements in the crustal rocks of the planet. Preliminary analysis suggests that Mercury may contain concentrations of uranium and thorium comparable to those found on Earth.

Weak luminosity detected on the dark side of Mercury appears to indicate the presence of additional gases in the atmosphere, including argon, neon, and possibly xenon. The occultation mode of the experiment allows one to set an upper limit on the total gas content of the planetary atmosphere. The surface pressure on Mercury is less than that of Earth by a factor of 10^{11}. The albedo of Mercury at ultraviolet wavelengths is similar to that of the Moon.

The Ultraviolet Spectroscopy Experiments were conducted by A. Lyle Broadfoot and M. J. S. Belton, of Kitt Peak National Observatory, and M. B. McElroy of Harvard University.

F. INFRARED RADIOMETER

1. Venus Encounter

The temperature of the Venus atmosphere increases with depth from a temperature of about 250 K (-9°F) near the top of the visible cloud deck to a temperature of 750 K (890°F) at the surface of the planet. Near the cloud tops the temperature is about 9 K (16°F) per kilometer of depth.

The Mariner 10 infrared radiometer obtained measurements of the temperature of the Venus atmosphere at a wavelength of 45 μm. At this wavelength the atmosphere above the cloud tops is not completely transparent. When the line of sight of the radiometer moves from the center of

the Venus disk toward the edge, it becomes more and more inclined to the visible "surface" at the point where it penetrates into the Venus atmosphere. As a consequence, the average depth of the layers that contribute to the observed temperature becomes smaller and smaller. Since the temperature increases with depth, this means that the average temperature of the contributing layers becomes smaller as the edge of the disk is approached. This effect, called limb darkening, was observed by the Mariner 10 radiometer.

Figure 27 illustrates the single scan made of Venus by the radiometer. Although the scan did not pass across the center of the planetary disk, extrapolation from the observed temperatures yields a disk center temperature of 255 ± 4 K (0 ± 7°F). The corresponding temperature at the edges of the disk is 222 K (-60°F).

The bottom half of Fig. 28 illustrates the observed limb darkening. From these data one can infer that the 45-μm absorption coefficient is 0.24 km through the atmosphere. In other words, near the cloud tops of Venus, one-half the thermal energy at 45-μm wavelength is absorbed each 3 km of passage through the atmosphere.

The deviations from a smooth limb darkening are illustrated in the upper half of Fig. 28. They indicate that the atmosphere is not completely homogeneous, that significant deviations from uniformity do exist. An attempt was made to correlate these infrared features with ultraviolet markings noted in the television images of Venus. Unfortunately, this area of the cloud cover of Venus was unobservable until 2 or 3 days after the infrared data was obtained. Although the gross scale of the ultraviolet markings was comparable to the scale of the infrared features, no direct correlation could be established. However, television viewing of these areas of Venus (30 to 50° N latitude) was quite oblique. Also, specific markings in the ultraviolet tend to lose their individual identity within a day or two at most.

The information obtained by the radiometer is a significant contribution to our understanding of the structure of the Venus atmosphere.

2. Mercury Encounter

The Mariner 10 infrared radiometer has measured the surface temperature of Mercury from the blistering heat of the day side to the extreme cold of the unilluminated hemisphere, revealing that the uppermost layers of the soil are porous and highly insulating. The thermal properties of Mercury are thus similar to those of the Moon. The night-time temperatures, which are crucial for the determination of the nature of the soil, have never before been measured.

The infrared radiometer, constructed by Santa Barbara Research Center, consists of twin 1-in. telescopes with detectors sensitive to the thermal radiation from Mercury. The short-wave telescope can measure temperatures in the range from 700 to 200°K (about 800 to -100°F), and the long-wave telescope is sensitive from 300 to 80°K (about 80 to -320°F). The linear resolution at the surface of Mercury varies from 10 to 50 km, depending on the distance of the spacecraft from

the planet. Data were obtained during the hour in which Mariner swept past the planet, extending from the illuminated part of the planet across the night side and back again to the sunlit surface. Over the latter part of this scan the spacecraft was in Earth occultation, and the observations were tape-recorded for later transmission to Earth. The data presented here is limited to the observations received in real time, spanning the near-equatorial temperatures from mid-afternoon until nearly midnight of Mercury local time. (Since the rotation rate of Mercury is very slow, the length of a Mercurian day is equal to that of 176 terrestrial days. Thus an "hour" of local time of Mercury corresponds to more than seven days on Earth).

On the illuminated side of Mercury, the temperature is extremely high, ranging from about 570 to 700°K (about 566 to 800°F), depending on the distance of the planet from the Sun. (The orbit of Mercury is more eccentric than that of any other planet except Pluto, resulting in substantial variations in distance from the Sun and, hence, in the surface temperature at local noon.) Venus is the only planet that is hotter than Mercury. At the time Mariner reached Mercury, it was near its maximum distance from the Sun, so that the noon temperature was near the lower limit of the above range. The planet temperature at mid-afternoon, was 460°K (about 370°F). As the instrument's field of view swung past the terminator into the night side, the temperature plummetted rapidly to below 150°K (about -200°F), and then declined slowly and steadily, just as would be expected for a thermally insulating surface. At local midnight, the equatorial temperature was down almost to 100°K (about -280°F), and an extrapolation of our data to just before dawn, where the Sun has not shone for nearly three Earth months, gives a minimum temperature of approximately 90°K (about -300°F). Thus, the range of equatorial temperature during a Mercurian day is about 1000°F, much greater than that on any other planet.

The surface temperature of a planet, and particularly the rate of cooling of the surface during the night, are sensitive to the physical properties of the upper few inches of the surface soil. In a sense, then, the radiometer experiment has an extraordinarily high resolution, for it allows us to isolate and investigate the nature of this very thin surface layer of the planet. In general, the lower the temperature at night the more insulating is this surface layer: like a blanket, an insulating layer of dust keeps the heat in and results in a cold surface. The very low temperature observed on the night side of Mercury, which are nearly the same as the night temperatures on the Moon, show that the thermal conductivity of the soil of Mercury is similar to that of the Moon. For both objects, this thermal conductivity is much lower than we encounter on Earth, where moisture and wind compact the soil and increase its ability to conduct heat. Only in the near vacuum at the surfaces of Mercury and the Moon can the continuous "gardening" of the soil by meteoric impacts maintain the low-density dust layer required to match the observed temperatures.

When examined in detail, the temperature scan across Mercury reveals small variations (up
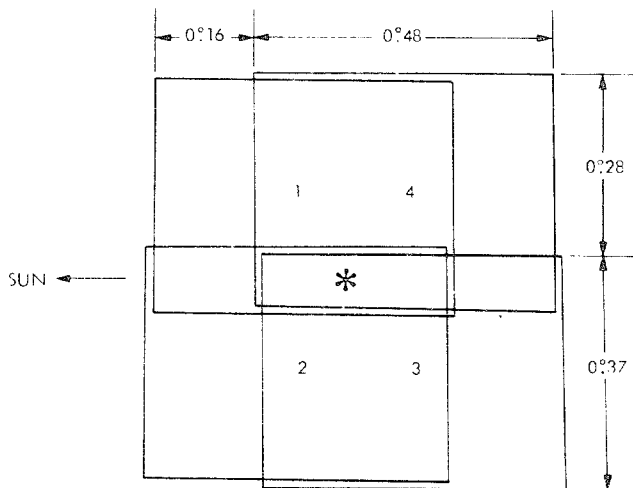
Fig. 26. Television frame mosaic of Kohoutek's nucleus
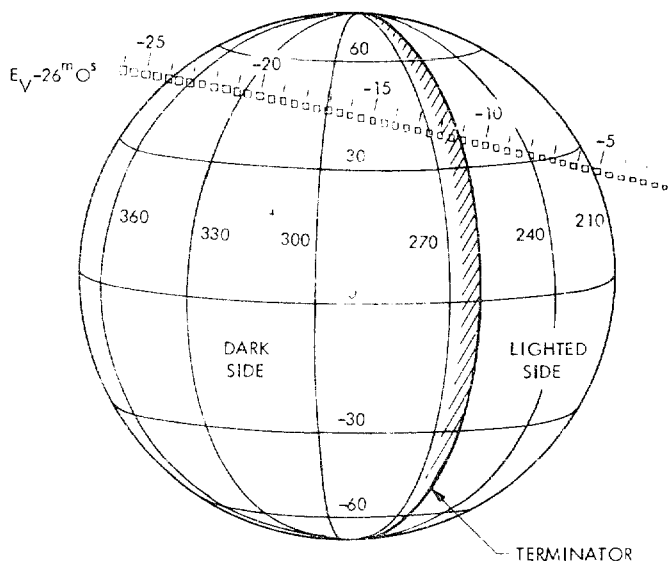
Fig. 27. Swath of the radiometer's field of view across the disk of Venus
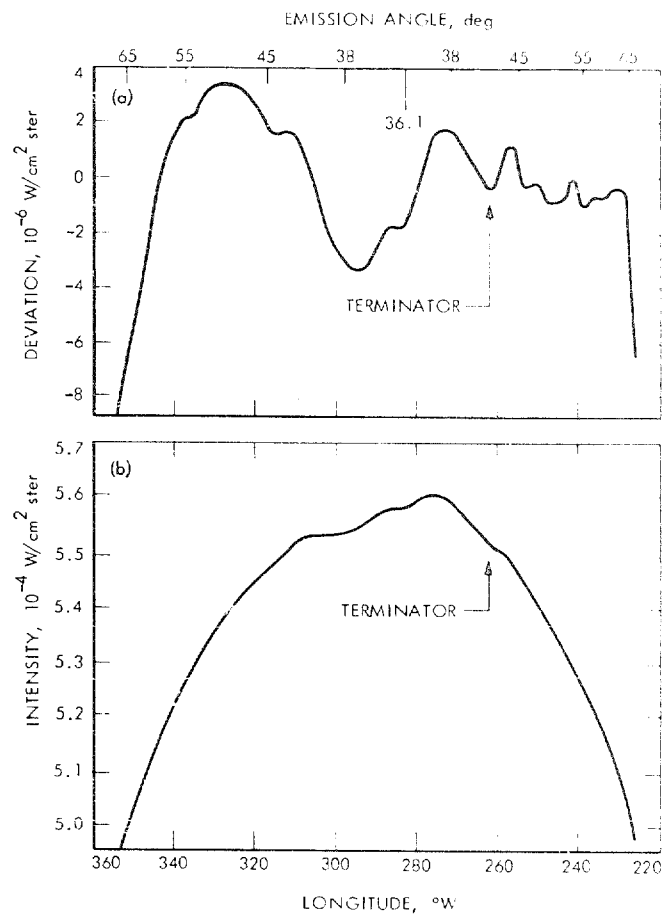
Fig. 28. Infrared radiometer temperature measurements of Venus

to 2 degrees) from the smooth temperature decline expected for a completely homogeneous material. Such variations were anticipated and are seen also on the Moon. Since the observed fluctuations are so small, however, it is concluded that in the part of Mercury observed in this experiment the surface is generally homogeneous in the upper few inches, with few outcroppings of rocks that are not blanketed by the pervasive layer of insulating dust.

Quantitatively, the main parameter of the soil that was derived from the measurements of the night-side temperature is the inverse thermal inertia, a quantity proportional to the reciprocal of the square root of the product of thermal conductivity and density. For Mercury the value of this thermal parameter is 600 $(cal^{-1} cm^2 s/K)^{1/2}$ for comparison, its value is about 800 for the Moon and 150 for Mars. The opacity of the soil to microwave radiation is almost exactly the same as that of the Moon, and the density of the upper few inches of the Mercurian soil is between 1.0 and 1.5 times that of water. The porosity of the soil must therefore be about 50%; probably it has an appearance and bearing strength very similar to that of the lunar soil.

The members of the Mariner 10 Infrared Radiometer Team are: Stillman Chase of Santa Barbara Research Center; Ellis Miner of JPL; David Morrison of the University of Hawaii; and Guido Munch and Gerry Neugebauer of the California Institute of Technology.

G. CELESTIAL MECHANICS AND RADIO SCIENCE EXPERIMENT

The Mariner 10 celestial mechanics and radio science experiment was a new one in that it transmits two frequencies from the spacecraft to Earth. It had both scientific and technological goals using both S- and X-band signals.

The prime scientific goals centered around the planetary ionospheres, atmospheres, gravity fields, and masses. The technological goals were pioneering ones designed to open new communication channels for the deep space probes of the future.

The key Celestial Mechanics questions about Venus concerned the shape of the planet and the intensity and structure of the gravity field. The analysis has revealed that we have close to our hands the most refined measurement of the mass of Venus and for the first time a good picture of the details of its gravity field and harmonic structure. This was regarded as a marginal experiment in our early planning but became a very strong one as the true nature of Mariner 10's radio system became apparent during the week before encounter.

The prime interest of the Radio Science experiment centered around the structure of the ionosphere and atmosphere of the planet. It is certainly an unusual atmospheric structure having a high cloud deck in the 60 km above the surface region and a lower one extending from approximately 35 to 52 km. The combination of Mariner 5, Russian, and astronomical results suggested that the upper cloud layer is thin, broken and, while rapidly moving, stable in its

configuration. The lower one is dense, thick and perhaps highly absorbing to radio waves of high frequency.

Thus the radio experiments were designed to use two frequencies and clearly measure the differential absorption in these layers in an attempt to sort out the many theories of their formation and constituency. The answer perhaps holds the key to the origin and evolution of Venus.

Mariner 10 provided for the experiment particularly well in that its high-gain transmitting antenna is fully articulated and driven by an onboard computer. Using our team's previous knowledge of the Venus atmosphere and the Navigation team's precise knowledge of the spacecraft position relative to the planet, JPL and Boeing engineers were able to program Mariner's computer so that the high-gain antenna was directed to point throughout occultation in such a way that Venus' atmosphere would always bend the radio signal toward Earth.

This program, known as the "teardrop" worked perfectly and will, like the X-band radio system, become an integral part of all new outer planet missions.

1. Venus Encounter

Figure 29 shows the S-band signal as Mariner 10 approached the planet and went into occultation. The frequency scale is relative to the nominal 2295 MHz signal transmitted by the spacecraft. If the spacecraft were receding from the Earth at a uniform velocity the downward trend would be a straight line. It, however, was being accelerated by Venus gravity field and the downward trend was ever increasing causing curvature. Suddenly as the Mariner 10 radio signal hits the atmosphere the frequency reversed direction and at the same time begins to fade away. The spacecraft high-gain antenna under computer control was steered to keep the Earth in focus. Very quickly the spacecraft went behind the planet but the signals remained locked on to by the Earth receivers. About six minutes behind the planet Mariner 10's receivers lost lock of the signal transmitted from Earth and the spacecraft switched to its backup oscillator. Since its frequency is different from that on Earth the ground-based receivers lost lock — but they picked it up in less than a minute and tracked it for an additional 30 seconds.

At the same time these signals were received by some receivers that do not lock on but instead recorded all the frequencies of interest. These are called the "open loop" receivers. The penalty paid for recording everything is the necessity to later computer process the data. It was slow, but very detailed and completely adaptable. There is no error, for the computer can fly by the planet as many times as you ask it to. It is safe to say that we can penetrate deeply into the lower cloud deck at both frequencies and be able to provide accurate differential absorption profiles and temperature profiles.

There are several preliminary results of interest. First that the dayside ionosphere of Venus confirmed the Mariner 5 results. Second, closed-loop quick-look S-band signal penetrated

to an altitude of 45 km above the surface of Venus while the X-band signal suffered an entirely different fate: At an altitude of 52 to 53 km it disappeared. This is the top of the lower cloud layer and the suggestion is that the layer is highly absorbing to the signal at 8415 MHz. Analysis of this differential absorption is proceeding. The analysis requires large computational power and time.

The mass derived from the Mariner 10 data is slightly less than that gleaned from Mariner 5. The data quality is so high that our knowledge of Venus' mass will improve by a factor of 2 to 5 — thus increasing the accuracy to equal that of the Earth's mass determination. Further it is now apparent that Venus is distinctly circular as compared to the Earth — about 100 times less oblate.

2. Mercury Encounter

The geometry at Mercury during the Mariner 10 occultation as seen from Earth is shown in Fig. 30. Conduct of the experiment is nearly identical to that described for Venus encounter. The doppler variations for Mercury encounter, which contain much of the Celestial Mechanics and Radio Science data, are shown in Fig. 31.

Since this was the first flyby of the planet Mercury, the Celestial Mechanics Experiment Team expected to greatly improve some basic physical constants describing the planet. Our knowledge of the mass of Mercury should be improved by at least 100 times our present knowledge. Since the encounter doppler data are of very high quality, if the oblateness of Mercury should be as small as a hundredth that of the Earth, we should be able to detect this in the data.

The extremely refined mass which was deduced from the Mariner 10 data (Fig. 32) will allow us to more precisely compute the motion of planets on which Mercury exerts an influence and thus improve our knowledge of planetary motions within the solar system. This will have an immediate and strong impact on the relativity solutions contained in data from previous missions such as Mariners 6, 7 and 9. A preliminary indication of improvement is shown in Fig. 32.

The ultimate sensitivity of the radio science experiment to an ionosphere and atmosphere is about 100 electrons/cubic centimeter and 1/100 of a millibar, respectively. Thus if the atmosphere were as large as a hundred thousandth of the Earth's, it was detectable by Mariner 10's radio system.

Immersion occurred approximately at the equator on the night side of Mercury. Within the sensitivity of the experiment neither an ionosphere nor an atmosphere was detected. The day-side high-latitude emersion data are only partially available. It can be said that no interaction was detected above 100-km altitude. Open-loop data, now being processed, hold the clue to any dayside interaction. If there is an ionospheric layer or layers on the day side, it exists below 100-km altitude.

Fig. 29. Mariner 10 celestial mechanics
and radio science experiment

Fig. 31. Doppler variation during
Mercury encounter
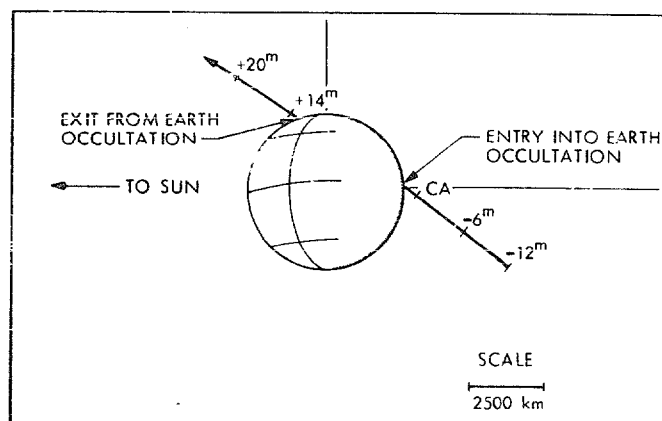
Fig. 30. View from Earth, showing
Earth occultation
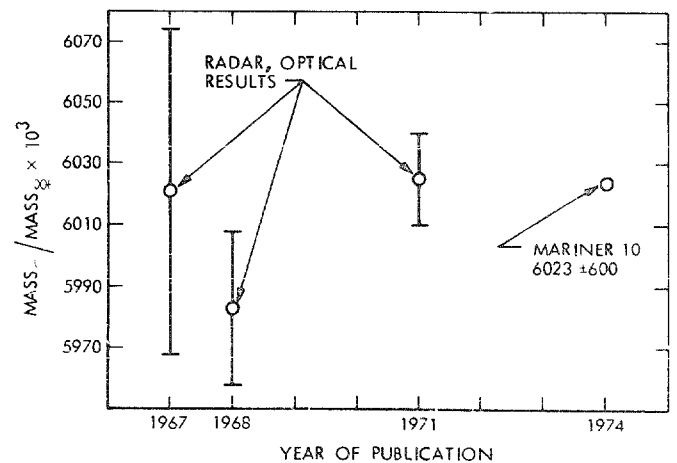
Fig. 32. Mercury mass determination

IV. MISSION SEQUENCE WORKING GROUP

The Mission Sequence Working Group (MSWG) was formed approximately 18 months prior to launch and included many of the key people who participated in the mission profile development. Consequently the MSWG became knowledgeable in spacecraft subsystem performance characteristics very early in the project.

A. ORGANIZATION

The majority of the MSWG team members played dual roles in the operations organization, since many members were also on other MOS teams. This dual role accomplished three functions. First it provided knowledgeable people to design flight sequences, second it kept all key members of the MOS team aware of the planned mission activities, and third it kept the total MOS manpower within the scope of the Project budget.

B. FUNCTION

The primary function performed in MSWG activities was non-real-time planning and preparation of executable sequences, the final product being the CC&S load and associated ground commands required to perform the sequence.

Non-MSWG functions were centered around performing the planned sequence, and solving to any problem occurring during sequence execution. This proved to be a very valuable working arrangement, since MSWG members were aware of spacecraft idiosyncracies and difficulties that might be encountered during implementation of a sequence.

C. SOFTWARE FUNCTIONS

The most significant aspect of sequence development was the proper use of all the software programs. Each program performed a specific task, and linked one or more programs to accomplish each job. The MSWG software set and the functions performed are discussed in the paragraphs that follow.

1. TVS Operational Sequence Table (TSOST)

TSOST is a general-purpose science input program providing basic sequence structure. It interfaces with SEG, POGASIS, SPOP, and COMGEN, and is used primarily for generating first cut at encounter sequences. It also provides critical interface from POGASIS to SPOP, and performs rudimentary constraint checking. The SCOUT conic trajectory program was used for trajectory information.

2. Sequence of Events Generator (SEG)

SEG merges the spacecraft command files with other sequence inputs to provide the integrated sequence output. It is used to prepare planning sequences for review/critique by using TSOST card interface for the bulk of spacecraft sequence inputs. This technique provided planning sequences in the same format as flight sequences.

3. Planetary Observation Geometry and Science Instrument Sequence (POGASIS)

POGASIS provides a precision science platform pointing supplied with plot outputs for accurate pointing analysis. It is employed after initial sequence development and for final platform initial position commands to obtain initial pointing parameters.

4. Scan Platform Operations Program (SPOP)

SPOP generates proper scan platform pointing values considering offsets, biases, and backlash compensation and final pointing parameters to COMGEN. In the processing mode, SPOP uses the COMGEN spacecraft command files to provide an as-programmed spacecraft command pointing profile for LIBPOG.

5. Command Generation (COMGEN)

COMGEN provides final spacecraft command files; integrates all spacecraft commands for both CC&S and ground commands; performs the bulk of sequence generation activities by simulating CC&S, AFS, FDS, and DSS spacecraft subsystems; and provides the command deck for ground commanded sequences and interface files for SEG and SPOP.

6. Library POGASIS (LIBPOG)

LIBPOG produces the final pointing values with a plot capability to show pointing results from those actually obtained from COMGEN files, and performs the extremely important function of checking programmed values, in particular, initial positions and backlash compensation.

D. SCHEDULING

The very nature of sequence development, being tied with software programs used by cognizant team members, lends itself to milestone scheduling. Each software program performs one or more functions in the sequence development process. Figure 33 combines the schedule with a logic diagram approach. This technique was utilized often to maintain visibility. Extreme difficulty was usually encountered in trying to keep the sequence development process on schedule. Operating the software identifies many items which are not foreseeable in the early planning phase. This often required modification and reiteration through some of the software processes.

E. SEQUENCE STRUCTURE

The major spacecraft constraint to sequence design was the limitation due to CC&S programmable storage (512 words). Tradeoffs were continually performed between the desired sequence and the implementable sequence. Two ways to partially overcome this problem are to reload the CC&S and to augment the CC&S using ground
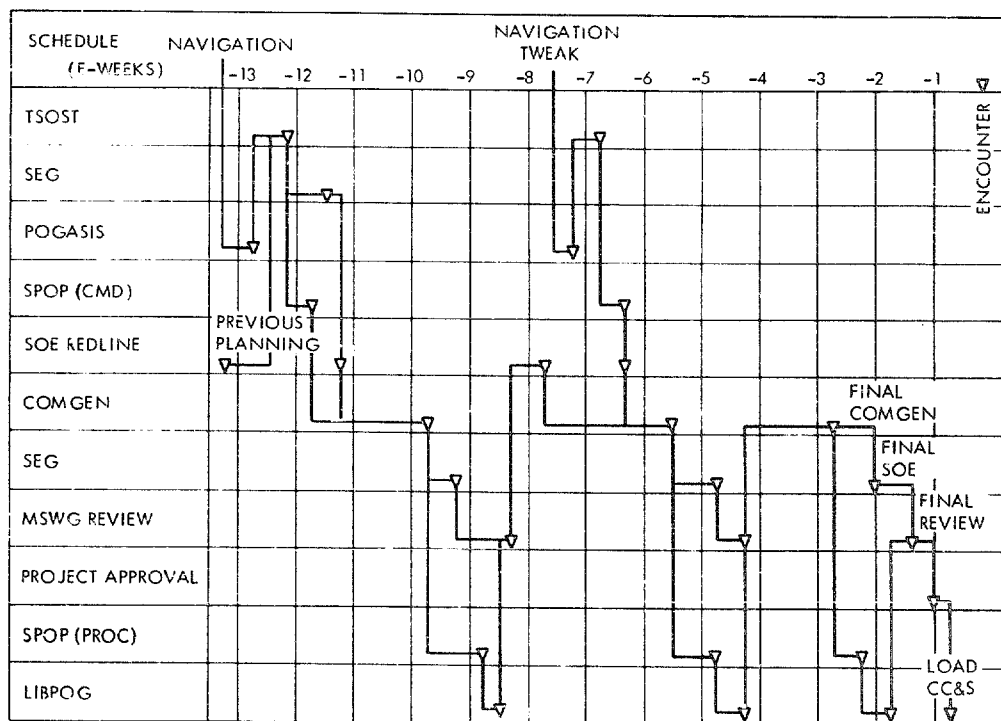
Fig. 33. Schedule/logic diagram for typical encounter sequence development

commanded sequences. For Mercury encounter, augmentation with ground commands proved to be the more desirable choice.

Trajectory correction maneuver sequences and specialty items such as UVS astronomy contained ground commands in order to provide real-time sequence flexibility. TCMs 1, 2, and 3 were initiated by ground commands which, in turn, started CC&S controlled maneuvers. In the case of UVS astronomy, the desire was to be able to control the initial pointing by ground command and let the CC&S execute the lengthy incremental slew sequences. Utilization of these types of sequence structure made possible the implementation of complex sequences within mission limitations.

V. MISSION OPERATIONS SYSTEM

A. INTRODUCTION

The primary responsibility of the Mission Operations System (MOS) organization was to plan, coordinate, and execute operations from the prelaunch planning phase through the end of the mission.

To accomplish these responsibilities, a Mission Operations Design Team (MOSDT) was organized in July, 1971, for the purpose of defining the Mission Operations System (MOS) functional design and support requirements for the entire MOS complex of personnel, hardware, software, procedures, organization, and facilities required to accomplish mission operations, Ground Data System (GDS) testing, and personnel training for the MVM'73 mission. The membership of the team was composed of representatives of all elements of the Mission Operations System.

The MOSDT interpreted the mission design in terms of operational functions to be performed, specified the MOS functional design for all Project, Mission Control and Computing Center (MCCC), and Deep Space Network elements required to support the mission, specified the relationship between all MOS functional requirements and the mission design requirements specified in the MVM'73 Mission Specification. The system functional design requirements were documented in a MOS Design Book which was used by the implementing agencies.

The Support Instrumentation Requirements Document (SIRD) was generated in parallel with the MOSDT activities, since many of the requirements evolved from this team.

Table 2 contains an abbreviated sequence of MVM'73 mission highlights. The purpose of this table is merely to point out the type and level of activity that the MOS teams were involved in during the actual mission, starting at launch. The line chart shown in Fig. 34 also illustrates the activity including the problems that were encountered during the flight operations portion of mission operations.

Table 2. Mission summary

Item	GMT Date	Comment
Launch	Nov. 3, 1973	05:45 GMT
Spacecraft separation	Nov. 3, 1973	06:23 GMT
Sun acquisition	Nov. 3, 1973	07:09 GMT
TV Optic heater failure	Nov. 3, 1973	PFR No. 5001
CC&S update U-0.1	Nov. 3, 1973	
Vega acquisition	Nov. 4, 1973	
Earth/Moon TV calibrations	Nov. 4, 5, 1973	Three Earth and four Moon calibrations were successful
CC&S update U-0.2	Nov. 5, 1973	
PSE power on and scanning	Nov. 5, 1973	System normal except for SEA count PFR No. 5007
UVS Earth slews	Nov. 6, 1973	
Earth/Moon TV calibrations	Nov. 6, 1973	Fourth Earth and fifth Moon TV calibration
RCM No. 1	Nov. 6, 1973	
CC&S update U-0.4	Nov. 7, 1973	
Pleiades star picture	Nov. 7, 1973	
PSE/SEA trouble shooting	Nov. 7, 1973	
CPT calibration	Nov. 8, 1973	

Table 2 (contd)

Item	GMT Date	Comment
PSE/SES turn on and low scan	Nov. 8, 1973	
Partial RCM	Nov. 9, 1973	
Earth/Moon TV calibration	Nov. 9, 1973	Fifth Earth and sixth Moon TV calibration Excellent TV data obtained
CC&S update U-0.2	Nov. 10, 1973	
TCM No. 1	Nov. 13, 1973	Maneuver successful
RCM No. 2 (first POR)	Nov. 21, 1973	PFR No. 5013
RCM No. 3	Dec. 7, 1973	Second POR, PFR No. 5017
First indication scan platform sticking	Dec. 18, 1973	Occurred during UVSAG SCAN PFR No. 5019
RCM No. 4	Dec. 19, 1973	No POR during eight roll calibration maneuvers
HGA anomaly	Dec. 25, 1973	Drop in RF power, thought to be in feed and temperature dependent. PFR No. 5020 HGA feed temperature increasing
HGA healed	Jan. 3, 1974	
HGA failure	Jan. 6, 1974	
Spacecraft switched to standby power chain (POR 3)	Jan. 8, 1974	PFR 5021
Kohoutek observation	Jan. 16, 1974	TVS & UVS observations
TV heaters ON	Jan. 17, 1974	
TCM 2	Jan. 21, 1974	Performance good
RCM 7 (8 rolls)	Jan. 28, 1974	Oscillation at end of roll sequence
CC&S Venus Encounter load	Jan. 29, 1974	
Venus CA	Feb. 5, 1974	
CC&S Venus FE load U-10.0	Feb. 6, 1974	
DSS tape recorder	Feb. 9, 1974	Tape recorder stuck. PFR 5023 and 5025
CC&S load U-12.2	Feb. 12, 1974	Enable RCM No. 8
Gyro test	Feb. 14, 1974	Investigate structural oscillation
Loss of Canopus	Feb. 18, 1974	Numerous bright particles are causing occasional loss of Canopus acquisition
CC&S load U-12.6	Feb. 23, 1974	Enable RCM No. 9
HGA healed	Mar. 4, 1974	Downlink gain up ~6 dB. Close to predict
Spacecraft placed in solar sailing mode	Mar. 9, 1974	Conservation of attitude control gas
Loss of Canopus	Mar. 11, 1974	Bright particle
Gyros on (POR 5)	Mar. 16, 1974	

Table 2 (contd)

Item	GMT Date	Comment
TCM 3 (POR 4)	Mar. 16, 1974	Successful
-X solar panel anomaly	Mar. 16, 1974	Differential solar panel currents PFR 5027
First FE TV&UVS	Mar. 23, 1974	Excellent data
Mercury diameter experiment	Mar. 28, 1974	
CC&S in control of Mercury	Mar. 28, 1974	
Encounter for 32 hours		
Mercury CA 90 W	Mar. 29, 1974	Success!
Post-encounter power anomaly	Mar. 30, 1974	PFR 5031
X-band transmitter anomaly	Mar. 30, 1974	Output dropped to 0 DN. Several days of diagnostic tests revealed X-band transmitter output erratic (PFR 5032)
LGA deploy	April 8, 1974	Last pyro squib operated properly. LGA to Extended Mission configuration
DSS ON/OFF toggle	April 28, 1974	Possibly due to power anomaly on Mar. 30, 1974
Spacecraft perihelion	April 5, 1974	Closest approach to the Sun
TVS OFF	April 11, 1974	
CC&S load for Extended Mission U-20.0	April 16, 1974	

B. MISSION OPERATIONS ORGANIZATION

The MVM'73 Mission Operations System (MOS) organization is shown in Fig. 35. The MOS was composed of a Mission Control Team, Spacecraft Team, Navigation Team, Science Team, Deep Space Network Operations Team, and a Mission Control and Computing Center (MCCC) Team.

1. Mission Control Team

The Mission Control Team (MCT) was composed of five Assistant Chiefs of Mission Operations (ACMOs), five Data Chiefs and two Command Operators. The Command Operator position was supplemented by Viking personnel who volunteered for the experience. These were people who had worked on the MM'71 Project. All the ACMOs had training on the Command System.

The ACMO and Data Chief positions were staffed 24 hours per day, seven days per week. The ACMO handled the interfaces between the Project and the DSN Operations Team, the MCCC Operations Team and the Analysis Teams within the Project. The Data Chief interfaced with the real-time data system.

The ACMO was also responsible for activating the Beep Alert whenever problems occurred

that required key technical personnel. Fifteen beepers with a range of 80 miles from the center of Los Angeles were distributed to the Project Manager, Spacecraft System Manager, CMO, DCMO, Command Operator, Science Team Chief, Spacecraft Team Chief, and one to each of the technical divisions within the Spacecraft Team. This system is recommended for all projects.

All ACMOs and Data Chiefs became involved in GDS testing at an early stage. It was important that personnel in these positions have a good understanding of the Ground Data System to enable them to recognize problems and respond rapidly, especially during critical periods.

All ACMOs became knowledgeable of the command system, proficient in its operations and familiar with the interfaces.

2. Spacecraft Team

The Spacecraft Team was the principal source of knowledge of the spacecraft design, test history, and system and subsystem analyses. The team consisted of a Spacecraft Team Chief, Buss Chiefs, System Analysts, and engineering and science subsystem analysts.

Members of the Spacecraft Team were also members of the Mission Sequence Working Group and were key participants in sequence design.

The subsystem analysts were key factors in the resolution of anomalies and recommendations for alternate operational modes as in the case of the roll axis structural interaction anomaly (which was resolved by operating in a mode that prevented the gyros from coming on without ground command action).

3. Science Team

The Science Team was composed of a Science Team Chief and two assistants, the Principal Investigators (PIs), a TV Analyst and an NIS System Analyst, and instrument performance analysts. The Science Team also included a Data Section, accountable for the production of data records.

Both television and nonimaging science elements of the Science Team were members of the MSWG and were major contributors to sequence design. The Science Team Chief coordinated inputs and resolved conflicts between Principal Investigator requirements.

4. Navigation Team

The Navigation Team headed by the Navigation Team Chief performed trajectory analysis, orbit determination, maneuver design, assisted the Science Team in the design and analysis of instrument scan sequences, and generated probe ephemeris tapes for use by the DSN in the generation of station predicts.

During launch phase, the team evaluated the launch performance and the resulting impact on trajectory correction requirements. The team monitored and evaluated spacecraft/launch vehicle separation and the launch vehicle deflection maneuver, and performed orbit determination estimates and estimated encounter conditions.

The Navigation Team coordinated the charged particle calibration effort using S/X-band doppler and range data, and determined trajectory correction maneuvers required to obtain desired aim point at both Venus and Mercury encounters.

Members of the Navigation Team were also members of the Mission Sequence Working Group and participated in the definition of the Mission Sequence Design.

5. DSN Operations Team

The DSN Operations Control System is the mechanism for controlling the operations of the DSN facilities and systems in support of flight projects, and is the function of the DSN Mission Independent Operations Organization headed by the Network Operations Chief. The DSN Operations Team for the Mariner Venus/Mercury 1973 Project was basically a subset of the DSN Mission Independent Operations Organization.

The Network Operations Project Engineer was responsible for detailed planning of standard operations. He interfaced with the Project through the CMO, and was a member of the MSWG to ensure that DSN inputs were integrated into the sequence. He also assisted in the area of scheduling.

The Network Operations Chief interfaced with the real-time operations through the ACMO. Normal operations and real-time problems were handled through this interface. This position was staffed 24 hours per day, 7 days per week.

The DSN provided Network Analysis Teams (NAT Telemetry, NAT Command and NAT Tracking) for exchange of technical information and for coordination not involving direction and control with counterparts on the Project Mission Operations Teams.

The NAT teams analyzed the effectiveness of the DSN systems, and isolated the cause of anomalies to specific facilities.

6. MCCC Operations Team

The MCCC Operations Control Team was responsible for the management and operations of all MCCC-committed facilities which supported the MVM'73 Project. This included hardware, software, and operational personnel.

The non-real-time interface with the Project was the MCCC Manager and the Facility and Operations Project Engineer. This interface included the implementation of the Mission Support Area (MSA), required computer systems support and access control.

The real-time interfaces were between the ACMO (ACE) and the Operations Control Chief (OPSCON) for real-time operations control and requirements. The Command Operator had a real-time interface with MOAT CMD for command system verifications. These interfaces were active 24 hours per day, seven days per week.

C. COMMAND OPERATION

A unique approach was utilized in providing the command function of the MOS. The multi-position Command Team of previous missions was reduced to a single position for MVM, that of Command Operator, who reported directly to ACE-1. All command analysis and validity checking was performed by the specialists in the Spacecraft Team. As a result, there were only two individuals designated as full-time Command Operators. Three other individuals were available (and provided support) on a part-time basis as Command Operators.

Prior to Launch, all ACMOs received training in the Command Operator position. The CMO and the DCMO participated in some of the command training. This training necessarily included information on the 360/75 and Deep Space Station capabilities. Consequently, the ACEs had a better understanding of the MOS ground system; traditionally, the ground command system has been a black box to the ACEs who have relied on specialists for all command operations support.

The Command Operator position was normally staffed only 8 to 16 hours per weekday, except for the encounters, for a short period following launch, and a few other short periods during which 24-hour coverage was provided. Further, only during very high command activity

1973

NOVEMBER

| DATE | 3 | 5 | 10 | 15 | 20 | 25 | 30 | 1 | 5 |

307 310 315 320 325 330 335

MISSION EVENTS

LAUNCH VEGA ACQUIRED PSE COVER OPENED RCM-1 CANOPUS ACQUIRED PSE TEST PSE DIAGNOSTIC PRM TCM-1 TWT HI POWER RCM-2 (ABORTED), POR NO. 1 HGA CAL BEST LOCK FREQ TEST

ACTIVITY PERIODS

TVS
MAG
CPT
PSE
IRR
UVS   MARS

GYROS
ENG. TEST
CC&S (LOAD)

3 4 5 6 7 8 9 10 11 12 13 14 15 16 17 18 19 20 21 22 23 24 25 26 27 28 29 30 1 2 3 4

DSN COVERAGE

DSS 12
DSS 14
DSS 42
DSS 43
DSS 62
DSS 63

DECEMBER   JANUA

| 5 | 10 | 15 | 20 | 25 | 30 | 31 | 1 | 5 | 10 |

| 340 | 345 | 350 | 355 | 350 | 365 | 001 | 005 | 010 |

EO TEST

RCM-3 POR NO. 2
HGA CAL

PANEL TILT
SCAN CAL.

RCM-4 HGA CAL
PSE TEST

HGA MALFUNCTION

HGA CURE
HGA MALFUNCTION

RCM-5
HGA CAL HGA CURED HGA CAL
HGA CAL
HGA CAL
HGA MALFUNCTION
SCAN ACT. TEST
POWER SWITCHOVER POR NO. 3
(SCAN ACTUATOR TEST POSTPONED)

SCAN ACT. TEST XTX EXP
PCU VCO FREE-RUN

KOHOUTEK DATA

| 2 | 3 | 4 | 5 | 6 | 7 | 8 | 9 | 10 | 11 | 12 | 13 | 14 | 15 | 16 | 17 | 18 | 19 | 20 | 21 | 22 | 23 | 24 | 25 | 26 | 27 | 28 | 29 | 30 | 31 | 1 | 2 | 3 | 4 | 5 | 6 | 7 | 8 | 9 | 10 | 11 | 12 | 13 | 14 |

JANUARY

FEBRUARY

| 10 | 15 | 20 | 25 | 31 | 1 | 5 | 10 | 15 | 20 |

| 010 | 015 | 020 | 025 | 030 | 035 | 040 | 045 | 050 |

ST
R SWITCHOVER POR NO 3
(SCAN ACTUATOR TEST POSTPONED)
SCAN ACT TEST XTX EXP
PCU VCO FREE-RUN TEST
RCM-6 (CANCELLED)
HGA CAL
TV HEATERS ON
GYROS ON
VENUS ORT
TCM-2
SCAN ACT TEST
SCAN CAL
VENUS ORT
RCM-7 ROLL INSTABILITY
GYROS INHIBITED (DC-40)
GYROS ENABLED (DC-19)
VENUS CLOSEST APPROACH
PANELS TILTED
ROLL LOOP TEST
PANELS TILTED
LOST CANOPUS, GYROS ON
REACQUIRED CANOPUS
DSS TES

KOHOUTEK DATA

| 9 | 10 | 11 | 12 | 13 | 14 | 15 | 16 | 17 | 18 | 19 | 20 | 21 | 22 | 23 | 24 | 25 | 26 | 27 | 28 | 29 | 30 | 31 | 1 | 2 | 3 | 4 | 5 | 6 | 7 | 8 | 9 | 10 | 11 | 12 | 13 | 14 | 15 | 16 | 17 | 18 | 19 | 20 | 2 |

15 20 25 28 1 5 10 15

050 055 060 065 070 075

345 350 15 20

L LOOP TEST
PANELS TILTED

LOST CANOPUS, GYROS ON
REACQUIRED CANOPUS

DSS TEST

HGA CAL AND FLIP FLOP

SCAN ACTUATOR TEST

PANELS TILTED

HGA CAL

HGA CURED
VCO DRIFT TEST

PANEL TORQUE TEST
PANEL ZENER FAILED
START SOLAR SAILING

HGA CAL AND MERCURY OAT

TCM J POH NO

PANEL TILT
SCAN CAL

RCM A H

| 15 | 16 | 17 | 18 | 19 | 20 | 21 | 22 | 23 | 24 | 25 | 26 | 27 | 28 | 1 | 2 | 3 | 4 | 5 | 6 | 7 | 8 | 9 | 10 | 11 | 12 | 13 | 14 | 15 | 16 | 17 | 18 |

| 11 | 12 | 13 | 14 | 15 | 16 | 17 | 18 | 19 | 20 |

JANUARY

20	25	30	31	1	5	10	15	20	25
355	360		365	001	005	010	015	020	025	030

RCM-4 HGA CAL
PSE TEST
HGA MALFUNCTION
HGA CURE
HGA MALFUNCTION
RCM-5
HGA CAL HGA CURED HGA CAL
HGA CAL
HGA CAL
HGA MALFUNCTION
SCAN ACT TEST
POWER SWITCHOVER POR NO 3
(SCAN ACTUATOR TEST POSTPONED)
SCAN ACT TEST XTX EXP
PCU VCO FREE-RUN TEST
RCM-6 (CANCELLED)
HGA CAL
TV HEATERS ON
GYROS ON
VENUS ORT
TCM 2
SCAN ACT TEST
SCAN CAL
VENUS ORT
RCM-7 ROLL INST
GY

KOHOUTEK DATA

| 18 | 19 | 20 | 21 | 22 | 23 | 24 | 25 | 26 | 27 | 28 | 29 | 30 | 31 | 1 | 2 | 3 | 4 | 5 | 6 | 7 | 8 | 9 | 10 | 11 | 12 | 13 | 14 | 15 | 16 | 17 | 18 | 19 | 20 | 21 | 22 | 23 | 24 | 25 | 26 | 27 | 28 | 29 | 30 |

1974

FEBRUARY

| 31 | 1 | 5 | 10 | 15 | 20 | 25 | 28 | 1 | 5 | 10 |

| 030 | 035 | 040 | 045 | 050 | 055 | 060 | 065 | 070 |

RCM-7 ROLL INSTABILITY
GYROS INHIBITED (DC-40)
GYROS ENABLED (DC-19)
VENUS CLOSEST APPROACH
PANELS TILTED
ROLL LOOP TEST
PANELS TILTED
LOST CANOPUS, GYROS ON
REACQUIRED CANOPUS
DSS TEST
HGA CAL AND FLIP FLOP
SCAN ACTUATOR TEST
PANELS TILTED
HGA CAL
HGA CURED
VCO DRIFT TEST
PANEL TORQUE TEST
PANEL ZENER FAILED
START SOLAR

| 28 | 29 | 30 | 31 | 1 | 2 | 3 | 4 | 5 | 6 | 7 | 8 | 9 | 10 | 11 | 12 | 13 | 14 | 15 | 16 | 17 | 18 | 19 | 20 | 21 | 22 | 23 | 24 | 25 | 26 | 27 | 28 | 1 | 2 | 3 | 4 | 5 | 6 | 7 | 8 | 9 | 10 | 11 | 1 |

Fig. 34. Mariner 10 major events time line

35

Fig. 35. MVM'73 Mission Operations Organization

periods and at shift changes were two Command Operators present. During the cruise phases, the on-duty ACE also served as Command Operator when the position was not otherwise staffed—normally at least 8 hours per day and most weekends. The ACE often sent commands in the off-hour periods.

One of the full-time Command Operators was always on call during the off-hours via an ACE-controlled beeper. This on-call individual was only called in during spacecraft emergencies and on one or two occasions when a high command activity period occurred unexpectedly.

1. Reliability and Command Summary

The reliability of the command function was very high during the Mission as measured by the number of attempted command transmissions which were actually received by the spacecraft (15307 received out of 15334 transmitted). This produced a command reliability of 0.9982. A summary of command anomalies is shown in Table 3.

D. SIMULATION

The Simulation Team began its support of the Mission Operations Test and Training program on July 3, 1973, with the training test identified as "MOS Verification Test and Training." The test profile included cruise and trajectory correction maneuver (TCM) phases of the mission. The Simulation Team concluded its support of MOS training with the final Launch near-earth operational readiness test (L - 2 to L + 6 hr) on

Nov. 1, 1973. The simulation system provided the capability to prepare the mission operations teams to function as one professional unit.

The training, however, was not accomplished without problems. Initially, too many real-time requests were made and action taken to correct the problem areas noted in those requests. In many cases, the cure was more painful than the malady and resulted in reducing the effectiveness of the simulation for the purpose of training. Such results were largely due to the fact that there was not sufficient time to continue supporting the test and evaluate the necessary remedy and its effect on the total simulation system. To combat this problem all real-time change requests were channeled through the CMO or Deputy CMO for approval.

A major problem of the Simulation System was associated with the transmission of both low-rate and high-rate data from the Mission Control and Computing Center (MCCC) in Pasadena, California to the remote tracking stations, where the data was processed and retransmitted to the MCCC (long-loop). Because of the high bit rate (22.05 kbits/s) of the science data, the simulation system was overloaded when trying to simulate encounter sequences. The training value which the team members received was greatly reduced because many hours were spent resolving simulation problems directly related to getting the data out to the remote tracking stations.

For future missions, it is recommended that MOS training involving encounter sequences or high activity periods be conducted internal to the MCCC (short-loop), and that data flow tests which involve sending data either from the remote tracking stations to the MCCC or from the MCCC to the remote tracking stations and back be conducted. The tests could be supported by a minimal number of personnel and would validate the correct receipt of data at the MCCC and the operations at the remote tracking stations.

E. RECOMMENDATION SUMMARY

The recommendations have been summarized and placed in various categories of mission operations.

1. Organization and Planning

The original plan for handling the scheduling of resources for the Project was through the DSN Network Operations Project Engineer (NOPE) and the MCCC Facility and Operations Project Engineer (FOPE). The NOPE and the FOPE were members of the MSWG and were to participate in the development of mission sequence from which they would obtain resource requirements for Project scheduling purposes. This approach did not function as anticipated due to the workload of other DSN and MCCC functions for which the NOPE and the FOPE were responsible and which limited their participation in the MSWG. This resulted in Project requirements being scheduled by a combination of MSWG attendance and interfacing with the Deputy Chief of Mission Operations (DCMO).

Table 3. Command anomaly summary

Type of anomaly	Number of anomalies
Intentional aborts	4
Hardware aborts	
Exciter/transmitter failures	5
CMA/confirm loop	3
DSS operator procedure abort	1
Unreceived commands	
DSS hardware anomalies	4
DSS processing errors	0
LGA null	0
Transmit too early	5
Unresolved	0
Ignored commands	3
Rejected commands	2
Total command anomalies	27

Scheduling is an important function within the structure of a project and requires time, knowledge of the MOS interfaces, other project requirements, and a thorough knowledge of the mission sequences. From the experience gained on MVM'73, it is recommended that future projects assign one person full-time to handle scheduling of resources.

It is recommended that planning and scheduling of tests during the MOS training period be limited to one test per week. During MVM'73, it was established that a reasonable amount of time was required for pretest briefings, post-test critiques, closeout of action items from previous tests, and contingency time for possible rerun of a previous test. Without the time being available to work problems they were repetitive in follow-on tests and usually caused morale problems.

It is recommended that ACMOs and Data Chiefs become involved in Ground Data System testing early. It is important that these positions have a good understanding of the GDS to enable them to respond to problems that occur during operations, especially during the critical periods of a mission.

2. Procedures and Practices

The incident surprise anomaly (ISA) should be recognized by the DSN and the MCCC as the vehicle for identifying problems during GDS integration.

GDS Functional Requirements Documents should consider use of the Level 3 and Level 4 concept that was initiated on MVM'73. This concept identified interfaces, forced early and orderly definition of requirements, and brought about design integration.

The ground data system engineer (GDSE) should put subsystem requirements on a priority basis early in the development phase.

Principal investigators (PIs) should be involved in GDS constraints early in the project. This will help the MOS to design for maximum information return.

3. Operations

The project-to-outside command function interfaces were much too complex. The basic problem was the time-consuming coordination with NAT CMD under the OPSCHIEF and MOAT command under the OPSCON before the project could access the command system. It is recommended that this interface be simplified.

It is recommended that all persons occupying the ACMO position during flight operations be knowledgeable of the command system, become proficient in its operations and familiar with the interfaces involved.

The ACMO and Command Operator operational positions should be colocated.

This section describes the performance of the spacecraft subsystems, the anomalies that occurred during flight operations and their effect on the mission, and recommended alternate operating modes.

All commands used in this document are defined in Tables 4, 5, and 6.

A. TELECOMMUNICATIONS

The prime mission spanned the time of GMT Day 307, Nov. 3, 1973 to GMT Day 105, April 15, 1974. During the mission three trajectory correction maneuvers (TCMs), two planetary flybys, (Venus and Mercury) and Cruise Science events occurred, as well as several noncatastrophic failures. The above events will be described in this report as separate elements, but the failures will not be described except as they relate to the telecommunications systems.

1. Trajectory Correction Maneuvers

a. TCM-1. During TCM-1 the data recorded for comparison to predicts was downlink AGC and SNR on the IBM 360/75, and uplink AGC, downlink AGC and SNR on the Mission and Test Computer (MTC). During the TCM DSS 14 transmitter power was not at 20 kW, so the uplink uncertainty is large.

The plot in Fig. 36 is a comparison of expected uplink AGC and the actual AGC as recorded by the MTC. Figure 37 is a comparison of downlink AGC plotted by the MTC and the expected profile plotted by hand over the MTC plot. The two nulls are due to the pitch turn moving the Earth vector near the low-gain antenna bicone 0-deg point, and the actual AGC followed the predict very closely. This data was taken on the DSS 14 Receiver Number 1, Block III.

Figure 38 is a further comparison of downlink AGC, but using hand notation of Receiver Number 2 AGC from the 360 every 30 sec. This shows the performance to be above expected, but not as high as receiver number 1, pointing out the inconsistency of AGC calibrations at the stations. The plot also shows some sort of time lag during the nulls, which could be a data display lag or a hand notation error.

The large deviations, before the first roll and at the end of the unroll, are due to the high-gain antenna pointing at Earth. The HGA boresight gain, and the circulator switch isolation, produce a higher effective radiated power along the HGA boresight than from the LGA when in the transmit LGA configuration. This produces large interferometry deviations when the spacecraft is in this mode and this geometry occurs.

The downlink ST/N_0 was considered the most critical of the observable parameters. The values taken by hand and compared to the predicted design value ST/N_0 are shown plotted in Fig. 39. This also shows the same time lag and HGA interferometry as the AGC plots, but the

deviation from predicts appears to be (excluding the nulls) about 0.2 to 0.3 dB.

b. TCM-2. Due to a power chain transfer to the redundant power chain, TCM-2 required the TWTA to be in the low power configuration with transmission on the low-gain antenna. The Earth cone angle at the start of the maneuver was 163 deg and at the motor burn attitude 123 deg. These cone angles translate into a LGA uncertainty of ±2.4 dB and ±1.7 dB, respectively.

In addition, the normal uncertainties of low power on the TWTA, modulation angles, DSIF receiving antenna gain and ST_B/N_0 calculations at the TCP would produce a composite uncertainty of ±5.3 dB at the burn attitude. The plot of ST_B/N_0 actual versus ST_B/N_0 predicted (Fig. 40) shows the burn attitude delta to be -1.3 dB at 33 1/3 bps.

During the actual burn the data rate was increased to 2.45 kbits/s and recorded at the spacecraft. The transmitted data at 2.45 kbits/s was below 0 dB ST/N_0 and was not acquired, but carrier lock was maintained.

The actual data shows a time shift from the predicted data due to the use of a maneuver orientation predict which is generated well in advance of the actual maneuver time. Although the roll and pitch durations are correct, the absolute start times are arbitrary until the real-time CC&S clock is started, at the time of the maneuver.

c. TCM-3. Due to the roll axis structural interaction exhibited by the spacecraft, and also thermal constraints, the third TCM was executed in a Sun/Canopus orientation without any roll or pitch. This allowed the high-gain antenna to be used throughout the burn, producing a signal level very much greater than any required threshold.

2. Venus Encounter

The prime telecommunication mode at Venus encounter (VE) was dual channel 117.6 — kbits/s/ and 2.45 kbits/s. The high rate was used for imaging and the low rate was a time multiplex of nonimaging science and engineering, modulation interplexed with the high rate.

A detailed comparison has been made for uplink AGC, downlink AGC, and low-rate SNR. The high-rate SNR cannot be compared, since the actual measured SNR was not sent over the ground communications lines with the telemetry information.

The high-rate SNR was sent by way of monitor information, but this data source is not recorded in a form recoverable by the telecommunications analysis program. The data is recoverable by tape dump, manual conversion from octal to Data Number to dB units, to punched cards, and finally input to the telecommunications program. This has not been done with the high-rate SNR for VE due to time constraints.

Table 4. Description of direct commands

Command	Destination	Function	Effect on spacecraft
DC 1	FDS	Selects redundant memory states	Each DC 1 advances the FDS "memory-in-use" state one step in the following sequence: 1. Memory A only 2. Memory B only 3. A & B-fixed engineering format 4. A & B
DC 2	MDS	Selects TMU 1	Applies power to TMU 1, and removes power from TMU 2
DC 3	—	Not used	———
DC 4	DSS	Switches the DSS to its READY mode of operation from any other mode of operation	Sets DSS controller in the READY mode
DC 5	Pyro	Deploys LGA to extended mission position	Actuates pinpuller, releasing LGA and allowing it to deploy
DC 6	RFS	Enables and disables S-band ranging	1. Enables or inhibits DC 9 applying power to the S-band ranging channel 2. When ranging is ON, the ranging channel detects the ranging signal transmitted to the spacecraft and phase modulates the spacecraft-transmitted RF carrier with the ranging signal.
DC 7	RFS	Selects redundant TWT and associated power supply	Unregulated dc power from the power subsystem is switched from TWT 1 power converter to TWT 2 power converter or vice versa.
DC 8	RFS	Selects the alternate exciter in the event a malfunction is indicated in the operating exciter	Incoming 2.4 kHz single-phase square wave power is switched from exciter 1 power supply to exciter 2 power supply, or vice versa.
DC 9	RFS	Turns X-band ranging OFF if it is ON, or vice versa; toggles S-band ranging ON and OFF if DC 6 is in effect	1. Ranging control is by means of a relay in the receiver power supply which toggles +15 Vdc ON or OFF to the ranging channel. 2. When ranging is ON, the ranging channel detects the ranging signal transmitted to the spacecraft and phase modulates the spacecraft-transmitted RF carrier with the ranging signal
DC 10	RFS	Selects LGA for transmission	Causes the control unit to switch the voltages on the two RF circulator switches to switch the output of the operating TWT to the LGA

Table 4 (contd)

Command	Destination	Function	Effect on spacecraft
DC 11	RFS	Selects HGA for transmission	Causes the control unit to switch the voltage on the two RF circulator switches to switch the output of the operating TWT to the HGA
DC 12	Attitude Control	Steps Canopus tracker brightness gate to lower (more sensitive) values cyclically	Each DC 12 command will advance the brightness gate level one step in the sequence 1, 2, 3, 1, 2, 3, 1 ···
DC 13	CC&S	Aborts any maneuver sequence and switches the CC&S maneuver logic to the NON-TANDEM STANDBY state	1. Resets all maneuver relays. DC 13 will terminate a burn in progress. (7M1-5, 8M1) 2. Halts and resets the fixed sequencer 3. Resets the maneuver logic relays, resulting in the NON-TANDEM STANDBY mode 4. Sets flipflop flag 3 in the CC&S processor 5. Resets relay K9
DC 14	Attitude Control	Returns control to celestial sensors; enables autopilot power (resets DC 61)	
DC 15	Attitude Control	Allows the spacecraft to acquire (in roll) any object of sufficient brightness to produce a roll error signal (>0.02 Canopus)	Sets relay K14 to remove brightness gate requirements from Canopus acquisition logic
DC 16	—	Not used	———
DC 17	Attitude Control	Advances cone angle setting to next position cyclically	Each DC 17 will advance the Canopus tracker cone angle one step in the sequence 1, 2, 3, 4, 5, 4, 3, 2, 1, 2 ···
DC 18	Attitude Control	The first DC 18 will place the roll axis on inertial control; each subsequent DC 18 will turn the spacecraft approximately +2 deg in roll	1. Turns on gyro with roll axis in inertial control 2. Inhibits Canopus tracker input to switching amplifier
DC 19	Attitude Control	Resets DC 15, DC 18 DC 20, and DC 40	1. Restores brightness gate requirements to Canopus acquisition logic if DC 15 removed them 2. Takes spacecraft from inertial to celestial if DC 18 has established this state (if no other inertial commands are in effect)

Table 4 (contd)

Command	Destination	Function	Effect on spacecraft
DC 19 (contd)			3. Enables roll search to be initiated by loss of roll reference if DC 20 had inhibited it
			4. Enables gyro power if DC 40 had inhibited it
DC 20	Attitude Control	Removes the Canopus tracker as the source of roll position error information	1. Canopus tracker power is turned OFF
			2. Canopus tracker input to the switching amplifier is inhibited
			3. Inhibits initiation of roll search by loss of roll reference
			4. Roll gyro remains OFF; spacecraft uncontrolled in roll
DC 21	Attitude Control	1. Overrides star acquisition and initiates a roll search 2. Step roll axis -2 deg (if DC 18 in effect)	1. If the gyros are OFF with a roll reference acquired, DC 21 will cause the Canopus tracker to reject the acquired object, turning ON the roll gyro and initiating a roll search
			2. If roll search has been inhibited by ~30 sec CCW gas jet firing, DC 21 will reset the inhibit
			3. If the roll gyro is in inertial, each DC 21 will turn the spacecraft approximately -2 deg in roll
DC 22	—	Not used	————
DC 23	—	Not used	————
DC 24	Power	Enables or disables switchover from high rate to low rate charger caused by high temperature or high voltage	Enables or disables the battery voltage and temperature detector output signals
DC 25	FDS	Selects oscillator B, or enables oscillator failure detection circuit to select operational oscillator	Toggles a flipflop in the FDS. One state of flipflop inhibits oscillator A, causing the failure detector to select oscillator B. The other state enables the failure detector to select oscillators
DC 26	Power	Supplies power, either direct from battery or 30 Vdc from regulator if enabled, to PYRO and enables the engine solenoid valve	DC 26 allows SM1 to apply power to the engine solenoid valve

Table 4 (contd)

Command	Destination	Function	Effect on spacecraft
DC 27	CC&S	Initiates CC&S maneuver: tandem, parallel, or sequencer only	1. Causes CC&S event 7M1, turning ON the attitude-control gyros for warmup 2. Sets midcourse (sequencer) relay in the CC&S maneuver logic, removing the mid-course clamp on the fixed sequencer and thus initiating the fixed maneuver sequence 3. During these maneuvers, the fixed sequencer will set Flag 1 4096 sec after DC 27, simultaneously with 7M2 and 7M4 4. The fixed sequencer will set and reset 7M2, 7M3, 7M4, and 7M5 to A/C; and 8M1 to PYRO, switching 30 Vdc power to Propulsion (if engine value is ENABLED)
DC 28	APS	Selects channel 1 or channel 2 of APS electronics	Toggles APS between channel 1 and channel 2 electronics
DC 29	CC&S	Disables tolerance detector such that the CC&S will not be inhibited if the 2.4 kHz input power falls out of tolerance	Disables the RESET input of the power monitor relay
DC 30	CC&S	Inhibits CC&S computer output actuators, halts computer operations, and resets all flags except flag 6. Flag 6 is set	1. Sets the CC&S power failure relay, thus halting any scan in progress and preventing any further scans from being initiated 2. Computer relay drivers are inhibited 3. All flag flipflops except 6 are reset; flag flipflop 6 is set 4. Sets the power monitor relay if it is in the reset state
DC 31	CC&S	Enables CC&S computer output actuators, initiates computer operations, and resets all flags except 6. Flag 6 is set	1. Resets the CC&S power failure relay 2. Enables computer relay drivers 3. Resets all flag flipflops except 6; flag flipflop 6 is set
DC 32	CC&S	Initiates either a computer-only or a parallel maneuver, depending upon the maneuver logic state	1. Set flag flipflop 5 2. Sets the computer relay in the maneuver logic, allowing the computer to control the maneuver relay drivers if the tandem relay is reset

Table 4 (contd)

Command	Destination	Function	Effect on spacecraft
DC 33	CC&S	Places the maneuver logic in the TANDEM STANDBY state, or initiates a TANDEM maneuver, depending on the maneuver logic state	1. Sets the tandem relay in the maneuver logic 2. Disables computer control of the maneuver relay drivers
DC 34	Power	Turns OFF the 30 Vdc regulator	Transfers the PYRO-PROP load from the 30 Vdc regulator to the battery bus
DC 35	MDS	Selects TMU 2	Applies power to TMU 2, and removes power from TMU 1
DC 36	FDS	Select which memory (or memories), if any, will remain in use in the event of a power failure in the memory voltage supplies	Steps a four-stage counter which provides memory power failure override in the following sequence: 1. A override 2. B override 3. A and B override 4. No override
DC 37	Power	Toggles share boost converter	Enables or disables boost converter
DC 38	Power	Toggles battery charger ON and OFF	Toggles raw dc power to the battery charger
DC 39	DSS	Positions tape in parking window	The DSS is placed in tape pass 4 and enters slew mode. Upon receipt of LEOT the DSS goes to READY mode, pass one
DC 40	Attitude Control	Turns OFF and unconditionally inhibits turn-on of gyro power	Sets relay K19
DC 41	—	Not used	———
DC 42	RFS	Switches TWTs to high-power output mode	Causes the control unit to switch the appropriate voltage to the TWTs to place them in a high-power mode. A substantial increase in raw dc power consumption results
DC 43	RFS	Switches TWTs to the low-power output mode	Causes the control unit to switch the appropriate voltage to the TWTs to place them in a low-power mode. A substantial reduction in raw dc power consumption results
DC 44	—	Not used	———
DC 45	Pyro	Unlatch scan platform from launch-stow position	Fires dual bridgewire squib, permanently releasing scan platform latching mechanism
DC 46	Power	Toggles magnetometer No. 2 ON and OFF	Toggles 2.4 kHz power to magnetometer number two ON and OFF
DC 47	Power	Toggles DSS ON and OFF	Toggles 2.4 kHz power to DSS; turns ON DSS replacement heaters when DSS is OFF

Table 4 (contd)

Command	Destination	Function	Effect on spacecraft
DC 48	Power	Turns TVS OFF	Turns OFF 2.4 kHz power to TVS; raw dc power to replacement heaters is turned ON when TVS is turned OFF
DC 49	Pyro	Unlatches HGA dish from launch-stow position	Actuates pinpuller, freeing HGA dish for articulation
DC 50	Power	Used to assess battery condition in flight, and in reconditioning battery in flight	Switches battery power to the 50-ohm test load. The battery output voltage and current are monitored to assess battery condition. Battery reconditioning is accomplished by discharging the battery about 60% and recharging at high rate
DC 51	—	Not used	———
DC 52	CC&S	Provides capability to change CC&S computer program by setting Flag 7	Sets flag flipflop 7
DC 53	Pyro	Deploys PSE boom	Actuates pinpuller, releasing PSE boom and allowing it to deploy
DC 54	Power	Turns ON power to S-band TWT power amplifier	Switches raw power to the TWT power converter
DC 55	Power	Turns OFF power to S-band TWT power amplifier	Switches raw power from the TWT power converter
DC 56	DSS	Start low-rate record (2.45 kbits/s)	Sets DSS controller in the low-rate record mode
DC 57	DSS	Starts high-rate record (117.6 kbits/s)	Sets DSS controller in the high-rate record mode
DC 58	DSS	Starts high-rate playback (22.05 kbits/s)	Sets DSS controller in the high-rate playback mode
DC 59	DSS	Starts low-rate playback (7.35 kbits/s)	Sets DSS controller in the low-rate playback mode
DC 60	DSS	Start tape slew	Sets DSS controller in tape slew mode
DC 61	Attitude Control	Inhibits autopilot power, switches celestial sensors out of control loop, turns gyros ON, and places all axes under inertial control	Sets Relay K9 1. Turns ON all gyros in INERTIAL 2. Inhibits Canopus tracker input to switching amplifier 3. Inhibits power to autopilot
DC 62	Power	Toggles HGA actuator supplemental heaters ON and OFF	Toggles raw dc power to HGA actuator heaters
DC 63	Power	Toggles PSE supplemental heater	Toggles raw dc power to PSE supplemental heaters
DC 64	Power	Toggles one of the propulsion supplemental heaters and the CPT supplemental heater ON and OFF	Toggles raw dc power to the CPT and propulsion supplemental heaters

Table 4 (contd)

Command	Destination	Function	Effect on spacecraft
DC 65	Power	Selects FDS power converter A or B	Toggles 2.4 kHz power to FDS between power converter A and B
DC 66	Power	Toggles one of the propulsion supplemental heaters, the sun sensor supplemental heater, and the APS solar panel supplemental heaters ON and OFF	Toggles raw dc power to the sun sensor, the propulsion, and the APS solar panel actuator supplemental heaters
DC 67	Power	Toggles TV optic heaters ON and OFF	Toggles raw dc power to the TV optic heaters
DC 68	Pyro	Removes PSE cover	Fires dual bridgewire squib, releasing PSE cover latch and allowing cover to open
DC 69	Power	Toggles gyro and science bay 6 supplemental heaters ON and OFF	Toggles raw dc power to bay 6 (science) and 7 (gyro) supplemental heaters ON and OFF
DC 70	Power	Toggles IRR ON and OFF; the IRR replacement heater is OFF when the IRR is ON and vice versa	Toggles 2.4 kHz power to IRR electronics and replacement heater
DC 71	Power	Toggles X-band transmission ON and OFF	Toggles raw dc power to X-band exciter ON and OFF
DC 72	Power	Toggles Magnetometer No. 1 ON and OFF	Toggles 2.4 kHz power to magnetometer No. 1 ON and OFF
DC 73	Power	Inhibits the engine valve opening (inhibits engine burn)	Turns OFF power to PYRO and PROP
DC 74	—	Not used	————
DC 75	Power	Toggles CPT ON and OFF	Toggles 2.4 kHz power to CPT (and CPT replacement heater) ON and OFF; turns ON CPT replacement heater when CPT is OFF
DC 76	Power	Toggles UVS occultation ON and OFF	Toggles 2.4 kHz power to UVS occultation and replacement heater; replacement heater is turned ON when UVS occultation is OFF
DC 77	Power	Toggles UVSAG ON and OFF	Toggles 2.4 kHz power to UVSAG and replacement heater; replacement heater is turned ON when UVSAG is OFF
DC 78	Power	Turns TV subsystem ON	Turns 2.4 kHz power to TVS ON; replacement heaters are turned OFF
DC 79	Power	Toggles PSE ON and OFF	Toggles 2.4 kHz power to PSE and replacement heater; replacement heater is turned OFF when PSE is ON
DC 80	Power	Turns ON the 30 Vdc regulator	Transfers the PYRO-PROP loads to the 30 Vdc regulator

Table 4 (contd)

Command	Destination	Function	Effect on spacecraft
DC 81	Power	Selects either low-rate or high-rate battery charger	Switches the high or low rate charger into the charging loop. High-rate current is nominally 2.0 A and low-rate 0.65 A
DC 82	—	Not used	————
DC 83	—	Not used	————
DC 84	CC&S	Provides capability to change CC&S computer program by setting Flag 6	Sets flag flip-flop 6
DC 85	CC&S	Enables the tolerance detector such that the CC&S will be inhibited if the 2.4 kHz input power falls out of tolerance	Enables the RESET input of the power Monitor relay
DC 86	CC&S	Provides capability to change CC&S computer program by setting flag 8	Sets flag flipflop 8

Table 5. CC&S Commands without dc equivalents

Command	Destination	Function	Effect on spacecraft
2A	RFS	Selects the standby TWT or exciter if the on-line TWT or exciter has failed	Unregulated dc power may be switched from TWT 1 power converter to TWT 2 power converter, or vice versa; similarly, 2.4 kHz power may be switched from one exciter power supply to the other
2F	RFS	Turns off S- and X-band ranging	Ranging control is by means of a relay in the receiver power supply which toggles +15 Vdc ON or OFF to the ranging channels When ranging is ON, the ranging channel detects the ranging signal transmitted to the spacecraft and phase modulates the spacecraft transmitted RF carrier with the ranging signal
4J	Power	Toggles all supplementary heaters (including TV optic heaters)	Toggles power to supplementary heaters ON and OFF
5B	CC&S	Removes sequencer control before an automatic reacquire can be issued, allowing a computer-only unwind	Resets the midcourse relay putting the maneuver logic in the specified state:
5C	CC&S	Enables FDS frame start pulse to initiate a computer scan	5C enables frame start to set Flag 4, initiating a computer scan

State before 5B	Sequencer Maneuver	Parallel Maneuver	Tandem Maneuver
State after 5B	Non-tandem Standby	Computer Maneuver	Tandem Standby

Table 5 (contd)

Command	Destination	Function	Effect on spacecraft
7A	Attitude Control	Turns on attitude control (backup to PAS S-4)	Turns ON attitude control, cruise sun sensor power, and enables acquisition sun sensor power (if not already performed by PAS S-4)
7B	Attitude Control	Turns on Canopus tracker, initializing it in brightness gate 1	Applies power to the Canopus tracker. Turns ON attitude control cruise sun sensor power, and enables acquisition sun sensor power. 7B is backup to 7A and PAS S-4
7E	Attitude Control	Places the spacecraft under inertial control without enabling the auto-pilot	Turns ON gyros (if not already turned ON or inhibited by DC-40) and puts them in INERTIAL mode, inhibiting roll search. 7E enables pitch and roll turns
7M1	Attitude Control	Turns gyros ON and reforms gyro feedback loop capacitors	Turns ON attitude control, Canopus tracker, sun sensors, and gyros
7M2	Attitude Control	Places spacecraft under inertial control with the autopilot enabled	Turns ON gyros (if not already ON), turns ON autopilot power if DC 61 is not in effect, and puts the gyros in inertial mode, inhibiting roll search. 7M2 enables pitch and roll turns
7M3	Attitude Control	Permits roll and pitch turns of positive polarity	Sets command (gyro torquer) current polarity for positive pitch and roll turns
7M4	Attitude Control	Initiates a roll turn	7M4 inhibits a pitch turn and initiates a roll turn by applying current to the gyro torquer
7M5	Attitude Control	Initiates a pitch turn	7M5 initiates a pitch turn by applying current to the gyro torquer
8A	PYRO	Deploys from launch position; the solar panels, magnetometer boom, HGA boom, and the LGA	Fires the respective squibs to accomplish the deployment of the solar panels, magnetometer boom, HGA boom, and the LGA
8M1	PYRO	Perform engine burn	Opens engine solenoid valve, resulting in a trajectory correction maneuver engine burn

At this point in the mission the HGA was in a failed condition, and after careful in-flight measurements the VE low-rate data was compared with a HGA with 3.9 dB less gain than preflight tests.

Figures 41-49 show the results of these comparisons at DSS 14 on the day of Venus encounter. Tables 7 and 8 list the deviations for all stations.

3. Mercury Encounter

The telemetry requirement for the Mercury encounter was 22.05 kbits/s with an error rate of less than 5 bits in 100. The goal was 117.6 kbits/s with an error rate of less than 3.33 bits in 100. Both required the simultaneous transmission of a second channel at 2.45 kbits/s with an error rate of less than 1 bit in 10^4. Figure 50 is a block diagram of the portion of the system detailing the physical implementation of the Mercury telemetry requirement and goal.

During the preliminary analysis of measured data it became apparent that if the new super-cooled maser at the DSS 14 could really achieve a noise temperature of 13.5 K, and if the spacecraft telecommunications system performance was at its design value, and if the ground station performance was at its design value, 117.6 kbits/s at Mercury was indeed achievable. Figure 51 displays the prediction of expected bit error rate at Goldstone DSCC on the day of Mercury encounter using preflight data. The change in error rate is due to the change in system noise temperature as a function of elevation angle at the station.

The in-flight measurement of performance was made difficult by the temporary partial failure of the spacecraft S-band HGA. The track of the Earth vector from the spacecraft required the HGA feed to go from Sun illuminated to shadowed on December 25, 1973, and from shadow to sunlit on March 4, 1974. The first
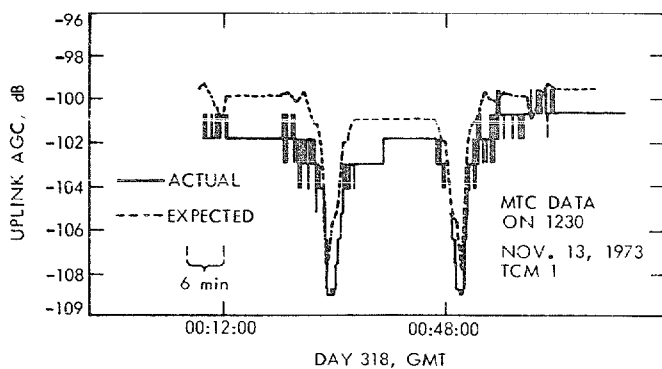
Fig. 36. Uplink AGC--
Nov. 13, 1973
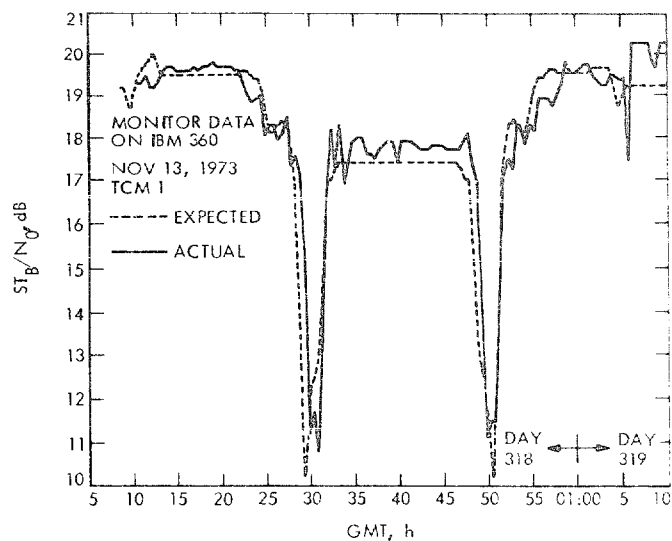
Fig. 39. Downlink ST_B/N_0, Nov. 13, 1973
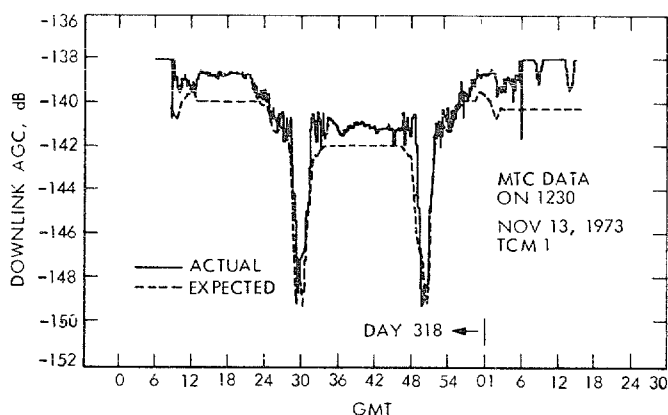
Fig. 37. Downlink AGC--Nov. 13, 1973
(MTC data on 1230) (1730)
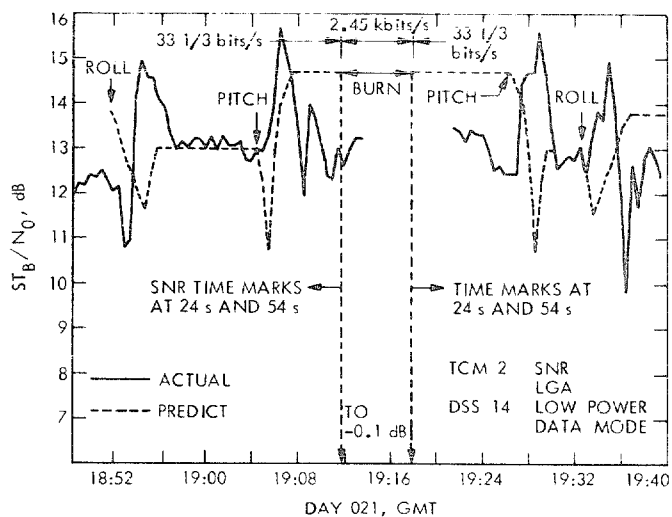
Fig. 40. ST/N_0 versus GMT
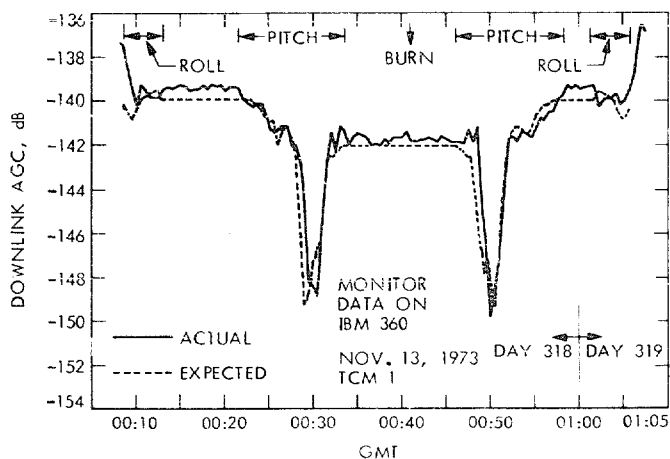
Fig. 38. Downlink AGC--Nov. 13, 1973
(Monitor data on IBM 360)
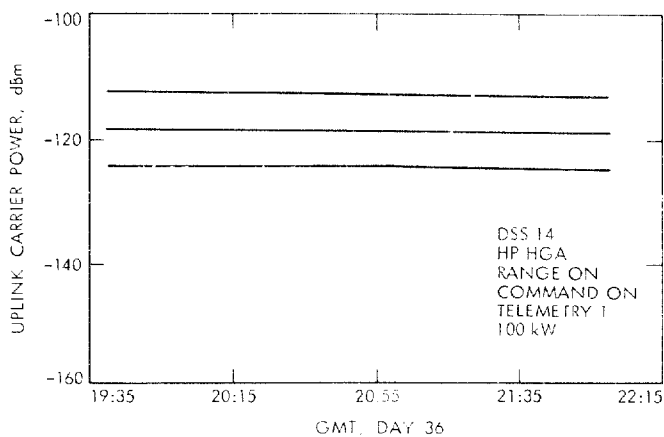
Fig. 41. Uplink carrier power comparison
analysis
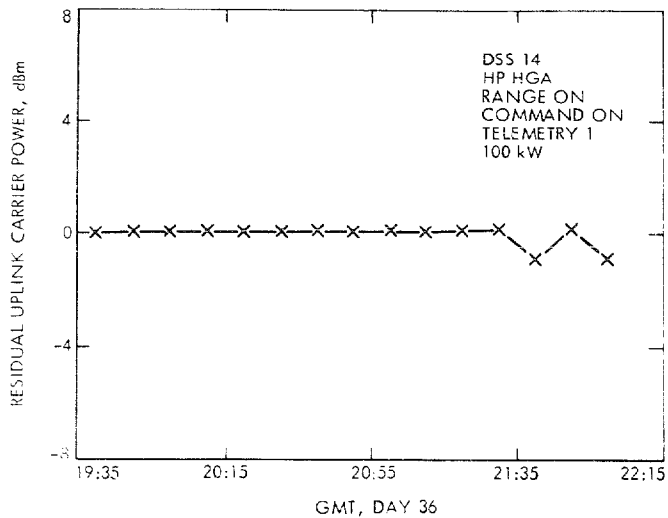
Fig. 42. Residual uplink carrier power comparison analysis
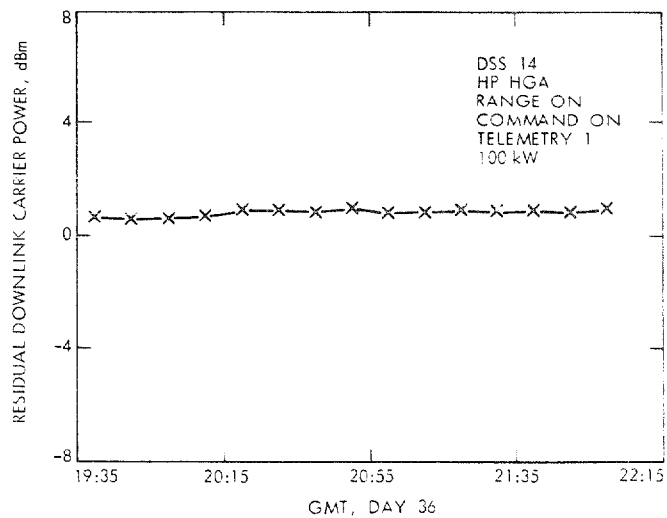
Fig. 45. Downlink carrier power comparison analysis
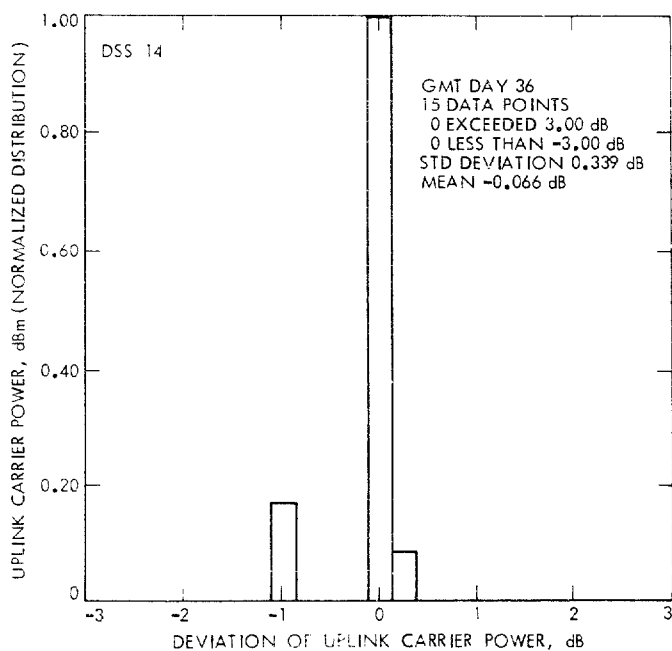
Fig. 43. Uplink carrier power
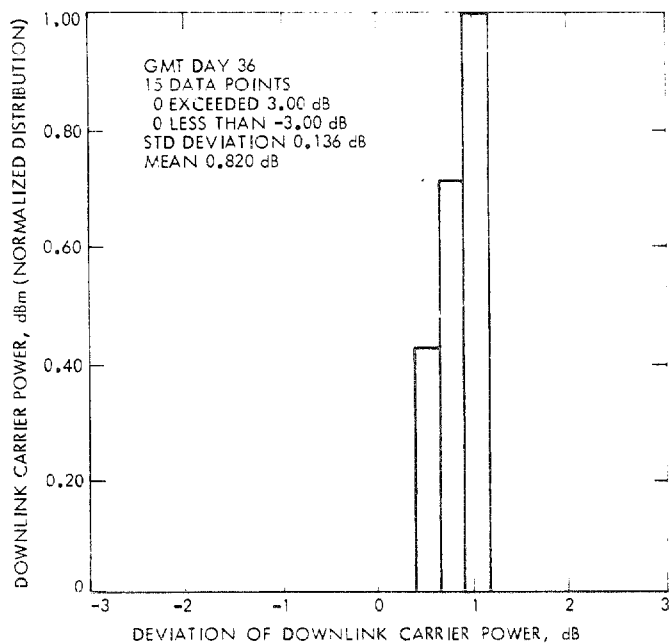
Fig. 46. Downlink carrier power
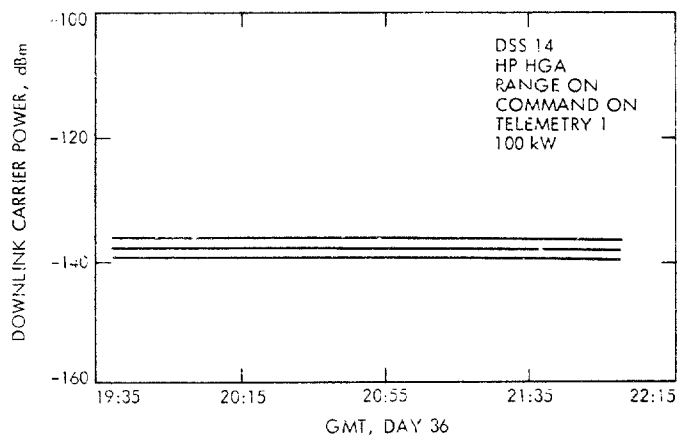
Fig. 44. Downlink carrier power comparison analysis
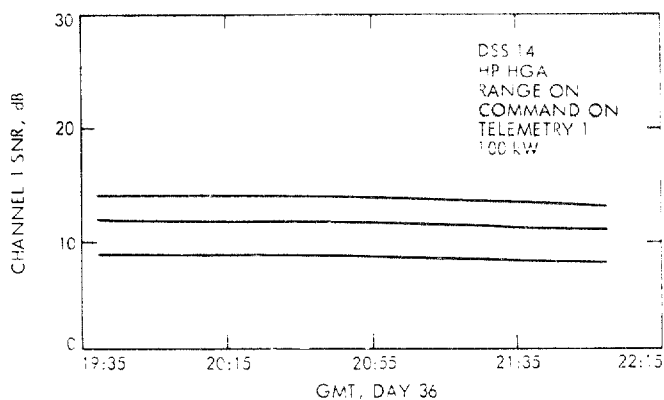
Fig. 47. Channel 1 signal-to-noise ratio comparison analysis
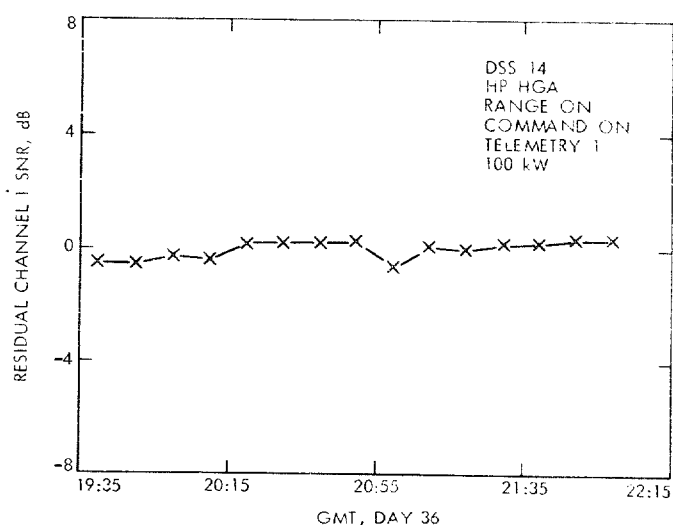
Fig. 48. Residual channel 1 signal-to-noise
ratio comparison analysis
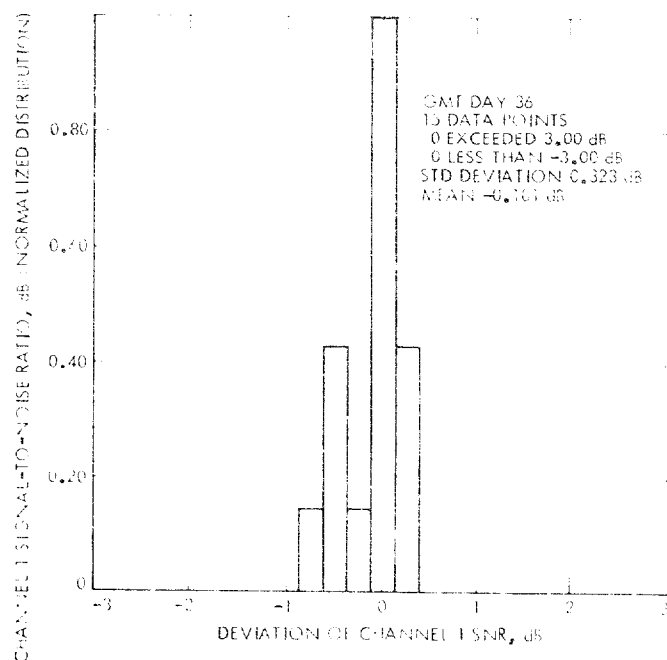
Fig. 49. Channel signal-to-noise ratio
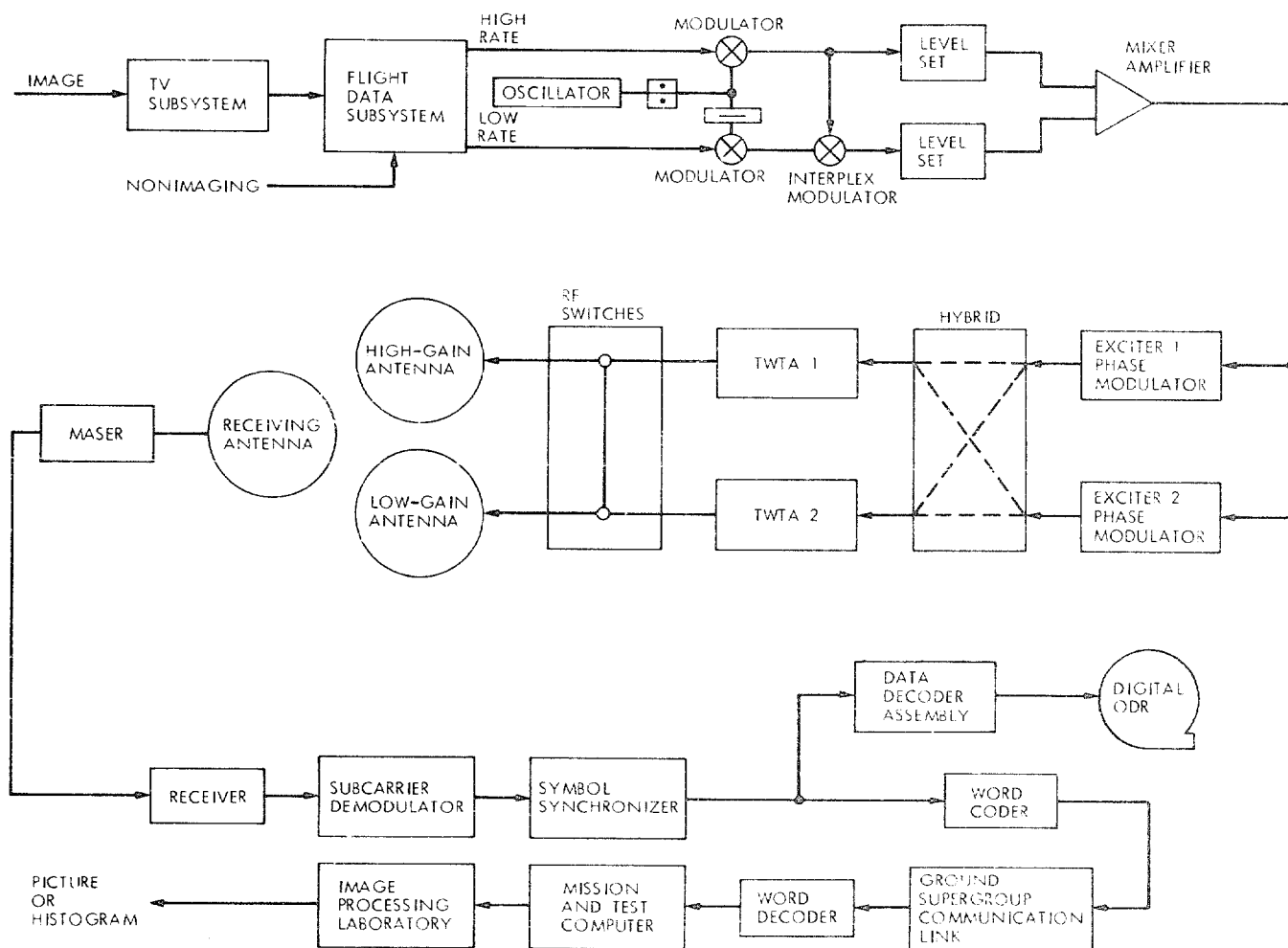
Fig. 50. Block diagram of 117.6 kbits/s elements

Table 6. DC equivalents to CC&S commands

CC&S	DC
2B	DC 10
2C	DC 43
2D	DC 42
2E	DC 11
4A	DC 81
4B	DC 38
4C	DC 76
4D	DC 77
4E	DC 78
4F	DC 79
4G	DC 71
4H	DC 47
4I	DC 46
4K	DC 65
4L	DC 75
4M	DC 48
4N	DC 54
4P	DC 55
4Q	DC 70
4R	DC 72
4S	DC 26
4T	DC 73
5A	DC 27
5D	DC 32
7C	DC 12
7D	DC 17
8C	DC 45
8D	DC 49
8E	DC 53
8F	DC 68
8G	DC 5

antenna failure occurred on December 25, and in the succeeding two months the S-band downlink varied between 2 dB to 6 dB below design value. The antenna healed on March 4, and on March 12, the first 117.6 kbits/s performance tests were run using DSS 14 and DSS 43 configured for minimum noise temperature mode (low noise temperature maser and no transmission). The spacecraft had attitude-control difficulties at the time which placed the HGA boresight off Earth by a significant amount. This effect was calculable and added only a small residual uncertainty.

The ground antenna was moved off track to produce a "synthetic" attenuation of the signal from the spacecraft without modifying the noise temperature conditions at the station. The ground antenna offsets were designed for approximately -2, -3, and -4 dB from the current link conditions. This eliminated, to a large extent, the dependence on absolute values and predicts, and substituted the range distance increase from the test time to encounter, automatically including all nonlinear effects at these signal to noise ratios.

The range increase would produce a 3.50-dB decrease in received signal level, so a plot of bit error rate (BER) as a function of dB down from current conditions would indicate the expected error rate at encounter within the uncertainty of the measurement of the data points.

Since the total link BER measurement was in question, including the ground data-processing system, it was decided to use the video histograms as a measure of BER and convert this value to SNR. The spacecraft TV system was turned off and the Flight Data Subsystem (FDS) was commanded to interrogate the TV at the 117.6 kbits/s rate. This produces a black picture with a slight amount of residual noise at the spacecraft.

The FDS quantifies the elements of the picture into 8-bit binary pixels. This is then biphase modulated on a high-rate subcarrier, interplexed with the low-rate stream and modulated on the downlink carrier. The end result, after reception, demodulation, synchronization, and dequantization is either a picture or a histogram of the decimal values of

Table 7. Comparison of predicted versus actual AGC, 117.6 kbits/s SNR and 2.45 kbits/s SNR using degraded HGA

Station	Predict (HGA - 3.9 dB) corrected for T_s AGC/117.6 kbits/s SNR/2.45 kbits/s SNR	Actual AGC/117.6 SNR/2.45 SNR	Δ
DSS 14	-136.6/7.6/12.9	-136.0/6.8/12.3	+0.6/-0.8/-0.6
DSS 43	-136.6/7.8/13.2	-137.6/7.1/11.6	-1.0/-0.7/-1.6
DSS 63	-136.7/7.3/12.6	-136.7/7.4/13.2	0.0/+0.1/+0.6
DSS 12	-144.6/ - /13.3	-143.3/ - /14.9	+1.3/ - /+1.6
DSS 62	-144.7/	-143.3/	+1.4/

T_s = system noise temperature

Fig. 51. Bit error rate at Goldstone DSCC compared to predicts--117.6 kbits/s on March 29, 1974 encounter day)

Fig. 53. Goldstone 117.6 kbits/s bit error rate test

Fig. 52. Bit error rate from picture No. 1029955 versus number of bits per pixel used, March 12, 1974

Fig. 54. One-way and two-way 117.6 kbits/s tests at DSS 14

DSN
ANT 64 m
POWER LISTEN ONLY
EL 70°

S/C
ANT HGA
POWER 20 W
DATA MODE 117.6 kbits/s

Fig. 55. One-way 117.6 kbits/s test
at DSS 43

Fig. 57. Residual channel 1 signal-to-noise
ratio comparison analysis--DSS 63

Fig. 56. Residual downlink carrier power
comparison analysis--DSS 63

GMT DAY 88
13 DATA POINTS
0 EXCEEDED 3.00 dB
0 LESS THAN -3.00 dB
STD DEVIATION 0.216 dB
MEAN -0.750 dB

Fig. 58. Downlink carrier power--DSS 63

Fig. 59. Channel 1 signal-to-noise
ratio--DSS 63
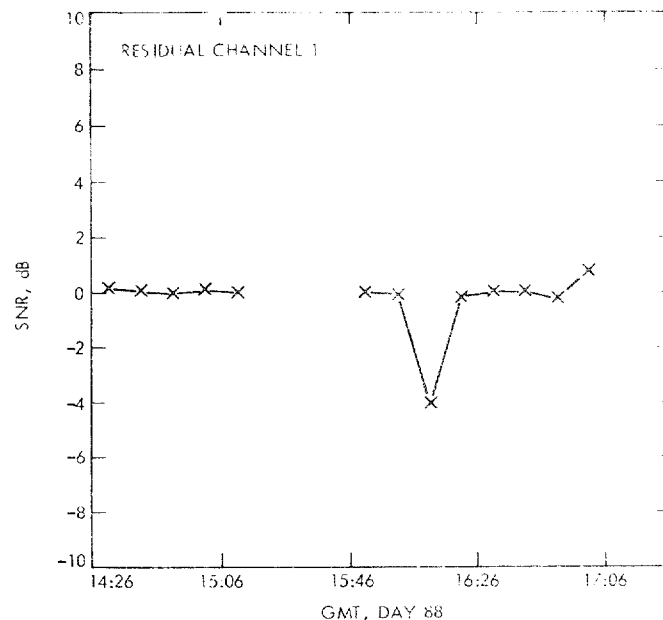
Fig. 61. Residual channel 1 signal-to-noise
ratio comparison analysis--DSS 14
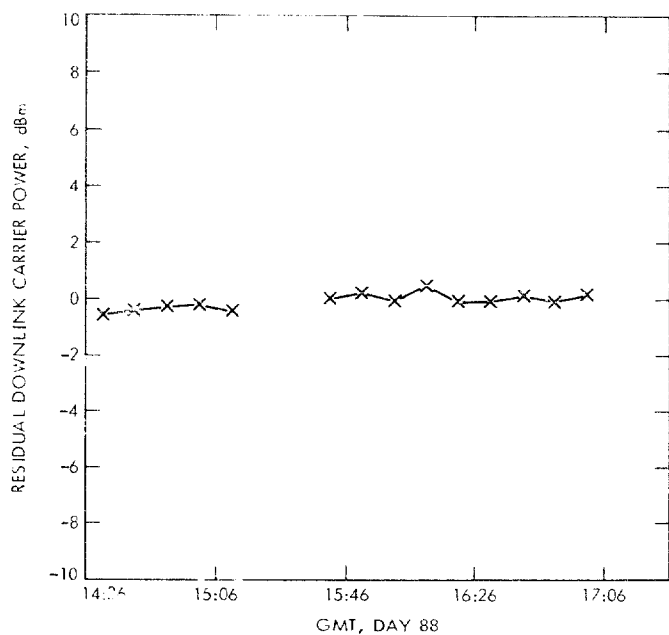
Fig. 60. Residual downlink carrier power
comparison analysis--DSS 14
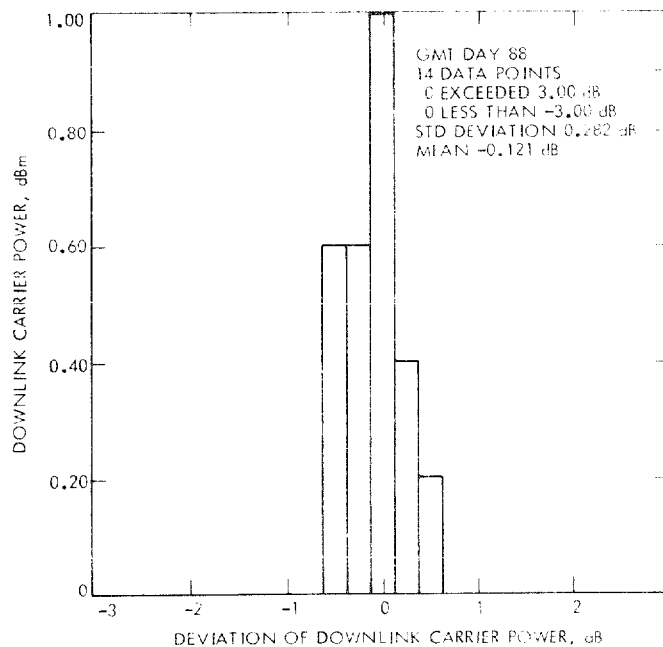
Fig. 62. Downlink carrier power--
DSS 14
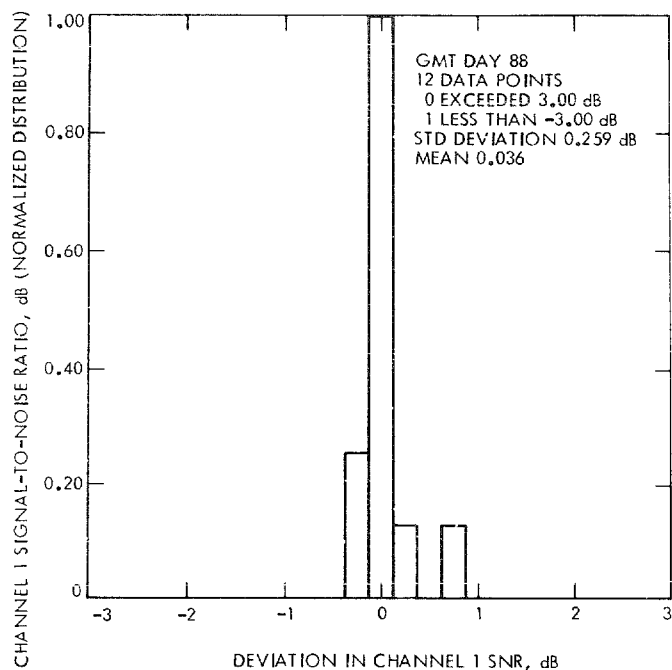
Fig. 63. Channel 1 signal-to-noise
ratio--DSS 14
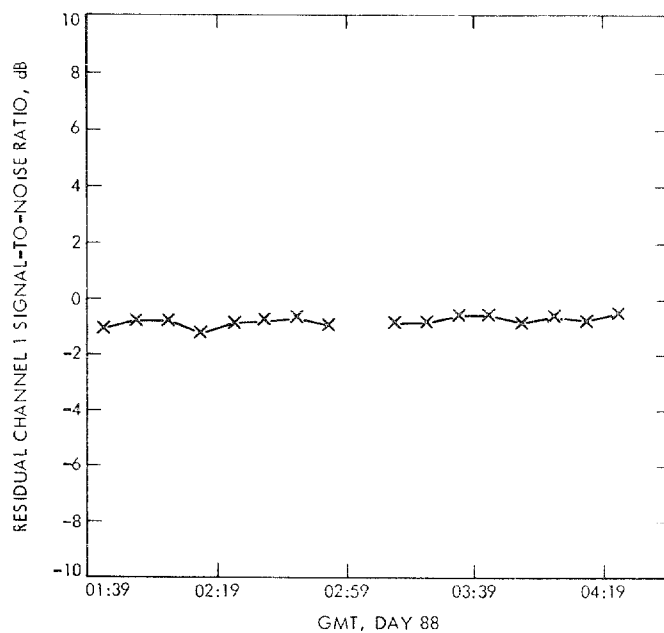
Fig. 65. Residual channel 1 signal-to-noise
ratio comparison analysis--DSS 43
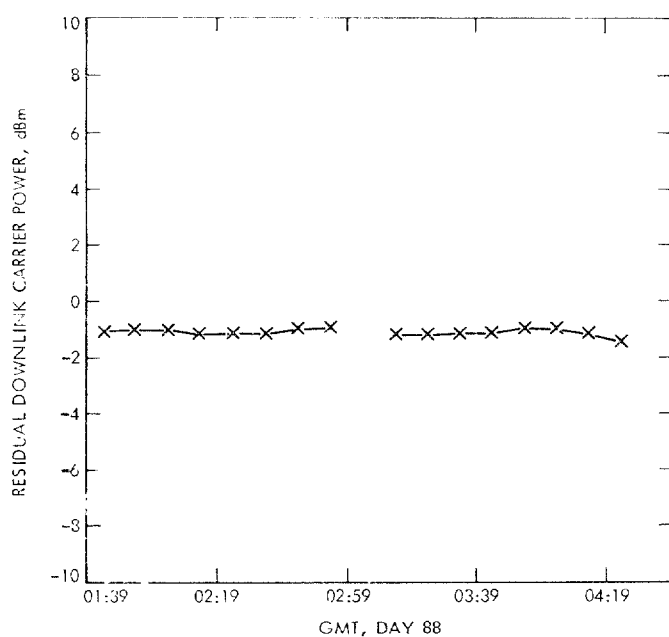
Fig. 64. Residual downlink carrier power
comparison analysis--DSS 43
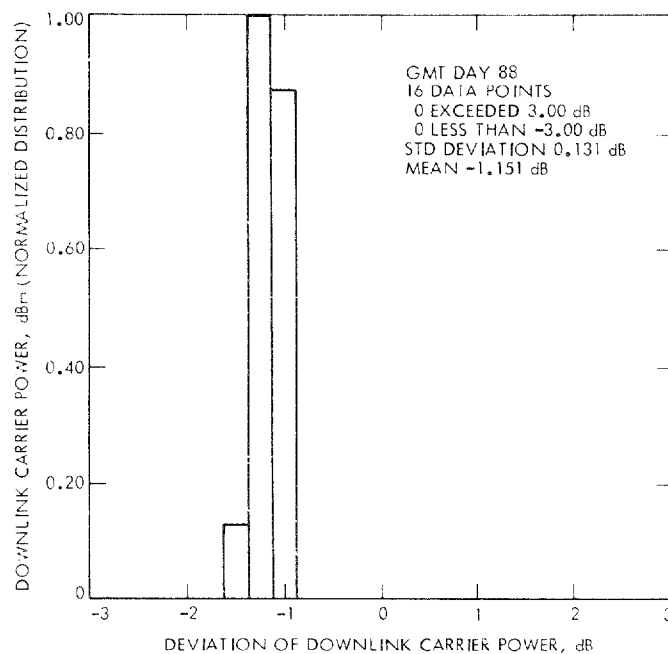
Fig. 66. Downlink carrier power--DSS 43
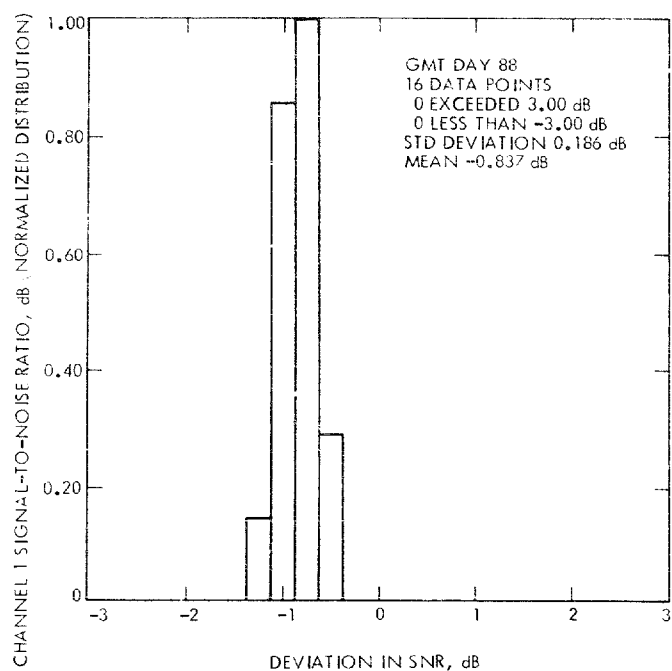
Fig. 67.   Channel 1 signal-to-noise ratio--
DAA 43

GMT DAY 88
16 DATA POINTS
0 EXCEEDED 3.00 dB
0 LESS THAN -3.00 dB
STD DEVIATION 0.186 dB
MEAN -0.837 dB
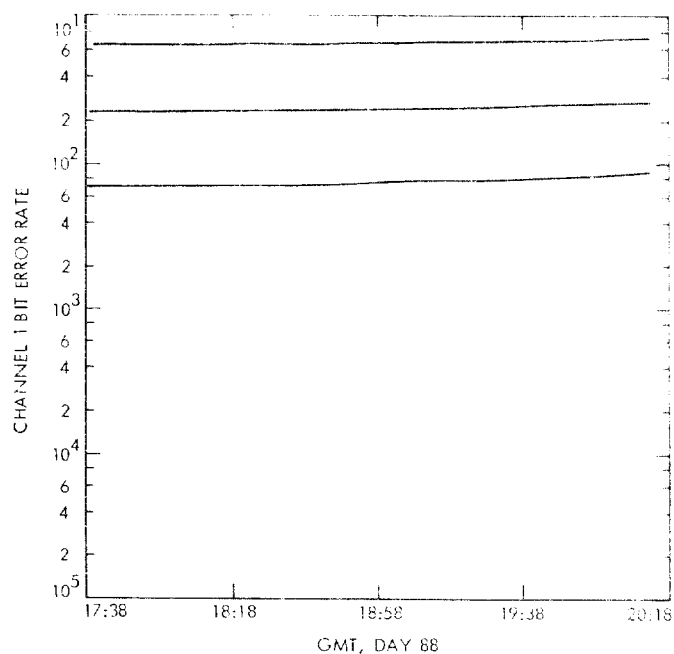
Fig. 69.   Channel 1 bit error rate
(117.6 kbits/s)--DSS 14
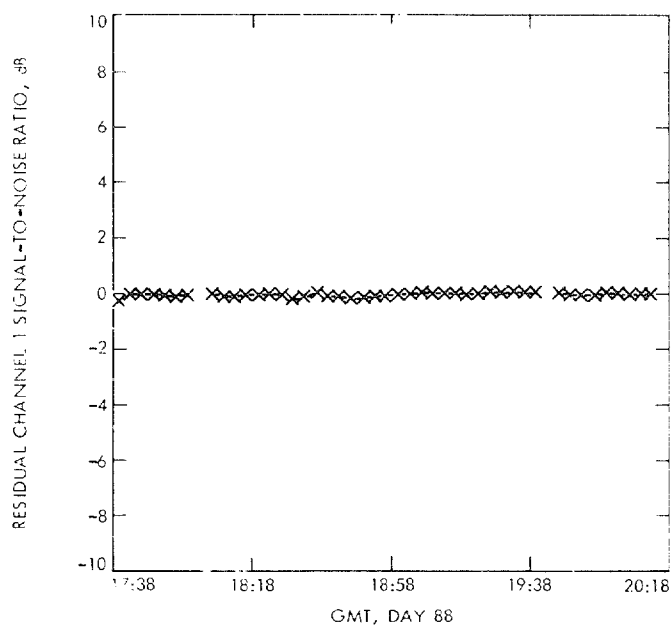
Fig. 68.   Residual channel 1 signal-to-noise
ratio comparison analysis--DSS 14

GMT DAY 88
45 DATA POINTS
0 EXCEEDED 3.00 dB
0 LESS THAN -3.00 dB
STD DEVIATION 0.087 dB
MEAN -0.035 dB
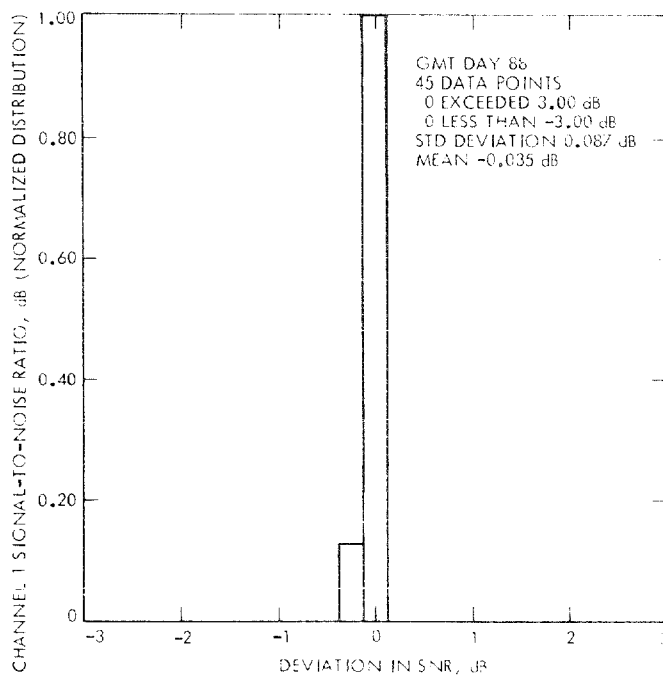
Fig. 70.   Channel 1 signal-to-noise ratio
(117.6 kbits/s)--DSS 14

Table 8. Comparison of predicted versus actual AGC, 22.05 kbits/s SNR and 2.45 kbits/s SNR, using degraded HGA

Station	Predict (HGA - 3.9 dB) corrected for T_s AGC/22.05 kbits/s SNR/2.45 kbits/s SNR	Actual AGC/22 SNR/2.45 SNR	Δ
DSS 14	-137.8/13.3/18.0	-138.0/13.5/18.1	-0.2/+0.2/+0.1
DSS 43	-137.8/13.5/18.2	-137.6/13.3/18.1	+0.2/-0.2/-0.1
DSS 63	-138.2/12.8/ -	-138.8/12.9/ -	-0.6/+0.1/ -
DSS 12	-146.7/ - / 6.1	-144.8/ - / 7.9	+1.9/ - /+1.8

T_s system noise temperature

each pixel. From the histogram it is now possible to measure the total link bit error rate and to eliminate the residual spacecraft noise.

The spacecraft noise will exist in the least significant bits, but the link noise will exist uniformly on all bits. To maximize the confidence level as many bits as possible must be used. Strong signal tests had indicated that only the two least significant bits would be affected by peak residual noise. This was checked by plotting the derived error rate as a function of the numbers of bits used and correlating this with the total number of bits per picture used to calculate the error rate. Figure 52 is an example of this plot for one particular picture. As can be seen, including the two least significant bits (bits 7 and 8), in the calculation increases the total error rate due to the spacecraft residual noise. The bits used for the link error rate measurement were the 6 most significant bits.

The result of all of the above was a set of points cross-correlating bit error rate, and dB decrease in signal. Since dB decrease is related to range increase which is, in turn, related to time by the trajectory. One may now plot BER versus time (Fig. 53). Time is deliberately set from right to left to correspond to a loss in dB. The 1-σ ellipses are SNR estimates converted to error rate in the ordinate and carrier level estimate deltas in the abscissa together with the tolerances. The histogram error rates are plotted as points.

As can be seen, the expected error rate at encounter was 3.8 in 100, while the TV experiment team goal was 3.33 in 100. But there were still several considerations that were not included.

The first is the elevation angle of the ground antenna. During the test it was peaking at 37.5 deg, but at encounter it would peak at 42 deg. This is about a 0.1-dB improvement. The second is that during critical periods of a mission there is more time allocated for station preparation and calibrations and more care is taken during tuning periods because requirements on the system are more stringent. This, although not a measurable number, is probably of the order of 0.2 dB.

The plan at this point was to run short tests at DSS 14 and 43 as the spacecraft approached Mercury and to compare these to the predicted curve, but in the meantime to commit to a 117.6/2.45 kbits/s sequence. These plots are shown in Figs. 54 and 55.

On March 20 a decision was made to switch exciters. This was in response to the Celestial Mechanics and Radio Science Team's analysis of the oscillator's phase noise spectrum. They found phase shifts of several degrees, which would tend to reduce the validity of any spacecraft generated carrier frequency data from Mercury. A switch in oscillators would also switch to a different telemetry phase modulator. The preflight test data indicated a potential improvement of 0.1 ± 0.30 dB. The improvement was of the order of ±0.1 dB.

Table 9 lists the various short tests (10 min) during the pre-encounter.

On March 27 (two days before encounter) the project requested a final error-rate predict for the encounter pass at Goldstone. The value given was 2.29 in 100, the equivalent SNR was 3.00 dB at 17:18:59 (h:min:s) on March 29, 1974.

The encounter data is shown in Fig. 51. Included are the design predict (10-18-72), preflight predict (10-4-73), and the in-flight predict (3-27-74). The mean deviation over the 2-1/2 hours at encounter was 0.2 dB from preflight data, and 0.0 dB from in-flight data.

Figures 56 through 67 are selected plots of downlink carrier and ST/N_0 residuals at 22.05 kbits/s at DSSs 63, 43, and 14. Figures 68-70 are plots of ST/N_0 residuals at 117.6 kbits/s at DSS 14 listen-only.

4.   Cruise Science

The prime data rate through most of the mission was 2.45 kbits/s block-coded single channel. This, included the 33-1/3 bits/s engineering data time multiplexed with the cruise science data to produce a composite 2.45 kbits/s. Figures 71 and 72 are plots of expected and actual uplink and downlink AGC. The drop in downlink AGC

Table 9. 117.6 kbits/s Tests

Day in March	Exciter	Mean SNR deviation from predicts, dB	
		DSS 14	DSS 43
12	1	-0.5	
13	1		+0.2
20	1	-0.4	
22	2	+0.0	
24	2		+0.3
25	2		+0.1
26	2	+0.0	+0.4
27	2		-0.1
28	2	+0.5	-0.1
Encounter			
29	2	+0.2	+0.1

Table 10. TCM 1 maneuver summary

Propulsion	
Burn time (at spacecraft)	317:16:41:50 PST
Burn magnitude (ΔV)	7.77785 m/s
Burn duration	19.90 s
Mass loss	1.8 kg

Turns	
Roll turn	+49.017 deg 265 s
Pitch turn	+127.572 deg 722 s
Off sun	30 min

Spacecraft parameters	
Scan position	
Cone	96.80 deg
Clock	267.01 deg
HGA position	
Cone	90 deg
Clock	302 deg
Antenna	
Turns	LGA
Burn	LGA
Nulls	None
Battery usage	3.4 A-h
Data modes	
Turns	D/M 17 — Primary format (2450)
Burn	DM/17 — Maneuver format (2450)

from day GMT 35° to GMT 71 is due to the previously mentioned HGA failure.

Figure 73 is a plot of residual AGC by station for a brief period of time. This plot uses two-hour averages of AGC over each station.

Due to the healing of the HGA, the extreme press of work to prepare for the Mercury encounter, the additional testing and analysis for the 117.6 kbits/s at Mercury, the departure of one telecom data analyst to return to school, and the lack of manpower, this plot (Fig. 73) was not continued. The real-time comparison was used (Fig. 72) instead.

B. SPACECRAFT TIME LINES AND ASSOCIATED MANEUVERS

1. TCM 1

The latest orbit determination results, which moved the estimated Venus encounter by approximately 15 km, coupled with revised estimates of turn rates have combined to indicate a positive roll turn should be used rather than the negative roll turn originally planned. A summary of the maneuver is shown in Table 10.

The Maneuver performance looked very good. The Navigation Team was able to monitor the roll turn and its polarity (+0.035 Hz max shift), the pitch turn and its polarity (+0.116 Hz at start, and -0.080 Hz at the end). These doppler shifts correspond to velocity changes as small as 2 mm/sec. The burn should have produced a +72 Hz doppler shift, but only a +71 Hz shift was observed. This corresponds to a 1.5% error, which is within specifications.

Subsequent to reacquiring celestial references, the Canopus tracker went into a roll search, apparently due to a bright particle. Analysis and corrective action achieved Canopus acquisition after the roll search.

Based on the orbital parameters as of Nov. 26, 1973, TCM 2 was required to correct for a miss of approximately 1560 km (970 miles) to attain the desired Venus flyby aiming point. The present orbit was 1560 km farther away from Venus than the desired aiming point. The maneuver would also have to correct for a timing error of 3 min (Mariner 10 would presently arrive at Venus 3 min earlier than desired). Figure 74 is a sketch of the desired flyby and post TCM 1 orbit points and the timeline is shown in Table 11.

DSSs 12, 14, 42, 62
F   FAVORABLE
D   DESIGN VALUE
A   ADVERSE

64 m

F
D
A

1973 ⟶⟵ 1974

F
D
A
26 m

V_E M_E

GMT DAYS

Fig. 71.   Uplink AGC

1973 ⟶⟵ 1974

DSS 12/14
DSS 42/43
DSS 62/63

−3.9 dB
HGA FIRST FAILURE

−5.7 dB
HGA SECOND FAILURE
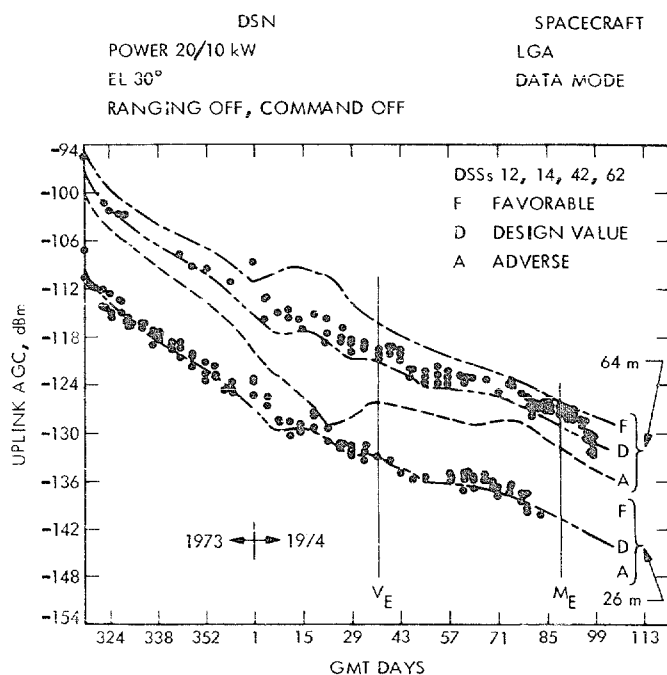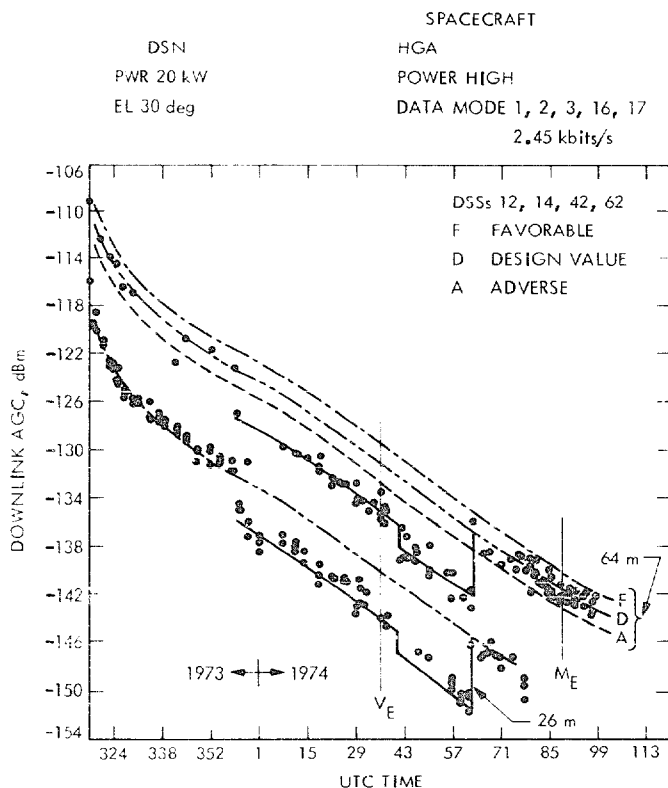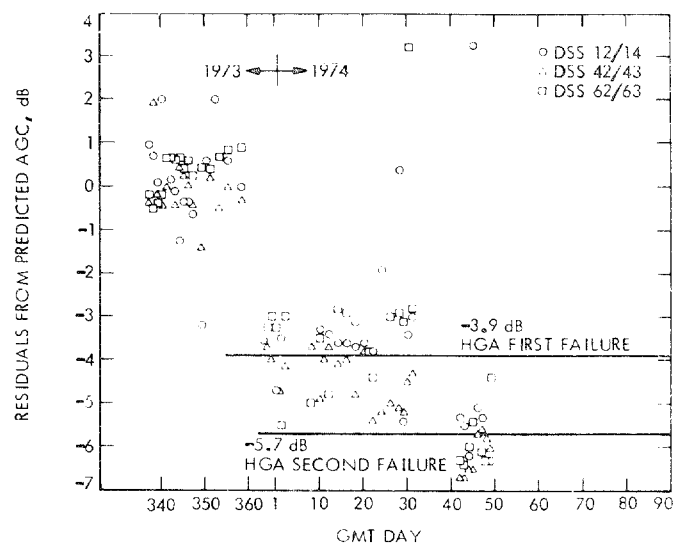
GMT DAY

Fig. 73.   Delta (residuals) from design

DSN

PWR 20 kW

EL 30 deg

SPACECRAFT

HGA

POWER HIGH

DATA MODE 1, 2, 3, 16, 17

2.45 kbits/s

DSSs 12, 14, 42, 62
F   FAVORABLE
D   DESIGN VALUE
A   ADVERSE

64 m

F
D
A

1973 ⟶⟵ 1974

M_E

V_E
26 m

UTC TIME

Fig. 72.   Downlink AGC

BIASED INJECTION AIM POINT

POST TCM 1 ORBIT

CAPTURE RADIUS − 10,000 km

POST INJECTION ORBIT

VENUS

DESIRED FLYBY POINT

55,000 km 3 hr LATE

1560 km AND 3 min EARLY
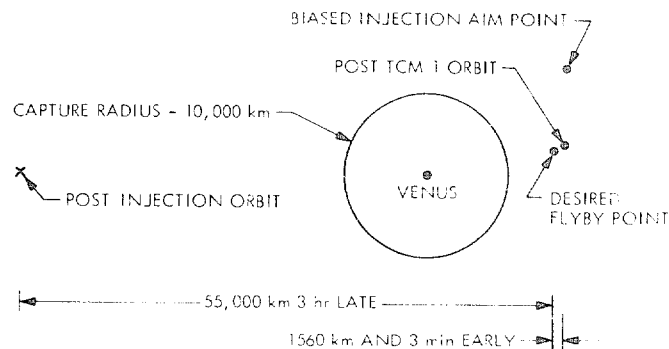
Fig. 74.   Desired flyby and post-TCM orbit points

EARTH

COMPONENT OF
ΔV IN THE EARTH
(4.01 m/s)

103 deg

α = 77 deg

TCM 3 VELOCITY
CHANGE, ΔV
(17.83 m/s)

SPACECRAFT
DIRECTION
OF MOTION, V

ROCKET
EXHAUST

SUN
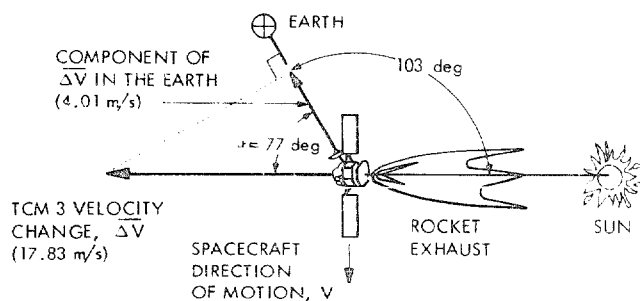
Fig. 75.   Spacecraft orientation relative to Earth and Sun for TCM 3

Table 11. TCM 1 timeline (GMT)

Day	GMT	Command	Event
317	20:59:21	DC 33	Initiate tandem maneuver
	21:00:21	DC 80	Enable 30 Vdc supply
	21:35:16	DC 79	PSE instrument off (replacement heater on)
	21:45:16	DC 52	Computer Flag 7 interrupt
	23:00:16	7MI	Gyros on
	23:11:16	CC-6A-0-1243	To 2450 bits/s engineering telemetry
318	00:08:32	7M4	Start roll turn
	00:12:57	7M4	Stop roll turn
	00:21:29	7M5	Start pitch turn
	00:33:31	7M5	Stop pitch turn
	00:41:32	DC 73	Enable solenoid valve
	00:42:03	8M1	Burn start
	00:42:23	8M1	Burn stop
	00:46:23	7M5	Start pitch unwind
	00:58:26	7M5	Stop pitch unwind
	01:01:26	7M4	Start roll unwind
	01:05:51	7M4	Stop roll unwind
	01:12:00	7M1	Gyros off
	01:13:51	DC 81	Battery charger to high rate
	01:40:58		Gyros on (loss of Canopus)
	01:45:17	CC-6A-0-1042	To 33-1/3 bits/s engineering telemetry
	01:54:36		Gyros off (particle acquired)
	02:05:16		Gyros on (roll search)
	02:40:38		Canopus acquired
	02:43:46		Gyros off
	03:21	DC 79	PSE instrument on

2. TCM 2

On January 21 at 19:50 GMT, Mariner 10 was commanded to roll 46 deg then pitch nearly 35 deg. At 12:14 PDT, the rocket motor fired for about 3.8 sec to change the spacecraft's speed by about 4.83 km/hr (3 mph). From the observed shift of -17.41 Hz in doppler frequency, which was within 0.04 Hz of the predicted value, it was concluded that excellent performance had been achieved in the radial component of the velocity change. The TCM 2 timeline is presented in Table 12.

3. TCM 3

The third trajectory correction maneuver (TCM 3) was successfully performed as a sunline maneuver. The maneuver had to be done at a particular time, i.e., 12:55 GMT on Saturday morning, March 16, in order to change the trajectory characteristics in the desired manner. The spacecraft orientation relative to the Earth and Sun is shown in Fig. 75. TCM 3 maneuver time line is shown in Table 13.

Usually, it is difficult to separate the effects of velocity magnitude and thrust direction during a maneuver, because the doppler shift that is seen in real-time is only a function of the magnitude of the velocity component in the Earth direction. However, during TCM 3 the Sun was constantly in the Sun sensor's view field, and an accurate estimate of spacecraft position in pitch and yaw relative to the Sun was obtained by telemetry. As shown by the drawing, the angular offsets were such that the angle o, nominally 77 deg, was determined to have been 76.75 deg. This 0.25-deg shift caused the Earth-line velocity component to be 2% larger than predicted.

Telemetered thrust chamber pressure data indicated that the rocket engine thrust was about 1% low, which would make the two velocity vectors 1% smaller than planned. The observed 63.4-Hz doppler shift was in fact 1% higher than predicted due to the summation of the two effects just described.

The result of the TCM 3 maneuver on the Mercury encounter geometry is shown in Fig. 76.

The current best estimate trajectory (BET) is seen to be well inside the desired target zone, which by definition is inside both the Sun and Earth occultation zones for obtaining information on any possible atmosphere on Mercury and possible magnetic field interactions with the solar wind. The displacement of the BET from the free-return contour means that one or more additional maneuvers would be needed after Mercury encounter to achieve a second close Mercury flyby about 176 days later (two Mercury years). On March 26, after 10 days of tracking, data was available for processing, the uncertainty around BET was reduced, and more accurate estimates of the required arrival time and exit occultation time were factored into the TV and Radio Science sequences which were developed. The spacecraft passed about 704 km (437 miles) above Mercury's surface, well within the 90% science value zone.

Table 12. TCM 2 Timeline, Day 021

Time, sec	Event
17:42:51	PSE off (4F)
18:04:51	Transmit LGA
18:19:03	TVS off, DC-48
18:24:40	Gyro heater off, DC-69
18:30:15	TWT low power, DC-43
18:34:30	PSE supplemental heater off, DC-63
18:40:03	MAG A off, DC-46
18:44:15	MAG B off, DC-72
18:50:07	Roll turn start
18:54:17	Roll turn stop
18:58:15	Propulsion heater off, DC-66
19:02:49	Pitch turn start
19:06:06	Pitch turn stop
19:14:38	Burn start
19:14:42	Burn stop
19:24:42	Start pitch unwind
19:27:59	Stop pitch unwind
19:30:59	Start roll unwind
19:35:09	Stop roll unwind
19:38:09	Reacquire
19:48:40	MAG A on, DC-46
19:53:00	MAG B on, DC-72
19:58:27	PSE supplemental heater on, DC-63
20:04:03	Propulsion heater on, DC-66
20:13:51	Transmit HGA
20:19:51	PSE on, 4F
20:29:15	TVS on, DC-78
20:33:27	TWT high power, DC-42
20:43:15	Gyro heater on, DC-69
20:50:51	-X panel to 45 deg
20:57:51	+X panel to 45 deg

Table 13. TCM 3 timeline, day 075 (L + 134 days)

Event time		Event
075	09:55:02	Slew scan platform to maneuver position
	11:19:18	PSE off
	11:43:18	Slew high-gain antenna to maneuver position
	11:54:02	7M1, Gyros on
	11:58:52	All-axis inertial
	12:00:52	Burn start
	12:01:43	Burn stop
	12:11:18	Reposition high-gain antenna
	12:38:18	PSE power on
	13:43:19	Reposition scan platform

C. THERMAL CONTROL

1. Performance From Launch Through Launch Plus 30 Days

The performance of Mariner 10 over the first 30 days of the mission was entirely normal with the exception of a few unexpected temperature control responses. The mechanical devices subsystem performed its various post-launch deployment functions without a hitch, and nothing occurred on the spacecraft that would suggest that performance was less than normal for the other applied mechanics subsystems and disciplines vital to the spacecraft design, specifically structures, cabling, materials, and packaging.

The thermal response of the spacecraft to the launch environment was slightly underestimated, resulting in typical cooldown rates that were more rapid than had been expected based on STV test data. This data is summarized in Table 14.

The failure of the TV optics heaters to function resulted in steady-state scan platform temperatures that were well below those anticipated, yet still above the FA limit for the TV vidicons and UVSA, and above the TA limit for the AES. Once the platform thermal predictor model was corrected for the absence of the optics heaters, it was able to reproduce actual flight temperatures fairly accurately, indicating that prelaunch platform predicts were reasonably correct.

Table 14. Comparison of near-Earth temperatures with predicts

MTC Channel No.	Temperature measurement description	Earth predicts		Day 312, 01:46		ΔT		Comments
		°C	EU, °F	°C	EU, °F	°C	EU, °F	
E065	Canopus tracker	-5.5	22	-10.5	13	-5	-9	
E066	GCA	14.4	58	16.7	62	2.2	+4	
E067	Sun Sensor	-25.5	-14	-23.3	-10	2.2	+4	
E068	+X/-Y N2	4.4	40	8.3	47	3.9	+7	
E069	-X/+Y N2	3.9	39	6.7	44	2.8	+5	
E070	TVCA	2.2	36	2.8	37	0.5	+1	
E106	PSE Electronics	13.9	57	17.2	63	3.3	+6	Bay 6
E107	PSE Platform	2.2	36	-2.8	27	-5	-9	
E301	CPT	-3.3	26	-2.2	28	1.1	+2	
E408	UVSA	10.5	51	-11.7	11	-22.2	-40	On scan platform
E409	UVSO	-25.5	-14	-25	-13	0.5	+1	
E454	Prop N2	10.5	51	15.5	60	5	+9	Not steady state
E455	Propellant	11.1	52	16.7	62	5.5	+10	
E456	Valve	22.2	72	23.9	75	1.7	+3	
E457	Thrustplate	22.2	72	22.2	72	0	0	
E500	IRR	-27.8	-18	-30.5	-23	-2.8	-5	
E602	Mag A	-37.8	-36	-57.2	-71	-19.4	-35	
E603	Mag B	-20.5	-5	-37.8	-36	-17.2	-31	
E604	Mag Electronics	20.5	69	24.4	76	3.9	+7	Bay 6
E605	Mag Proc.	21.1	71	25	77	3.3	+6	
E663	Aux. oscillator	8.3	47	8.9	48	0.5	+1	
E664	TWT 1	11.1	52	15	59	3.9	+7	
E665	TWT 2	6.7	44	9.4	49	2.8	+5	
E666	VCO	5.5	42	6.7	44	1.1	+2	
E667	Dish 1							
E668	Dish 2							
E669	Dish 3							
E670	SX Feed							
E671	X-band transmitter	8.3	47	8.3	47	0	0	
E750	Bay 1	8.9	48	11.1	52	2.2	+4	
E751	Bay 2	3.9	39	5.5	42	1.7	+3	
E752	Bay 3	1.1	34	2.2	36	1.1	+2	
E753	Lower blanket	-47.8	-54	-48.9	-56	-1.1	-2	
E754	Bay 5	6.7	44	11.1	52	4.4	+8	
E755	Bay 6	7.2	45	16.1	61	8.9	+16	
E756	Bay 7	10.5	51	13.9	57	3.3	+6	
E757	Sunshade	17.8	64	30	86	12.2	+22	
E758	HGA Boom			-10	14			
E800	TVA Opt F	5	41		—			On scan platform
E801	TVA Opt R	8.9	48		—			
E802	TVA video	14.4	58	-7.8	18	-22.2	-40	
E803	TVB Opt F	5.5	42		—			
E804	TVB Opt R	9.4	49	-16.1	3	-25.5	-46	
E805	TVB video	15	59	-6.7	20	-21.7	-39	
E806	AES	2.2	36		—			
E869	Battery	10.5	51	13.3	56	2.8	+5	
E870	+X solar panel 1	29.4	85	32.8	91	3.3	+6	
E871	+X solar panel 2	51.1	124	36.7	98	-14.4	-26	
E872	+X solar panel 3	51.1	124	37.8	100	-13.3	-24	
E873	+X solar panel 4	5.1	124	37.8	100	-13.3	-24	
E874	-X solar panel 1	29.4	85	35.5	96	6.1	+11	
E875	-X solar panel 2	5.1	124	37.8	100	-13.3	-24	
E876	-X solar panel 3	5.1	124	38.3	101	-12.8	-23	
E877	-X solar panel 4	5.1	124	40.5	105	-10.5	-19	

EU = engineering unit
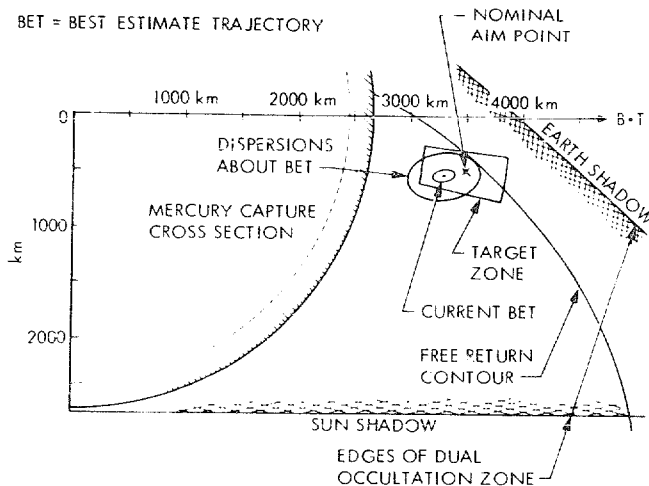
Fig. 76. Results of TCM 3 on the Mercury encounter geometry
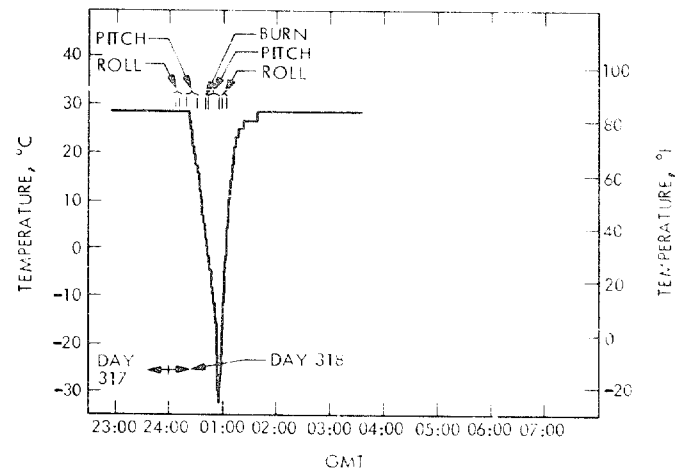
Fig. 79. TCM 1 maneuver transient, +X solar panel (zener) E870
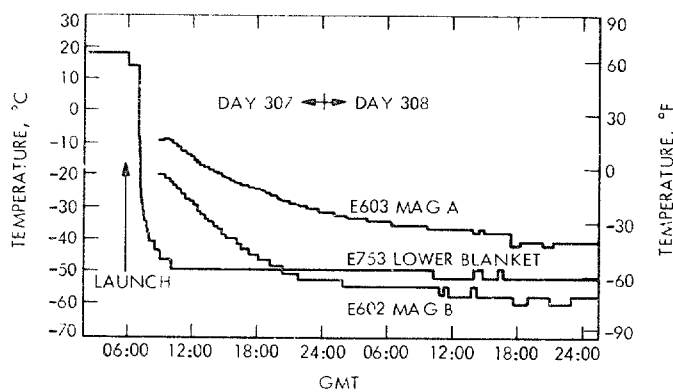
Fig. 77. Magnetometer A and B sensor and lower blanket launch transient temperature
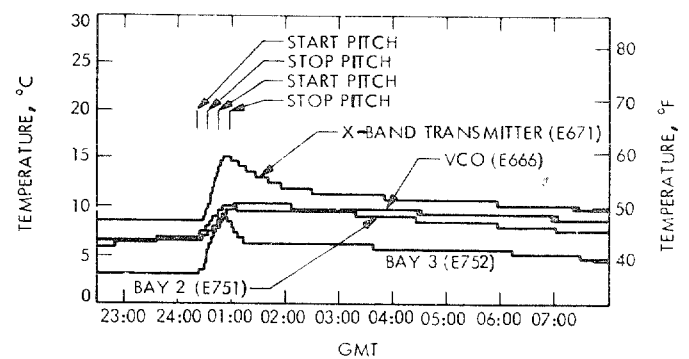
Fig. 80. TCM 1 maneuver transients--Bay 2 (E751), Bay 3 (E752), X-band transmitter (E671) and VCO (E666)
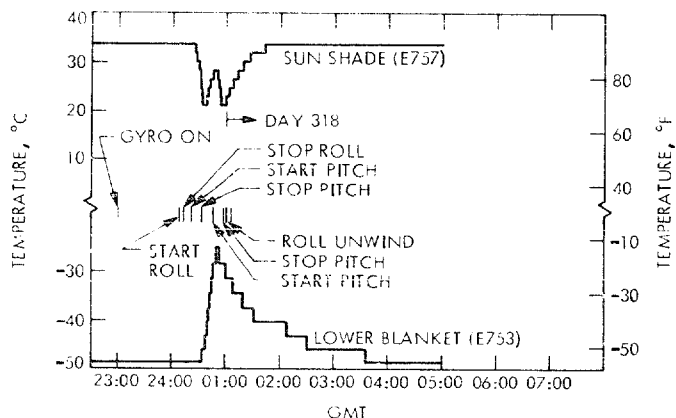
Fig. 78. TCM 1 maneuver transient-- sunshade (757)/lower blanket (753)
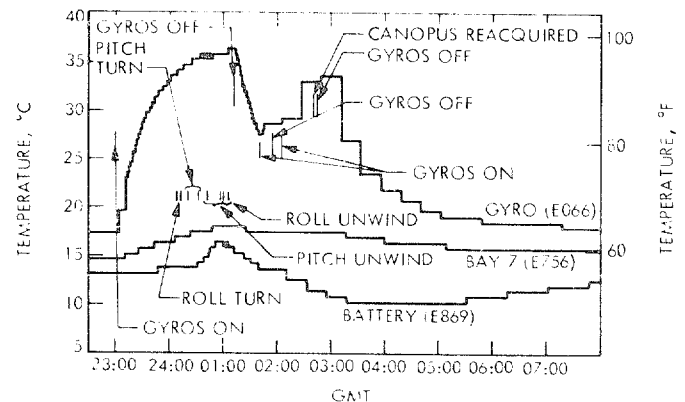
Fig. 81. TCM 1 maneuver transients--gyros (Bay 7) and battery

Significant temperature control surprises included the magnetometer temperatures, with the A and B sensors steadying out 17.2 and 19.4°C (31 and 35°F) below predicts, respectively (Fig. 77). Also surprising were solar panel temperatures, an average of 13.3°C (24°F) below predicts, and the Canopus tracker temperature, 5°C (9°F) below the prelaunch prediction.

TCM-1 served as an excellent thermal shakedown for subsequent maneuvers that were to be more severe due to longer engine burn durations and higher solar intensities. The thermal response (Figs. 78 through 81) of the spacecraft to TCM 1 was generally mild and indicated, at least tentatively that soakback temperature predictions based on hot firing tests conducted at ETS are conservative.

The spacecraft temperatures at lift-off were nominal and as expected based upon previous tests data. In general, most transients were more rapid than those observed during STV testing. The most obvious of these was the X-band transmitter transient shown in Fig. 82. Also apparent in Fig. 83 the effect of the Sun on the X-band transmitter temperature up through separation and solar panel deployment. DC 71, X-band transmitter power on, was sent at 06:43:30 on Day 307 to prevent the X-band transmitter from falling below the lower Design (3-210) limit of 5°C (41°F).

2. **Performance From Launch + 30 Days Through Launch + 70 Days**

For the 40-day period between L + 30 and L + 70 days, the spacecraft was in a thermally quiescent cruise mode. The only spacecraft configurational changes which influenced spacecraft temperatures during this period were the daily articulation of the high-gain antenna and the repositioning of the solar panels on Day 348/349 (the panels were initially articulated from 0 to 25 deg on Day 348, and then the +X panel moved to 12 deg and the -X panel to 40 deg on Day 349).

Three major spacecraft anomalies occurred during this period that affected high-gain antenna performance, power chain redundancy, and scan platform slewing capability. These anomalies will be discussed only to the extent that they affected spacecraft temperatures.

During this period, the solar flux at the spacecraft increased by 13.5% from 0.147 W/cm² to 0.197 W/cm² (136 to 183 W/ft²). The total accumulated solar exposure to date was 1914 equivalent sun hours (ESH).

The overall performance of the Temperature Control Subsystem was nominal with most spacecraft temperatures following predicts. Some temperatures, however, deviated significantly from predictions in the most critical direction, namely positive. Each of these cases is discussed, and for most of them the observed effect can be attributed to the thermal presence and particular geometry of the high-gain antenna or solar panels. These effects would not necessarily map into significant deviations from predict at Mercury. The remaining deviations were attributed to degradation of thermo-optical surface properties. These effects would map into deviations from predict at Mercury. However, the

spacecraft was thermally designed to accommodate extensive degradation, and none of the data suggested that degradation levels at Mercury will be anything but minimal. Thermo-optical property degradation, although accommodated in the design, was not included in the preflight predicts, because it is not sufficiently predictable, especially as a function of time and exposure.

a. Bus and Propulsion Module. Those assemblies located in the bus and in the propulsion module whose temperatures were deviating significantly from predictions were being influenced by either the nonstandard solar panel tilt configuration, reradiated energy from the high-gain reflector, or both.

Those assemblies noticeably affected by the high-gain antenna are clustered on the +Y side of the bus (specifically Bays 2, 3, and 4, the X-band transmitter mounted over Bay 3, and the Canopus tracker mounted over Bay 2).

The Canopus tracker temperature appeared to be very sensitive to high-gain antenna dish temperatures. On Day L + 62/63 of the mission, the high-gain antenna was positioned to warm the dish to a maximum. Shortly thereafter the Canopus tracker increased 1.1°C (2°F). When the high-gain antenna was subsequently returned to the Earth-pointing position, the Canopus tracker temperature decreased 1.1°C (2°F). The Canopus tracker was 2.8°C (5°F) above its predicted temperature.

The X-band transmitter temperature showed the same sensitivity to high-gain antenna temperatures as the Canopus tracker and is also 5°F above predict.

The measurements in Bay 2, Bay 3 and Bay 4 all exhibited a similar deviation from their respective temperature predictions. These discrepancies were attributed to the fact that the high-gain antenna average temperature and orientation with respect to the bus combined to provide a significant thermal input to the bus that was not anticipated and, hence, not reflected in the predictions.

For reasons of cost and complexity, the high-gain antenna reflector was not articulated in either the temperature control model (TCM) test or the flight spacecraft solar thermal vacuum (STV) test. However, the position selected for the dish in the TCM test was the Mercury position, and for the Mercury test mode the reflector was heated to the level appropriate for that orientation/solar flux combination. This would result in a correct input to the bus at Mercury, at least for the TCM. Unfortunately, this same technique was not used for the Mercury mode during the STV test. Although maintained at approximately the same temperature, the reflector was positioned differently, which resulted in a smaller input to the bus than there would be during the equivalent TCM mode. Since the flight predicts are based on the STV test results, it is probable that the Mercury predicts are lower than they should be for those assemblies whose temperatures are influenced by the high-gain antenna.

The propulsion module temperatures are sensitive to both the solar panel temperature and,

to a lesser extent, the high-gain antenna temperatures. The effect of tilting the solar panels at Day L + 42 and L + 43 is evident on all propulsion module temperatures (Propellant, Propellant N2, Thrustplate, and Propellant Valve). The effect was greatest on the thrust plate and thrust plate-mounted components, which exhibited a 2.2°C (4°F) decrease in temperature as a result of the solar panel tilt. As the solar panels warmed, the temperatures of the thrust plate and thrust plate-mounted components increased more rapidly than predicted, indicating the presence of an increasing extraneous input.

The TVCA temperature also indicated a sensitivity to solar panel tilt. The effect of tilting the solar panels was -2.8°C (-5°F), and here again it was apparent that the TVCA temperature increased at a slightly faster rate than the predict would indicate.

b. Appendages. The temperature of most appendage items were close to the predicted temperatures, with only a few exceptions.

The PSE scan platform package temperature showed a rate of temperature increase greater than predicted, but only after the solar panels were tilted. By tilting the -X solar panel to 40 deg, the view factor between the panel and the PSE scan package was increased significantly, resulting in a thermal input to the PSE that varies directly with solar intensity. This increasing input explains the deviation in slopes between the predicted and the actual temperature profiles.

The UVSO instrument also showed a sensitivity to the solar panel tilt. The UVSO temperature increased 1.7°C (3°F) due to tilting the +X solar panel to 25 deg. The next day, when the +X solar panel was returned to +12 deg tilt, the UVSO temperature decreased about 0.56°C (1°F). As the panel temperature increases and the solar intensity increases, the UVSO temperature diverges from the predict. The UVSO temperature is 2.2°C (4°F) higher than anticipated. The predictions do not include a variable solar panel tilt effect, but are based upon STV test data which was valid only for specific solar intensities and solar panel tilt angles. Between these data points the panel effects were neglected.

The IRR temperature increased 3.3°C (6°F) when the -X solar panel was tilted to 40 deg, even though the average panel temperature decreased 15.5°C (28°F). Here again, due to the fact that this input from the solar panel increases with solar intensity, the IRR temperature was increasing faster than predicted, which does not include this variable effect except at those mission points tested during STV.

The spacecraft sunshade continued to increase in temperature due to an increasing solar flux and beta-cloth degradation. The solar absorptivity (α_s) of the beta cloth increased to an indicated value of approximately 0.35. This was an increase of 0.01 over the preceding 40 days and represents less degradation than anticipated.

The predicts for the solar panel substrate temperatures pertain only to the outboard temperature measurement on each solar panel, since they are unaffected by the presence of the bus or

spacecraft sunshade. Actual data from the inboard measurement was plotted, however, to show the extent to which the inboard temperatures are influenced by the rest of the spacecraft.

The outboard solar panel temperatures followed predictions quite closely. On the +X panel, the temperature transducer was located on the outboard corner of the panel near the trailing edge, and was within 1.1°C (2°F) of predict (the predict having been revised for the actual tilt profile).

The transducer located outboard on the -X panel near the leading edge was within 4°F of predict.

The predicts for the +X solar panel zener temperatures have not been updated to reflect the differential panel tilt. In addition, zener power dissipation was affected by the nonstandard tilt profile, thereby significantly changing the shape of the actual data plot versus the obsolete predicted plot.

The high-gain antenna temperatures generally followed the predicted profiles. Only the center transducer was below the predict, probably as a result of being partially shadowed by the Y-bar and coaxial cabling on the back of the high-gain antenna reflector. The high-gain antenna boom temperature significantly higher than predicted. Part of the reason for this discrepancy is the large uncertainty in determining the boom radiative properties and solar input as a function of high-gain antenna dish position.

With the dish in a 160-deg cone angle position, it provided a sizeable energy input to the high-gain antenna boom and at the same time blocked the view of the boom radiator to space. As the dish cones away from the anti-Sun direction, the radiator becomes exposed, thereby relieving the situation considerably.

Blockage of the high-gain antenna boom radiator was not foreseen, due in part to the fact that during the high-gain antenna thermal development test the configuration was such that blockage of the radiator did not occur as the dish was articulated through the range of mission cone angles.

The high-gain antenna feed temperature was higher than predicted due to the reoccurring high-gain antenna feed anomaly. The feed was approximately 6.7 to 8.3°C (12 to 15 F) above prediction. The high-gain antenna was positioned to 160 deg cone at L + 62 days in an attempt to maximize the feed temperature without illuminating it in order to prevent the anomaly from reoccurring. Four days later, the high-gain antenna was repositioned to automatically track the Earth along the antenna boresight. The effect of this high-gain antenna movement was readily observed in all high-gain antenna temperature measurements.

c. Scan Platform. The scan platform temperatures continued to be colder than predicted prior to launch due to the TVS optics heater failure. Scan platform temperatures have been found to be sensitive to scan platform cone angle and to solar panel tilt angles. Tests on the temperature control model indicated the scan platform was not sensitive to solar panel tilt and

temperature; however, the scan platform was stowed at 255-deg clock in that test. In flight, the scan platform was stowed at 94-deg clock/61-deg cone, looking out toward a solar panel tilted 40 deg to the Sun.

d. Temperature Data Associated With Spacecraft Anomalies. On Day L + 52, the high-gain antenna S/X band feed temperature increased 11.7°C (21°F) over a two and a half hour period. The reason for this sudden increase was an apparent failure in the S-band portion of the feed which caused some of the RF energy normally radiated toward Earth to be reflected within the feed and dissipated as heat. The temperature transient was preceded by other indications in spacecraft telemetry and on the ground that a partial feed failure had occurred. Subsequent thermal analysis indicated that the additional energy dissipated in the feed amounted to something between 1.0 and 1.6 W. RF subsystem personnel estimated the energy loss to be between 2.0 and 2.5 W.

Subsequent to the initial failure, the feed anomaly cleared and re-failed twice. S/X-band feed temperature is shown in Fig. 83 for each of these occurrences.

On Day 008 (L + 64 days) failure logic in the power subsystem automatically switched from the main power chain to the standby chain. Since this switch was irreversible, the power conditioning equipment was no longer redundant. There were no abnormal spacecraft temperature indications either before or after this event.

The scan platform was continuously plagued by an anomaly that causes the cone slewing rate to decrease at cone angles in the 150 to 180° range. In order to cause the observed slowing of the platform, an extraneous torque in the neighborhood of 11.3 N·m (100 in.-lb) is required. Various hypotheses have considered cable bundle stiffness at low (-18°C or 0°F) temperatures, cone bearing galling or distortion, thermal blanket interference and actuator malfunctions. No temperature effect has been observed that was peculiar to these anomalies.

3. Performance From Launch + 70 days Through Launch + 110 Days

For the 40-day period between L + 70 and L + 110 days, the Mariner 10 spacecraft was thermally active. Thermally significant events were the gyro turn on/trajectory correction maneuver 2/solar panel tilts, television subsystem on/off sequences and the recovery of the TV optics heaters, roll calibration maneuver (RCM 7) and the associated gyro anomaly, Venus encounter, special gyro tests, and supplemental heater turn offs. The events are chronologically listed in Table 15.

Several spacecraft anomalies occurred during this period affecting the high-gain antenna performance, gyro performance, TVS heater operation, and the scan platform slewing capability. These anomalies will be discussed only to the extent that they affected spacecraft temperatures.

During this period, the solar flux at the spacecraft increased 66.7% from 0.197 W/cm² (183 W/ft²) (1.45 solar constants) to 0.3 W/cm² (305 W/ft²) (2.42 solar constants). Since launch the solar intensity at the spacecraft has increased 142.3%. The total accumulated solar exposure was 3733 equivalent sun hours. The overall performance of the Temperature Control Subsystem was nominal with most spacecraft temperatures following predictions. In Section VI-C-2 it was noted that several temperatures were diverging from prediction due to reradiated energy from the HGA. This effect has diminished but was still evident during this period.

The only cause for concern in the realm of temperature control at that time was the HGA boom temperature which was representative of the HGA APS actuator temperatures. The HGA boom temperature continued to increase at a rate well in excess of the predicted rate.

The other spacecraft temperatures deviating from prediction did not appear in any danger of violating allowable temperature limits through the remainder of the mission.

a. Bus and Propulsion Modules

Those assemblies located in the bus and the propulsion module whose temperatures deviated significantly from predicts were influenced by solar panel tilts, reflected and reradiated energy from the HGA reflector, and spacecraft power states. Those assemblies most notably affected by the HGA are clustered on the +Y side of the spacecraft, namely Bays 2, 3, 4, the X-band transmitter, and the Canopus tracker.

The Canopus tracker temperature continued to be influenced by the HGA and the solar panels. The departure from predicts noted in Section 6.3.2 diminished due to the cooling of the HGA. The solar panel effect was more noticeable due to the large decrease in panel temperature when tilted. On L + 104 days, the panels were tilted from 45 to 58 deg and the Canopus tracker temperature dropped 1.1°C (2°F). The Canopus tracker was less than 2.2°C (4°F) above predictions.

The X-band transmitter temperature was also returning to predicts due to the decreasing HGA effect and was less than 2.2°C (4°F) above predicts.

The temperatures for Bay 2, Bay 3 and Bay 4 all exhibited a similar tendency to return to normal values as the HGA effect diminished. Solar panel effects were evident on both Bays 2 and 4.

The response of the propulsion module and the TVCA to supplemental heater turn offs and solar panel tilts is listed in Table 16. Due to the extremely long time constant of the propellant tank, however, temperature changes in the tank were effectively reduced by the increasing solar intensity. The propulsion module temperatures seemed to be following predictions reasonably well, thereby providing additional confidence in the ability to project temperatures for future

Table 15. Thermally significant events occurring between L + 70 and L + 110 days

Day from launch	GMT time (Earth received time)		Event
	Day of year	Hours	
L + 73	016	16:11	-X solar panel to 12 deg
L + 74	017	16:36-18:51	Gyro turn-on sequence
	017	16:54	TVS heaters on, both/both
	017	21:58	TVS heaters to low/low
L + 75	018	16:22	UVSO power on
	018	21:48	UVSO power off
L + 77	020	22:16	UVSO power on
L + 78	021	16:22-20:44	TCM 2
	021	20:52	-X solar panel to 45 deg
	021	20:59	+X solar panel to 45 deg
L + 80	023	17:32	PSE scan stop
	023	18:19	PSE scan low
L + 81	024	03:16	TVS off
	024	16:30	PSE scan on, low
L + 82	025	18:35	TV heater to hi/hi
L + 85	028	15:41-21:00	RCM 7
		21:00-21:37	Gyro anomaly/gas leak
	028	23:37	PSE scan on, high
L + 86	029	00:33	TVS on
	029	04:14	IRR on
L + 93	036	17:01	Ey closest approach
	036	19:27	IRR off
	036	21:34	PSE scan on, low
L + 94	037	17:03	UVSO power off
L + 95	038	23:26	PSE scan stop
L + 96	040	21:39	TVS off
L + 97	041	03:03	TVS on
	041	04:03	TVS off
	041	07:03	TVS on
	041	10:03	TVS off
	041	17:03	TVS on
	041	18:03	TVS off
L + 98	042	01:03	TVS on
	042	02:03	TVS off
	042	02:54	TVS on
	042	10:04	TVS off
	042	17:03	TVS on
	042	18:04	TVS off
L + 99	043	05:03	TVS on
	043	06:03	TVS off
	043	17:03	TVS on
	043	18:03	TVS off
L + 100	044	05:03	TVS on
	044	06:04	TVS off
	044	17:04	TVS on
	044	18:30	TVS off
L + 101	045	18:33	Gyro test
L + 102	046	00:41	-X solar panel to 58 deg
	046	01:41	+X solar panel to 58 deg
	046	16:36	PSE scan on, low
	046	22:36	DC 66 off
L + 105	049	07:05	Lost canopus/gyros on

maneuvers. The TVCA was 3.9°C (7°F) below its prediction. This was due in large part to the solar panel tilts, which are different from those used during STV testing and assumed in the predicts.

The gyros were turned on on L + 76 days (GMT day 017 17:37) and remained on through the maneuver, TCM 2, until L + 87 days (GMT day 028 21:37) at which time an anomaly was observed. The gyro turn-on sequence was elaborate and designed to prevent any excess stress of the power system since the switch to the standby power subsystem elements was at that time an unresolved event. The sequence is presented in Table 17. Figure 84 presents the TWT base temperatures during the gyro turn-on sequence. Figures 85 to 88 present the propulsion module temperatures, PSE platform temperature and the gyro temperature. The gyro reached a steady-state temperature of 41.7°C (107°F). When the TVS was turned off on L + 82 days, the
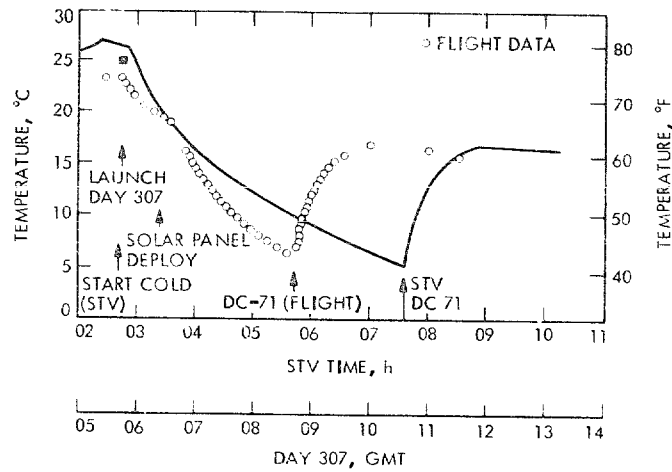
Fig. 82. X-band transmitter cooldown--
STV test
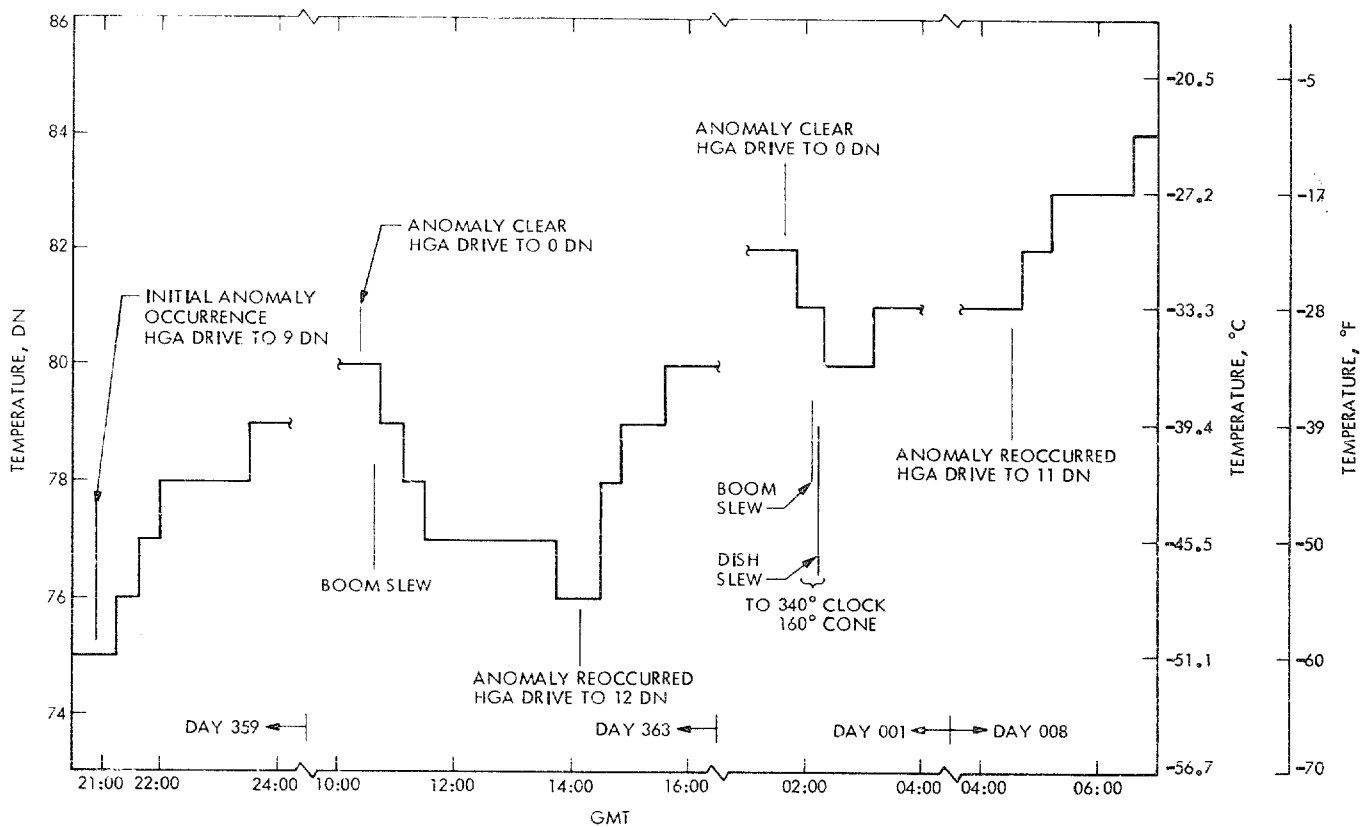
Fig. 83. S/X-band feed temperature (E670) response to feed anomalies
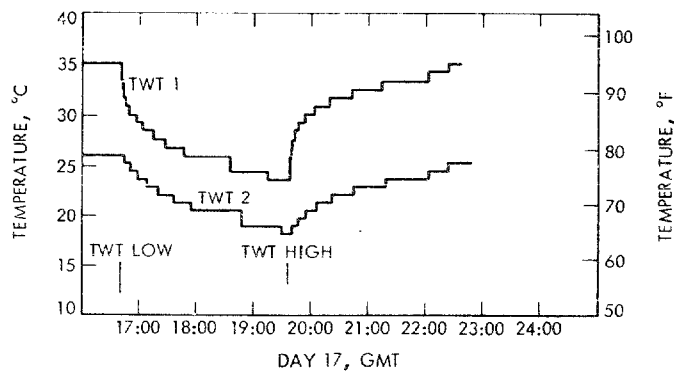
Fig. 84. TWTA base temperature

Table 16. Propulsion module temperature response to supplemental heaters off and solar panel tilts

Time	Event	ΔT, °C (°F)			
		E070 TVCA	E455 Propellant	E456 Valve	E457 Thrust plate
L + 76 Days 1654 Day 017	DC 64 supplemental heater off 13.5 W on thrust plate -X solar panel from 40 to 12 deg	-2.8 (-5)	-1.1 (-2)[a]	-7.8 (-14)	-8.9 (-16)
L + 80 Days 2052 Day 021	Solar panels tilted from 12 to 45 deg	-6.7 (-12)	[a]	-3.9 (-7)	-5.6 (-10)
L + 104 Days 0100 Day 046	Solar panels tilted from 45 to 58 deg	-3.9 (-7)	[a]	-2.2 (-4)	-2.2 (-4)
L + 105 Days 2236 Day 046	DC 66 supplemental heater off 13.5 W on thrust plate	-4.4 (-8)	-2.2 (-4)[a]	-12.8 (-23)	-12.8 (-23)

[a] Difficult to determine due to the very long time constant of the propellant tank.

Table 17. Gyro turn-on sequence

Time, GMT	Event
017 16:11:32	-X solar panel to 12 deg
017 16:36:32	TVS off (DC 48)
017 16:41:32	TWT low power (DC 43)
017 16:51:32	APS supplemental heater off (DC 62)
017 16:54:32	Propulsion/CPT heater off (DC 64) TVS Optics heaters on
017 16:57:32	Propulsion/Sun sensor heater off (DC 66)
017 17:00:32	Gyro heater off (DC 69)
017 17:03:32	PSE supplemental heater off (DC 63)
017 17:28:32	MAG B off
017 17:31:32	MAG A off
017 17:37:38	Gyros on
017 17:51:38	TVS on (DC 78)
017 17:58:32	MAG B on (DC 72)
017 18:01:32	MAG A on (DC 46)
017 18:11:32	PSE supplemental heater on (DC 63)
017 18:26:32	Propulsion/Sun sensor heater on (DC 66)
017 18:31:32	Gyro heater on (DC 69)
017 18:51:32	Transmit LGA
017 19:21:38	Transmit HGA
017 19:36:38	TWT high power (DC 42)

effect upon the gyro was approximately -1.1°C (-2°F). Other gyro turn-ons and transients will be presented in a later section.

The television subsystem was turned off on L + 82 days (GMT day 024, 03:16), then turned on again at L + 88 days (GMT Day 029 00:33), and then off again at L + 99 days (GMT Day 040 21:39). The TVS affects all of the Bay 6 assemblies and, to a lesser extent, Bays 5 and 7. The PSE electronics changed approximately 3.9°C (7°F) due to the TVS switching. The gyro effect is about 1.1°C (2°F) on the PSE electronics. The Magnetometer processors, also located in Bay 6, changed approximately 2.2°C (4°F) due to the TVS switching. The Bay 6 temperature changed about 3.3 C (6°F) due to the TVS switching. The gyro had only a 0.5°C (1°F) effect upon the average Bay 6 temperature. The TVS switching has only a 1.1 C (2°F) effect on the average bay temperature of Bays 5 and 7. The TVS optics heater turn-on will be discussed in the section on the scan platform.

The CPT supplemental heater, commandable with DC 64, was turned off at L + 76 days. This resulted in a 5.6°C (10°F) drop in CPT temperature. This change was expected, based upon the results of the STV test. There was an additional temperature drop expected when the gyro heater, DC 69, was turned off. The ΔT would be approximately 2.2°C (4°F).

b. Appendages. The temperatures of most appendage items were close to predictions with only a few exceptions.

The cruise sun-sensor temperature decrease was only 11.1°C (20°F) when the DC 66 supplemental heater was turned off. The expected temperature decrease was 16.7°C (30°F).

The PSE scan platform temperature sensor exhibited several interesting signatures. On L + 87 days (GMT day 028 23:37) the scan rate was increased from 1 deg/sec to 4 deg/sec and the average scan platform temperature decreased ~2.2°C (~4°F). Turning the scan off resulted in a 2.8°C (5°F) decrease in temperature. This decrease was due mainly to the scan motor and electronics being turned off. Solar panel tilting also seemed to have approximately a 1.1°C (2°F) effect upon the PSE scan platform temperature. The PSE temperatures followed the predict with a slight deviation, indicating some degradation of the Sun facing silvered teflon surfaces.

The UVSO experiment was turned on for the first time on L - 76 days (GMT day 018 16:22) and then off at GMT day 018 21:48. The transient response is shown in Fig. 88. The UVSO was turned on for Venus encounter at L + 79 days (GMT day 020 22:16) and an expected 3.9°C (7°F) temperature drop was observed. The replacement heater for this instrument was larger than the actual dissipated power by about 0.3 W. The UVSO was turned off at L + 96 days (GMT day 037 1703) and again the temperature increased 4.4°C (8°F). When the sun sensor heater, DC 66, was turned off at L - 105 days, the UVSO temperature decreased 8.9°C (16°F) as expected. The temperature was 2.8°C (5°F) above that predicted for the UVSO off. Solar panel tilting seemed to have less effect upon the UVSO at the higher tilt angles in that the temperature did not toggle following a solar panel tilt.

The IRR temperature was difficult to interpret, since several changes occurred simultaneously, but it did seem to track the PSE scan platform temperature. For example, stopping the PSE scan platform on L + 82 days resulted in a 1.1°C (2°F) drop in IRR temperature. On L + 87 days, the IRR was turned on at the same time the PSE scan rate was set to 4 deg/sec. The result was a decrease in IRR temperature of about 1.7°C (3°F). At L + 95 days the IRR was turned off, and the PSE scan rate returned to 1 deg/s, resulting in a temperature increase of 3.9°C (7°F). At L + 104 days, the solar panel was tilted from 45 to 58 deg and the PSE scan was started. This resulted in an IRR temperature decrease of 3.3°C (6°F), indicating a significant solar panel effect, especially since the PSE temperature increased.

The two MAG sensor package temperatures continued to increase with an obvious solar panel effect. The various flip sequences were also evident on the outboard magnetometer. During the gyro turn on sequence, the MAG was turned off, and the resultant temperature drop was 5.6°C (10°F) at an initial rate of 11.1°C (20°F)/hour. The HGA reflector temperatures followed the updated predictions reasonably well. The original temperature predictions did not consider the fact that the equation that locates the line of flight transducers on the reflector is a double-valued function; at clock angles between 180 and 360 deg, the T1 transducer is toward the Sun for all cone angles; for clock angles between 0 and 180, the T3 transducer is toward the Sun. Therefore at approximately L + 79 days, the relative position of the transducers to the Sun changed. The S/X-band feed temperature, E-670, followed the predict reasonably well in spite of the temperature

perturbations caused by the intermittent feed anomaly. The HGA boom temperature (E-758) still deviated significantly from the original predictions. A review of the analytical model showed that the antenna dish effects were ignored. It was believed that these effects coupled with an increased solar input contributed to the error. However, such simple additions to the model are not enough to explain the continued deviation as the antenna moves away from the boom, decreasing cone angles and increasing clock angles.

The lower thermal blanket temperature (E-753) was obviously sensitive to solar panel tilt angle. During STV testing, tests were conducted at 35-deg tilt and 2.0 solar constants (equivalent to L + 97 days), and at 70-deg tilt and 4.8 solar constants (L + 156 days).

The spacecraft sunshade (E-757) continued to perform remarkably well. The temperature was 121.7°C (251°F) compared to a predicted temperature of 220°F. The sunshade was exposed to a total of 3733 equivalent Sun hours. The estimated degradation in solar absorptivity was only 0.07 at L + 110 days. This indicated a considerable slowing in the rate of degradation.

The solar panel temperatures (E-871, -872, -873, -875, -876, and -877) continued to follow predictions reasonably well. The analytical model used for the flight predictions did not account for spacecraft-induced effects. The model was corrected for edge effects and predicted the leading and trailing edge temperatures reasonably well. Table 18 presents a summary of the solar panel temperatures. Figure 89 presents a schematic of the spacecraft showing the solar panel transducers and temperatures for several tilt angles. As can be seen, E871, E873, and E876 are all trailing edge transducers and are tracking one another closely. Transducers E872 and E877 are leading edge transducers under the sunshade, and they, too, are tracking each other reasonably well.

c.   Scan Platform.   As reported in Section VI-C-1, the TV optics heaters failed to function at launch resulting in platform temperatures well below those anticipated. At L + 76 days, a power-down sequence for gyro turn-on was conducted during which the propulsion/CPT supplemental heater (DC 64) was turned off. As this heater was turned off, the TV optics heaters began to function normally. (See Section VI-C-3-d for further discussion and the response of platform temperatures to optics heater recovery.) A chronology of platform power changes including this occurrence is given in Table 19.

The scan platform achieved thermal equilibrium in three significant power configurations since launch:

(1) TVS on, optics heaters off.

(2) TVS on, optics heaters on.

(3) TVS off, optics heaters on.

A summary of scan platform temperatures for these three modes is provided in Table 20. For comparison, the analytical predictions are also presented for the case of 0 W optics heater

Table 18. Solar panel temperature summary

Time (L time)	Solar flux, W/m² (BTU/ft²/h)	Tilt, deg	Average panel temperature, °C (°F)	Predicted $T_{leading}$, °C (°F)	Predicted $T_{trailing}$, °C (°F)	Actuals[a] E871 +X °C (°F)	Actuals[a] E873 +X °C (°F)	Actuals[a] E875 -X °C (°F)	Actuals[a] E876 -X °C (°F)
						Panel temperatures			
L + 45	1589.5 (504.2)	12	60 (140)	55 (131)	47.8 (118)	47.2 (117)	48.3 (119)		
L + 61	1802.9 (571.9)	12	71.1 (160)	65 (149)	57.8 (136)	58.3 (137)	59.4 (139)		
L + 74	2057.3 (652.6)	12	83.3 (182)	76.1 (169)	68.3 (155)	70 (158)	71.7 (161)		
L + 45	1589.5 (504.2)	40	41.1 (106)	36.1 (97)	30 (86)			33.3 (92)	32.2 (90)
L + 61	1802.9 (571.9)	40	51.7 (125)	46.1 (115)	38.9 (102)			43.9 (111)	42.2 (108)
L + 74	2057.3 (652.6)	40	62.8 (145)	56.1 (133)	48.9 (120)			54.4 (130)	53.3 (128)
L + 81	2204.5 (699.3)	45	61.1 (142)	55.5 (132)	48.3 (119)	49.4 (121)	50.5 (123)	54.4 (130)	52.2 (126)
L + 85	2342.6 (743.1)	45	65.5 (150)		52.8 (127)	55 (131)	55.5 (132)	60 (140)	57.8 (136)
L + 97	2736 (867.9)	45	78.9 (174)	72.8 (163)	65 (149)	67.8 (154)	68.3 (155)	73.9 (165)	71.1 (160)
L + 103	2944.4 (934.0)	45	86.1 (187)	79.4 (175)	71.1 (160)	75 (167)	75.6 (168)	82.2 (180)	78.3 (173)
L + 104	2987.6 (947.7)	58	62.2 (144)	56.7 (134)	49.4 (121)	51.1 (124)	51.7 (125)	58.3 (137)	53.3 (128)
L + 108	3212.7 (1019.1)	58	67.8 (154)	62.2 (144)	55 (131)	55.5 (132)	57.2 (135)	65 (149)	58.9 (138)
L + 118	3836.3 (1216.9	58	83.8 (182)	77.2 (171)	68.9 (156)	70 (158)	70.6 (159)	79.4 (175)	72.8 (163)
L + 118	3836.3 (1216.9)	66	60.6 (141)	55.5 (132)	48.3 (119)	47.2 (117)	47.8 (118)	57.8 (136)	49.4 (121)
L + 128	4703.8 (1492.1)	66	77.8 (172)	72.2 (162)	64.4 (148)	59.4 (139)[b]	61.1 (142)[b]	75.6 (168)	65 (149)
L + 137	5584.9 (1771.6)	66	93.9 (201)	86.7 (188)	78.3 (173)				
L + 137	5584.9 (1771.6)	71	73.3 (164)	67.8 (154)	60 (140)				
L + 147	6262.7 (1986.6)	71	83.3 (182)	77.2 (171)	69.4 (157)				
L + 156	6479.6 (2055.4)	71	86.7 (188)	80.6 (177)	83.3 (182)				

[a]E875 leading edge; E871, E873, E876, trailing edge.
[b]Not at 66 deg.
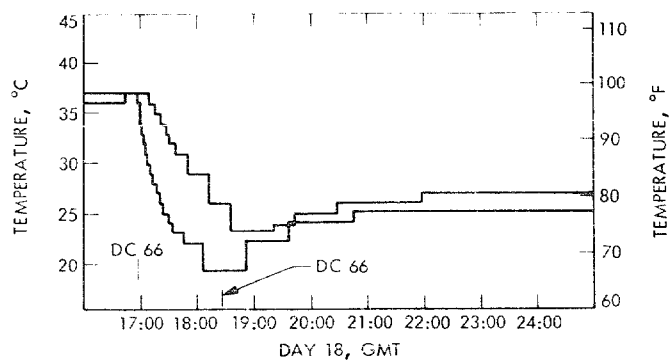
Fig. 85. Propulsion temperature
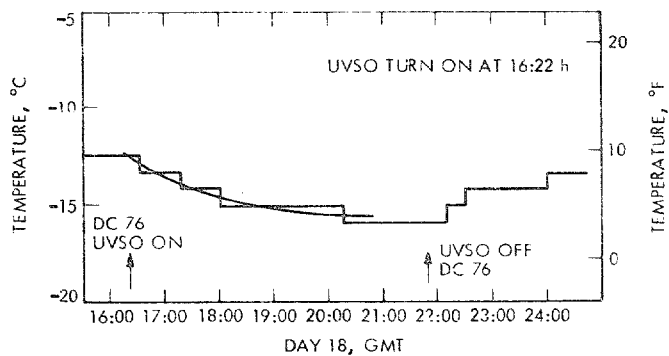
Fig. 88. UVSO temperature (E409)
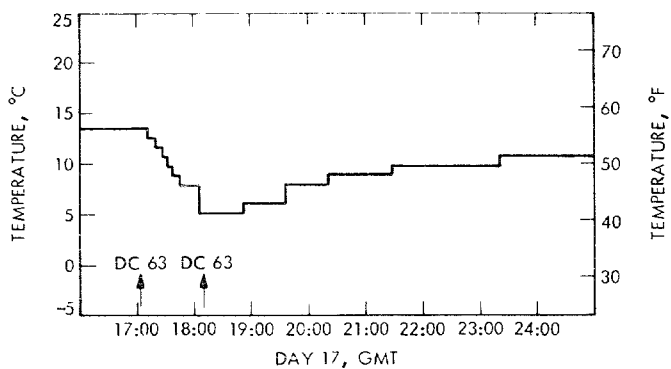
Fig. 86. PSE platform temperature
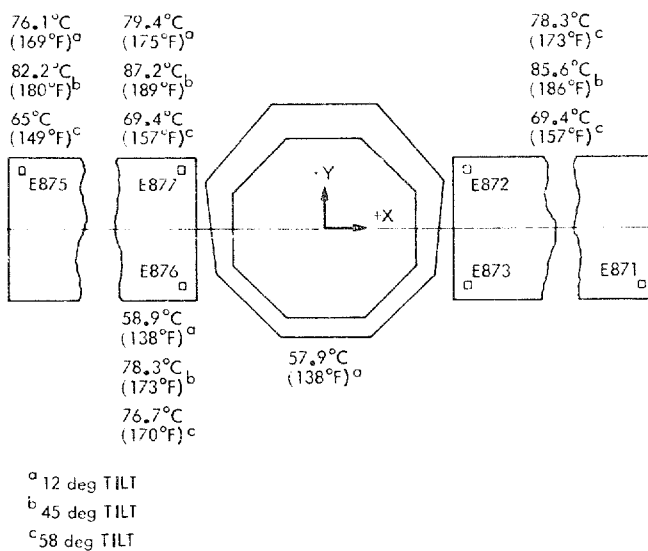
Fig. 89. Actual solar panel temperature distribution
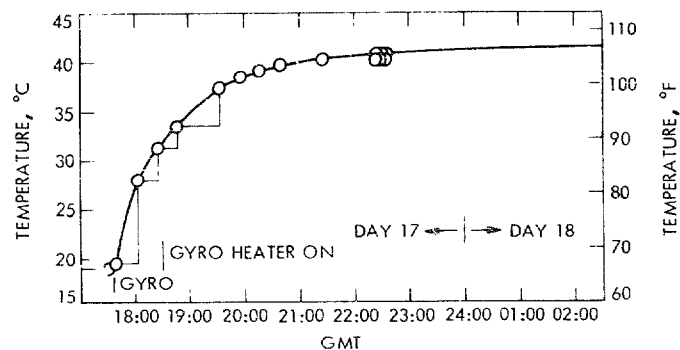
Fig. 87. Gyro temperature transient, TCM 2
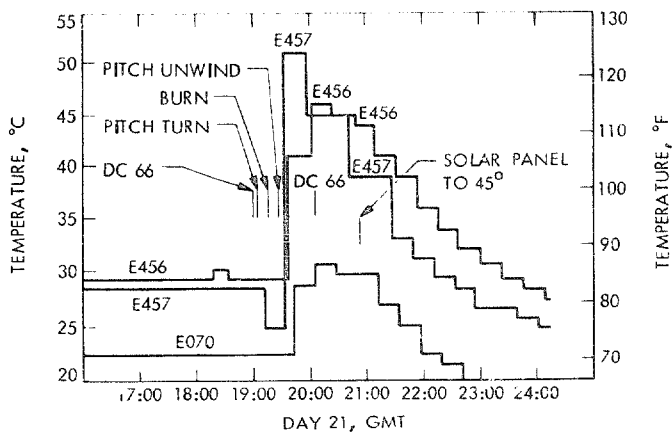
Fig. 90. Propulsion (E457), valve (E456), and TVCA (E070) temperatures for TCM 2
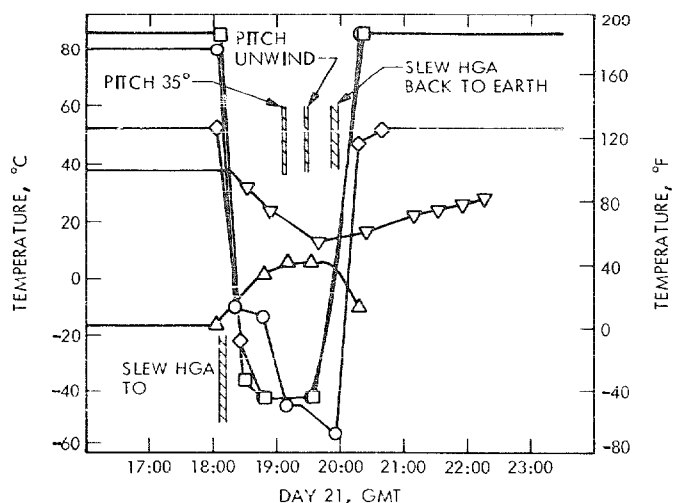
Fig. 91. TCM 2 high-gain antenna temperatures
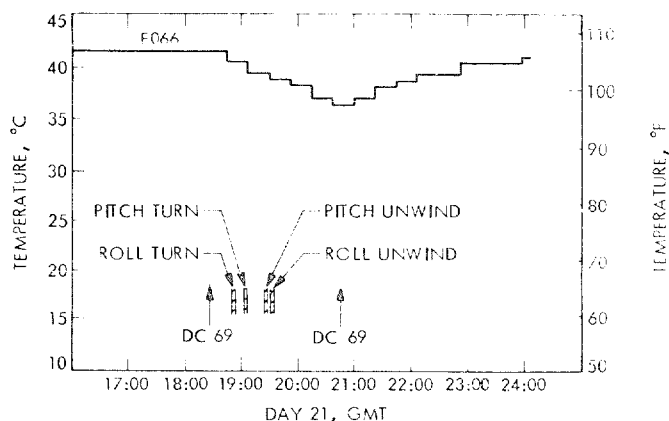
Fig. 94. Gyro temperature, TCM 2
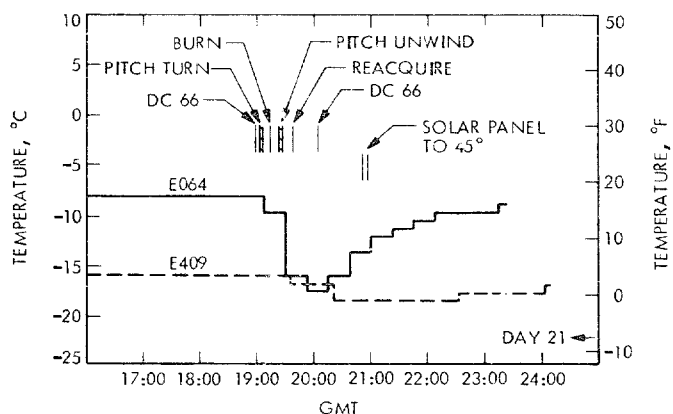
Fig. 92. Cruise sun sensor (E067) and UVSO (E409) temperatures, TCM 2
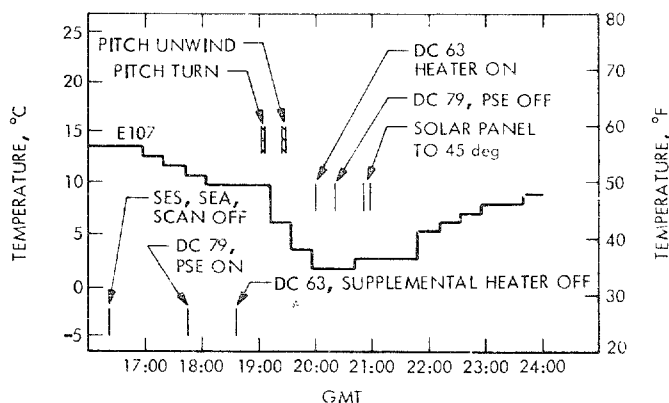
Fig. 95. PSE platform temperature, TCM 2
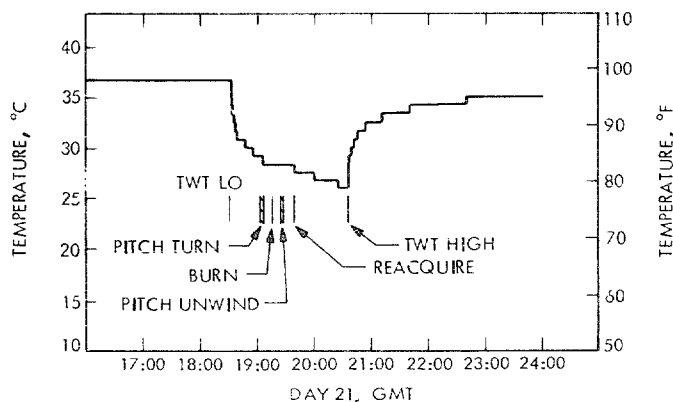
Fig. 93. TWTA base temperature, TCM 2
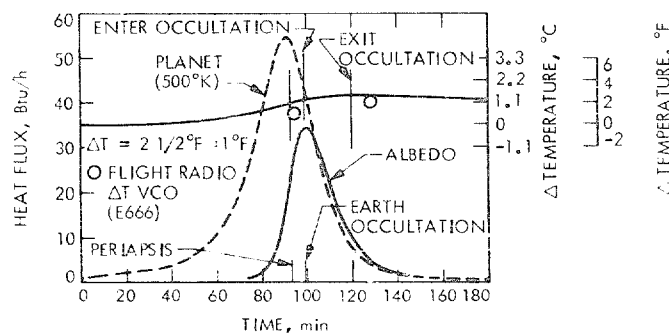
Fig. 96. Venus encounter heat loads
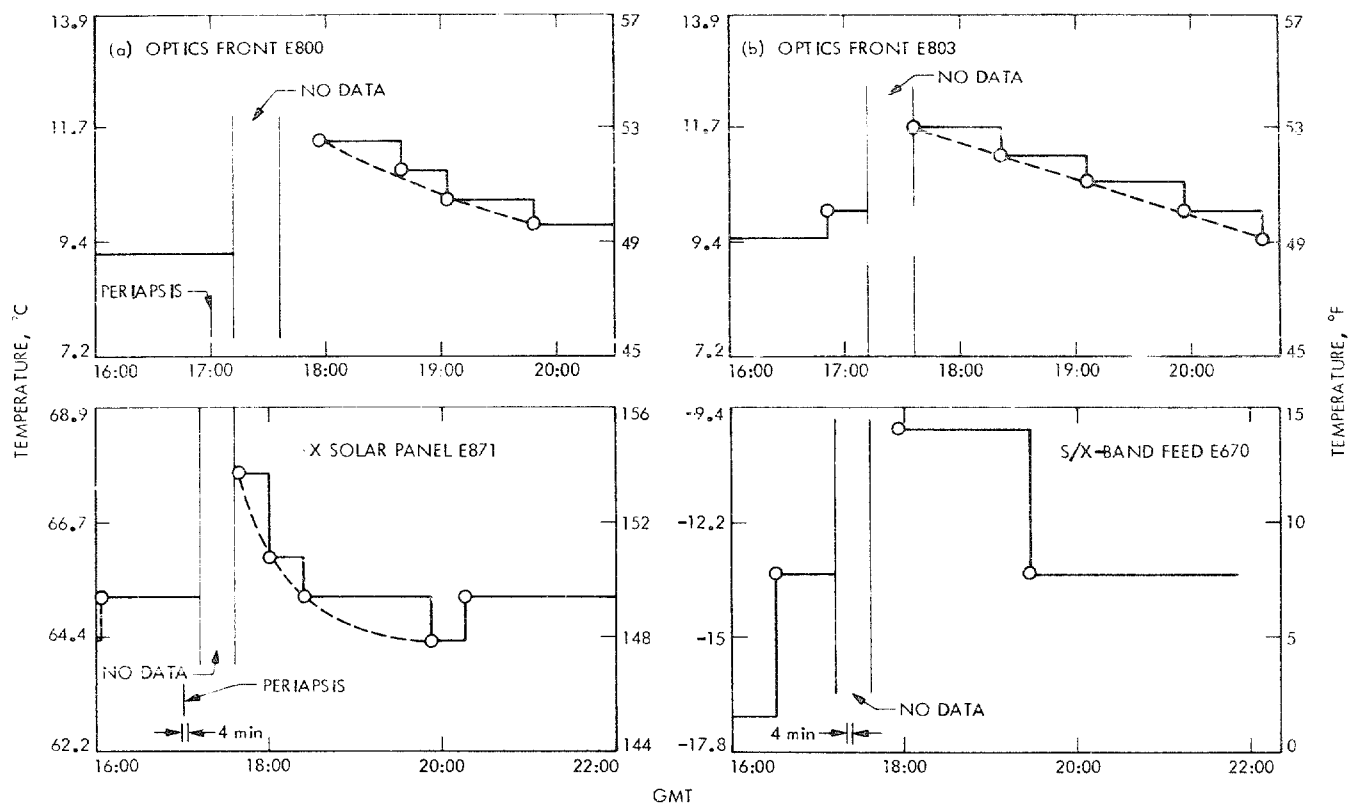
Fig. 97.   Mariner 10 Venus encounter
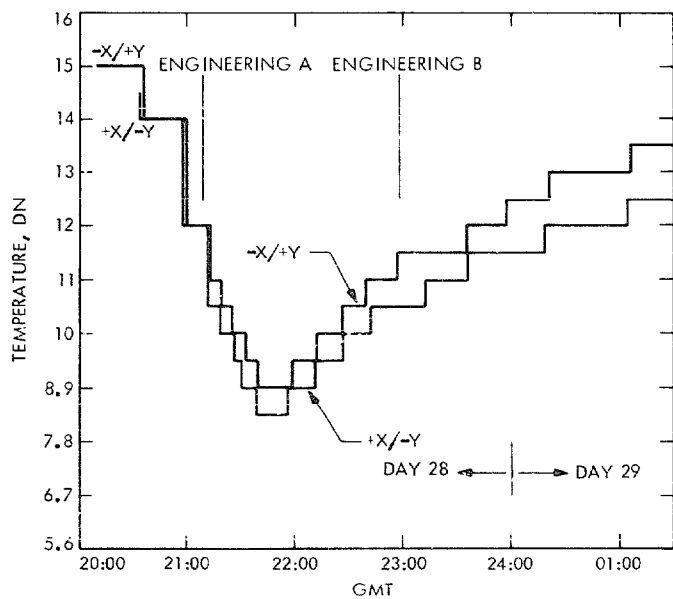
Fig. 98.   E068 (+X/-Y N$_2$) temperatures--
gyro anomaly, Day 028
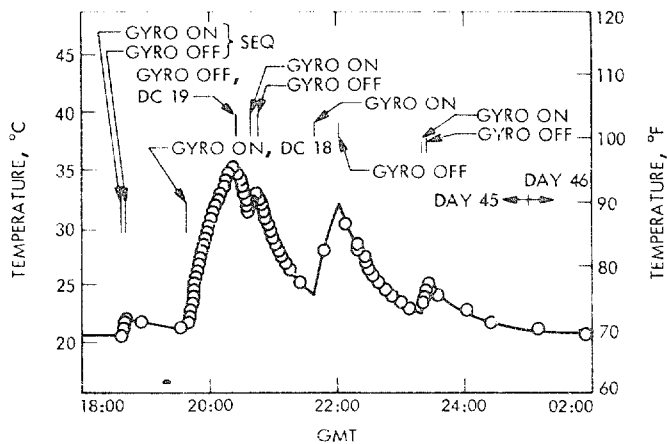
Fig. 99.   Gyro test, Day 045

Table 19. Platform power changes

L + Day	GMT		Event
	Day	h:min	
L + 74	016	16:54	Optics heater recovery in both/both state (8.3 W each)
L + 74	016	21:58	Heaters from both/both to low/low (8.3 W each to 3.7 W each)
L + 81	023	03:16	TVS off
L + 83	025	18:35	Heaters from low/low to high/high (3.7 W each to 6.0 W each)
L + 87	029	00:33	TVS on for Venus encounter
L + 98	040	21:39	TVS off after Venus
L + 99	041 to		TVS turned on for several hours each day for far encounter picture taking sequences
L + 101	043	18:33	TVS off

power dissipation (heater off) and for the case of 6.0-W optics heater power dissipation (heater on). The column headed ΔT is the difference between the predict and the flight temperatures. Since the analytical model is valid only for the case where the scan platform is stowed, the two operating cases show good agreement with the analysis. Therefore, the analytical model is adequate and provides reasonably accurate temperatures. Comparing the nonoperating case with the prediction gives about -11.7°C (-21°F) discrepancy. This difference is attributed to the effect of slewing the platform away from the upper blanket (higher cone angles), thereby exposing a greater area of the scan platform blanket to space.

d. TCM 2 Temperatures. A second trajectory correction was conducted prior to Venus encounter on GMT day 021. The power subsystem was "unloaded" to insure against any POR or battery share modes. All observed temperature responses to the maneuver were nominal. However, some responses were masked by the power subsystem "unloading." Figure 90 presents the propulsion module temperatures. The fact that the DC 66 heater was turned off prior to the turns complicates the soakback temperatures. The thrust-plate experienced a 27.2°C (49°F) rise in temperature due to the 3.75-s burn. The propellant valve experienced a 17.2°C (31°F) temperature rise and the TVCA a 8.4°C (15.5°F) rise in temperature. The expected soakback temperatures were significantly higher than those observed; expected valve ΔT was 37.8°C (68°F) and the expected ΔT at the TVCA was 20.5°C (37°F). Bus temperatures due to the pitch turn of 34.7 deg were minimal. Figure 91 presents the HGA temperatures for the HGA slew prior to and after the maneuver as well as during the maneuver. Figure 92 presents the cruise sun sensor and UVSO temperatures. Prior to the maneuver all supplemental heaters were turned off in order to "power down" the spacecraft, thus preventing a possible battery share mode. Figure 93 presents the TWT temperature transient when switched from high to low power and returned to high. Figure 94 presents the effect of DC 69 upon the gyros in Bay 7. Figure 95 presents the

PSE scan platform temperatures. The PSE scan was turned off, also the PSE and the supplemental heater. In all, the PSE scan package dropped 11.7°C (21°F) during the maneuver sequence, reaching a low of 1.7°C (35°F) — 1.7°C (3°F) above the flight temperature limit.

e. Venus Encounter. Temperature data during the Venus encounter sequence was not very dynamic. Venus closest approach (5800-km altitude) occurred at 17:01 on GMT day 036. Real-time data was lost from 17:12 until 17:36 as the spacecraft was occulted from the Earth by the planet. Figure 96 presents the performance of the radio bay (Bay 4) during the encounter. Presented in the figure are the calculated planet emitted and reflected heat loads on the Bay 4 shear-plate. Also shown is the calculated temperature rise of the Bay 4 shear-plate and radio components. The circles represent the actual flight spacecraft data for the VCO (E666). Figure 97 presents four of the most active temperatures on the spacecraft. First are the two TV optics temperatures which increased about 2.2°C (4°F) during encounter. The +X solar panel outboard transducer (E871) showed a 3.3°C (6°F) increase and the HGA S/X feed about 7°C (12.6°F). The HGA feed performance did not vary during this temperature transient.

f. Temperature Data Associated With Spacecraft Anomalies. An anomaly occurred on GMT day 028 21:00 hours at the conclusion of the roll calibration maneuver No. 7 (RCM 7). The roll axis began to oscillate and blow gas in both pairs of roll gas jets. The gyros were turned off at 21:37 and a normal cruise state was reestablished. Approximately 544 g (1.2 lbm) of gas was expended during the anomaly. Figure 98 presents the gas bottle temperatures during the anomaly. There was no change in gyro temperature. Beginning at 1833 on GMT day 045, a special gyro test was conducted to determine the condition of the roll gyro and to verify various postulated failure modes. Figure 99 presents the gyro temperature data from this test. The data indicates no degradation of the gyro which would change its temperature signature. At approximately

Table 20. Comparison of flight and predicted temperatures

| | Prediction | | Flight data | | | | | |
| | 0 W heater, °C (°F) | 6.0 W heater, °C (°F) | TVS on, heater off, scan stowed | | TVS on, heater on, scan stowed | | TVS off, heater on, scan at 157 deg cone | |
			Temperature °C (°F)	ΔT	Temperature °C (°F)	ΔT	Temperature °C (°F)	ΔT
Nonoperating								
TVA optics front	-32.2 (-26)	2.2 (36)					-8.9 (16)	-11.1 (-20)
TVA optics rear	-26.7 (-16)	6.7 (44)					-6.1 (21)	-12.8 (-23)
TVA	-21.1 (-6)	12.2 (54)					0.5 (33)	-11.7 (-21)
TVB optics front	-31.7 (-25)	2.8 (37)					-8.9 (16)	-11.7 (-21)
TVB optics rear	-26.1 (-15)	7.2 (45)					-5.5 (22)	-12.8 (-23)
TVB	-20.5 (-5)	12.8 (55)					0.5 (33)	-12.2 (-22)
AES	-36.1 (-33)	0 (32)					-9.4 (15)	-9.4 (-17)
UVSA	-24.4 (-12)	8.3 (47)					-3.9 (25)	-12.2 (-22)
APA	-26.7 (-16)	7.2 (45)						
Operating								
TVA optics front	-21.1 (-6)	8.9 (48)	—		10 (50)	1.1 (+2)		
TVA optics rear	-13.9 (7)	14.4 (58)	-16.1 (3)	-2.8 (-5)	12.8 (55)	-1.7 (-3)		
TVA	-5 (23)	22.8 (73)	-5.6 (22)	-0.56 (-1)	22.2 (72)	-0.56 (-1)		
TVB optics front	-20 (-4)	10 (50)	—	—	9.4 (49)	-0.56 (-1)		
TVB optics rear	-12.8 (9)	15.5 (60)	-13.3 (8)	-0.56 (-1)	13.9 (57)	-1.7 (-3)		
TVB	-4.4 (24)	22.8 (73)	-4.4 (24)	0	21.7 (71)	-1.1 (-2)		
AES	-18.9 (-2)	8.9 (48)	-15 (5)	3.9 (+7)	10.5 (51)	1.7 (+3)		
UVSA	-11.7 (11)	16.1 (61)	-8.9 (16)	2.8 (+5)	14.4 (58)	1.7 (+3)		
APA	-16.7 (2)	12.2 (54)						

07:12 on GMT day 049, Canopus was lost and the gyros came on. The gyro temperature data is presented in Fig. 100.

Since the initial partial failure of the S-band feed on L + 52 days, the failure has completely healed twice, partially healed once and partially failed six times. The temperature changes resulting from these various changes in the condition of the feed are presented in Table 21.

On L + 76 days, when the TV optics heaters began to function, the turning off of the propulsion/CPT supplemental heater (DC 64) apparently removed the postulated ground fault that had previously prevented the FDS MOSFET switches from closing. Figure 101 shows the temperature response of the scan platform to the recovery of the heaters which came on in the both/both state (8.3 W per camera).

4. Performance from Launch + 110 Days Through Launch + 163 Days

The 55-day period between L + 110 days and L + 163 days included the following events of primary thermal significance.

(1) The third trajectory correction maneuver (TCM3) at 3.88 suns.

(2) Mercury encounter with an 8-min solar occultation at 4.60 suns.

(3) Spacecraft perihelion at 4.79 suns.

One major spacecraft anomaly occurred during this period. The Day 090 (L + 148 days) power anomaly occurred the day after Mercury closest approach and caused a large additional and permanent power dissipation in Bay 1. The thermal consequences of each of these anomalies will be discussed in detail later in this report.

During this period, the solar flux at the spacecraft progressed from 0.33 W/cm^2 (305.3 W/ft^2) (2.42 suns) at L + 110 days to 0.65 W/cm^2 (603.2 W/ft^2) (4.79 suns) at perihelion (L + 153 days), then back to 0.6 W/cm^2 (553.6 W/ft^2) (4.40 suns) at L + 165 days. The total accumulated solar exposure was 8763 equivalent sun hours (ESH).

a. Summary. The only mechanical devices function performed during this period was the deployment of the low-gain antenna to its third position. This event occurred successfully on Day 098 (L + 156). Success was verified by telecommunications performance, since there is no microswitch indication for the third position.

The overall spacecraft thermal performance was normal with most spacecraft temperatures following predictions. The most troublesome of the temperatures not following predicts was the HGA boom temperature which exceeded its upper FA temperature for a period of several days between L + 147 and L + 154 days. The temperatures of most sunlit components of the spacecraft were higher than predicted due to an increase in solar absorptance resulting from prolonged exposure to the solar environment.

Table 21. HGA anomaly temperature data and derived feed power dissipation

Occurrence No.	Day	Before occurrence		After occurrence		ΔT, °C		ΔP, W
		Temperature, °C (°F)	Power, W	Temperature, °C (°F)	Power, W			
1	L + 52	-51 (-59.8)	1.07	-39.4 (-39.0)	2.77	11.5 (+20.8)		-1.70[a]
2	L + 56	-36.4 (-33.5)	2.38	-48.2 (-54.7)	0.68	-11.8 (-21.2)		-1.70[a]
3	L + 56	-48.2 (-54.7)	0.68	-36.4 (-33.5)	2.38	11.8 (+21.2)		+1.70[a]
4	L + 62	-30.1 (-22.2)	2.25	-36.4 (-33.5)	1.34	-6.3 (-11.3)		-0.91
5	L + 65	-33.3 (-27.9)	1.28	-23.7 (-10.6)	2.82	9.6 (+17.3)		+1.54[a]
6	L + 93	-9.9 (+14.1)	1.72	-9.9 (+14.1)	1.72	0	0	b
7	L + 93	-9.9 (+14.1)	1.72	-9.9 (+14.1)	1.72	0	0	b
8	L + 99	-13.4 (-7.8)	0.89	-13.4 (+7.8)	0.89	0	0	b
9	L + 107	-13.4 (+7.8)	0.89	-16.9 (+1.5)	0.17	-3.5 (-6.3)		-0.72
10	L + 108	-16.9 (+1.5)	0.17	-13.4 (+7.8)	0.89	3.5 (+6.3)		+0.72

[a]Tolerance +0.1 W
All other power Nos. ±0.8 W

[b]Since 1 DN ≈ 14.2°C (6.5°F), a ΔP of ≈0.8 W is possible with no apparent ΔT.

b. Temperature Control Performance

(1) Comparison of Flight Temperatures versus Predicts. Overall temperature control performance was reasonably close to that predicted. The single spacecraft temperature measurement that persistently eluded all attempts to predict its behavior was the HGA boom temperature (Fig. 102). The most probable reasons for this difficulty are: (a) the complex nature of an accurate analytical model, caused primarily by the varying HGA geometry, and (b) the likelihood of degradation in the solar absorptance of painted portions of the boom.

It is interesting to note that both the HGA boom temperature and the HGA S/X feed temperature (Fig. 103) abruptly start increasing at L + 140 days from previous temperature levels that are relatively steady. Although neither of these increases was predicted, closer study reveals that the HGA pointing vector passed through a cone angle of 90 deg on L + 140 days and continued to decrease as shown in Fig. 103. The probable explanation for the feed increase, therefore, is the effect of the additional solar load on the feed that is diffusely reflected from the concave side of the dish. The boom temperature may be responding to the same stimulus, but instead of the additional heat load consisting of reflected solar energy, the input would be reradiated IR from the back of the dish to the boom radiator located on the anti-Sun side of the boom.

Table 22 compares the actual flight temperatures at Mercury against those predicted prior to launch (Bibliographic ref. 7). The comparison shows the spacecraft to be generally warmer at Mercury than predicted, the only significant exception being the scan platform.

Table 23 lists the differences between actual flight temperatures and STV test temperatures for selected spacecraft components. The only corrections made to the raw STV test data are for power state differences and the solar intensity difference between the 4.8-sun STV test mode and the 4.6-sun actual Mercury encounter. The results of this comparison shown in Table 23 lead to the following conclusions.

(a) The fact that the flight bus temperatures match STV test temperatures so closely indicates that the STV simulation was of very high fidelity and that the bus is relatively insensitive to degradation in the solar absorptance of the spacecraft sunshade.

(b) The sun sensor and UVSO, both located under the same Alzak (clear anodized, polished aluminum) sunshade, were obviously the victims of degradation in the Alzak solar absorptance.

(c) The only other piece of Alzak on the spacecraft serves as the sunlit layer of the TVCA heat shield, and yet the TVCA, thrustplate, and propellant tank temperatures all decreased during the mission relative to the STV test data. This peculiar behavior becomes consistent with (b) above when one remembers that at the conclusion of the STV test, the Alzak surface of the TVCA heat shield was noted to have severely discolored, whereas this discoloration was conspicuously absent from the UVSO Sun sensor shade. Post-test measurements indicated that the average solar absorptance of the TVCA heat shield had increased almost 100% during the course of the test, while the absorptance of the UVSO/sun sensor shade was virtually unchanged. Since the flight predicts were based on STV test results, it is apparent that the TVCA heat shield degradation was greater during the STV test than during flight, and that the opposite was true for the UVSO/sun sensor shade.

(d) The Canopus Tracker remained below STV temperatures throughout the mission. Post-launch analysis (see PFR 5004) uncovered the fact that the tracker dissipates less internal power when acquired than it does when viewing a dark field. Hence, by obscuring the tracker field of view during STV, the power is increased above the flight value resulting in an unconservative temperature at the low end of the flight temperature range. Similar trackers have been flown on previous Mariners, but previous thermal designs have conductively coupled those trackers to the bus structure. Since the MVM tracker is somewhat decoupled from the bus, it is much more sensitive to small power changes. This would explain why large temperature differences between STV and flight have not been observed with previous trackers.

(2) Mercury Encounter Thermal Performance. Mercury encounter occurred on Day 088 (L + 146 days). The spacecraft passed through the dual occultation zone (Earth and Sun) at a closest approach altitude of 704 km from the planet surface. The encounter timetable is listed in Table 24.

The spacecraft temperature transients resulting from proximity to the planet and the solar occultation were generally mild with the exception of the low mass, sunlit appendage items such as the high-gain antenna, solar panels, and the spacecraft sunshade.

A temperature predict was generated for the radio bay (Bay 4) response to the encounter. Both the predict and the actual data are shown in Fig. 104. The predict indicated that the planetary effect was predominant, whereas the actual data shows a greater effect due to the solar occultation. The temperature changes were so small, however, that the predict inaccuracy did not prevent rapid signal reacquisition at Earth occultation exit and consequent satisfaction of radio science objectives.

Figures 105 through 109 show the encounter transients for the gyros, high-gain antenna, both solar panels, and the spacecraft sunshade, respectively.
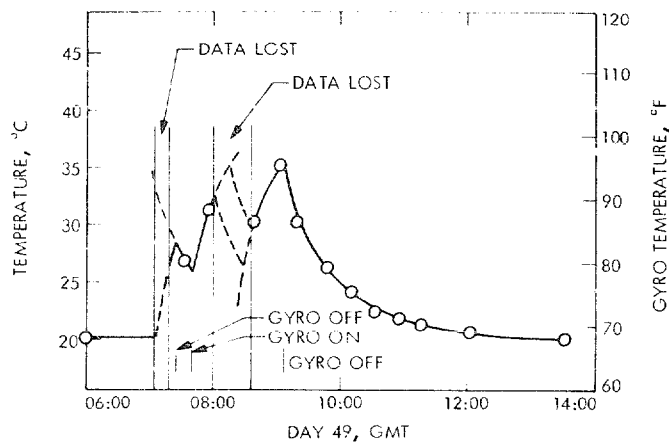
Fig. 100. Day 049 anomaly--lost Canopus/gyros ON
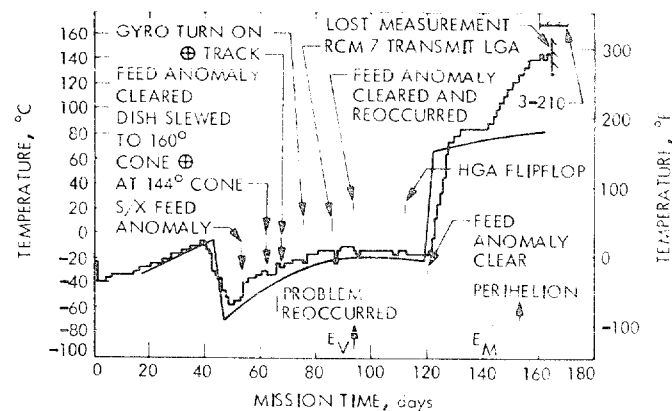
Fig. 103. S/X-band feed (E670) temperature
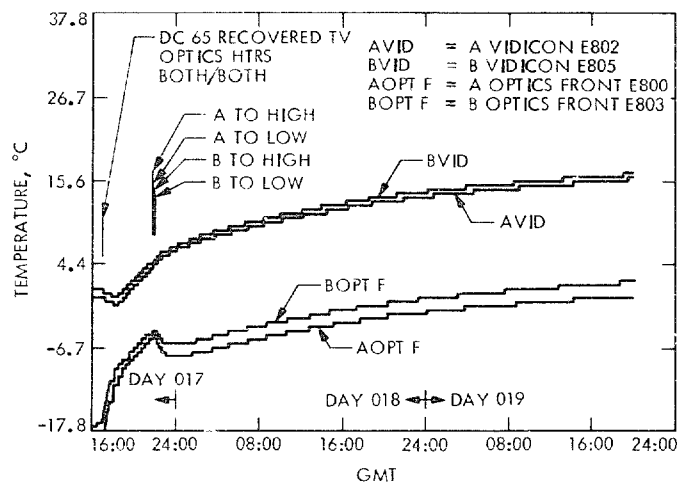
Fig. 101. TV temperatures resulting from TV optic heater recovery
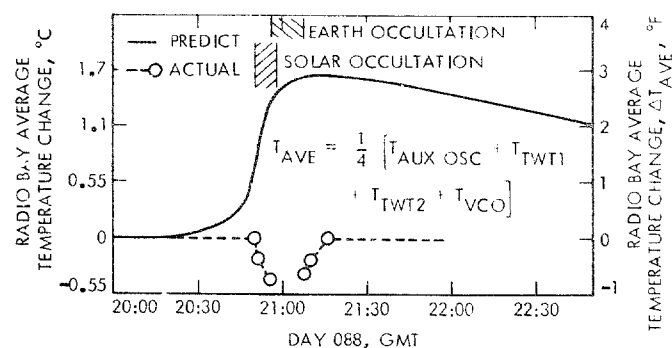
Fig. 104. Radio bay (Bay 4) average temperature response-- Mercury encounter

$$T_{AVE} = \frac{1}{4}\left[T_{AUX\ OSC} + T_{TWT1} + T_{TWT2} + T_{VCO}\right]$$
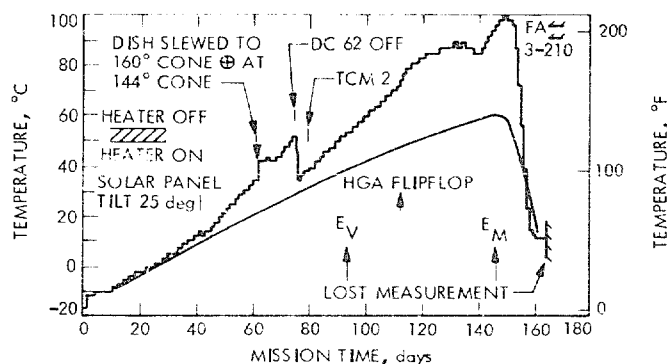
Fig. 102. High-gain antenna boom (E758) temperature
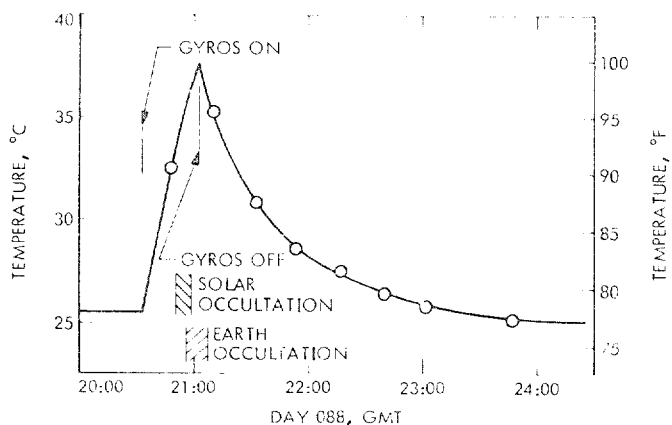
Fig. 105. Gyro temperature (E066) transient at Mercury encounter
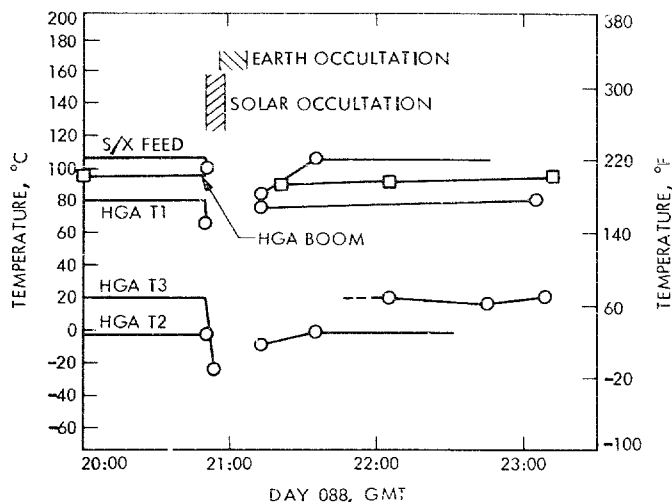
Fig. 106. High-gain antenna response to solar occultation at Mercury
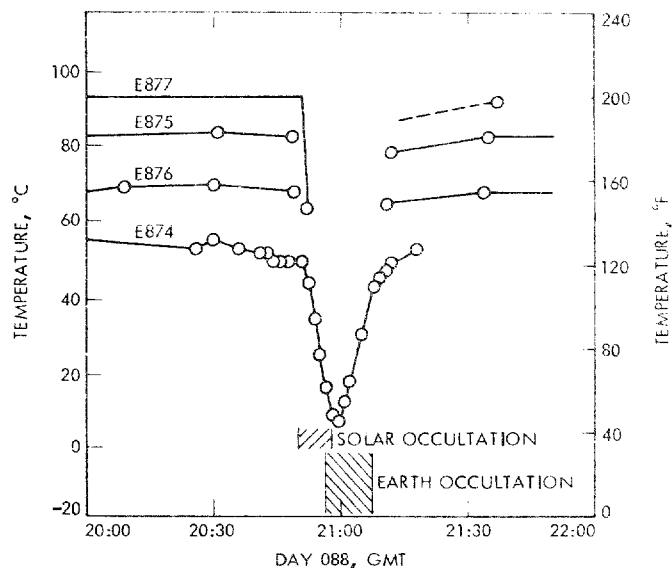
Fig. 108. -X solar panel temperatures--solar occultation at Mercury
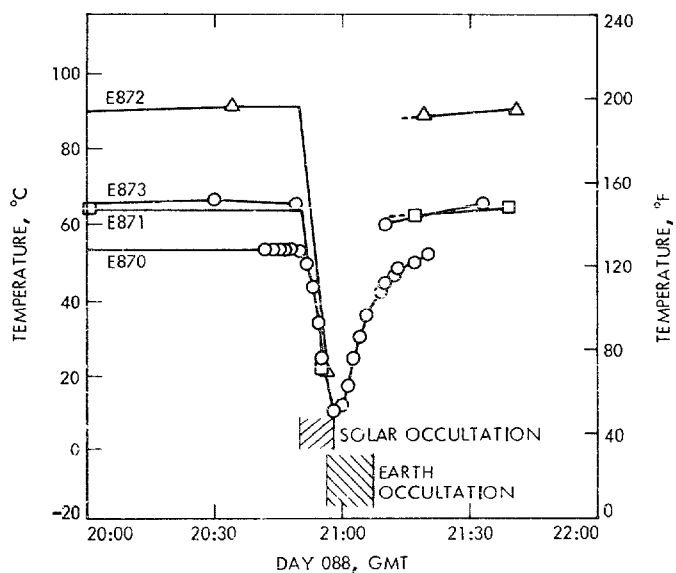
Fig. 107. +X solar panel temperatures--solar occultation at Mercury
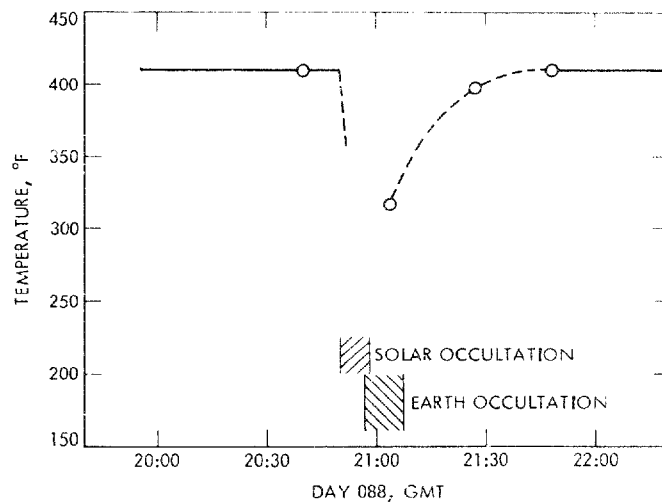
Fig. 109. Sunshade temperature response to Mercury solar occultation

Table 22. Flight temperatures versus prelaunch predicts at Mercury

MTC channel No.	Temperature measurement description	☿ Encounter L + 146-1/2 °C	(°F)	Prelaunch predicts °C	(°F)	ΔFlight-Predicted °C	(°F)	
065	Canopus tracker	4.4	(40)	7.2	(45)	-2.8	(-5)	Gyro heater on
066	GCA	25.5	(78)	17.2	(63)	8.3	(15)	
067	Sun Sensor	40.5	(105)	26.1	(79)	14.4	(26)	Alzak degradation
068	+X/-Y N2	20.5	(69)	17.2	(63)	3.3	(6)	
069	-X/+Y N2	23.3	(74)	18.3	(65)	5	(9)	
070	TVCA	75.6	(168)	69.4	(157)	6.1	(11)	
106	PSE Electronics	30	(86)	26.1	(79)	3.9	(7)	
107	PSE Platform	29.4	(85)	19.4	(67)	10	(18)	
301	CPT	3.3	(38)	-0.6	(31)	3.9	(7)	
408	UVSA	10.5	(51)	18.3	(65)	-7.8	(-14)	
409	UVSO	24.4	(76)	14.4	(58)	10	(18)	Alzak degradation
454	Prop N2	30	(86)	30	(86)	0	(0)	
455	Propellant	31.1	(88)	31.7	(89)	-0.5	(-1)	
456	Valve	58.9	(138)	52.2	(126)	6.7	(12)	
457	Thrustplate	60	(140)	57.2	(135)	2.8	(5)	
500	IRR	29.4	(85)	24.4	(76)	5	(9)	
602	Mag A	-20	(-4)	-11.1	(12)	-8.9	(-16)	
603	Mag B	-12.2	(10)	-10.5	(13)	-1.7	(-3)	
604	Mag Elect.	35	(95)	32.2	(90)	2.8	(5)	
605	Mag Proc.	36.1	(97)	34.4	(94)	1.7	(3)	
663	Aux. oscillator	31.1	(88)	29.4	(85)	1.7	(3)	
664	TWT 1	44.4	(112)	40.5	(105)	3.9	(7)	
665	TWT 2	35	(95)	32.8	(91)	2.2	(4)	
666	VCO	28.9	(84)	25.5	(78)	3.3	(6)	
667	Dish 1	80.6	(177)		—			
668	Dish 2	-5.5	(22)		—			
669	Dish 3	16.1	(61)		—			
670	S X Feed	105.5	(222)		—			
671	X-band transmitter	23.3	(74)	21.7	(71)	1.7	(3)	
750	Bay 1	20.5	(69)	18.3	(65)	2.2	(4)	
751	Bay 2	20.5	(69)	17.8	(64)	2.8	(5)	
752	Bay 3	22.2	(72)	19.4	(67)	2.8	(5)	
753	Lower blanket	-8.3	(17)	-6.1	(21)	-2.2	(-4)	
754	Bay 5	25	(77)	22.2	(72)	1.7	(3)	
755	Bay 6	23.3	(74)	20	(68)	3.3	(6)	
756	Bay 7	22.2	(72)	17.8	(64)	4.4	(8)	Gyros on
757	Sunshade	210.5	(411)	148.9	(300)	61.7	(111)	Beta cloth degradation
758	HGA Boom	95	(203)		—		—	
800	TVA Opt F	5.5	(42)	11.1	(52)	-5.5	(-10)	
801	TVA Opt R	9.4	(49)	16.7	(62)	-7.2	(-13)	
802	TVA VID	18.9	(66)	25	(77)	-6.1	(-11)	
803	TVB Opt F	5.5	(42)	12.2	(54)	-6.7	(-12)	Effect of slewing platform away from stowed position
804	TVB Opt R	10.5	(51)	17.8	(64)	-7.2	(-13)	
805	TVB VID	18.9	(66)	25	(77)	-6.1	(-11)	
806	AES	7.8	(46)	11.1	(52)	-3.3	(-6)	
869	Battery	20	(68)	16.7	(62)	3.3	(6)	
870	+X S/P 1	52.2	(126)					
871	+X S/P 2	62.8	(145)					
872	+X S/P 3	90	(194)					
873	+X S/P 4	65	(149)					
874	-X S/P 1	53.3	(128)					
875	-X S/P 2	82.2	(180)					
876	-X S/P 3	68.3	(155)					
877	-X S/P 4	92.2	(198)					

Table 23. Temperature comparisons - flight versus STV test

Item	⊕ 1.0 Suns ΔT,[a] °C (°F)	♀ 2.0 Suns ΔT,[a] °C (°F)	☿ 4.6 Suns ΔT,[a] °C (°F)
Bus			
Bay 1	-0.5 (-1)	0 (0)	-0.5 (-1)
Bay 2	-1.1 (-2)	-0.5 (-1)	0 (0)
Bay 3	-1.1 (-2)	-0.5 (-1)	-0.5 (-1)
Bay 4	-0.5 (-1)	-1.1 (-2)	0 (0)
Bay 5	0.5 (1)	0.5 (1)	0 (0)
Bay 6	2.2 (4)	0.5 (1)	0.5 (1)
Bay 7	0 (0)	0.5 (1)	0 (0)
Bay 8	0 (0)	0.5 (1)	0 (0)
Canopus tracker	-8.3 (-15)	-5 (-9)	-6.1 (-11)
Charged particle telescope	-1.1 (-2)	0 (0)	0 (0)
Propellant			
TVCA	-2.8 (-5)	-3.9 (-7)	-9.4 (-17)
Thrustplate	-1.7 (-3)	-2.8 (-5)	-6.1 (-11)
Propellant tank	0.5 (1)	0 (0)	-3.3 (-6)
Appendages			
Infrared radiometer	-1.1 (-2)	1.7 (3)	0 (0)
Sun sensor	-0.5 (-1)	5 (9)	11.7 (21)
UVS occultation	-0.5 (-1)	3.3 (6)	7.2 (13)

[a] $\Delta T = T_{flight} - T_{stv}$ where T_{stv} is corrected to correspond to the flight power configuration and to the Mercury solar intensity of 4.6 suns.

Table 24. Mercury encounter timetable

Event	Time (GMT)[a]
Gyros on	20:33:30
Enter penumbra	20:50:19
Enter umbra	20:50:23
Closest approach	20:55:09
Enter Earth occultation	20:56:25
Exit umbra	20:57:47
Exit penumbra	20:57:52
Exit earth occultation	21:03:05
Gyros off	21:07:39

[a] Times are in ERT (earth-received time)

(3) TCM-3 Thermal Performance. The third trajectory correction maneuver was performed on Day 075 (L + 133 days) with the following maneuver parameters:

Burn time start (ERT)	12:00:52 GMT
Burn duration	51.126 sec
ΔV	17.832 m/sec
Turns	None
Scan platform position	121 clock 143 cone
High-gain antenna position	80 clock 103 cone

Subsequent to the roll axis anomaly which occurred on Day 028 (L + 86 days), it was decided that future maneuvers would be constrained to be sunline maneuvers only (i.e., no turns), in order to minimize gyro-on time and eliminate commanded turns, thereby minimizing

NOMINAL AiM POINT

B • T ≈ 3590, TCA ≈ GMT DAY 088 20:30

B • R ≈ 525

MERCURY

B • R

B • T

E_v + 34 days

E_v + 41 days

SUNLINE MANEUVER DIRECTIONS

POST-TCM-3 DISPERSIONS

DUAL OCCULTATION ZONE

FREE RETURN CONTOUR

UNCORRECTED FLYBY POINT

B • T ≈ -12, 300 km

B • R ≈ 4220 km

TCA ≈ GMT DAY 088 20:211

Fig. 110. Post-Venus trajectory correction option

Fig. 111. TCM 3 temperature transients for TVCA (E070), thrustplate (E457), valve (E456), and GCA (E066)

Fig. 112. Comparison of the peak soakback temperatures from TCM 3 to those of TCM 1 and TCM 2: (a) TVCA actuators, (b) TVCA support ring

(a) TVCA ACTUATORS

DEVELOPMENT TEST

CALIB TEST

△ TEST DATA
O FLIGHT DATA

SOAKBACK ΔT, °C

(b) TVCA SUPPORT RING

BURN TIME, s

(a) THRUSTPLATE E457

SOAKBACK ΔT, °C

SOAKBACK ΔT, °F

△ TEST DATA
O FLIGHT DATA

Fig. 114. Apparent Beta cloth
degradation

RATE 1.95·10⁻⁵ ESH

VENUS

MERCURY
PERIHELION

APPARENT α ε AT LAUNCH

ESH

(b) PROPULSION VALVE

BURN TIME, s

-X
66 deg TO 60 deg

-X
66 deg TO 76 deg

-X
60 deg TO 76 deg

E872

E877

DATA MODE 1

DATA MODE 1

E871

E876

-X
76 deg
TO 60 deg

E877

E872

E876
E875

E871

0 DN

TEMPERATURE, °C

TEMPERATURE, °F

GMT
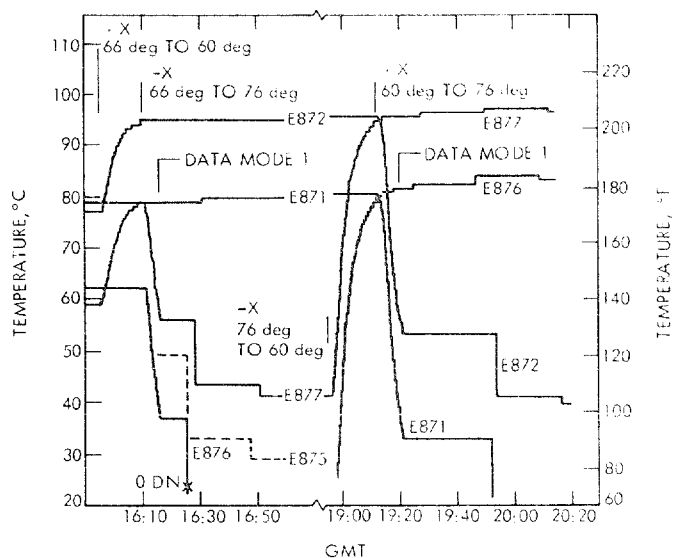
Fig. 115. Solar panel tilt test,
GMT Day 068

Fig. 113. Comparison of the peak soakback
temperatures from TCM 3 to those
of TCM 1 and TCM 2, (a) thrustplate,
(b) propulsion valve

the chance of a large attitude-control gas loss. Fortunately, the trajectory correction required to reach the aim point at Mercury was such that a sunline maneuver would suffice with only a small sacrifice in time of arrival. Once a maneuver is constrained to be sunline, however, the only design variables become the time at which the maneuver is performed (fixes the correction direction) and the applied impulse or ΔV (fixes the magnitude of the correction). For this reason the maneuver had to be performed much later than anticipated and at a much greater solar intensity (3.88 suns). Figure 110 shows the trajectory geometry for TCM-3 and Table 25 contains the timeline.

This maneuver was quite interesting from the thermal point of view since it was of long enough burn duration to elicit a significant temperature response, and the propulsion module temperature data was not confused by the thermal perturbations caused by spacecraft turns.

Figure 111 shows the propulsion module temperature data. Figures 112 and 113 compare the peak soakback temperatures from TCM-3 to the peaks from TCM-1 and -2, all of which are compared against the data obtained during pre-launch calibration tests at ETS. It would appear that the ETS data is conservative; however, none of the in-flight burns were of long enough duration to confirm this observation.

(4) Beta Cloth Sunshade Degradation. A preliminary comparison of the spacecraft sunshade temperature against solar fluence through the mission yields the data presented in Fig. 114 as solar absorptance to emittance ratio versus equivalent hours at one Earth Sun (ESH). It is interesting to note that the degradation increased linearly in terms of equivalent sun hours since before Venus encounter (fluence to Venus was ~2900 ESH). The sunshade temperature at Mercury encounter was 211°C (411°F), corresponding to an absorptance to emittance ratio α/ϵ of 0.494. Extrapolating this linear rate of increase in α/ϵ to Mercury II at about 17,000 ESH yields an α/ϵ of 0.69 and a resultant sunshade temperature of approximately 260°C (500°F), still well within the temperature capability of the Beta cloth [maximum design temperature 315°C (600°F)].

(5) Solar Panel Tilt Test Temperature Data. On Day 068 (L + 126 days), a solar panel tilt test was performed for the purpose of evaluating solar panel power performance. Figure 115 shows the transient data from two transducers on each of the two solar panels. Only the first two tilts for each panel are included. Table 26 lists the steady-state temperatures for each tilt position of each panel. Since the test occurred over the pace of two days during which the solar intensity increased 4%, the data in Table 26 is all normalized to 3.3 suns.

During this same test, on Day 069 (L + 127 days), the -X solar panel was accidentally tilted to 50 deg at a solar intensity of 3.37 suns. It was intended to increment the +X panel from 60 to 76 deg; however, the incremental command was addressed to the wrong panel resulting in a -X increment from 66 to 50 deg.

The temperature data for this incident is shown in Fig. 116. The maximum cell

Table 25. TCM 3 timeline, Day 075 (L + 134 days)

Spacecraft event time[a]	Event
10:56:08	Slew scan platform to maneuver position
11:11:08	PSE off
11:32:08	Slew high-gain antenna to maneuver position
11:49:30	7M1, gyros ON
11:52:42	All axis inertial
11:54:42	Burn start
11:55:33	Burn stop
12:01:08	Reposition high-gain antenna
12:32:08	PSE power ON
13:22:08	Reposition scan platform

[a]One-way light time = 6 min, 6.4 s

temperature calculated from the telemetry data was 133°C (272°F) compared to the FA temperature of 120°C (248°F) and the TA of 140°C (284°F). No solar panel damage or degradation was noted as the result of this occurrence.

(6) High-Gain Antenna Flip-Flop Temperature Data. On Day 053 (L + 111 days), the HGA was slewed in order to relieve the situation whereby the HGA coax cables were being wrapped about the boom as the antenna continuously tracked the Earth. Both the boom and the dish actuator were rotated 180 deg, thereby returning the dish to its initial pointing direction and at the same time "unwrapping" the cables 180 deg. The sequence was to first slew the antenna to approximately 90 deg cone by means of the dish actuator, then rotate the boom actuator 180 deg, and finally complete the 180 deg slew of the dish actuator.

The temperature data for the reflector and the S/X-band feed is presented in Fig. 117. Data from the HGA boom measurement is shown in Fig. 118.

c. Temperature Data Associated With Spacecraft Anomalies

(1) Day 090 Power Anomaly. At 0222 GMT on Day 90 (L + 148), the day after Mercury closest approach, an anomalous power glitch occurred on the spacecraft, the effects of which are characterized by the following symptoms.

(a) The power dissipation in the power bay (Bay 1) increased by approximately 87 watts as indicated by the increased power input to the boost regulator coupled with no change in boost regulator output loads.

	Solar Panel							
	+X				-X			
	Channel							
Tilt angle, deg	870	871	872	873	874	875	876	877
	Location[a]							
	Z	TO	LI	TI	Z	LO	TI	LI
	Temperature, °C (°F)							
50	--	--	--	--	76.1 (169)	116.1 (241)	109.4 (229)	120.6 (249)
60	58.3 (137)	80.6 (177)	95.6 (204)	81.1 (178)	57.8 (136)	91.7 (197)	84.4 (184)	97.2 (207)
61					55.5 (132)	88.9 (192)	80 (176)	95 (203)
62	56.1 (133)	74.4 (166)	91.1 (196)	75.6 (168)	53.3 (128)	86.7 (188)	78.3 (173)	92.2 (198)
64	56.1 (133)	65.5 (150)	84.4 (184)	68.3 (155)				
66	52.2 (126)	59.4 (139)	77.8 (172)	60.6 (141)	55.5 (132)	71.7 (161)	62.8 (145)	78.3 (173)
66.26	51.7 (125)	60 (140)	78.9 (174)	61.7 (143)				
66.54	50 (122)	59.4 (139)	77.8 (172)	60 (140)				
67	47.8 (118)	56.7 (134)	75.6 (168)	57.8 (136)				
68	46.1 (115)	52.8 (127)	72.2 (162)	53.9 (129)	47.2 (117)	65 (149)	54.4 (130)	73.3 (164)
70	38.3 (101)	43.3 (110)	65.5 (150)	45.5 (114)	39.4 (103)	56.1 (133)	45.5 (114)	65.5 (150)
72					32.2 (90)	48.3 (119)	36.1 (97)	58.3 (137)
76	16.7 (62)	22.2 (72)	40 (104)	23.3 (74)	8.9 (48)	28.9 (84)	22.8 (73)	41.7 (107)

[a]Location code

I = Inboard (closest to bus)
O = Outboard
T = Trailing edge (edge away from Sun)
L = Leading edge (edge toward Sun)
Z = Zener (on spar near zener diode)

Except for 870 and 874, transducers are mounted at panel corners on uncelled side of honeycomb substrate.

(b) The TV optics heaters went off indicating the probable presence of a ground fault similar to the one present at launch which prevented the solid-state FDS switches from activating the optics heaters.

(c) Several temperature telemetry channels became noisy, notably those with transducers located on the solar panels.

(d) The outboard temperature transducer on the +X solar panel (E871) increased 11°C (20°F) for no apparent reason.

The temperature response of the bus to this anomaly is presented in Figs. 119, 120, and 121. The scan platform response is shown in Fig. 122. Solar panel temperature data is presented in Fig. 123.

Table 27 lists the steady-state temperatures for the entire spacecraft both prior to the anomaly on Day 89 and after the transient caused by the anomaly steadied out on Day 91. Since the solar intensity increased from 4.65 to 4.73 suns between Days 89 and 91, this effect is removed from the Δ's to yield only the effect of the anomaly.

An analysis was performed using the thermal analyzer model of the bus to see if the steady-state temperature response of the bus was consistent with the observed 87 W power discrepancy in the boost regulator. Figure 124 shows the results of this analysis for two assumed additional power dissipations in Bay 1, and compares these results against the actual steady-state ΔT's. The match between the analytical results and actual temperatures is not very good, probably due to bay-to-bay coupling inaccuracies in the model.
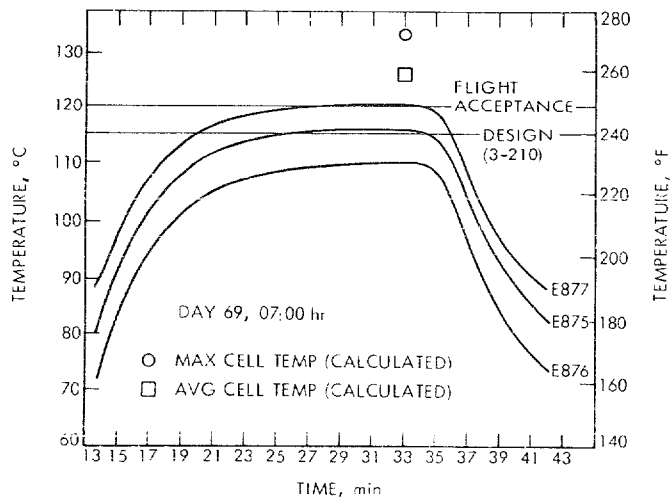
Fig. 116. Inadvertent -X solar panel tilt to 50-deg at 3.37 suns
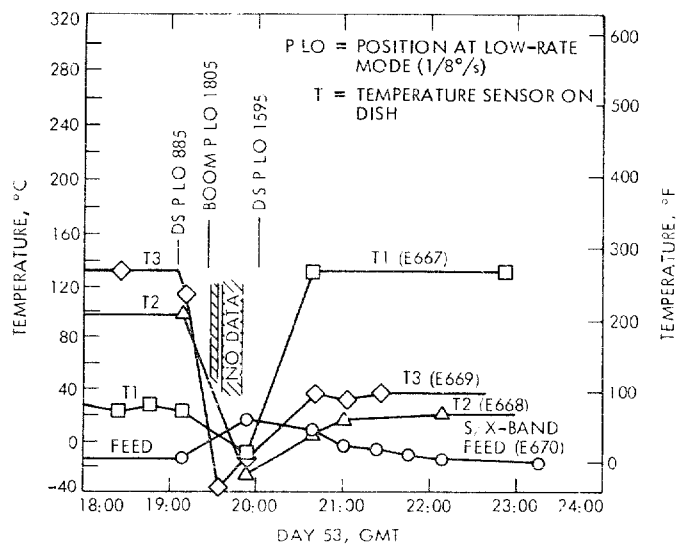
Fig. 117. High-gain antenna temperature response to HGA flipflop, Day 053
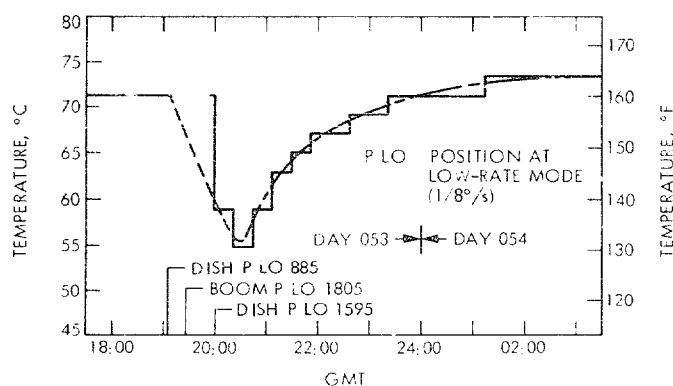
Fig. 118. HGA boom temperature response to HGA flipflop, Day 053
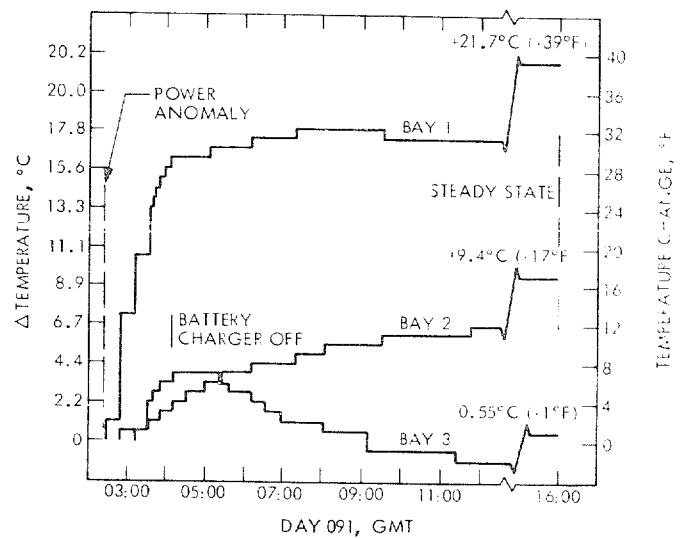
Fig. 119. Bus temperature response to power anomaly--Bay 1 and adjacent bays
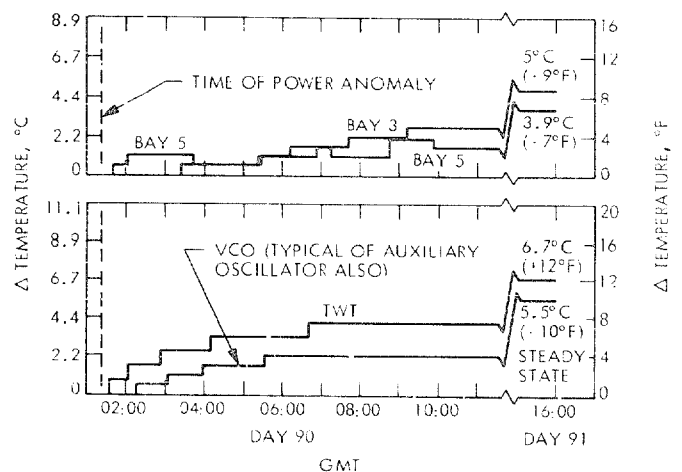
Fig. 120. Bus temperature response to power anomaly--Bay 4 and adjacent bays
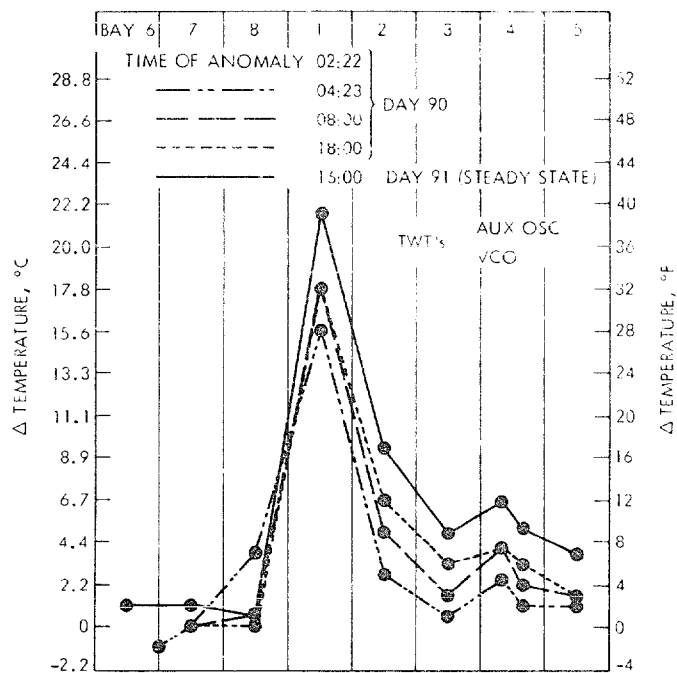
Fig. 121. Bus temperature response to power anomaly
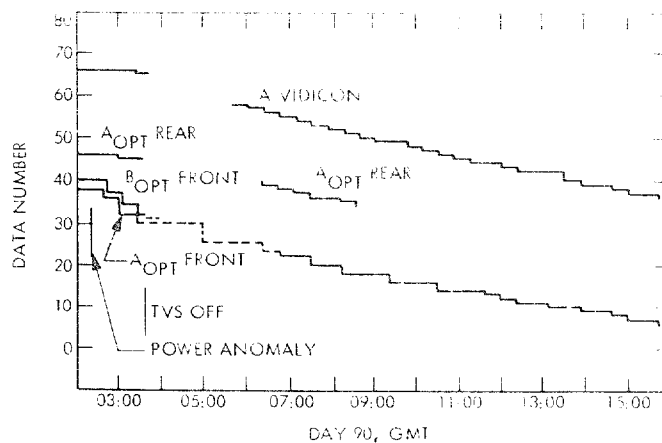
Fig. 122. TV temperature transient data
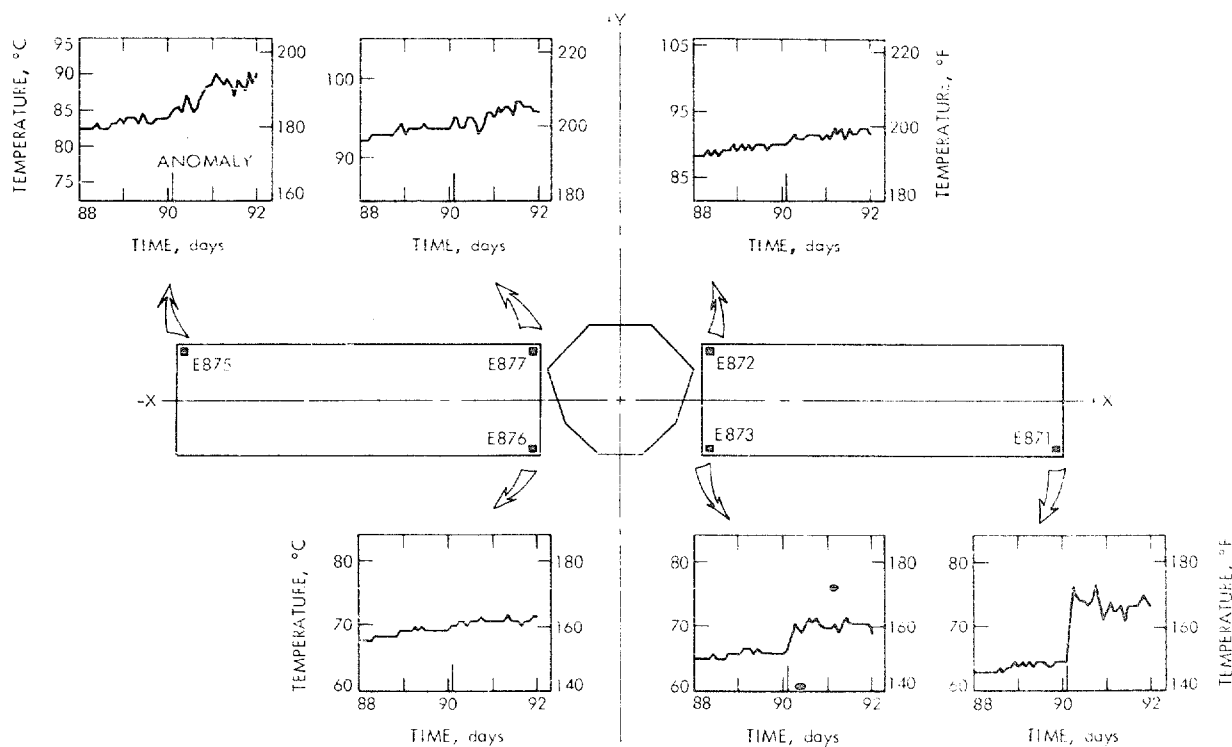
Fig. 123. Solar panel temperature response to power anomaly

Table 27. Steady-state temperature response to day 90 power anomaly

Temperature measurement description	Pre-anomaly Day 89 16:00 °C(°F)	Post-anomaly Day 91 16:00 °C(°F)	Steady-state Δ		Solar Δ °C(°F)	Anomaly Δ °C(°F)	Comments
			DN	°C(°F)			
Canopus tracker	4.4 (40)	9.4 (49)	9	5 (9)	3.3 (6)	4.4 (8)	Bus mounted
GCA	25.5 (78)	26.7 (80)	2	1.1 (2)	0 (0)	1.1 (2)	
Sun sensor	41.1 (106)	43.3 (110)	2	2.2 (4)	2.2 (4)	0 0	
+X/-Y N2	20.5 (69)	27.8 (82)	13	7.2 (13)	0.5 (1)	6.7 (12)	Bus
-X/+Y N2	23.3 (74)	28.9 (84)	10	5.5 (10)	0.5 (1)	5 (9)	
TVCA	75.6 (168)	78.9 (174)	3	3.3 (6)	2.2 (4)	1.1 (2)	
PSE electronics	30 (86)	31.7 (89)	2	1.7 (3)	0.5 (1)	1.1 (2)	
PSE platform	30.5 (87)	31.7 (89)	1	1.1 (2)	1.1 (2)	0 0	
CPT	3.3 (38)	5 (41)	2	1.7 (3)	0.5 (1)	1.1 (2)	Bus-mounted platform
UVSA	10.5 (51)	-7.2 (19)	-20	17.8 (-32)	0 0	-17.8 (-32)	
UVSO	28.3 (83)	30.5 (87)	2	2.2 (4)	2.2 (4)	0 0	
Prop N2	30.5 (87)	32.2 (90)	3	1.7 (3)	1.1 (2)	0.5 (1)	
Propellant	31.7 (89)	33.3 (92)	3	1.7 (3)	1.1 (2)	0.5 (1)	
Valve	58.9 (138)	62.2 (144)	3	3.3 (6)	2.2 (4)	1.1 (2)	
Thrustplate	60 (140)	63.3 (146)	3	3.3 (6)	2.2 (4)	1.1 (2)	
IRR	31.7 (89)	33.9 (93)	2	2.2 (4)	2.2 (4)	0	
Mag A	-19.4 (-3)	-20 (-4)	1	-0.5 (-1)	0 0	-	
Mag B	-11.7 (11)	-12.2 (10)	1	-0.5 (-1)	0 0	-	
Mag electronics	35 (95)	37.2 (99)	-2	2.2 (4)	0.5 (1)	1.7 (3)	
Mag processors	36.1 (97)	38.3 (101)	-2	2.2 (4)	0.5 (1)	1.7 (3)	
Aux. oscillator	31.1 (88)	36.7 (98)	10	5.5 (10)	0.5 (1)	5 (9)	Bus
TWT 1	44.4 (112)	51.1 (124)	8	6.7 (12)	0.5 (1)	6.1 (11)	
TWT 2	35 (95)	41.7 (107)	8	6.7 (12)	0.5 (1)	6.1 (11)	
VCO	28.3 (83)	34.4 (94)	9	6.1 (11)	0.5 (1)	5.5 (10)	
Dish 1	70.6 (159)	51.1 (124)	-4	-19.5 (-35)	-	-	HGA slewing
Dish 2	5.5 (42)	38.3 (101)	8	32.8 (59)	-	-	
Dish 3	20 (68)	28.9 (84)	2	8.9 (16)	-	-	
S/X Feed	111.1 (232)	116.7 (242)	1	5.5 (10)	-	-	
X-band transmitter	23.9 (75)	28.9 (84)	9	5 (9)	0.5 (1)	4.4 (8)	Bus mounted
Bay 1	20.5 (69)	41.7 (107)	39	21.1 (38)	0.5 (1)	20.5 (37)	Additional power dissipation in bus
Bay 2	21.1 (70)	30.5 (87)	17	9.4 (17)	0.5 (1)	8.9 (16)	
Bay 3	22.2 (72)	27.8 (82)	10	5.5 (10)	0.5 (1)	5 (9)	
Lower blanket	-4.4 (24)	-4.4 (24)	--	--	--	--	
Bay 5	25 (77)	27.8 (82)	5	2.8 (5)	0.5 (1)	2.2 (4)	
Bay 6	23.3 (74)	24.4 (76)	2	1.1 (2)	0 0	1.1 (2)	
Bay 7	22.2 (72)	23.3 (74)	2	1.1 (2)	0 0	1.1 (2)	
Sunshade	210.5 (411)	213.9 (417)	1	3.3 (6)	3.3 (6)	0 0	
HGA boom	97.2 (207)	99.4 (211)	1	2.2 (4)	2.2 (4)	0 0	

Table 27 contd

Temperature measurement description	Pre-anomaly Day 89 16:00 °C(°F)	Post-anomaly Day 91 16:00 °C(°F)	Steady-state Δ		Solar Δ °C(°F)	Anomaly Δ °C(°F)	Comments
			DN	°C(°F)			
TVA Opt F	5.5 (42)	-	-39	-23.3 (-42)	0 0	-23.3 (-42)	
TVA Opt R	9.4 (49)	-12.8 (9)	-41	-22.2 (-40)	0 0	-22.2 (-40)	
TVA vidicon	18.9 (66)	-2.8 (27)	-39	21.7 (-39)	0 0	-21.7 (-39)	
TVB Opt F	5.5 (42)	-	-41	-23.3 (-42)	0 0	-23.3 (-42)	Loss of optics heaters
TVB Opt R	10.5 (51)	-10.5 (13)	-39	21.1 (-38)	0 0	-21.1 (-38)	
TVB vidicon	18.9 (66)	-1.1 (30)	-37	-20 (-36)	0 0	-20 (-36)	
AES	7.8 (46)	-11.7 (11)	-36	-19.5 (-35)	0 0	-19.5 (-35)	
Battery	19.4 (67)	20.5 (69)	2	1.1 (2)	0 0	1.1 (2)	Battery charge off
+X S/P 1	52.2 (126)	52.2 (126)	--	-	-	-	
+X S/P 2	63.3 (146)	73.3 (164)	12	10 (18)	1.1 (2)	8.9 (16)	
+X S/P 3	90 (194)	92.2 (198)	3	2.2 (4)	1.1 (2)	1.1 (2)	
+X S/P 4	65.5 (150)	70.6 (159)	6	5 (9)	1.1 (2)	3.9 (7)	
-X S/P 1	55 (131)	53.3 (128)	-1	-1.7 (-3)	-	-	Noisy
-X S/P 2	82.8 (181)	88.9 (192)	7	6.1 (11)	1.1 (2)	5 (9)	
-X S/P 3	69.4 (157)	70 (158)	1	0.5 (1)	1.1 (2)	-0.5 (-1)	
-X S/P 4	92.8 (199)	96.7 (206)	4	3.9 (7)	1.1 (2)	2.8 (5)	

The general temperature distribution, however, is similar enough to the actual distribution to conclude that the power change observed in power telemetry was real and was being dissipated within Bay 1.

Another conclusion that may be drawn from both the transient and the steady-state data is that additional power (a few watts) is also being dissipated in the radio bay (Bay 4) in the vicinity of the TWTs. Not only do the TWT and VCO temperatures rise faster than either of the adjacent bays, but they rise farther. Since the VCO temperature trails the TWT temperature, this additional dissipation is apparently closer to the TWTs than to the VCO.

D. TELEVISION SUBSYSTEM (TVS)

When this subsystem was first turned on, it was observed that the A&B optics heaters had not come on. Problem Failure Report (PFR) 5001 thoroughly documents this anomaly.

The TV camera data obtained on the Earth and Moon mosaics indicated good subsystem performance despite the apparent loss of the optics heaters. Previously unplanned troubleshooting operations were conducted prior to the start of the first Earth mosaics at 22:00 GMT on Day 307. Preliminary analysis of Earth and Moon data indicate good optical focus.

After concluding a duty cycle analysis, it was determined that the camera electron beam and light flooding could normally be off to prolong vidicon life. Periodic diagnostic commands were sent to monitor cathode beam currents and provide continuing confidence that the electronic performance remained good. PFR 5012 analyzes and documents this anomaly.

On January 17, 1974, the TV optics heaters were observed to come on when the propellant/ CPT supplemental heaters were turned off with a DC 64 command. An attendant rise of scan platform temperatures was noted.

On February 9, 1974 (four days after Venus closest approach), the rate of decline of the TV cathode beam currents was observed to increase, coupled with more instability in the levels. Accordingly, the PI decided to turn off the TVS and discontinue the continuous (cyclic 2) mosaics. At this time, the A camera had dropped 50 DN in read current since launch to only 13 DN above beam starvation levels.

Cumulative statistics for TVS operations are as follows:

Power on   2832.9 h

Beams on   766 h

Filter steps	A, 289; B, 321
Shutters	3909 each

E. FLIGHT DATA SUBSYSTEM (FDS)

1. Performance During Flight

After all the problems experienced during subsystem test, flight of the FDS seemed relatively uneventful. However, there were two spacecraft problems associated with the FDS.

a. **TV Heater Problem.** Immediately after launch the TV optics heaters failed to operate. MOS switches in the FDS are used to turn the heaters on and off. Analysis revealed that the drains of the MOS switches were connected to the raw DC return and that a short to ground of the DC bus itself would put a negative bias across the switches, turning them off.

On January 17, 1974 an unrelated set of supplemental heaters was turned off and the TV heaters came on, indicating that the original hypothesis was very likely. During the spacecraft power anomaly that occurred on March 31, 1974, the heaters again went off and did not turn ON again (Bibliographic ref. 14).

b. **POR Problem.** The FDS has an internal circuit, called the power-on-reset (POR) circuit, that monitors the 5 Vdc logic voltage. If the voltage drops below about 22% (10% is the specification on the logic IC's), the circuit causes certain logic in the FDS to reset. Through June 30, 1974, the gyros were turned on 26 times, and 6 of those times the FDS unexpectedly experienced a POR. Analysis indicated that the most likely cause was a dip in the 2.4 kHZ voltage of over 25% combined with noise coupled into the FDS.

2. Critique

The capability to reprogram the engineering formats was a change from previous spacecraft, which had only a single hardwired engineering format. The ability to modify the formats without changing the hardware was useful before launch and decidedly advantageous after launch. In flight the engineering formats were reprogrammed numerous times, to optimize data return and to analyze problems.

F. DATA STORAGE SUBSYSTEM

In completing the primary mission the DSS accumulated approximately 960 passes and returned 1 x 10^{10} bits of data, and passed more than one-half million feet of tape past the magnetic heads. The performance of the DSS in accomplishing the primary mission was good but was not without incident.

1. Tape Stick

The 73-2 recorder had experienced some tape sticking in the parking window prior to launch. At first it was thought that the sticking was caused by static charge buildup. The decision was made to moisturize the tape recorder atmosphere. The stick appeared again, just prior to launch, even though the transport

atmosphere was at a relative humidity of about 30%. Since the problem was understood, and the tape recorder could recover from a stick by using synchronous motor torque, a decision was made to launch with the 73-2 unit. A tape unstick sequence was designed, tested, and adopted.

In the early part of February 1973 two tape sticks were observed. The first occurred in the parking window, when the unstick sequence was not used. The second occurred three or four days later and appeared to be on the oxide just outside the parking window. The second stick was cause for concern because a stick on the oxide had not occurred before, and it caused the project to reexamine the theories on the probable cause of the stick.

2. Power Toggling

After the Day 90 power anomaly, the power to the subsystem began intermittently to toggle on and off. After looking at all subsystem parameters which appeared normal, it was concluded that the problem was somewhere else. The power to the subsystem is supplied by the power subsystem through a relay located in another bay.

G. CENTRAL COMPUTER AND SEQUENCER

In-flight performance was flawless (no PFRs were issued against the CC&S). The following comments apply to the CC&S operation up through the conclusion of the first Mercury Encounter on April 5, 1974:

(1) 53 memory loads were made and check sums were properly received on all 53.

(2) The 53 memory loads involved the loading of 3,746 CC&S memory words.

(3) 364 discrete commands (relay closures) were sent to other subsystems by the CC&S.

(4) 490 FDS coded commands were sent by the CC&S.

(5) 7,087 APS coded commands were sent by the CC&S.

(6) 24 DC ground commands were received by the CC&S.

(7) 40 CC-4 commands were received by the sequencer for maneuver parameters.

(8) There was a single case on April 4, 1974 in which a noise glitch on the spacecraft ground line caused an unplanned jump in the CC&S memory and resulted in a TWT high power command not being sent by the CC&S. The unplanned jump in the CC&S memory was verified and understood, and it was postulated that the spacecraft ground line glitch was associated with the Day 90 power problem.

H. MECHANICAL DEVICES

1. Mechanical Devices Performance

Mechanical devices data (and pertinent supporting data) is presented in Table 28 and Fig. 125. Unfortunately, data sample rates were not sufficiently high near launch to allow an accurate comparison between predicted times for devices events and the times at which the events actually occurred. Nevertheless, the following observations can be made:

(1) Spacecraft separation occurred at 06:24:01, 7 sec after SOE predict. (This time is determined almost exactly by the V-band pyro event in Centaur telemetry.)

(2) The actual time (58 ± 1 s) required to deploy the PSE boom was very close to the nominal prediction (64 ± 10 s).

(3) The scan latch blowdown profile coincided closely with the "clean" curve in Fig. 125.

(4) The +X solar panel latched down between 0 and 168 sec after the -X solar panel.

The last primary mission-critical mechanical devices function was successfully performed on Day 348 (GMT) when the solar panels were tilted from 0 to 25 deg. Each panel latching mechanism performed as designed by first unlatching the panel from its launch support points on the trunnion, then locking the actuator linkage directly to the panel structure. Subsequent panel articulation verified that the mechanisms had performed in a completely nominal fashion.

On April 8, 1974 the last pyro squib was successfully fired to move the low-gain antenna to the extended mission configuration.

I. PROPULSION SUBSYSTEM PERFORMANCE

1. TCM 1 Summary

The Propulsion Subsystem performed as predicted during TCM 1. Impulse, mass expended, roughness, and soakback temperatures were all within specification. Tracking data indicates that the ΔV was only 1.8% higher than predicted and well within the requirement of 8%. Tank and engine thrust chamber pressure telemetry indicate that the error resulted primarily from small uncertainties in the thrust coefficient (C_F), the characteristic velocity (c*), the flow resistance, and the amount of heat transfer. These errors were reduced for the remaining maneuvers by modifying the appropriate Burn Time Estimation Calculation (BUTEC) computer program input.

a. Discussion. The first trajectory correction maneuver was successfully performed ten days after launch in order to correct launch vehicle injection errors which would have resulted in a 67,000-km miss at Venus. The desired velocity increment was 7.784 m/s and required a burn time of 19.9 s. As a result of the maneuver, the projected miss was reduced to 1500 km. The TCM is schematically depicted in Fig. 126 and the maneuver parameters are presented in Table 29. A simplified sequence of events is presented in Table 30.

Propulsion Subsystem performance during the maneuver was as predicted and within specifications. Tracking data indicated that the ΔV was 1.8% higher than predicted, but this is only slightly greater than a 1-σ error (Fig. 127) and significantly less than the 8% error allowed. Burn time, engine roughness and soakback temperatures were also within specification. The burn time was accurate to within 0.05 s. Peak-to-peak roughness in chamber pressure was less than half of the allowable 1.4×10^5 N/m² (20 psi), and the quality of tape playback was excellent. Soakback temperatures were approximately 8.3°C (15°F) lower than predicted and are plotted in Figs. 128 and 129. The propellant consumed during the maneuver was 1810 ± 22.7 g (3.99 ± 0.05 lbm), and the remaining ΔV capability was 114 ± 1 m/s. There were no predicted or observed effects on thrust due to the TVCA jet vane transient.

Although the Propulsion Subsystem performance was in close agreement with that predicted by BUTEC, the performance was further analyzed in order to improve predictability for the remaining TCMs. BUTEC's input parameters were then tweaked half-way between the original values, which were based on FA test data obtained at TRW, and the best estimates obtained from the flight telemetry.

Considering the uncertainties in flight data this was considered a valid approach, since BUTEC had also predicted slightly low on most of the TA and Calibration Subsystem tests performed at the Edwards Test Station. The errors estimated from the analysis of flight telemetry are compared with premaneuver predictions in Table 31 and are discussed in further detail below.

The flight telemetry indicated that the engine chamber pressure (P_c) was approximately 0.9% higher than predicted (Fig. 130). Since the ΔV was 1.8% higher than predicted, the thrust coefficient (C_F) must also have been 0.9% higher (corresponding to a 1.2 σ error). See Table 31.

The high chamber pressure was due to a higher than expected tank pressure, higher than predicted engine performance (C*), and a lower than predicted flow resistance.

The high tank pressure accounted for approximately 30% of the chamber pressure error. As indicated in Fig. 131 the error in tank pressure reached a maximum of 10.3×10^4 N/m² (2.5 psi) at the end of the burn. The error was due to a higher than predicted heat transfer between the tank walls and the pressurant gas and, to a lesser extent, to unmodeled effects of tank contraction and gas-out-of-solution during the "blowdown." The heat transfer was determined from BUTEC simulations and the 1.7×10^4 N/m² (15 psi) recovery in tank pressure at the end of the burn. The results indicated that the heat transfer was 50% higher than predicted (corresponding to a 0.5 σ error) and that this affected tank pressure by a maximum of 0.76×10^4 N/m² (1.1 psi) and total impulse by 0.12%. Since a review of some
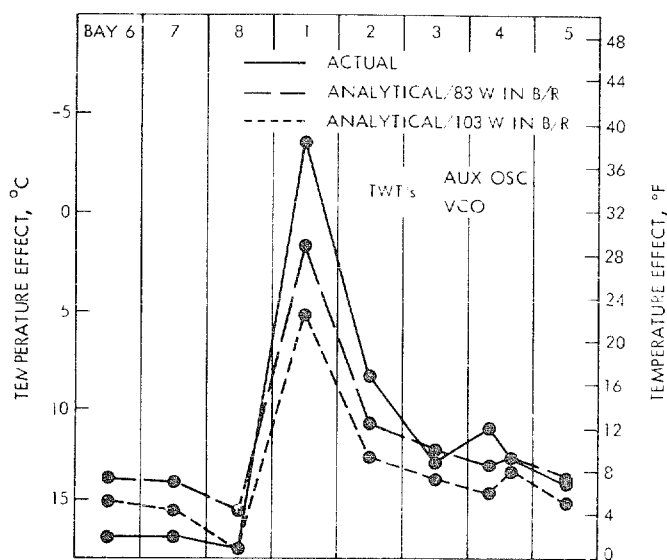
Fig. 124. Temperature effect of power anomaly referenced to preanomaly temperatures
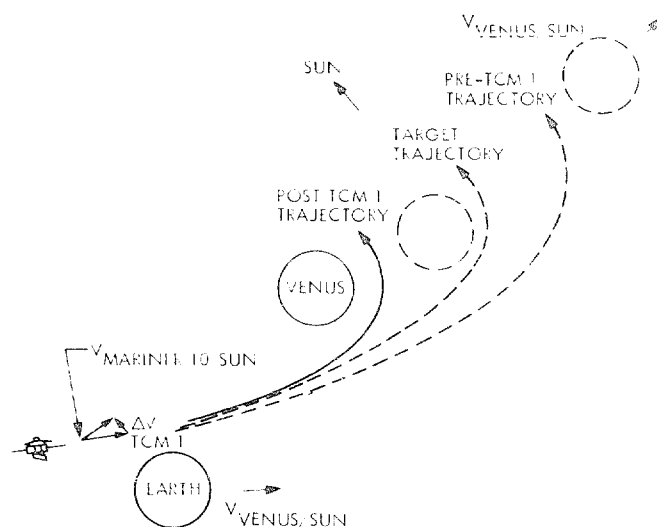
Fig. 126. Schematic presentation of the pre- and post-TCM 1 trajectories and the target trajectory
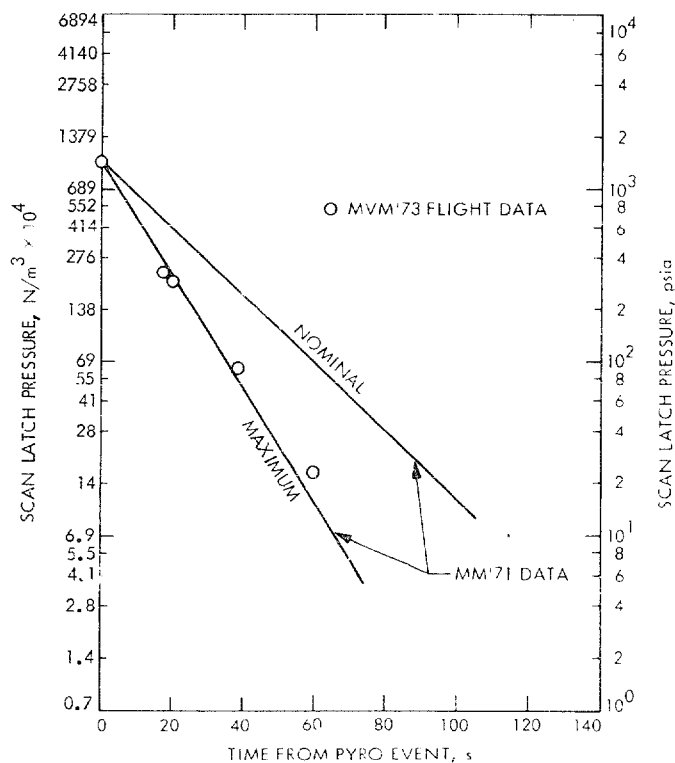
Fig. 125. Scan latch pressure
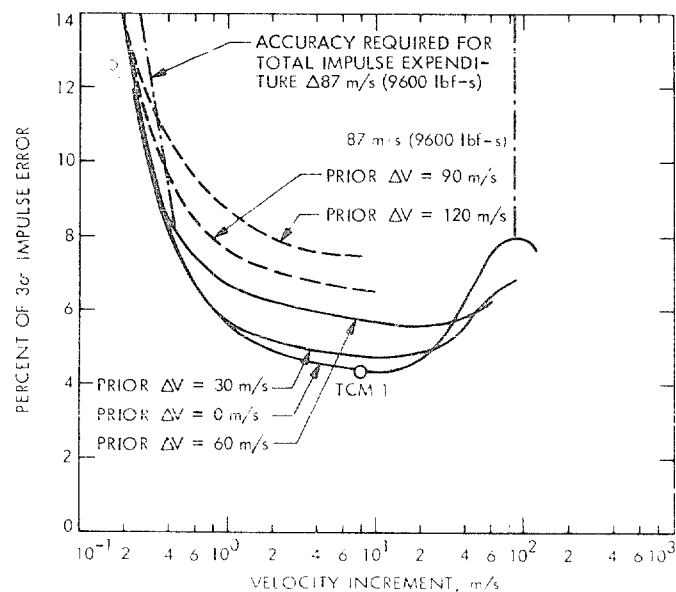
Fig. 127. 3σ impulse error

Table 28. Mechanical devices data launch day 307

Event	Event[a] source	Predicted event time (sequence of events), GMT	Earliest confirmation of event in data, GMT	Latest confirmation of no event in data, GMT	Data sample rate
Spacecraft separation					
Pyro arming switch	M	06:23:54	06:25:47	Prior to space-craft separation	84 x
V-band	p[b]		06:24:01	Prior to space-craft separation	<1 ms
Release relay hold			06:25:05	06:22:17	84 s
Separation initiated times T3	M	06:27:39 (SEP + 225 s)	06:28:35	06:22:11	84 s
Separation initiated timer T4 (unlatch solar panel, MAG, HGA, LGA)	P	06:27:45 (T3 + 6 s)	06:38:43	Prior to space-craft separation	22.4 min
-X solar panel deployment	M	06:29:15 ± 20 s) (T4 + 90 ± 20 s)	06:29:59	06:28:35	84 s
LGA deployment	M	06:27:50 (T4 + 5 sec)	06:29:59	06:28:35	84 s
+X solar panel deployment	M	06:29:15 ± 20 s (T4 + 90 ± 20 s)	06:31:23	06:29:59	84 s
HGA deployment	M	06:31:40 ± 65 s (T4 + 235 ± 65 s)	06:32:47	06:31:23	84 s
MAG boom deployment	M	06:28:05 (T4 + 20 s)	06:38:43	Prior to space-craft separation	22.4 min
PSE boom unlatch	P	06:45:00	06:45:01	06:44:40	21 s
PSE boom deployment	M	06:46:04 ± 10 s (Unlatch + 64 ± 10 s)	06:45:59	06:38:18	143 ms
HGA dish unlatch	P	07:35:00	07:35:04	07:34:43	21 s
Scan platform unlatch	P	07:38:00	07:38:13	07:37:52	21 s

[a]Event source: M = microswitch   P = pyro

[b]Centaur telemetry
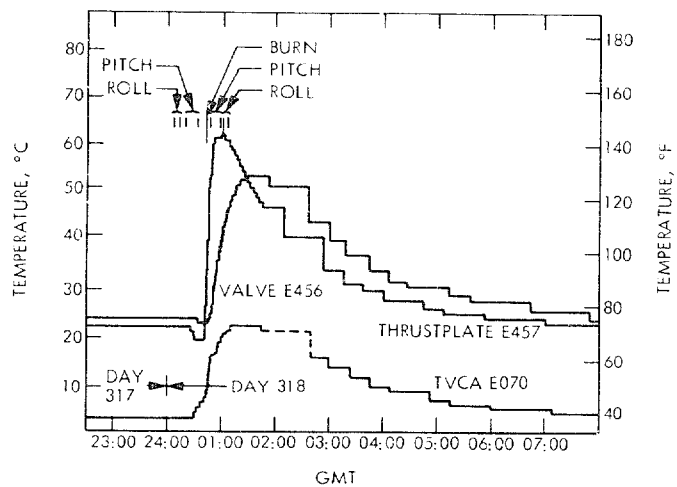
Fig. 128. TCM 1 maneuver transients--propulsion valve (456), thrustplate (457) and TVCA (070)
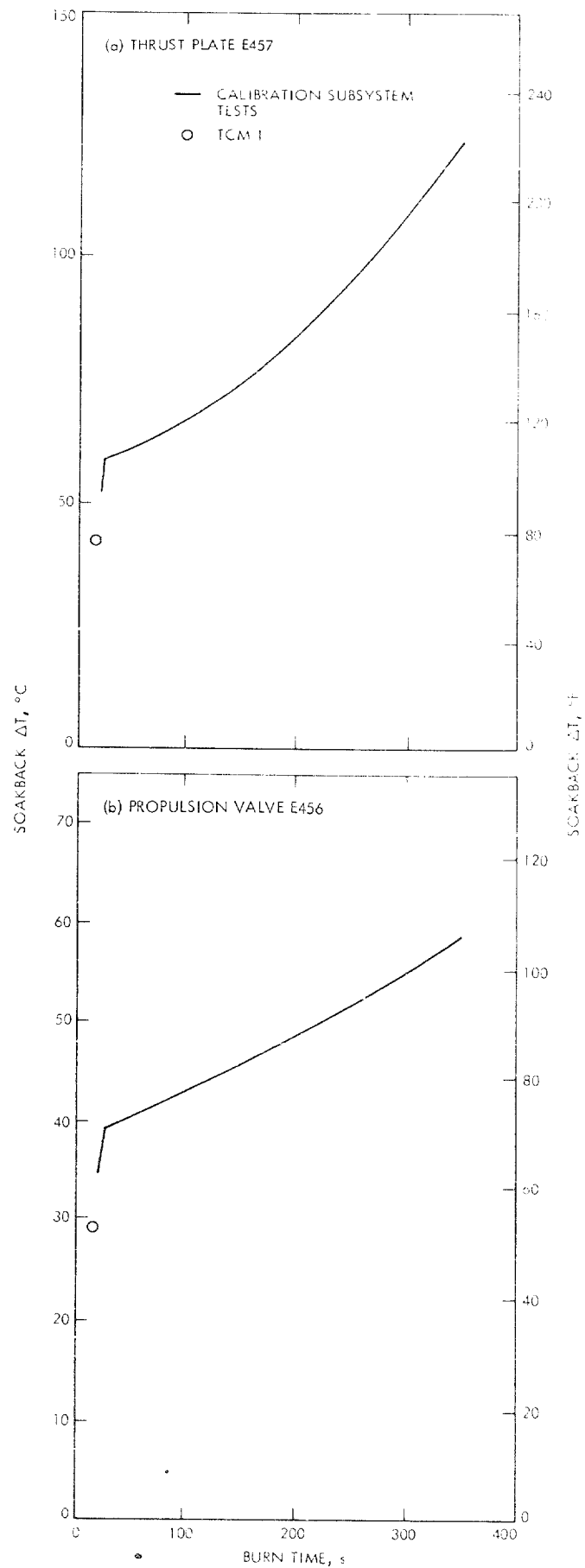
Fig. 129. Maximum soakback ΔT

Table 29. TCM 1 maneuver parameters

Trajectory Parameters

	Pre-TCM 1	Target
B · T	-51,305 km	15,142 km
B · R	-180 km	-4,998 km
Time of closest approach to Venus	036:20:12:17 GMT	036:17:02:34 GMT
Required ΔV		7.784 m/s
BUTEC ΔVT		7.778 m/s

Turn parameters

Roll	49.017 deg
Pitch	127.552 deg

Burn parameters

Initial spacecraft mass	502.3 kg (1107.388 lbm)
Initial propellant mass in tank	28.7 kg (63.262 lbm)
Initial tank pressure	255×10^4 N/m^2 (307.2 psia)
Initial temperatures	
Nitrogen	14.3°C (57.7°F)
Propellant	14.9°C (58.8°F)
Valve	23.9°C (75°F)
Maximum thrust	205 N (46.1 lbf)
Burn time	19.9 s

earlier tank expulsion tests confirmed these flight results, the BUTEC heat transfer was increased by the full 50%.

The errors due to the unmodeled tank contraction and gas-out-of-solution during the blowdown were determined using a version of BUTEC which had been modified to simulate the effects. The results indicated that tank pressure was affected by less than 0.55×10^4 N/m^2 (0.8 psi) and total impulse by less than 0.15%. Although these errors are very small, they were compensated for on all remaining maneuvers.

The remaining error in P_c resulted from errors in C* and flow resistance. Since the errors are difficult to separate, based on the telemetry, an analysis was performed to calculate the most probable magnitudes. The analysis was based on the two errors' opposite effect on mass expended (ΔM) and on uncertainties in the values of ΔM, P_c, C* and flow resistance. ΔM and P_c were determined from the telemetry, and C* and flow resistance had been calculated from

Table 30. TCM 1 sequence of events

GMT[a]	Command/event	Description
317:21:00:02.808	DC 33	Switch CC&S to tandem standby
317:21:01:02.809	DC 80	Enable 30-V regulator
317:21:45:02.846	DC 52	Issue 5A turning on sequencer at next hours pulse plus 22 min
317:22:38:02	CC&S hours pulse	
317:23:00:02	CC&S 5A	Sequencer on
317:23:23:02	CC&S 2B	Transmit low-gain antenna
318:00:08:18		Start roll
318:00:12:43		Stop roll
318:00:21:15		Start pitch
318:00:33:17		Stop pitch
318:00:37:18	CC 6A	Switch to maneuver format
318:00:41:47	CC&S 4S	Enable PSA
318:00:41:49	8M1	Start burn
318:00:42:08.9	$\overline{8M1}$	Stop burn
318:00:42:11	CC&S 4T	Disable PSA
318:00:42:13.995	DC 73	Backup to 4T
318:00:42:49.995	DC 34	Disable 30-V regulator
318:00:43:39	CC 6A	Switch to primary format
318:00:46:09		Start unwind

[a]CC&S times are 1 sec earlier than predicted. Correction is based on predicted time of the 8M1 command and the actual time when chamber pressure first increased. Times noted are actual times. One-way light time was 13.480 s.

Table 31. TCM 1 impulse errors

Error source	Effect of error on ΔV, %	Magnitude of error, % $\frac{\text{(Predicted - actual)}}{\text{Predicted}}$	A priori 1σ Estimate, %	Correction factor for TCMs 2 and 3, %
Thrust coefficient C_F	0.90	-0.90	± 0.75	+0.45
Flow resistance	0.39	+1.20	± 3.0	-0.60
Characteristic Velocity $C*$	0.29	-0.425	± 0.5	+0.2125
Heat transfer	0.12	-50	+ 50 / -100	+50
Tank contraction	0.09			
Transducer accuracy	<0.09			
Gas out of solution	<0.06			
Jet vane transient	<0.05			

test data. The results indicated that C* was 0.425% higher and flow resistance 1.2% lower than predicted. As can be noted in Table 31, these errors are consistent with premaneuver predictions.

The effect of all of the above errors on tank pressure and P_c can be noted in Figs. 131 and 132.

2. TCM 2 Summary

Propulsion subsystem performance was satisfactory during TCM 2 and TCM 3. The impulse errors, chamber pressure roughness values, and soakback temperatures were within specification for both burns. The delivered velocity increment was approximately 1.4% greater than predicted for TCM 2 and 0.8% less than predicted for TCM 3. These values were well within the requirement of 8% and the a priori 3 σ error estimates of 5.2 and 4.6%. Analysis of telemetry and previous test experience indicates that most of the observed impulse prediction error is due to variations in engine catalyst bed pressure drop.

a. Discussion. TCM 2 was performed 15 days before Venus encounter to move the flyby point approximately 1400 km closer to Venus. The geometry is shown in Fig. 133. This required a burn of 3.70 s and a velocity correction of 1.359 m/s of the 114 m/s correction capability before the burn.

The maneuver was performed in the conventional manner by the computer and sequencer operating in tandem. Conventional roll and pitch turns were performed before the burn. The only unconventional feature of the burn was the operation of the valve from the battery instead of the 30-V regulator.

This was done because the regulator contains diodes which were suspect as a result of the failure of the main power chain. The pyro switching assembly and the RHD valve operated properly, as expected, although initial battery voltage was 37.5 V rather than the 30 V for which the valve and PSA are designed.

TCM 2 chamber pressure roughness reached a maximum value of 6% peak-to-peak versus a specification requirement of 10%. The soakback temperatures were low due to the short burn duration, and no valve leakage was observed after the burn.

The major TCM 2 burn parameters are summarized in Table 32, and the predicted and actual chamber and tank pressures are shown in Figs. 134 and 135.

The propulsion determination of impulse error was made by curve-fitting the telemetered P_c data and integrating the resulting curve-fit equation. This method determined that 1.55 ±1.2% more impulse was delivered than predicted. This relatively large 3 σ uncertainty is due largely to uncertainties in shutdown impulse. The navigation determination of impulse error was made by finding the most probable combination of doppler, pointing, and propulsion errors.

Table 32. TCM 2 summary

Maneuver date Jan. 21, 1974	(GMT 021 19:14)
Duration of burn	3.70 sec
Predicted velocity increment	1.359 m/s
Actual velocity increment	
Navigation	1.376 m/s
Propulsion	1.380 m/s
Initial tank pressure	22.6×10^4 N/m^2 (325.8 psia)
Impulse prediction error	
Navigation	+1.25%
Propulsion	+1.55 ±1.2% (3σ)
3σ a priori impulse error	5.2%
Initial spacecraft mass	500 kg (1102.27 lbm)
Initial propellant mass in tank	27 kg (59.272 lbm)
Propellant expended in maneuver	345 g ± 2.7 g (0.76 ±0.006 lbm (3σ))
Initial temperatures	
Nitrogen	20°C (68°F)
Propellant	20°C (68°F)
Valve	28.8°C (84°F)
Turn parameters	
Roll	47.95 deg
Pitch	35.17 deg

This method determined that 1.25% more impulse was delivered than predicted.

Considerable difficulty was experienced in obtaining this level of agreement between the propulsion and navigation ΔV estimates. This was largely due to the following circumstances:

(1) There were relatively large uncertainties in the pre-TCM 2 orbit determination.

(2) The post-burn tracking data could not be used to determine ΔV because the trajectory was perturbed only seven days after the burn by a large amount of attitude control gas expended during the first roll axis structural oscillation incident.

(3) The doppler data received during the burn was extremely sensitive to small errors in pointing.

These errors fortunately combined in a way that canceled out the TCM 2 ΔV error, and the resulting pass by Venus was within approximately 10 km (0.1 d) of the target point.
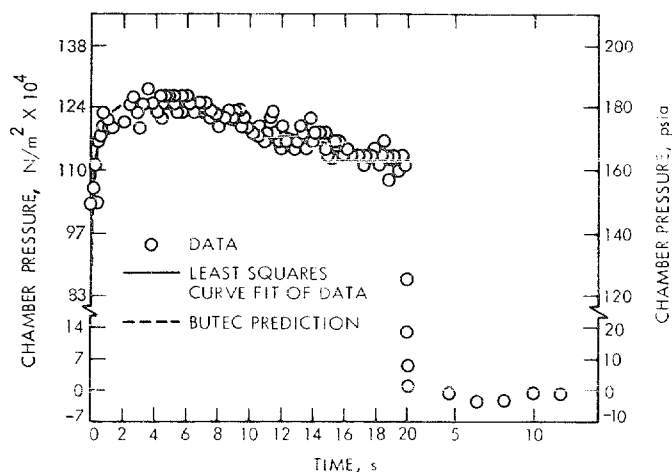
Fig. 130.   TCM 1 chamber pressure
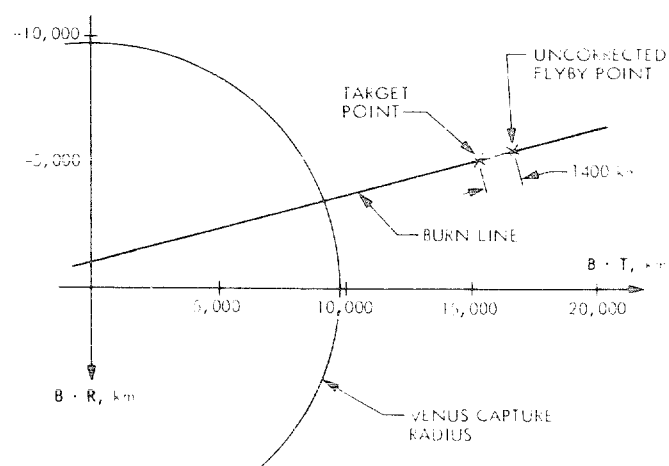
Fig. 133.   TCM 2 maneuver geometry
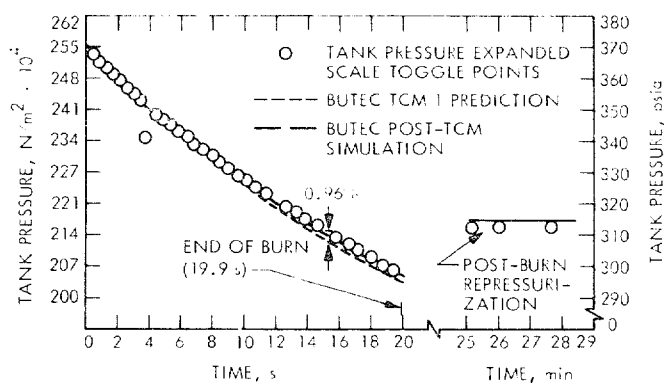
Fig. 131.   TCM 1 tank pressure
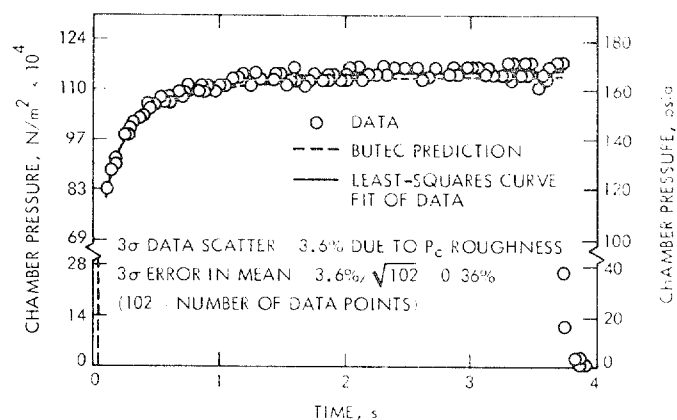
Fig. 134.   TCM 2 chamber pressure
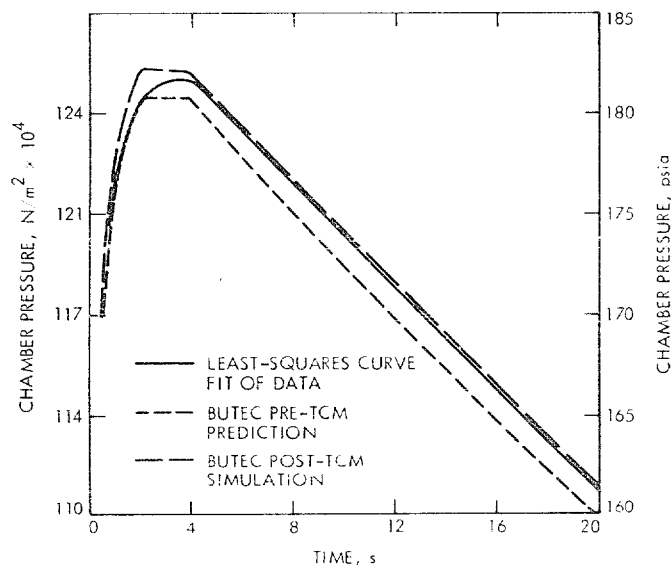
Fig. 132.   BUTEC simulation of TCM 1
chamber pressure
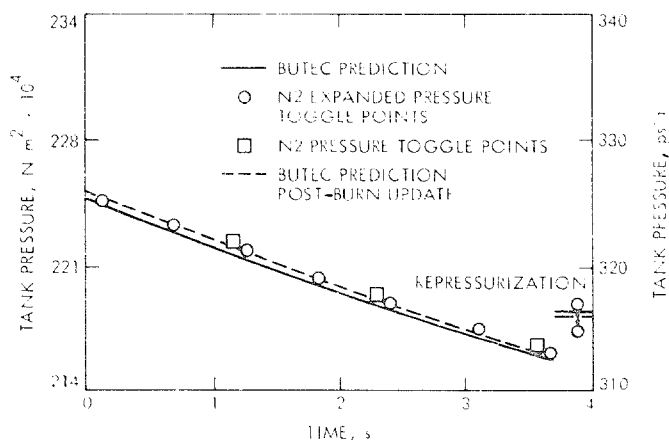
Fig. 135.   TCM 2 tank pressure

The 1.55% impulse error consisted of a 0.45% C_F error (based on the C_F determined from TCM 1 tracking) and a 1.1% integrated P_c error. The 1.1% integrated P_c error was made up of a 1.5% error due to the high catalyst bed pressure drop prediction plus a 0.1% error due to a low tank pressure prediction minus a 0.5% BUTEC transient simulation error. The BUTEC transient error of approximately 0.5% occurs for short burns because BUTEC P_c rises more rapidly than measured P_c. This was discovered during TCM 1 data analysis. The resulting error was negligible in TCMs 1 and 2 and was compensated for in the TCM 2 prediction by only making half of the 0.9% C_F correction indicated by TCM 1.

3. TCM 3 Summary

TCM 3 was a sunline maneuver performed 13 days before Mercury encounter in order to correct the Mercury flyby point. The geometry is shown in Figs. 136 and 137. The uncorrected flyby point was on the wrong (sunlit) side of Mercury. The desired flyby point was within the 90% science return zone shown on the dark side of Mercury. It was also desired that the flyby point be inside but close to the free return contour so that sunline maneuvers with the remaining propellant could be performed during the extended mission to attain the second Mercury encounter in late September 1974.

A sunline maneuver is one performed with the spacecraft in normal cruise attitude with the rocket nozzle pointed directly at the Sun. This is done to reduce the probability of a roll axis structural interaction oscillation occurring and to eliminate the attitude control gas usage that exists during the roll and pitch turns of a conventional maneuver. The gyros must still be on during the burn to control the jet vanes.

It was determined that a sunline maneuver could be executed to correct the trajectory errors that existed following the Venus encounter. The sunline maneuver had to be performed close to the Mercury encounter and involved a greater propellant expenditure, than that of an unconstrained maneuver.

The Venus flyby was so accurate that the sunline maneuver required only 17.83 m/s of the 113 m/s ΔV capability before the burn. (An unconstrained maneuver performed six days after Venus encounter would have required only 4.5 m/s compared with a prelaunch mean ΔV requirement of 25.1 m/s.)

The major TCM 3 burn parameters are shown in Table 33, and the predicted and actual chamber and tank pressures are shown in Figs. 138 and 139. Figure 138 does not show the actual P_c data points due to their large number.

TCM 3 chamber pressure roughness was approximately equal to the specification requirement — 10% peak-to-peak. The engine valve again operated properly on battery power, peak soakback temperatures were less than predicted, and no valve leakage was detected after the burn.

The burn time for TCM 3 was not a multiple of 0.050 s because the maneuver was performed

Table 33. TCM 3 Summary

Maneuver date	GMT 21:01 Day 075
Duration of burn	51.153 s
Predicted velocity increment	17.831 m/s
Actual velocity increment	
Navigation	17.702 m/s
Propulsion	17.671 m/s
Initial tank pressure	222×10^4 N/m^2 (322.0 psia)
Impulse prediction error	
Navigation	-0.72%
Propulsion	-0.90% ±0.7% (3σ)
3σ a priori impulse error	4.6%
Initial spacecraft mass	498.5 kg (1099.04 lbm)
Initial propellant mass in tank	26.5 kg (58.512 lbm)
Propellant expended in maneuver	3.9 kg ± 0.027 kg (8.69 ±0.06 lbm (3σ))
Initial temperatures	
Nitrogen	23.6°C (74.5°F)
Propellant	24.4°C (76.0°F)
Valve	45.6°C (114.5°F)
Turn parameters	
Roll	0 deg
Pitch	0 deg

using the computer only. This minimized the gyro on time and thus the possibility of gas loss due to roll axis oscillation.

The propulsion and navigation estimates of TCM 3 impulse errors were made in the same way as for TCM 2. The agreement was excellent since propulsion determined that delivered impulse was 0.9 ± 0.7% less than predicted and navigation obtained 0.7%.

The 0.9 % error consisted of a 0.07% error due to a 0.23×10^4 N/m^2 (+0.34 psia) error in predicted tank pressure and a 0.83% error due to a -2.8×10^4 N/m^2 (-4.0 psi) error in predicted catalyst bed pressure drop. Inspection of Fig. 138 also shows that the BUTEC tank pressure model did not work perfectly — predicted

tank pressure was lower than measured from 10 to 30 s and higher after 40 s. This did not cause a significant impulse error because the high and low tank pressure periods compensated for each other.

The TCM 3 impulse prediction error thus was almost entirely due to an error of 2.8×10^4 N/m^2 (4.0 psi) in predicting the catalyst bed pressure drop. This occurred because the large decrease in bed ΔP that occurred from TCM 1 to TCM 2 20.8×10^4 N/m^2 to 17.7×10^4 N/m^2 (30.2 to 25.7 psi) was projected forward to obtain a TCM 3 predicted bed ΔP of 15.9×10^4 N/m^2 (23.0 psi). This projected decrease did not occur; the indicated TCM 3 bed ΔP was actually 0.90×10^4 N/m^2 (1.3 psi) higher than that determined for TCM 2.

Figure 137 shows the post-maneuver flyby point which was approximately 180 km inside the aim point. The maneuver was considered highly successful since no additional pre-Mercury maneuver was required, the flyby point was within the extended 90% science value zone, no attitude-control gas was wasted by roll axis oscillation, and sufficient propellant remained to correct the trajectory for Mercury II with sunline maneuvers.

Figure 140 shows the catalyst bed pressure drop for the various firings of the flight engine (S/N 206) and the calibration test engine (S/N 205). The two engines behave similarly, and it was expected that the flight engine catalyst bed pressure drop would not vary significantly from its TCM 2 and 3 values during future engine firings.

Table 34 summarizes the prediction error magnitudes for TCMs 1, 2, and 3. Table 35 summarizes the BUTEC model changes made to predict and simulate the three burns.

J. POWER SUBSYSTEM

The spacecraft power subsystem performed well during the mission with three significant exceptions. The first was the power chain switchover that occurred on January 8, 1974. The second was the solar panel current anomaly that occurred on March 9, 1974. The third exception was the 87-W power increase that occurred on March 31, 1974. A brief summary of the analysis of these anomalies is presented in this section.

Table 34. TCM 3 prediction errors

| TCM | A priori 3σ impulse error | Error magnitudes | | | | Comments |
		Integrated percent of P_c	Percent of C_F	Percent of total	σ	
1	4.3%	0.9%	0.9%	1.8%	1.26	Navigation determined the 1.8% total error from post-burn tracking. The major causes of the P_c error were C_F, resistance, and heat transfer model errors. Essentially all the P_c error and half the C_F error were corrected for TCM 2
2	5.2%	1.1%	0.15%	1.25%	0.72	Navigation determined the 1.25% ΔV error by statistically analyzing the doppler, pointing, and propulsion errors. The major cause of the P_c error was a decrease in the catalyst bed pressure drop
3	4.6%	0.9%	0.2%	0.7%	0.46	Navigation determined the total error as in TCM 2. The major cause of the P_c error was an extrapolated catalyst bed pressure drop. The bed pressure drop for TCM 3 was actually almost the same as for TCM 2
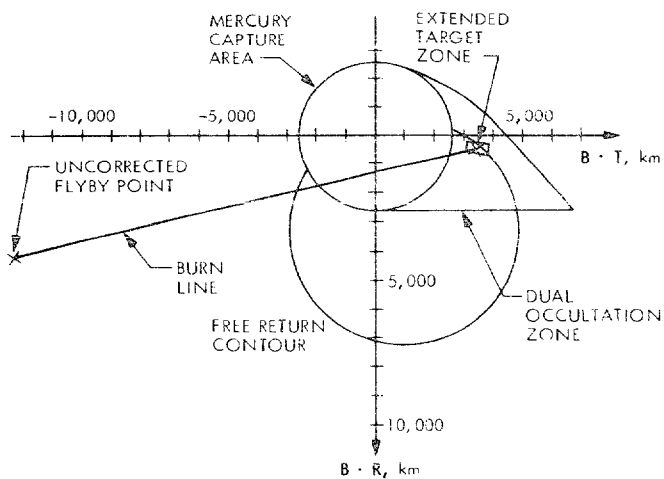
Fig. 136. TCM 3 maneuver geometry

Fig. 137. Post TCM 3 Mercury delivery
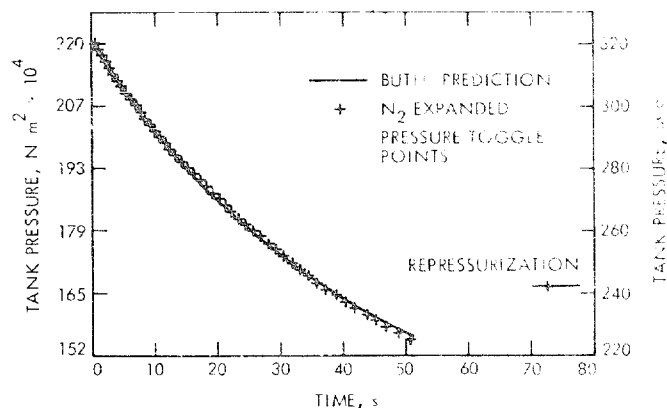
Fig. 139. TCM 3 tank pressure
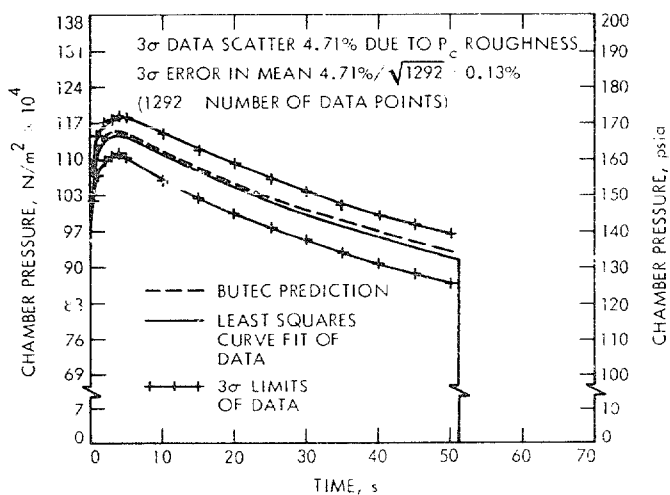
Fig. 138. TCM 3 chamber pressure
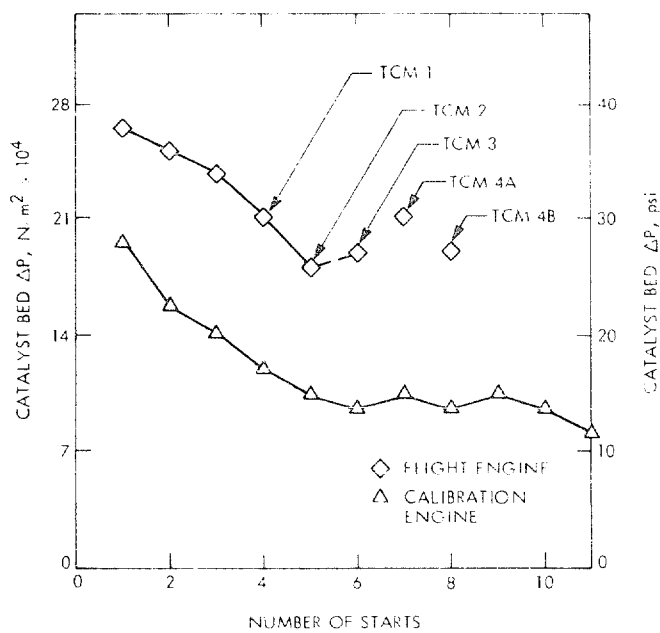
Fig. 140. Catalyst bed pressure drop variation

Table 35. BUTEC model changes

TCM 1 prediction	Reference model. All values are directly from test data except catalyst bed pressure drop which was 2.1×10^4 N/m^2 (3 psi) less than the average of the last two FA tests.
Post-TCM 1 simulation	C* increased 0.425%, liquid and catalyst bed resistances decreased 1.2%, C_F increased by 0.9%, heat transfer to ullage gas increased by 50%, tank contraction and gas out of solution added to model. These changes increased impulse 1.8% for the burn duration and 2.10% for a 50-s burn.
TCM 2 prediction	C* increased 0.2125%, liquid and catalyst bed resistances decreased 0.6%, C_F increased 0.45%, heat transfer increased 50%. (Effects of tank contraction and gas out of solution were negligible for this short burn.) These changes increased impulse 0.9% for the burn duration and 1.14% for a 50-s burn duration.
Post TCM 2 simulation	C* increased 0.425%, C_F increased by 0.45%, catalyst bed pressure drop decreased to 17.7×10^4 N/m^2 (25.7 psi), heat transfer increased 50%. These changes increased impulse 2.15% for the burn and 2.39% for a 50-s burn duration.
TCM 3 prediction	C* increased by 0.425%, catalyst bed pressure drop decreased to 16×10^4 N/m^2 (23.0), C_F increased to 0.75%. Tank contraction, gas out of solution simulated, heat transfer increased 50%. These changes increased performance 3.55% for the burn and for a 50-s burn duration.
Post TCM 3 simulation	C* increased by 0.425%, and catalyst bed pressure drop increased by 19×10^4 N/m^2 (27.0 psi), heat transfer increased 50%, C_F increased by 0.75%. Tank contraction and gas out of solution simulated. These changes increased impulse 2.66% for the burn and for a 50-s burn duration.

All percentage changes are referenced to the values used for the TCM 1 prediction.

The TCM 1 and TCM 3 simulations matched the integrated chamber pressures for those burns. The TCM 2 simulation matched the mean chamber pressure at 3.7 s.

---

1. Power Chain Switchover

The switchover occurred at 008:14:39:53 GMT[1] (L + 66 days). The relationship of spacecraft events associated with this failure was as follows:

008:14:39:53.271	NIS data goes bad
39:53.290	88.55 kHz subcarrier vanishes
39:54.570	88.55 and 177.1 kHz subcarriers appear[2]
39:55.930	Two pseudosubcarriers appear
39:56.090	Two pseudosubcarriers fade out
40:30.620	Battery voltage at 116 DN (down 2 DN)
40:41.120	Battery voltage at 117 DN (down 1 DN)
47:47.281	Battery voltage at 118 DN (normal)

When data reappeared on the line printers, the FDS was in data mode 10 (indicating an FDS power on reset), and the 2.4-kHz inverter input current was at 2 DN, which indicated that the spacecraft was on the standby chain, or that the 2.4-kHz inverter input current sensor had failed. The power chain switchover had no major impact on the mission.

a. Analyses and Tests

(1) During this period, 1N3892 diode failure were detected during VO'75 screening and type-approval (TA) testing. Three diodes from the same lot were used in the Mariner 10 booster regulator (BR). A

---

[1] All times in this report are Earth-received times.

[2] 1.28-s gap with no subcarrier.

diode from the same lot failed during MM'71 TA testing.

(2) Tests were conducted in the JPL power laboratory on the breadboard booster-regulator (BR) to determine the operating characteristics during the failure of the three diodes (CR11, 12 and 13). It was determined that the BR input current increased to approximately 18 A, and the BR output voltage dropped to a value slightly lower than the input voltage during the following failures:

Device	Failure Mode
CR 11	Short or open
CR 12	Short or open
CR 13	Short

An open-circuit failure of CR 13 had little effect.

(3) Analyses were performed to predict the solar array capability. It was concluded that the power subsystem would have gone into the solar array/battery share mode and that the battery would have discharged at 6 to 10 A until the transfer was made to the standby chain (this current was later estimated to be 10 A). The time for the failure sensor to react to an out-of-specification voltage or frequency condition was measured on the flight equipment as varying from 1.38 to 1.50 s.

(4) Tests were conducted on the battery to simulate a BR failure that would cause the battery to discharge at 8 A for 1.28 s (the time that the subcarrier vanished). The recharge characteristics of the test battery matched the battery flight data following the switchover reasonably well. The fact that the test was conducted at 8 A for 1.28 s versus a calculated current of 10 A for as much as 1.50 s would have little impact on the recharge characteristic.

(5) An analysis was performed to determine if the Earth-received data could be correlated with the expected response of the power subsystem for a power chain failure that would cause the battery to discharge at ≈10 A for 1.28 to 1.50 sec, and the BR output voltage to drop to the approximate input voltage. All of the significant responses of the spacecraft to the anomaly were considered, and all could be accounted for under the hypothesized failure.

The CC&S clock gained one second in the 10-day period prior to the anomaly. This would indicate that the 2.4-kHz inverter frequency had increased above the expected operating frequency; however, this could still have been within the performance specification (0.01%). Regardless, there is no apparent relationship between the frequency increase and the power chain switchover.

It was concluded that the switchover was caused by a component failure that resulted in a reduction in 2.4-kHz voltage.

b. Action Taken. It was considered that there may be a relationship between the power chain transfer and the power-on-resets (PORs) encountered by the Flight Data Subsystem (FDS) on some occasions when the gyros were turned on. The gyro turn-on transients are relatively large, and it was considered feasible that the transients were degrading one or more power subsystem components and finally causing a failure. In order to reduce possible stress on the power chain, the following action was taken:

(1) L + 75 days (GMT 017): gyros were turned on supposedly for the remainder of the mission.

(2) L + 79 days (GMT 021): reduced loads for TCM 2 to avoid the solar array/battery share mode and its associated transients. On L + 86 days (GMT 028), the spacecraft roll axis started to oscillate because of a structural dynamic coupling problem, so the gyros were turned off. The policy of reducing stress on the power chain continued:

(3) L + 103 days (GMT 045): reduced the loads for a gyro test.

Normal operations were later resumed because cognizant power subsystem design personnel completed an analysis which concluded:

(1) Switching loads off prior to each gyro turn-on did not reduce the risk of damaging the power chain; it may even increase the risk slightly.

(2) There was no significant stress on the power chain when transferring out of the share mode.

c. Relation to Preflight Problems/Performance. There is no evidence of any part problems other than the 1N3892 diodes. Only one 1N3892 diode was known to have failed the MM'71 testing program, none failed the Mariner 10 testing, and no failures were detected in the VO'75 testing until after Mariner 10 was launched. The problem with the 1N3892 diodes could have been detected under an expanded test program.

d. Recommendations. Component testing should be maintained at the same level on future programs because of the increased costs associated with an expanded program. However, the screening tests of 1N3892 diodes have been modified to limit the diode junction temperature to 150°C. Previous test methods allowed temperatures as high as 222°C.

The switchover design philosophy was reevaluated, with consideration of adding the capability to switch back to the main power chain if proven to be operating properly by in-flight tests. This approach was rejected because of the added design complexity, and of the successful record of the present design.

2. Solar Panel Current Anomaly

The following is a brief summary of the solar panel current anomaly that occurred on March 9, 1974 (GMT on Day 068).

a. Description. During the solar panel differential tilt test of March 9, 1974, the panel current sensors were changing as a result of the -X panel tilt being changed from 76 to 60 deg. At approximately Day 068 19:04 GMT, the No. 1 current sensor of the -X panel decreased 9 DN (-0.36 A) and the other three panel current sensors increased by 3 DN each (a total of +0.36 A). The general trend during this portion of the transient was 1 DN difference per change.

b. Analysis Effort. Initially, this anomaly was diagnosed as a shorted zener diode on one of the three electrical sections associated with the No. 1 current sensor of the -X panel. This diagnosis was later shown to be incorrect.

On the same day of this anomaly, twelve hours later, the -X solar panel was unintentionally tilted to a tilt angle of 50 deg. As a result of this error, the panel temperature went up to the type-approval temperature, and the PS&L voltage decreased to 39.73 V. An analysis of the flight data during the 50-deg tilt showed that the ratio of the -X panel current sensors 1 and 2 started to change immediately as the PS&L voltage changed, and increased continuously to the point where the voltage reach a minimum value. Had the anomaly been a shorted zener, the ratio of the current sensors would have been expected to remain approximately constant until the PS&L voltage reached ≈ 40 V (the regulation voltage of a solar panel section with a shorted zener diode). Further, a large increase in the ratio would have been expected when the PS&L voltage fell below the regulation voltage of the partially shorted zener diode string. The fact that a gradual change instead of an abrupt change in current was seen is solid evidence that the anomaly was not the result of a shorted zener diode.

Based on the assumption that the anomaly was caused by a failure (short) of some series-parallel configuration of solar cells, an analysis was conducted to determine what series-parallel configuration of shorted cells would match the ratio of the -X panel current sensors in flight. Two cases were considered:

(1) Both panels at 66-deg tilt

(2) -X panel at 50 deg; +X panel at 76 deg

The analysis showed that a group of shorted cells having five in parallel by four in series provided the best fit for the data at both of the above cases. This is somewhat unrealistic in that the solar panels are made-up modules having 3 or 4 cells in parallel. In spite of this discrepancy, the 5 by 4 configuration has been used in succeeding analyses of solar array prediction.

The analyses of this anomaly cannot be considered conclusive because of the limitations of the flight data. However, it is certain that the anomaly was not a shorted zener diode in the solar array regulator.

c. Effect of Problem. There was no impact on the mission from this anomaly other than to reduce the useful power of the solar array by a small amount.

The reporting system was altered to place more emphasis on monitoring the panel current data and the ratio of section currents within a panel. The mission was not altered because of this problem.

d. Relation to Preflight Problems and Performance. A short across a number of submodules could be caused by shorts from the solar panel substrate to the solar cells. Voids were detected in the dielectric insulation of some of the substrates, but these were repaired. Also, there is a layer of adhesive between the cells and the dielectric which provides additional protection from shorts. There would have to be at least two shorts between the substrate and the solar cells[3] in order to have a power loss (the substrate is separated from the solar array power return by a 5000 Ω resistor). It is unlikely that this sort of failure occurred, and it is doubtful that an expanded test program would have significantly reduced the possibility of this type of failure.

There was a problem with the solar cell manufacturing process that resulted in many of the solar cells having corner cracks. It is possible, but unlikely, for a corner piece to come loose and short a submodule,[4] but the analyses (to date) suggest a number of series cells (or submodules) were shorted. Therefore, it is unlikely that this problem was the source of the anomaly.

An interconnector[5] corrosion problem was discovered during the solar panel assembly and testing program. The interconnectors were found to have an acid residue which caused the corrosion when exposed to water vapor. This problem was resolved by cleaning the interconnectors and replacing a few where the corrosion was extensive. It was assumed that no corrosion would take place in flight because of the absence of water vapor. This problem may not be related to the solar panel anomaly, as the corrosion problem would tend to cause an open circuit, whereas the analyses suggest that the anomaly was caused by a short across a group of cells. If the corrosion problem was the source of the

---

[3] Unless the chassis was shorted to the power return line at some other point in the system.

[4] A group of parallel cells.

[5] A device used to connect solar cells in series and parallel.

solar panel anomaly, it could possible have been prevented by life testing[6] solar cell modules that had the acid residue. However, had it been determined from the life test that in-flight corrosion was possible and that a refabrication of the solar panels was required, the refabrication would have been expensive and could have jeopardized the launch date.

It is possible for the solar panel anomaly to have been caused by a piece of debris which fell across the panel and shorted a group of cells. This obviously would have no bearing on preflight testing.

c. Recommendations. It is recommended that no changes be made in the solar panel development and test philosophy as a result of this anomaly because of the following:

(1) There is no strong evidence indicating the mechanism of failure.

(2) The development and test philosophy used on the Mariner 10 program has proven to be successful on other programs.

3. 87-W Power Increase

a. Description. The following is a brief summary of the power anomaly of March 31, 1974, 09 GMT. The initial response to the anomaly was as follows:

(1) Booster regulator input current sensor increased ≈1.9 A (93 W).

(2) PS&L voltage decreased ≈0.75 V.

(3) Raw DC load power decreased ≈9 W (TV optics heaters became inoperative).

(4) Spacecraft power increased ≈77 W.

(5) Spacecraft bay temperatures began to increase (particularly Bay 1 where much of the power equipment is located).

(6) Battery voltage began to drop (because of temperature increase).

(7) Temperature sensor 2 on each solar panel showed an (artificial) increase.

(8) Zener temperatures began to drop.

The long-term response to the anomaly was:

(a) BR input current sensor indicated an additional load of ≈87 W.

(b) PS&L voltage was down slightly (as expected).

• (c) TV optics heaters remained inoperative.

(d) Spacecraft power demand up by ≈78 W.

(e) Temperature sensors 2 on each solar panel remained high (artificial).

(f) Zener temperatures remained low (as expected).

(g) Bay temperatures remained high (particularly Bay 1).

Although their relationship to the problems in the power subsystem is unknown, these subsystems were also affected by the anomaly:

(1) DSS power relay toggled occasionally.

(2) Many telemetry signals were noisy.

(3) X-band transmitter failed occasionally.

(4) MDS failures. The TWT would not respond to DC 42 (high power) or DC 43 (low power).

(5) PSE SES erratic.

b. Analysis Effort

(1) A BR failure analysis was performed to determine the maximum current the BR could draw under a failed condition and still regulate the output voltage proper. The maximum current increase for this failed condition was calculated as 0.6 A.

(2) The BR input current was plotted versus the 2.4-kHz inverter output current to determine if the increased demand at the BR input was related to the output load of the power chain. There was no relationship established which indicates that the failure is not in the BR or the 2.4-kHz inverter. From this, one can conclude that the additional load is between the BR current sensor (in 4A8) and the standby BR (4A10).

(3) A partial analysis of harness wiring was conducted to determine if there was a relationship between the failure characteristics within the power subsystem. No relationship was established.

(4) A review of the circuit diagrams was conducted to determine if there were any obvious failure modes that would result in a 2-A current increase. There was none.

(5) Many analyses were performed by other subsystems to evaluate the response of their respective subsystems to the failure.

c. Effect of Problem. This anomaly occurred during the Mercury far encounter. The first reaction was to reduce the loads to see if this would have any impact on the failure. The X-band transmitter and magnetometers were

---

[6]A limited life test was performed by Boeing, but no corrosion was detected.

turned off separately for approximately 25 min each, and the TVs were turned off for almost 15 hours. The TWT was on low power for one week, and the battery charger was off for over 17 days.

The additional spacecraft load resulted in a larger battery discharge during off Sun maneuvers.

d. Action Taken. The major impact of this anomaly on the power subsystem is the additional load of ≈87 W. The solar array power margin was adequate to permit normal operation of the spacecraft load in spite of the increased power demand and the solar array failure of March 9, 1974.

e. Relationship to Preflight Problems and Performance. There was no evidence before launch that this problem existed. It is doubtful that any reasonable test program could have discovered the source of this anomaly when considering that the hardware operated successfully for 148 days if it was associated with the primary power equipment, or for 82 days if it was associated with the standby power chain.

K. ARTICULATION AND POINTING SUBSYSTEM FLIGHT PERFORMANCE

1. Summary

A brief summary of the flight performance of the MVM'73 Articulation and Pointing Subsystem (APS) is presented. This is a summary of the data accumulated during the primary phase of the mission.

The APS demonstrated successful flight performance throughout the primary mission. There were, however, several anomalies observed in flight. The types of anomalies range from APS command overrides to a possible structural problem in the scan cone axis control. There were neither component failures nor performance degradation in the APS electronics.

2. Introduction

Figure 141, a simplified diagram, illustrates the various functions that APS performs on the Mariner 10 spacecraft. As shown, the APS performs six pointing control functions. It controls the pointing of the high-gain antenna (HGA) by articulating in the boom and dish axes, the pointing of the scan platform in the clock and cone axes and the updating of the tilt angles of the ±X axes solar panels. Figure 142, a detailed diagram, shows the actual configuration of the six actuators.

This report presents a brief performance summary of the following APS functions:

(1) APS electronics

(2) Solar panel control

(3) HGA pointing control

(4) Scan pointing control

3. APS Electronics

The APS electronics performed successfully throughout the primary mission. There were no observed hardware failures.

The APS electronics, as shown in Fig. 143, consists of dual redundant control channels. Each channel is multiplexed among six control actuators. Both feedback and incremental position modes are utilized to control the positioning of the six actuators.

Since there is a common power switch for the two channels, both channels were turned on together prior to launch and remained powered for the rest of the mission. The Channel 1 electronics was used throughout the primary mission while the Channel 2 remained as a standby unit. The telemetry outputs used to monitor the APS status in flight are shown in Fig. 142.

One anomaly was recorded by Day 330 (Nov. 26, 1973) when a command from the Flight Command Unit (FCU) was interpreted within the APS with an incorrect slew polarity. The cause of the problem was thought to be noise in the FCU-APS interface circuitry.

4. Solar Panel Control

The APS successfully controlled and updated the tilt angle of the solar panels. The tilt angle update was periodically performed to adjust the surface temperature of the solar panels. Figure 144 illustrates the panel tilt angle updates as a function of days from launch through Mercury encounter. Table 40 shows a summary of predicted and actual telemetry data numbers (DN) for the tilt angle update operation. As shown, the positioning of the solar panels was achieved within ±1 DN (±0.04 deg) of the predicted fine telemetry value.

From the 126th day to Mercury far encounter, solar sailing was effected by differentially positioning the solar panels to generate a control torque and achieve roll-axis attitude control without the use of the roll attitude-control gas jets. During this operation, the panels were rotated between 60 and 76 deg.

5. HGA Pointing Control

The APS successfully controlled the pointing of the HGA throughout the primary mission. One operational anomaly was recorded on Day 5, (Jan. 5, 1974) when an interference occurred between the HGA structure and the uncoiling cable bundle wrapped around the HGA boom.

On the same day, the HGA dish actuator was commanded incrementally to a dish angle of -4.5 deg, which was outside of the nominal operational range. The dish apparently encountered an obstruction before the final position was reached and stalled at -3.9 deg.

The slew was terminated by a subsequent stop command. It was determined that the actuator had stalled when the HGA dish Y-bar was
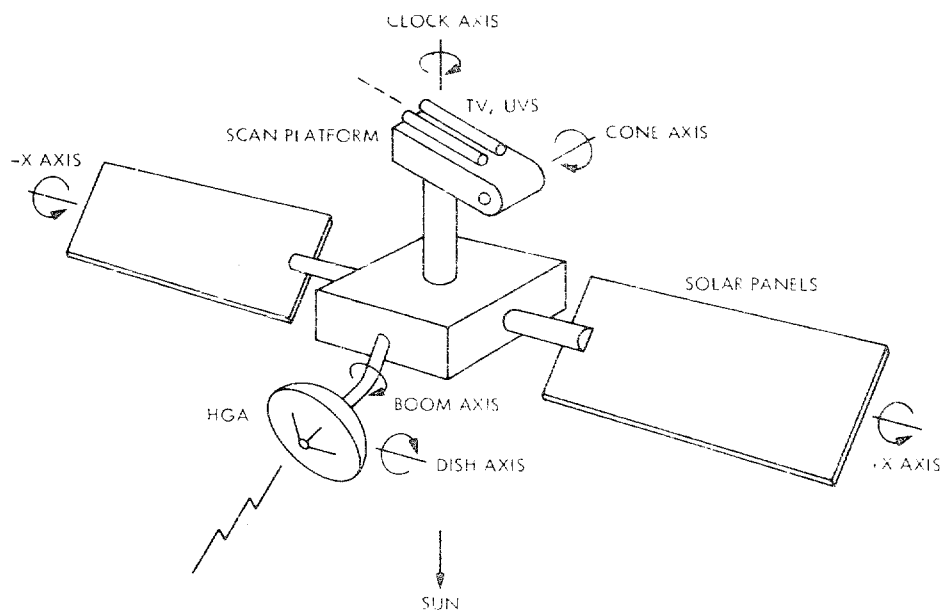
Fig. 141. APS functions
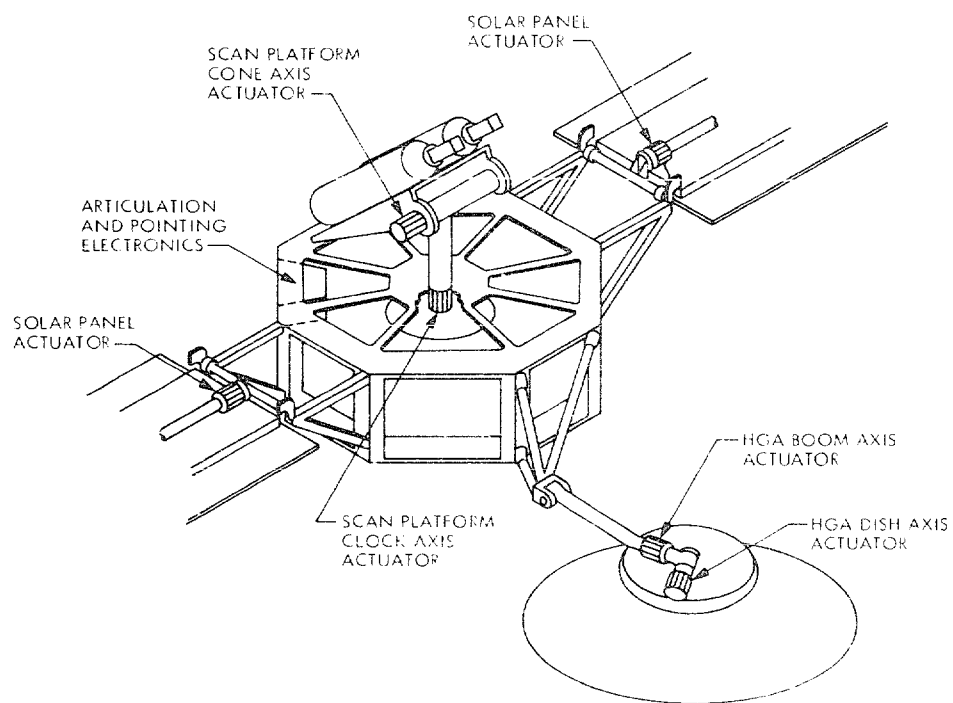
Fig. 142. APS configuration

pressed against the uncoiling cable wrapped around the HGA boom.

a.   Initial Deployment.   The boom and dish actuators were not connected at launch to their respective gimbals to avoid launch vibration that could be transmitted to the actuator shafts.   After launch the HGA structure was first unlatched by the spacecraft separation-initiated timer (SIT). After the Sun had been acquired, but prior to initial star acquisition, the dish and boom actuators were slewed.   A dish angle of -16 deg and boom angle of 13.9 deg were commanded to enable the drive pin engagement between the actuators and the gimbals.   After drive pins had been engaged, the dish gimbal was unlatched by ground command DC 49.   The dish gimbal was then slewed back to 87 deg.   The boom gimbal remained at 13.9 deg during the deployment operation.   The deployment chronology is shown in Table 37.

b.   Performance.   Both position and incremental modes were used in the pointing control of the HGA.   The position slew was verified (i.e., the actual value matches the predict) within 1 ~ 2 DN (0.04 ~ 0.08 deg) on the fine telemetry readout.   The incremental slew, particularly a short slew of 100 increments or less, was normally predicted exactly (i.e., within the readout resolution of the fine telemetry).

The backlash observed in the dish and boom axes were about 1 to 2 DN (0.04 ~ 0.08 deg) and 3 DN (0.12 deg), respectively.   An increase in dish axis backlash was observed during the HGA flip-flop operation on Day 53, when the dish gimbal was at 4.7 deg.   At a higher dish angle such as 85 deg, the backlash was typically 1 DN. The increased backlash was probably due to a similar interference between the Y-bar and the boom cable as observed in the Day 5 anomaly.

Some HGA boom axis positions were attained by CW and CCW slews.   This pair of position data provided a measure of hysteresis in the position mode.   The hysteresis observed was typically 1 DN (0.04 deg) and was repeatable.

6.   Scan Platform Pointing Control

The APS successfully controlled the clock and cone axes pointing of the scan platform throughout the primary mission.   There were some anomalies observed in the high cone angle operations.   As a result, some high cone angle slews (greater than about 163 deg) were deleted from the Venus encounter TV/UVS mosaics. Several engineering tests were performed in flight to investigate the problem.   Both position and incremental slews were used to achieve pointing of the platform.

7.   Scan Platform Unlatch and Deployment

After the Sun had been acquired but prior to initial star acquisition, the scan platform was unlatched by a CC&S 8C command.   Subsequently, the platform was slewed from 47-deg cone stow position to 58.9 deg, clearing a non-reversible pin latch at 58.4 deg.   This pin latch became the lowest cone angle physical limit after initial cone deployment (see anomaly in the second engineering test).   The platform remained in

the 255-deg clock stow position until Vega acquisition.   Table 36 shows a simplified sequence of APS events following the spacecraft separation from the launch vehicle.   Note that the UVS mosaic sequence originally planned to be performed after Vega acquisition was deleted due to a delay in acquisition.

8.   Scan Clock Control

The scan clock axis control was performed without any anomaly during the primary mission. An example of a typical scan clock axis slew performance is shown in Fig. 145.   Backlash observed in incremental slews was typically 3 to 4 DN (0.12 to 0.16 deg) in the fine telemetry readout.   In incremental slews, particularly those slews shorter than 100 increments, the final actuator position had been normally predicted exactly (within the telemetry readout resolution).   In position slews, the actuator positions had been predicted within 1 to 2 DN (0.04 to 0.08 deg) of the actual telemetry values.

Typical clock axis stepping characteristics and the fine telemetry dead zone characteristics recorded by the fine telemetry readout are shown in Figs. 147 and 148, respectively.

9.   Scan Cone Control

The scan cone axis control experienced some problems at high cone angles.   The first problem was noticed on Day 349 (Dec. 15, 1973) during a scan calibration sequence when an unexpectedly large backlash of 8 to 10 DN (0.32 to 0.40 deg) was observed at an angle of 161 deg in cone.   A nominal backlash observed prior to this date at much lower cone angles was consistently about 4 DN (0.16 deg).   The slew signature is illustrated in Fig. 148.

On Day 352 (Dec. 18, 1973) during the UVS helium wind experiment, a very sluggish cone axis movement was observed at angles between 160 and 179.7 deg.   An apparent slowing of cone axis motion is shown in Fig. 149.

As a result of these anomalies, a series of five scan engineering tests was performed between Day 7 and Day 57 (Feb. 26, 1974) to obtain more pertinent data on the cone axis slew signatures.   The tests covered a range of cone angles from 58 deg to 167 deg.   A sample slew pattern from the first engineering test is illustrated in Fig. 150.   As shown, the slew increments appeared normal, but increased backlash was observed at higher cone angles.   Also it appeared that the increased backlash is independent of the clock angle.

Figures 151 through 153 show some of the cone axis slew signatures recorded during the scan engineering test.   Figure 151 shows the start of a slew against backlash of 10 DN (0.4 deg) at a cone angle of 166.6 deg.   Figure 152 shows a normal cone actuator slew without backlash at a lower cone angle.   Figure 153 shows the end of a position slew when slowing occurred. Note that the actuator did reach the correct final position.

The result of the test indicated the following:
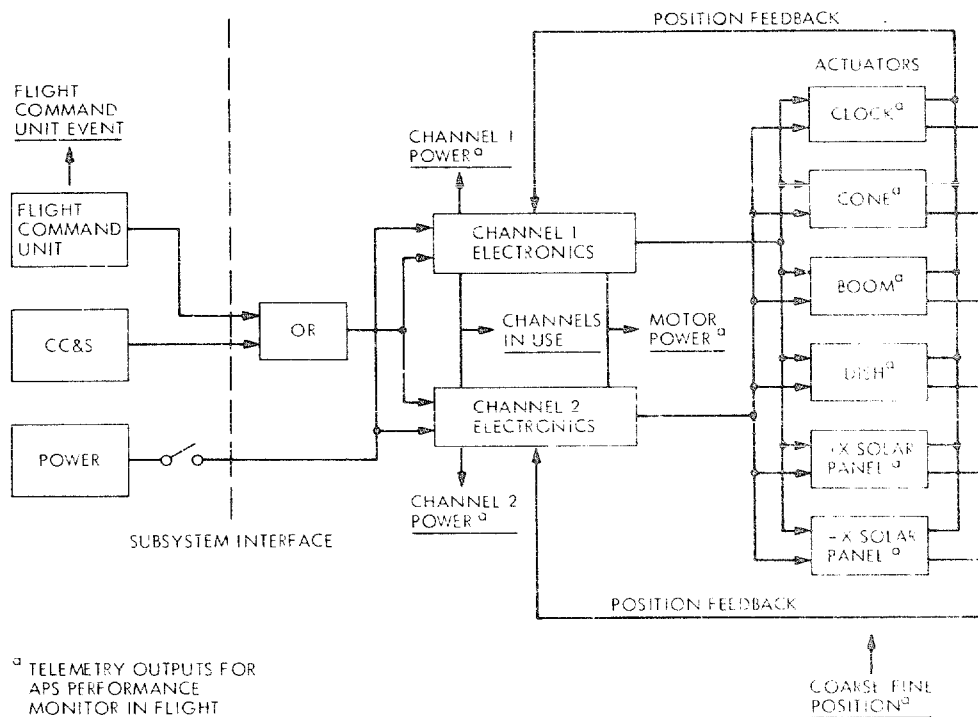
Fig. 143. APS block diagram
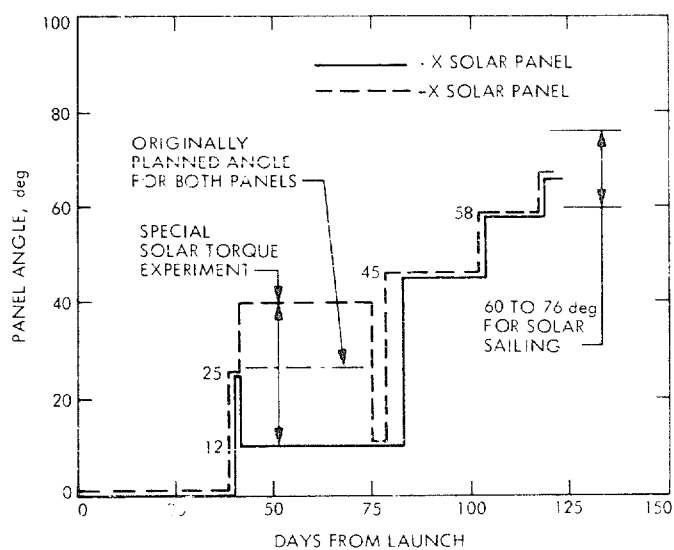
Fig. 144. Solar panel tilt profile

BL   BACKLASH
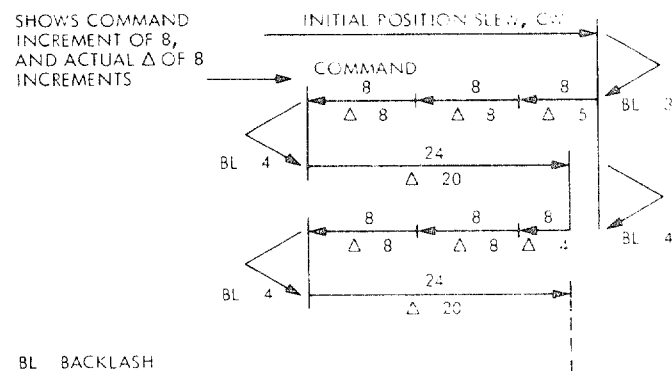
Fig. 145. Typical scan clock axis slew performance during TV mosaics

Fig. 146. Clock slew

127 DN

2 DN WIDE (≈0.08 deg)

1 DN (0.04 deg)

0 DN

1 in./sec

18:16:18   18:16:24

DAY 18, GMT
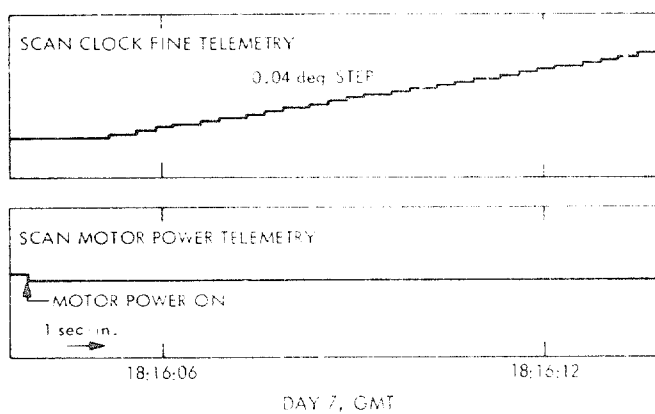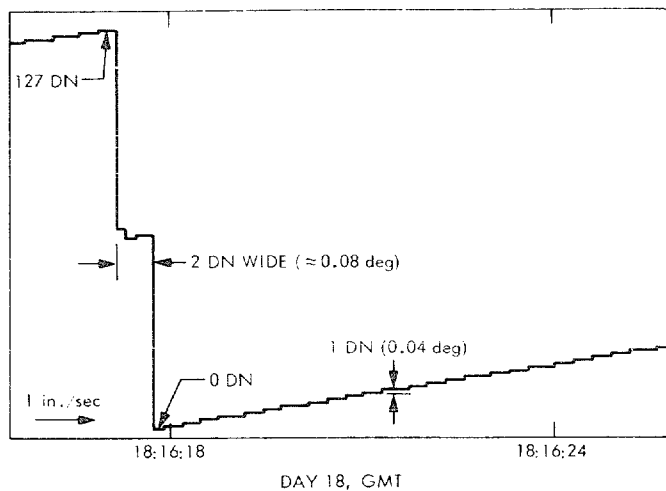
Fig. 147. Scan clock telemetry potentiom-
eter dead zone and stepping
characteristics

BL   10 DN[a]   BL   10 DN[a]

161.1 deg

15 Δ 15   14 Δ 6   14 Δ 6

P 1823
160.5 deg   19 Δ 9

BL 8 DN[a]

BL   BACKLASH

P   POSITION COMMAND

[a]UNEXPECTEDLY LARGE
BACKLASH OBSERVED
1 DN ≈ 0.04 deg

P 1246

CW DIRECTION
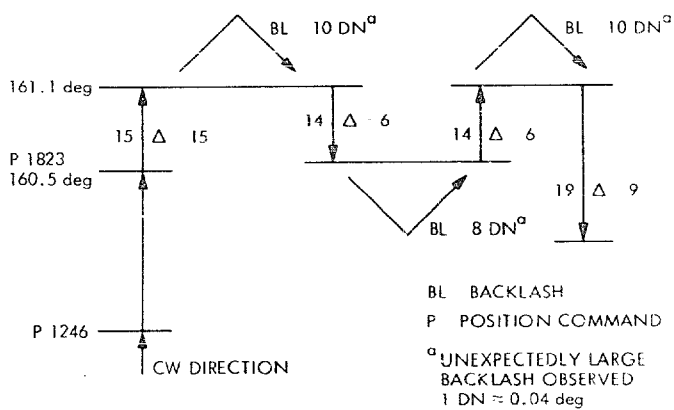
Fig. 148. Cone anomaly, GMT Day 350
(Dec. 15, 1973)

EXPECTED SLEW
PATTERN FOR
POSITION COMMAND
1976

179.7

176.1
ABORTED BY AN
ALL-ZERO
STOP COMMAND

170.8
ACTUAL SLEW
PATTERN

165.5
TELEMETRY
SAMPLES

160.3

42 s   SAMPLING INTERVAL

155
0   42   84   126   168   210   252

16:26:27   16:29:57

TIME, sec

GMT
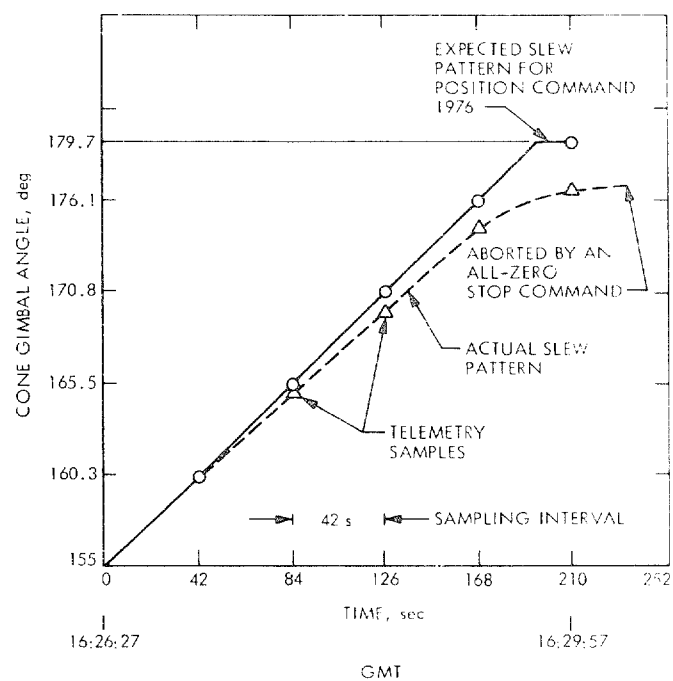
Fig. 149. Scan cone slew anomaly,
GMT Day 352 (Dec. 18,
1973)
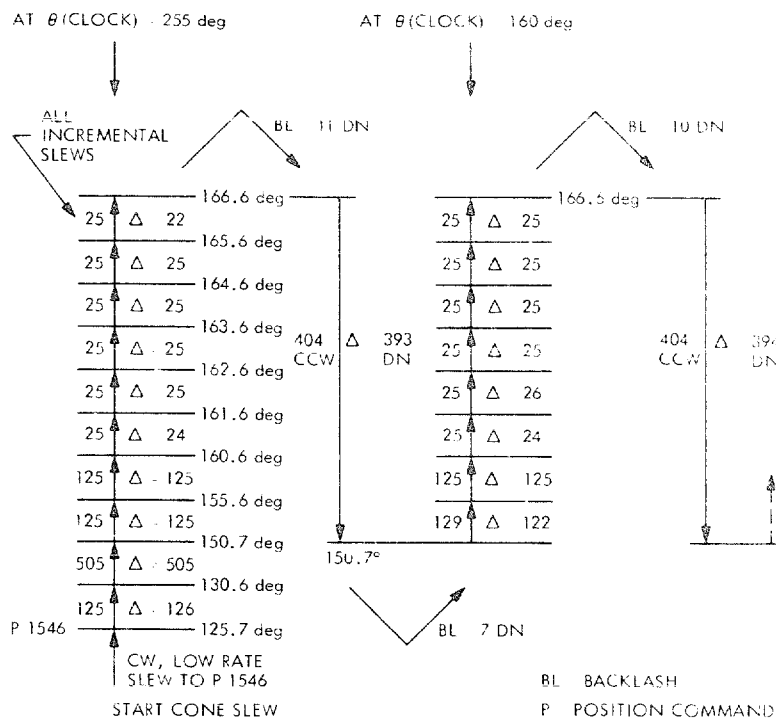
Fig. 150. Typical test slew pattern
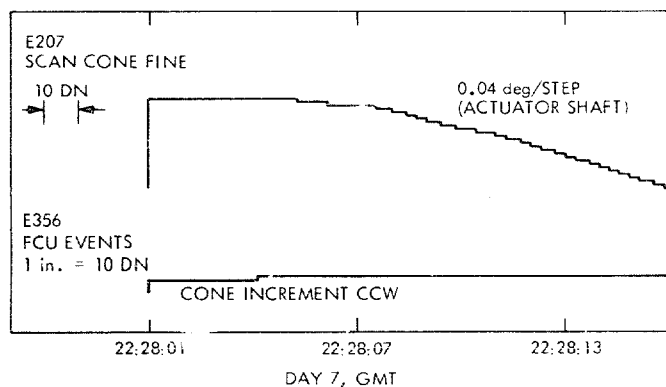
Fig. 151. Cone slew, 166.6 to 150.6 deg
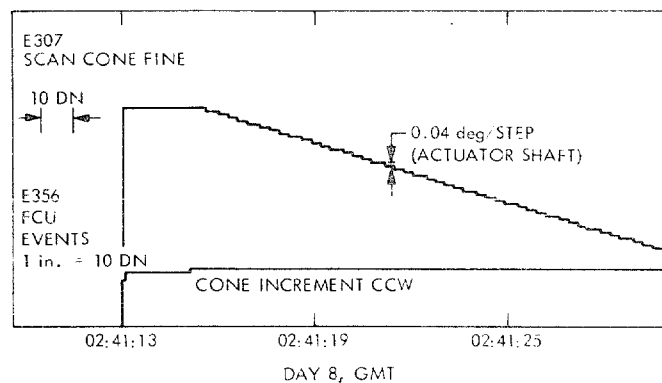
Fig. 152. Cone slew, 120.9 to
81.2 deg
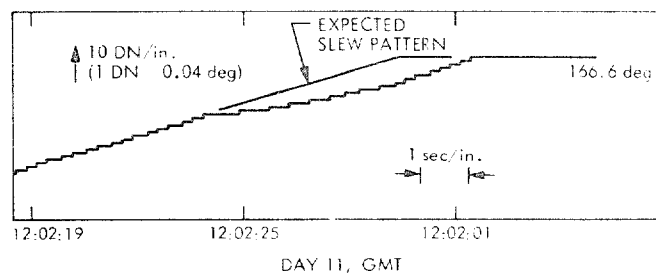
Fig. 153. Cone slew, 60 to 166.6 deg

Table 36. Summary of predicted versus actual telemetry data numbers for tilt angle updates

Days after launch	+X panel			-X panel		
	Tilt	Predict	Actual	Tilt	Predict	Actual
	deg	DN, Coarse/fine		deg	DN, Coarse/fine	
	0			0		
41 Days	25	75/53	76/52	25	51/77	50/76
42 Days	12		69/118	40		43/89
76 Days	12		69/118	12		57/15
79 Days	45	86/35.5	85/35	45	41/89	40/89
103 Days	58	92/99.5	91/99	58	34/20.4	34/20
117 Days	66	96/41.2	95/41	66	30/77.8	30/77
126 Days	60-76			60 to 76		

One fine DN $\approx$ 0.04 deg at actuator output shaft.

Table 37. Launch phase deployment summary

GMT, day 307	Event
06:24:00	Spacecraft separation
06:27:15	Began Sun acquisition
06:45:00	Unlatched solar panels, MAG boom, LGA, HGA
07:09:14	Sun acquired (sun gate)
07:00:00	Dish pin engaged
07:05:00	Boom pin engaged
07:24:23	Unlatch HGA Dish by DC 49
07:38:00	Scan platform unlatched by CC&S-8C
07:45:00	Dish axis slew, CW 1000 steps
07:51:00	Dish axis slew, CW 1000 steps
08:57:00	First scan cone position slew
09:38:00	Canopus tracker turned on
10:08:00	Expected Vega acquisition time
11:05:00	Scan mosaics for UVS helium experiment, deleted
16:45:00	Vega acquired

(1) Some slowing was observed at a cone angle as low as 150 deg.

(2) Slowing becomes more evident at cone angles above 160 deg.

(3) Backlash increases with increasing cone angle and sharply increases above 165 deg. A summary of backlash as a function of cone angles is shown in Fig. 154.

(4) When reversing the slew direction, from CW to CCW, a peculiar startup transient was observed. An example is shown in Fig. 151.

An initial list of candidates that were considered to be the cause of anomalies included the following:

(1) Binding and twisting of the scan platform cable bundle.

(2) Increased cone axis bearing friction.

(3) Actuator clutch slippage.

(4) Motor stalled.

(5) Interference with the platform thermal blanket.

(6) Low temperature effect due to the TV heater failure.

Subsequent investigation provided the following information:

(1) A special twist test performed on a simulated scan cable showed that a

maximum torque generated by the wound-up cable, at -17.8°C (0°F), would be about 0.68 N-m (6 in.-lb). This torque would be too small to cause the anomaly.

(2) Thermal blanket fit was checked at high cone angles at Eastern Test Range (ETR) prior to launch and the last blanket tie was deleted to insure necessary clearance at high cone angles.

(3) A special actuator test was performed at JPL using a prototype actuator. The test indicated that the clutch could not have slipped when driven by the actuator motor unless the clutch slip torque decreased in flight. In this test the motor stalled when the actuator output shaft was held stationary. The clutch slip torque, when back driven, was a minimum of 56.5 N-m (500 in.-lb).

When the motor is stalled, the power supply current should increase slightly and the amount of increase reflected on the supply voltage is a function of the APS power supply dynamic impedance. The power supply voltage fluctuation could have been monitored during the anomalous slews if it had been on a higher rate telemetry channel.

Figure 155 shows a sample of the APS power supply voltage fluctuation during a normal slew. Note that no fluctuation is observed in the clock axis slew shown in Fig. 146.

(4) The temperature of the cone actuator and the gimbal during the TV heaters malfunction was estimated to be about -17.2°C(1°F), a temperature well within the Flight Acceptance test temperature of -20°C (-4°F). The TV heaters which came on unexpectedly on Day 17 (Jan. 17, 1974) raised the actuator temperature to about 7.2°C (45°F). Examining the result of the fourth and fifth engineering tests which were performed after the Day 17, it was evident that a higher platform temperature did not eliminate the anomalous cone slew characteristics. Therefore, the effect of the low temperature was ruled out as a single cause of the anomaly.

No conclusion has been drawn to explain the cause of the anomaly. It has been hypothesized that the most probable cause is an excessive friction torque in either gimbal bearing or drive link mechanisms.

10. Anomaly During Engineering Test

An anomaly occurred on Day 11, 1974 during the second engineering test when the cone actuator was commanded to 58.6 deg. The platform apparently hit an obstruction at 58.8 deg and stalled the motor. The commanded cone angle was just within the operational low limit of 58.4 deg. It was hypothesized that this obstruction could be an HGA support strut that had not folded out of the way completely.

After the anomalous slew into the obstruction, the actuator was commanded away from it incrementally. This slew pattern is shown in Fig. 156. Subsequently, the cone actuator was slewed to 59.2 deg in cone, without encountering the obstruction, and slewed back incrementally to 61.1 deg. This slew pattern, shown in Fig. 157, is a normal slew signature against a backlash.

11. Fine Telemetry Potentiometer Deadzone

Figure 155 shows a trace of signal through the deadzone of the fine telemetry potentiometer. The deadzone is about 1.5 DN wide. This corresponds to 0.06 deg referred to the actuator output shaft or about 4.2 deg on the fine T/M potentiometer. Note the length of the zero-DN region. It is almost 0.1 deg referred to the actuator output or 6.7 deg on the fine telemetry potentiometer. Note that the clock actuator has a much shorter 0-DN region as shown in Fig. 147.

L. ATTITUDE CONTROL

1. Introduction

This section documents the Mariner 10 launch performance from launch to the end of the primary mission on April 15, 1974.

2. Launch

The Mariner 10 liftoff occurred at 307 05:45:59. The launch sequence of events is illustrated in Fig. 158 and was executed within the performance prediction envelope. The spacecraft separation from the lauch vehicle occurred at 307 06:24:00. The events subsequent to separation pertinent to the attitude control subsystem are listed in Table 38. Figure 159 illustrates the attitude-control celestial and inertial sensors error signals following the separation event. The next few paragraphs will describe spacecraft occurrences as interpreted from Fig. 159.

a. Sun Acquisition. The initial rate-reduction Sun search was initiated immediately after separation; however, the solar panels did not begin to unlatch until 307 06:27:39 and were not completely deployed until 307 06:29:15. The implications of the above event sequence are as follows: Prior to solar panel deployment, the spacecraft pitch and yaw axes search for a celestial null which may or may not be near the actual celestial null. The data observed during this period is obscured by data outages, and no definite statements on tipoff rates or orientation can be made.

During the solar panel deployment, the sun sensor fields of view are moving rapidly, resulting in changes in the rate of search polarity in both the pitch and yaw axes.

Following solar panel deployment, the yaw axis had apparently found an approximate celestial sensor null. This is indicated by the yaw position sensor signal within the sun gate limits, (about 6 deg), and a gyro rate reduction.

Following solar panel deployment, the pitch axis appeared to go into sun search for about
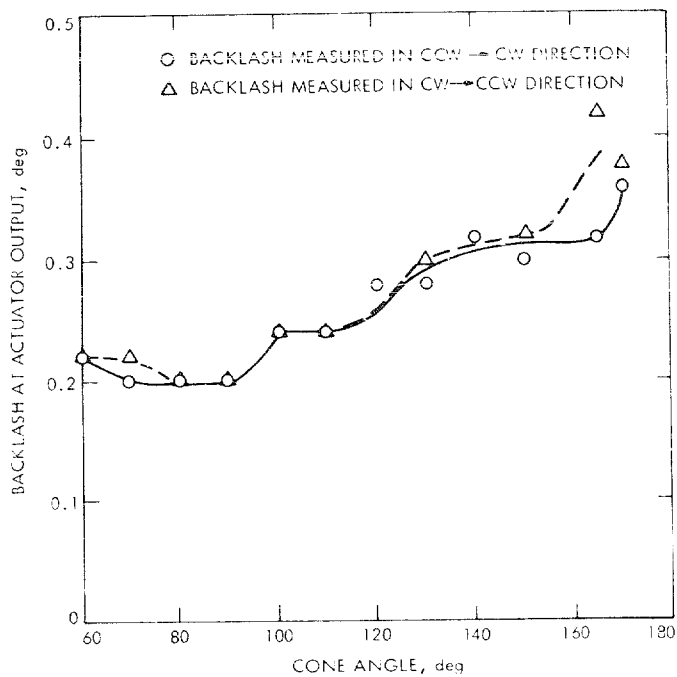
Fig. 154. Cone axis backlash as a function of cone angle
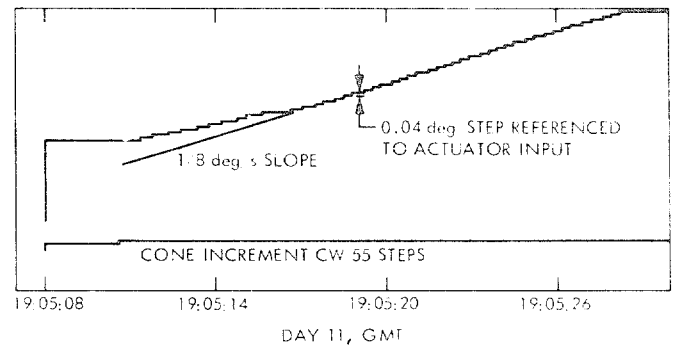
Fig. 156. Cone slew, 58.8 to 60.6 deg
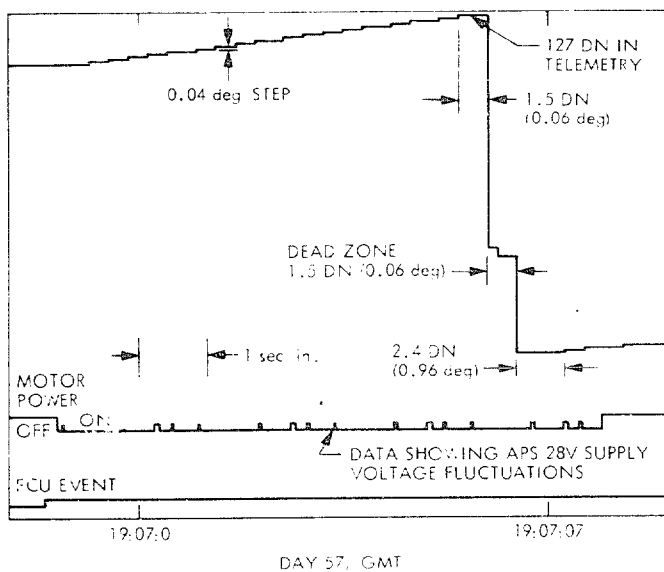
Fig. 155. Cone slew showing telemetry fine potentiometer dead zone
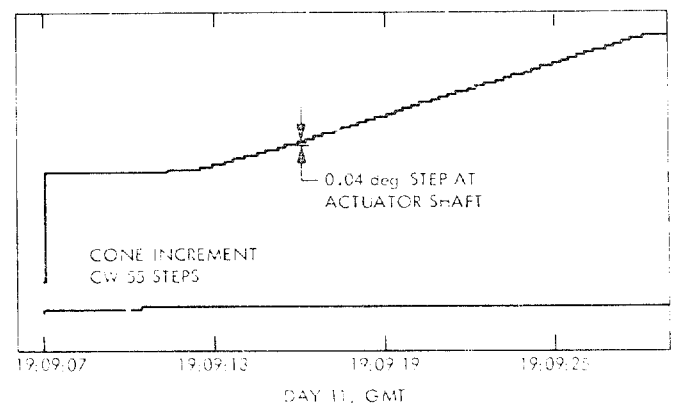
Fig. 157. Cone slew, 59.2 to 61.1 deg

Fig. 153. Launch sequence of events

Table 38. Launch events through celestial acquisition

Spacecraft event time (GMT)	Day	h	min	Spacecraft event time (GMT)	Day	h	min
Atlas centaur liftoff	307	05	45	DC 19 start roll search (reset DC 18)	307	10	50
Spacecraft separation and start of Sun acquisition	307	06	24	DC 18 roll inertial (end roll search and +2 deg turn)	307	11	07
Unlatch solar panels, mag boom and HGA	307	06	45	DC 12 steps adaptive gate to Gate 3	307	15	20
Apparent Sun acquisition (no sun gate)	307	06	33	7M1-7M2-7M4 start of positive roll command turn	307	15	21
Unlatch and deploy PSE boom	307	06	45	DC 19 reset DC 18 roll inertial	307	15	25
Engage HGA dish actuator pin	307	07	00	7M4 end of roll commanded turn	307	15	34
Begin final yaw Sun search	307	07	02	DC 13 (reset 7M2) and start roll search	307	15	46.0
Engage HGA boom actuator pin	307	07	05	DC 18 roll inertial -- stop roll search and +2 deg turn	307	15	46.4
Sun acquired (sun gate)	307	07	09	DC 19 reset DC 18 and start roll search	307	16	30.5
Unlatch Sun platform	307	07	38	DC 18 roll inertial -- stop roll search and +2 deg turn	307	16	31
Enable lower scan cone stop	307	08	57	DC 19 start roll search	307	16	40
Turn on Canopus tracker (begin star search)	307	09	38	Canopus null	307	16	41
Acquire reflected earth light	307	09	43	Gyros off	307	16	43
DC 18 rc'l inertial	307	10	10				
Last of 17 DC 21 (-2 deg roll turn)	307	10	47				

five minutes at an average rate of about 0.2 deg/s. These events would imply a pitch offset of about 75 deg from the pitch sun sensor null, (60 deg search to the linear field of view and about 15 deg from the edge of the linear field to the celestial null). During the transition of the linear field of view to the pitch axis celestial null, a sun gate signal should have been issued if indeed the Sun was within the sun gate field of view. Based on the telemetry data, the sun gate should have been issued at about 307 06:34.

Beginning at about 307 07:02 a yaw axis sun search was gradually initiated which resulted in a sun gate signal at 307 07:09. The yaw axis false celestial null was probably less than 80 deg and probably more than 20 deg from the actual celestial null. There are three possible reasons for the observed behavior:

(1) The planet Earth was a large bright object 2.15 × 10^4 lumens/m^2 (≈2000 ft-cd) at the time of the initial acquisition. This could have biased the acquisition sensor to a false celestial null.

(2) The Earth illumination would bias the acquisition sensor off of the actual celestial null, but probably not more than about 5 to 6 deg. However, the yaw acquisition sun sensor on Mariner 10 is a unique four-detector configuration that does have potential nulls at about 90 ± 30 deg cone.

(3) The four detector configuration is uniquely susceptible to detector open failures. If one of the two forward looking yaw sun detectors or circuitry had failed to open, a false celestial null could have been achieved if the Sun passed through a region that would have illuminated only the failed detector.

The events described in this Sun acquisition were not anticipated, but a similar event had occurred on Mariner 5.

b. Vega Acquisition. The Vega search was initiated by turning on the Canopus star tracker at 307 09:38. A normal roll search results when the Canopus star tracker (CST) output signal is

saturated, indicating that no star is in the field of view, and the roll gyro, in the rate mode, produces an error signal that effectively cancels the saturated CST signal when the roll axis is at the roll search rate. When a star of the correct intensity enters the field of view, that star is tracked, reducing the CST error signal and consequently the roll gyro rate.

At 09:43:37 a series of false star acquisitions were initiated that continued until the roll axis was placed in the roll inertial mode by a ground commanded DC 18 at 307 10:10. During this period of false Canopus acquisitions, stray light reflected from Earth would cause a star acquisition signal that would very shortly be lost due to reduced light intensity. When the acquisition signal was lost, the Canopus tracker is designed to fly back, i.e., drive the CST field of view in a direction opposite to the roll search direction in 10 ms. Following the flyback, a "sweep" is initiated which brings the CST field of view back to the roll search position in about 7 sec. At about the time the roll search position was reached, stray light from Earth was acquired again, and the sequence was repeated. During this series of false acquisitions, the gyro and gas jets attempted to track and reduce the CST disturbance and as a result about 141 g (0.31 lb) of attitude-control nitrogen gas was used.

Following the DC 18, seventeen DC 21's (negative 2 deg turns) commands were sent to step through the stray-light interference. This command sequence required about 68 g (0.15 lb) of nitrogen gas.

The roll search for Vega was reinitiated with a DC 19, which reset the DC 18 and removed roll inertial control. Vega was observed by the CST during the search, but an acquisition did not occur because the CST had been desensitized by the long exposure to the intense Earth's light. The roll search was stopped at 307 11:07 with a DC 18 (roll inertial mode). To prevent exposing the CST to Earth's light in an attempt to roll through Earth again, a commanded turn was programmed in a direction opposite to the roll search direction. In addition, a DC 12 stepped the CST adaptive gate to Gate 3, which allows for acquisition of objects of less intensity than the star Vega. This action was devised to allow the desensitized CST to initiate acquisition when Vega reentered the field of view.

The CC&S started a positive roll turn at GMT 15:21:00 and ended at 15:34:52 with an intensity indication that Vega had passed through the CST linear field of view and also indicated that the star would not be acquired with a roll search. The star map indicated that the commanded turn had ended with the trailing edge of the CST field of view about 16.72 deg past Vega.

A roll search was initiated at 15:45:01 with a DC 13 (reset the 7M2 all-axis inertial command from the CC&S) and was ended at 307 15:46:26 with a DC 18. This should have resulted in a peak displacement of about 19.72 deg so that Vega was at a maximum 3 deg within CST field of view. Since the DC 18 resulted in a +2 deg turn, Vega ended up within the CST field of view about 1 deg after turn (Fig. 160).

The next attempt at Vega acquisition was initiated with a DC 19 at 16:30:31, but was stopped with a DC 18 at 307 16:31:00. The telemetry data indicated the center of CST field of view had moved to within 0.6 deg of null but the +2 deg turn resulting from the DC 18 moved the spacecraft outside the CST linear field of view once again. However, a position error was developed by tracking the star, indicating that an acquisition had in fact occurred, and no further DC 18's were required. The final roll search to Vega was initiated by a DC 19 at 16:40:30, celestial null was achieved at 307 16:41, and the gyro power went off automatically at 16:43:40 signalling the end of the acquisition sequence.

3. Pitch Axis Disturbance Torque Observations

On GMT 004:02:10:51 there was an abrupt change in the polarity and magnitude of the pitch axis disturbance torque. The limit cycle plots for this period are illustrated in Fig. 161. The change in the disturbance torque appears to begin at about the same time as a HGA Boom low rate slew from 169.3 to 160.29 gimbal degrees. Solar pressure acting on the HGA surface is a major contributor to the disturbance torque in the pitch axis. However, between Day 004 00:40 and 02:10 the HGA boresight changed from a spacecraft clock angle of about 305 deg and a cone angle of about 150 deg to a clock angle of 301 deg and a cone angle of 157 deg. This small change in the HGA position should result in very small changes in the HGA area projected in the pitch-yaw plane and therefore the resultant disturbance torque. It must, therefore, be concluded that other forces acting on the spacecraft caused the observed change in pitch disturbance torque.

a. Observations That Support a Pitch Axis Gas Leak. The limit cycle plot in Fig. 161 verified that the force which caused the disturbance in the pitch axis does not result in any change in the disturbance torque in either the yaw or roll axes.

Figure 162 plots the pitch and yaw torque until the disturbance returns to normal at about Day 005 03:00. The total leakage angular momentum is about 0.64 N-m-s (0.47 ft-lb-s) resulting from the leakage of about 8.75×10^{-4} g (1.93×10^{-6} lb) of gas. This amount of gas would result in the change of spacecraft linear velocity by about 0.36 ± 0.04 mm/s in either the plus or minus Z-axis direction.

During the leakage period the MVM navigation team observed a net spacecraft velocity change of about 0.6 mm/s in the -Z direction. From Fig. 163 it can be observed that this could be caused by leakage from the yaw valve on the +Y axis with the nozzle opening in the +Z direction (thrusting in the -Z direction).

b. Observations That Are Inconsistent With a Leaking Pitch Axis Gas Valve. Figure 161 indicates that the last observable firing of the negative polarity pitch gas jets occurred at about 01:50:00. If a gas-jet leak induced by contaminated N_2 gas is hypothesized, then the last negative polarity pitch gas jet firing should signal a change in the observed disturbance torque polarity. Figure 161 demonstrates that this did not happen.
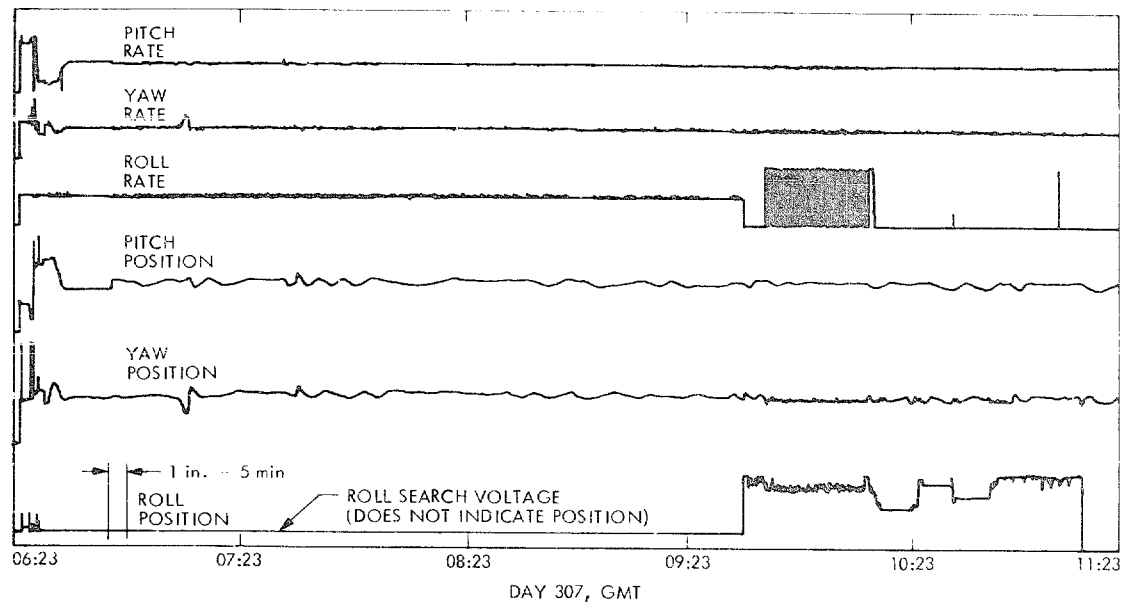
Fig. 159. Celestial acquisition
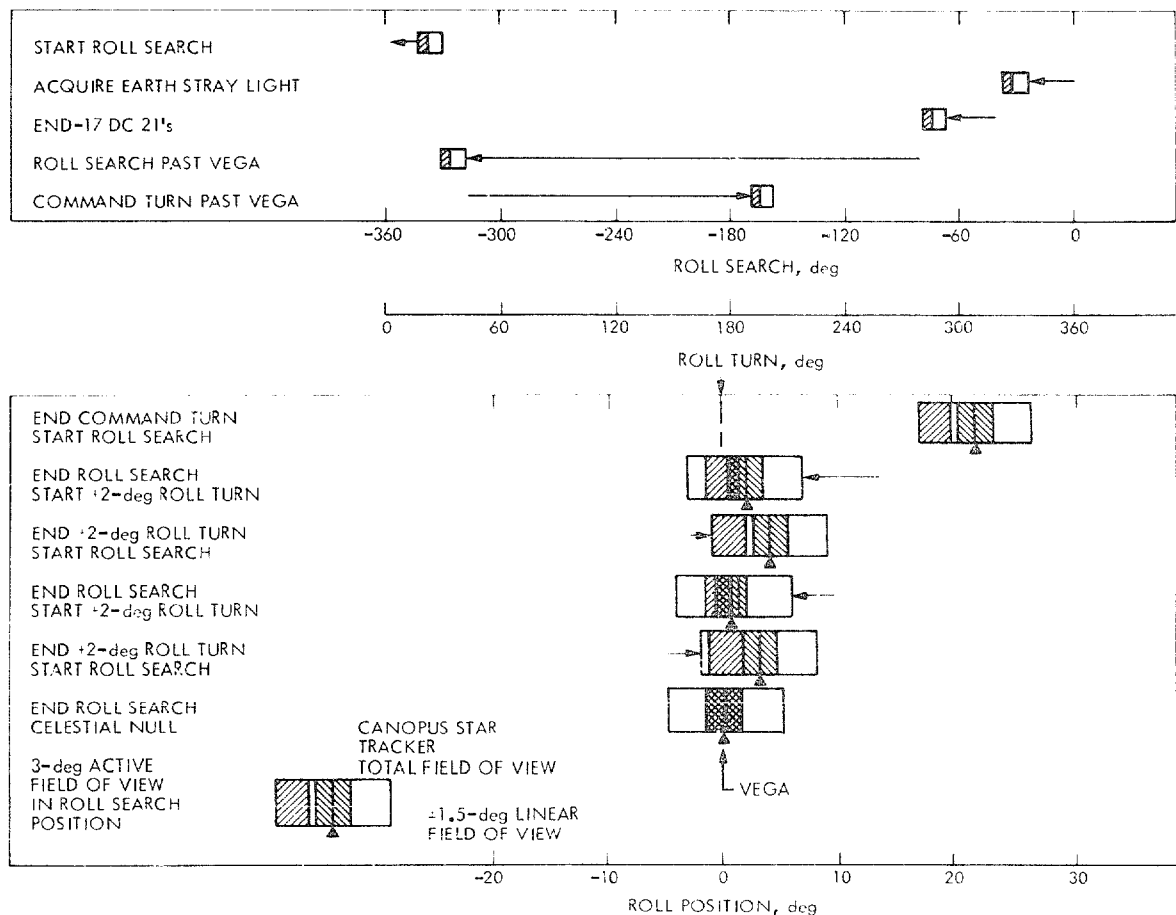
Fig. 160. Vega acquisition

PITCH AXIS

YAW AXIS

ROLL AXIS

5 min

01:30:00

02:00:00

02:30:00

DAY 004, GMT
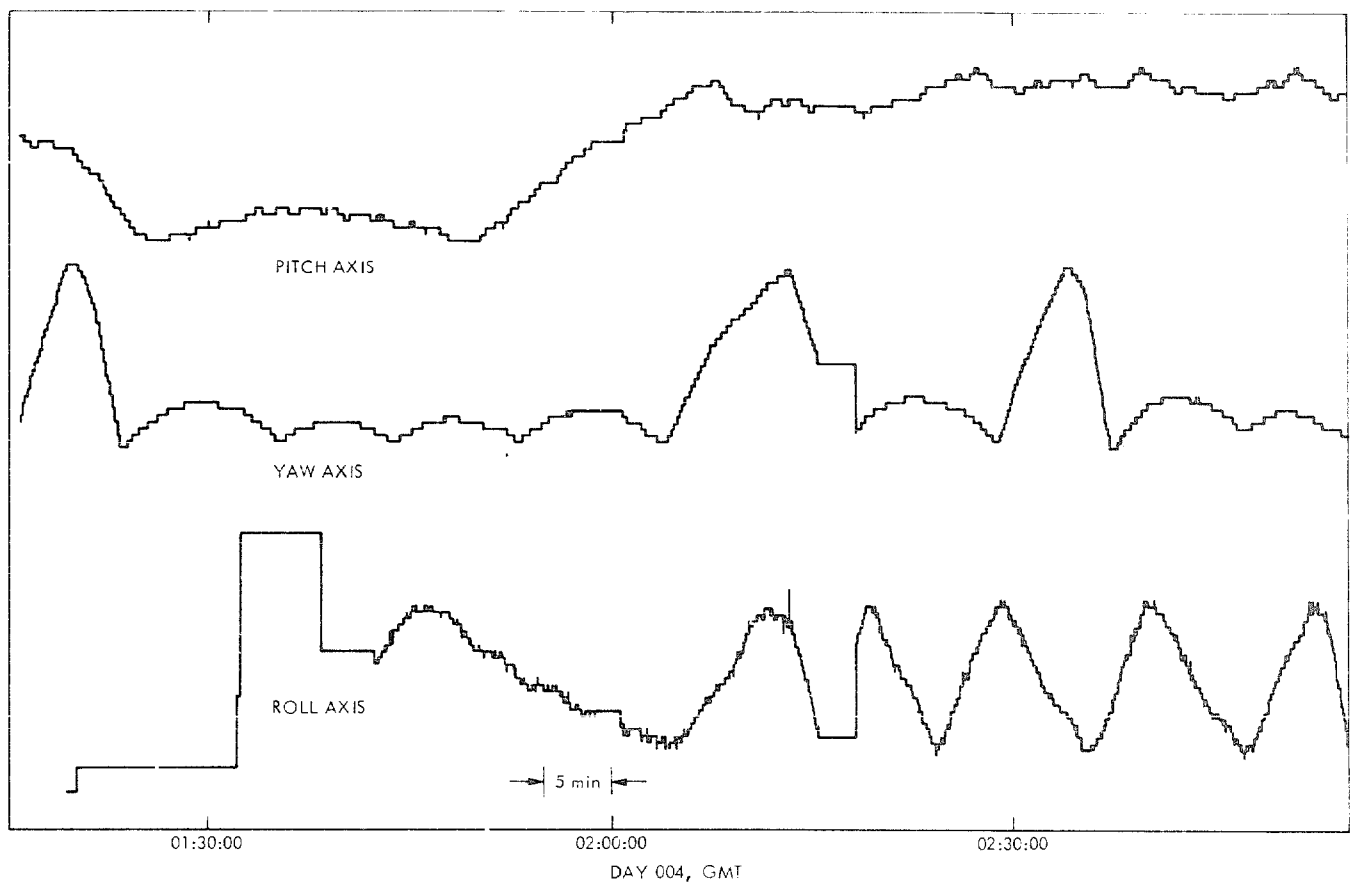
Fig. 161. Limit cycle plots, GMT Day 004

There are two possible negative pitch axis rate increments in the time interval a leak may have started. At about 02:09:20 a 11.74×10^{-6} rad/s rate change may have occurred, and at about 02:10:20 a 19.95×10^{-6} rad/s rate change may have occurred. Each of these rate increments were evaluated from about three telemetry changes, which, in general, is not enough to establish conclusive evidence of a gas jet firing. If either of these pitch rate changes are attributed to gas jet firings, then they must have been caused by noise with a magnitude on the order of 80% of the deadband width, i.e., a noisy spike equivalent to 7.04 mrad of error signal.

4. In-Flight Problem Summaries

This section provides a brief summary of selected MVM'73 in-flight problems.

The problems discussed are:

(1) Initial Canopus acquisition

(2) Roll-axis oscillation

(3) Bright particles

(4) Scan platform cone axis performance

a. Initial Vega Acquisition

(1) Description. During the initial star (Vega) acquisition beginning with Canopus star tracker (CST) turn-on at Day 307, 09:38 GMT, the stray light of Earth was acquired, resulting in a series of false Canopus acquisition signals followed by flyback and sweeps. Seventeen DC 21's were necessary to command through the stray-light region, but the extreme light intensity had desensitized the CST so that Vega was not acquired when it first passed through the CST's field of view. A commanded turn was programmed to turn back to Vega but uncertainty in the initial roll position resulted in a 20 deg turn past Vega with no indication that a star acquisition would take place.

Three roll searches followed by DC 18's (roll inertial commands) brought Vega within the CST field of view and an acquisition occurred.

(2) Analysis Effort. Turn magnitude analysis, and turn rate evaluation from the star maps indicated GCA performance was satisfactory.

A Canopus tracker stray-light characteristics analysis using MM'71 and MVM'73 data resulted in improved CST stray-light modeling. The improved stray-light model was validated in the Venus flyby sequence where stray-light interference margins were very small.

(3) Effect of the Problem. The principal effect of the anomalous Vega acquisition was the consumption of about 209 g (0.56 lbm) of attitude-control nitrogen gas. This excessive gas usage had little effect on mission planning until after other anomalies had resulted in the excess consumption of another 558 g (1.23 lbm) of gas.

(4) Actions Taken. The net effect of the excessive gas usage was a gas conservation operational procedure that has resulted in a very ambitious extended mission plan.

(5) Relation to Preflight Problems/Performance. CST stray-light interference has been a problem for all Mariners prior to MVM'73. It is very difficult to evaluate the stray-light effect with ground tests, and as a result flight performance data is important.

MM'71 experienced stray light while in Mars orbit and a stray-light model was developed which was eventually used on MVM'73.

(6) Recommendations. Evaluation of celestial sensor performance under a variety of flight conditions requires that modeling and/or test techniques be developed which have predicted or verified flight performance in the past.

b. Roll Axis Gyro Structural Interaction

(1) Description. On GMT Day 028 following a roll search after a roll calibration maneuver (RCM), what appeared to be an oscillation started and could not be stopped with two commanded DC 18's. A DC 13 reset the 7M1, which had held the gyros on in the rate mode and stopped the oscillation by allowing the gyros to turn off after the use of about 558 g (1.23 lbm) of attitude-control gas.

Similar oscillations occurred on two separate occasions on GMT Day 45 during an evaluation test sequence, and twice more on Days (049) and (065) during Canopus reacquisitions following particle-induced star losses. The total gas usage due to the gyro oscillation was about 726 g (1.6 lbm). Following the first oscillation the gyro was on without the apparent gyro structural interaction for three tests, two roll reacquisitions following particle-induced star losses, TCM 3 and the all axes inertial -- Mercury encounter -- Sun occultation sequence.

(2) Analysis. An analytic single-axis model was developed that included structural and gyro models that predicted the observed gyro-structural interaction.

A single-axis computer simulation was also done at JPL which verified the analytical conclusions.

Boeing analysts performed computer simulations and analysis that indicated that a potential gyro-structural interaction was possible but not probable.

(3) Effect of Problem. This problem resulted in termination of the continuous use of gyros in the rate mode and the magnetometer

calibration sequences, and severe restriction on the use of gyros.

In anticipation of large gas usages during the required TCMs and the Mercury occultation periods, gas conservation methods were instituted which maximized the gas reserves. Since the gyro-structural interaction did not occur during TCM 3 and the Mercury Encounter occultation periods, a gas reserve large enough for a Mercury II and possibly a Mercury III Encounter exists.

(4) Actions Taken. The action taken was to restrict unnecessary use of the gyros. After many particle-induced star losses had increased the danger of excessive gas usage during the automatic reacquisition sequences, a control mode was initiated that prevented gyros from coming on without a ground command.

The planned two TCMs with commanded turns were reduced to one sunline TCM with no commanded turns. This resulted in a ΔV penalty, but minimized the risk of excessive gas usage.

The Mercury encounter Sun occultation period was of fixed duration, but the planned occultation mode had the gyros on for many minutes before and after the actual occultation. This time was reduced significantly to minimize possible excessive gas usage.

(5) Relation to Preflight Problems and Performance. Ground testing could not have discovered this problem. A more detailed computer model and simulations may have discovered the interaction problem; however, the flexible body interactions on this spacecraft had been more intensively investigated than on any past Mariner and has set precedents for future spacecraft dynamic analysis.

(6) Recommendations. Continue the policy of detailed computer modeling of the spacecraft dynamics and attitude-control subsystem implementations.

c.   Bright Particles

(1) Description. During the months of February and March of 1974, an excessive number of bright particles caused the Canopus tracker to flyback and sweep and lose celestial lock four times during the February-March period (six times total). On many occasions the observed roll-axis performance was probably caused by multiple bright particles.

It is also interesting that on all occasions when the star was lost, the roll search inhibit was set.

(2) Analysis Effort. Each of the star losses was analyzed to see if the performance was

consistent with expected roll axis performance. In all cases, spacecraft gyro and dynamic performance was verified as bright particle-induced disturbances.

The source of the bright particles was hypothesized to be the HGA paint, and the mechanism of the particle acceleration into the tracker field of view as a static electric dipole.

(3) Effect of the Problem and Actions Taken. The effect of the flyback and sweeps was increased spacecraft gas usage averaging about 4.5 to 9 g (9.9 mlbm to 19.8 mlbm) a day for the flyback and sweeps alone. This excessive gas usage combined with the danger of gyro-structural interaction gas usage during roll searches resulted in an operational philosophy change.

The gyros were unconditionally inhibited from coming on without a ground command. This action prevented the spacecraft from automatically reacquiring the celestial references if they were lost for some reason.

Operationally, the bright particle problem with gyros off and others made off-hour MOS team response time critical. The team was notified of spacecraft problems in progress by a radio beacon (beeper) system.

Figure 164 indicates that the number of bright particles dropped significantly just prior to Mercury Encounter. This drop is also coincident with the fact that the HGA boresight is approaching a cone angle of 90 deg. There are bright particles after the HGA passed the 90-deg cone angle, but no multiple, extremely bright particles were noted.

5.   CONCLUSIONS

All of the Attitude-Control Subsystem performances during the initial acquisition sequence, following launch, with the exception of the false yaw axis Sun acquisition, were predictable. This acquisition sequence demonstrated a need for more conservative use of hardware models until actual flight performance has been established.

The limit cycle characteristic of the pitch axis disturbance torque is similar to the leaking gas jet valve signatures observed on MM'71, but a leak of about 0.9 g (0.2 lbm) cannot be confirmed since the storage vessel pressure-temperature measurements that can be converted to gas weight with a resolution of about 14 g (0.033 lbm). After the launch of MM'71, many days passed before a roll axis gas leak was observed, but after the first one, the leaks occurred with increased frequency. Therefore, if the observed pitch disturbance was due to a gas leak, more would have been expected.
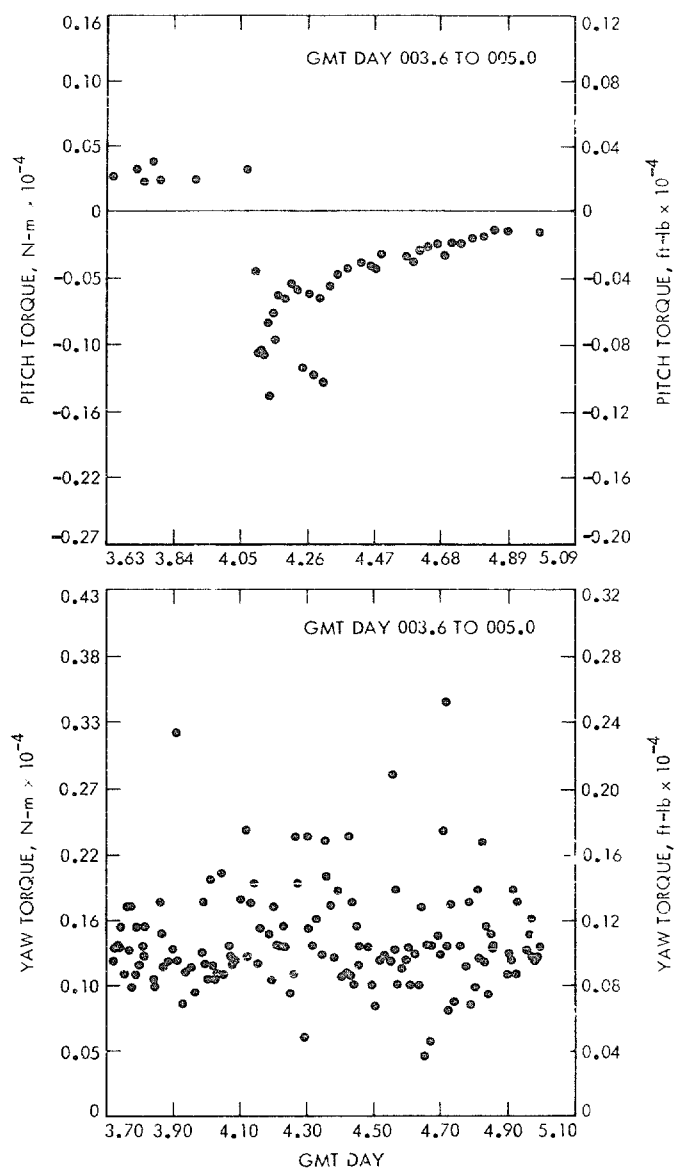
Fig. 162. Pitch and yaw disturbance torques
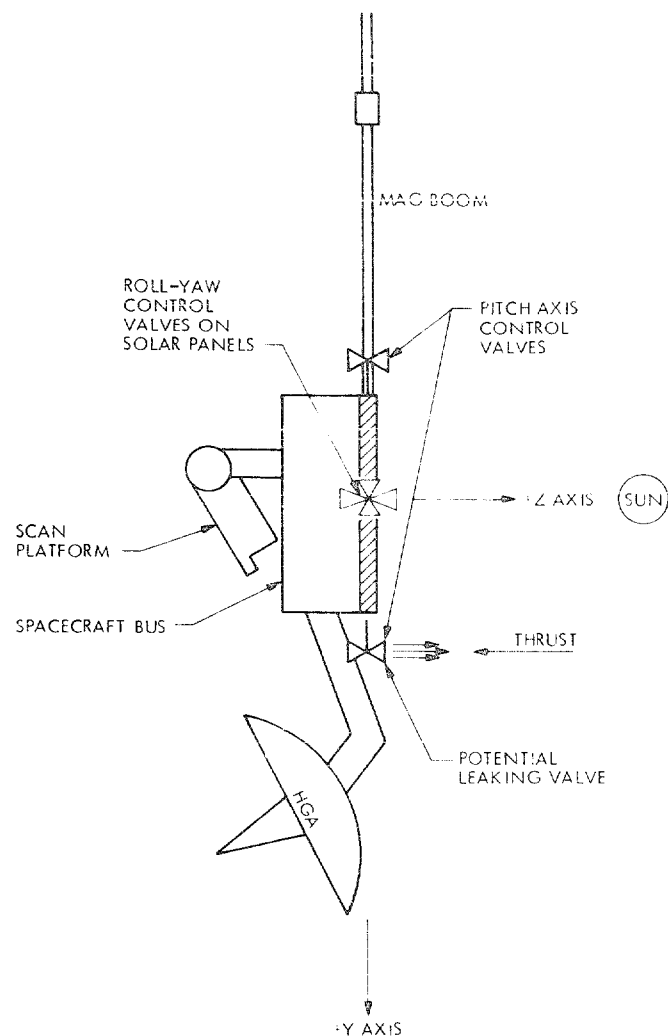
Fig. 163. RCA valve configuration
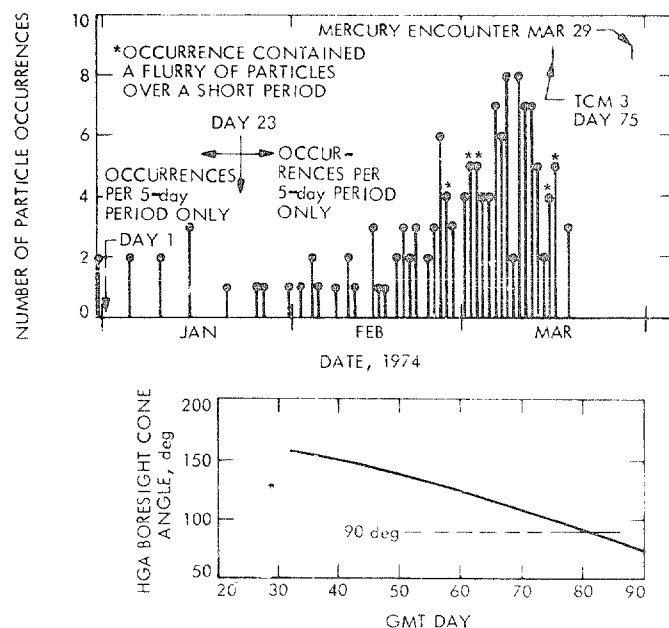
Fig. 164. Canopus tracker particle occurrence histogram

A. INTRODUCTION

This first gravity swingby mission was highly
dependent on accurate navigation to Venus in
order to properly exchange energy with that planet
and "fall in" toward the Sun so that Mercury's
orbit would be intersected (Fig. 165). A direct
Mercury transfer for the spacecraft (weighing
about 500 kg) would not have been possible with an
Atlas Centaur launch vehicle. However, the
proper alignment of the planets allowed the mis-
sion to utilize the less costly launch vehicle, and
as a secondary mission objective obtained very
good Venus science data.

For the Navigation Team, the flight path may
be considered as six separate phases, character-
ized by maneuvers or encounters, as follows:

1. Launch to First Trajectory Correction Maneuver, TCM 1 (11/3 to 11/14/73)

Near-Earth tracking allowed rapid orbit
determination convergence, and TCM 1 was
designed to correct for the built-in targeting bias
plus the actual launch vehicle injection errors.

An ambitious Earth-Moon TV sequence was
designed and executed.

2. TCM 1 to TCM 2 (11/14/73 to 1/18/74)

A long data arc was required for an accurate
orbit redetermination. TCM 2, designed to cor-
rect the TCM 1 execution errors, was done long
enough before Venus encounter so that, if neces-
sary, an additional pre-Venus maneuver could
have been performed. Both Venus and Mercury
Science sequences were being developed.

3. TCM 2 to Venus Encounter, E_V (1/18 to 2/5/74)

Just before a really adequate amount of track-
ing data had been accumulated to allow strong
orbit determination convergence, a large gas
expulsion took place on January 28, just 8 days
before E_V. (A structural vibrational mode,
resonant with roll gyro frequencies, was excited,
causing the roll jets to fire almost continuously
for about an hour.) Using the batch sequential
filter, the orbit determination program was able
to process all the tracking data and estimate the
effect of these nongravitational forces.

The Venus science sequence was adjusted to
decrease the chances of reinitiating the roll-gyro
oscillation.

4. Venus Encounter to TCM 3 (2/5 to 3/16/74)

After the close flyby of Venus, it was evident
that the spacecraft had passed extremely close to
the desired aim point, and that TCM 3, if per-
formed at E_V + 4 days as nominally planned,
would only require 4.5 m/s. (Preflight statistics
had estimated a mean value of 27 m/s.) Since it
was believed that an unconstrained maneuver
would excite the then not-understood gyro reso-
nance mode and expel an inordinate amount of
attitude-control gas, a sunline maneuver,

requiring no turns at all, was also calculated,
pending further spacecraft tests.

In order to maximize the excellent photo-
graphic data being returned from Venus, no tests
were performed until February 14, at which time
it was demonstrated that commanding a roll turn
did excite the gyro resonance. The decision was
made to perform a sunline maneuver, which
would have to be done when that sunline direction
of the motor orientation would move the Mercury
flyby position in the desired direction. That
proper time was March 16, 1974 at 11:54:42 GMT.

A hybrid Mercury Science Sequence that could
operate at either 117 or 22 kbits/s was developed
to accommodate the actual HGA performance
which periodically lost and then regained half its
output power.

5. TCM 3 to Mercury Encounter (3/16 to 3/29/74)

TCM 3 was biased slightly short of the "free-
return" locus such that a post-Mercury sunline
maneuver would move the Mercury II flyby posi-
tion in the right direction. The net result of this
bias plus the maneuver execution errors was that
the flyby altitude was 704 km from the planet
surface instead of the nominal 1000 km, satis-
fying all the experimenters' requirements.

B. MISSION ANALYSIS

Navigation responsibilities include preflight
studies leading to optimum trajectory selection
and science sequence design to assist in maximiz-
ing the science return as well as preparing for
and executing the orbit determination and trajec-
tory correction maneuvers.

1. Trajectory Selection

A major accomplishment of the mission
analysis performed for the Mariner 10 Mission
was the selection of a trajectory based on opti-
mizing the science return from the mission.
This analysis utilized simple equations called
"science value functions" as a means of coordi-
nating the requirements of Mariner 10's seven
science experiments and communicating these
requirements to project management. The value
functions also facilitated communication between
the mission analyst and the Principal Investiga-
tors and Team Leaders in charge of the experi-
ments. The value functions were unweighted,
that is each experiment was regarded as being
equally valuable, and were normalized to 1.0
maximum value. The relative value for each
candidate trajectory was plotted for each experi-
ment and a total value for each trajectory was
determined by a simple averaging process. This
revealed a clear scientific preference for launch
dates in early November. Since the range of
energy feasible launch dates was from early
October to early December the analysis was used
to demonstrate the wisdom of discarding nearly
half the available launch period. The final project
decision to launch on Nov. 3, 1973 was influenced
heavily by the value function analysis. The space-
craft was actually launched on this date, passed

Venus on Feb. 5, 1974 and encountered Mercury on March 29, 1974 at 20:47 GMT.

The seven Mariner 10 experiments include: three particles and field experiments (Charged Particle Telescope (CPT), Plasma Science Experiment (PSE), and Magnetometer), a dual-frequency Celestial Mechanics/Radio Science (CMRS) experiment, an Extreme Ultraviolet Spectrometer (UVS) experiment, a Television Science Experiment (TV), and an Infrared Radiometer (IRR).

The particles and fields experiments sample the energetic particle and magnetic field environments around the planets. They placed similar requirements on the trajectories, i.e., the trajectory at Mercury encounter was required to pass through the solar shadow and close to the surface in order to sample the solar wind wake.

The Celestial Mechanics Radio Science (CMRS) experiment constrained the Venus and first Mercury encounter to include an Earth occultation, with specific trajectory optimization for occultation entrance and exit characteristics. A close approach to Mercury was also required.

The UVS experiment comprises two instruments, a body-fixed occultation spectrometer and a scan platform mounted airglow spectrometer. This experiment required solar occultation at Mercury and placed constraints on the Mercury arrival date to optimize Hermian atmospheric measurements. A calibration of the UVS airglow spectrometer on the Earth and Moon following launch was also assigned value.

The TV experiment, initially compromised by the Mercury solar occultation requirement, imposed relatively weak constraints on the trajectory selection.[7] Earth/Moon calibration and Mercury lighting conditions and telecommunication distances were considered in assigning value to the various trajectories.

The IRR is a body-fixed instrument, which required a near-equatorial trajectory at Mercury to scan the surface. The experiment was located on the spacecraft to optimize its data for a November 3 launched trajectory.

The science value functions for each experiment were developed in an iterative process which, in some cases, revealed subtle requirements and capabilities that had not been previously considered in trajectory design. For example, the initial B-plane aiming point at Mercury was selected in the center of the zone where both Sun and Earth occultation would occur (the dual occultation zone). The value function process determined that being near the edge of the zone was preferable, because this provided passage through the anti-sunline (a particles and fields experiment desire) a nearly optimal trajectory for the radio science experiment as well as allowing a Mercury reencounter. The improvement of navigation capabilities during the prelaunch mission design allowed such an aiming

point to be selected without danger of missing the dual occultation zone.

The trajectories analyzed had the following characteristics:

(1) Mercury encounter provided a dual occultation.

(2) Both Venus and Mercury encounters occurred when the spacecraft could be in radio contact with DSS 14.

(3) Aiming points at Mercury allowed return for a second Mercury encounter.

The value function analysis revealed that the "middle launch period" (early to mid-November) was superior or equal to the "early" or late launch periods for every experiment. The early launch period (October) was very poor for the CMRS experiment. Most late launch days (late November) degraded the IRR and Particles and Fields experiments severely. The UVS and TV moon calibrations were of low value for both early and late launches. The optimal trajectories were for November 3 or 4, 1973 launches and March 29 or 30, 1974 Mercury arrivals. Improvements in the Atlas/Centaur launch vehicle performance that provided launch capability into early December gave the project leeway to allow selection of a scientifically optimal trajectory. The Mariner 10 mission did successfully accomplish all its scientific objectives.

2. Mercury Aiming Zones

The initial Mercury aiming point was chosen at $\theta = 21$ deg and $h_p = 1000$ km because this point was centered in the dual occultation zone. When the maneuver strategy of Mariner 10 was revised to include a fourth maneuver, thereby providing a high probability of an accurate encounter, the aim point could be optimized for science and could be near the edge of the dual occultation zone. This satisfied the particles and field experiments desired passage through the anti-sunline, θ's between 0 deg and 11 deg for "90% science value" based on value dropping off with $(\theta_{anti-sun} - \theta)^4$.

The IRR was mounted on the spacecraft in an optimal position for a θ of 8 deg. Deviations from this θ resulted in decreasing probability of overlap of the fore and aft fields of view. Since this overlap was very desirable, θ was restricted to be between 2 and 14 deg.

The radio science experiment required aiming points in the Earth occultation zone. Trajectories entering Earth occultation at Mercury's equator and exiting at 70 deg north latitude were desirable and were achievable at θ's of 2 deg or more.

The particles and fields and celestial mechanics experiments required passage as close to Mercury as possible in order to measure solar wind wake structure and gravitational

---

[7]The second Mercury encounter was optimized for television, with a midsoutherly latitude sunny-side closest approach point at an altitude of 48,070 km.

characteristics. This desire placed an upper limit of B = 4000 km on the aiming point. At the other extreme the two IRR fields-of-view could not intercept the planet at the same time so that a black space reference would always be available. Since the FOVs were 120 deg apart a lower limit on B of 3100 km was established. Thus the zone of optimal science return was established to be between $2 \leq \theta \leq 11$ deg and 3100 km $\leq$ B $\leq$ 4000 km. This zone was referred to as the "90%, value zone," since 90% of the maximum science value was achievable with flybys in this zone. The achieved flyby had θ 8.°5, B 3340 km.

3. Venus High-Gain Antenna Slewing

In December 1970 Dr. Gunnar Fjeldbo proposed a scheme for slewing the Mariner 10 high-gain antenna (HGA) to keep the radio beam continuously directed toward the Earth during Earth occultation at Venus. He developed a set of probable atmospheric radio beam refraction angles based on previous data on the Venus atmosphere. The shape of the slew pattern depended on the trajectory flown, but in general, in cone and clock space, resembled a teardrop.

In order to perform the "Venus Teardrop" a computer program called the High-Gain Antenna Slewing Program (HGASP) was written to read a DPTRAJ save tape, calculate the refraction angles required, calculate the teardrop cone and clock angles at 42-sec intervals, convert the cone and clock angles to high-gain antenna boom and dish actuator angles, and give output in printout and plot form of the required angles. Because the Antenna Pointing Subsystem (APS) could move only one of the six spacecraft actuators at a time (scan platform cone or clock, HGA boom or dish or +X or -X solar panel, and because the scan platform was being slewed frequently for the near-Venus TV sequence during Earth occultation, the design of a stepped HGA slew sequence was necessary to approximate the desired teardrop.

The sequence was designed to:

(1) Share the 42-sec CC&S frame with the TV sequence.

(2) Approximate the teardrop to within 0.5 deg in the early and late portions of Earth occultation.

(3) Fit into CC&S core as part of the automatic sequence.

(4) Allow flexibility for trajectory errors a. CC&S/FDS clock drifts. In order to achieve these goals:

   (a) TSOST was modified to accept HGA slew cards.

   (b) Minor compromises in both teardrop approximation and TV picture coverage were made.

   (c) As many repetitive CC&S frame command sequences as possible were used.

(d) Three separate HGA slews were designed, one for a nominal encounter time, one for a 42-sec early encounter and one for a 42-sec late encounter (the nominal was ultimately used).

(e) Specific steps for final teardrop selection were included in the sequence of events.

(f) Frequent HGA pointing calibrations were made to ensure accuracy of the slew strategy and pointing angles.

(g) Both high and low rate (1 and 1/8 deg/sec) HGA slew rates were used.

In order to monitor the teardrop during its execution a block substitution in the FDS was made, moving the fine boom and dish actuator readings from once per 22 min to once per 10.5 sec.

The HGA slew sequence was performed during Venus Earth occultation and resulted in the maintenance of a two-way radio communication to new depths in the Venus atmosphere.

C. SOFTWARE DEVELOPMENT

In accordance with the hard-line decision to keep costs down to an absolute minimum, every attempt was made to "make do" with as much as possible of existing software and to make only necessary changes or additions. There were several mission-peculiar requirements, however, which needed incorporation into the large navigation programs:

(1) Compensation of the articulating spacecraft's members effect on solar pressure forces.

(2) High-accuracy requirement at Venus and susceptibility to process noise coupled with a passage through zero declination (i. e., bad tracking geometry) at the end of December 1973.

(3) New operational ranging machines and an R&D range machine at DSS 14 resulting in two new tracking data types.

(4) An X-band transponder on the spacecraft so that both S- and X-band doppler and ranging data were generated.

(5) Targeting to Mercury on the pre-Venus maneuvers, rather than choosing a Venus aim point and later choosing a Mercury aim point.

(6) Required support of science sequence design for the two flyby sequences both of which were extremely ambitious sequences.

An ambitious schedule was developed in the attempt to produce the flight version of the "mission build" early enough so that testing and

training could begin about four months before the launch. The software packages were modified and certified and delivered on schedule, but when testing and training activities began, problems in interfaces, reactions to hardware idiosyncrasies, and inordinately long run times became apparent. One of the reasons for holding the full-dress rehearsal training sessions was to uncover these types of problems and to correct them prior to the launch. By the time launch readiness tests were being performed, the "bugs" had been corrected, or "work-around" procedures had been developed. One such procedure resulted in a rather cumbersome series of steps in the sequence design process. This consumed many long hours of operational effort, but it did work.

D. INFLIGHT NAVIGATION PERFORMANCE/ ORBIT DETERMINATION

1. Orbit Determination Strategy

a. _Data._ Tracking data were essentially continuous from launch through the first Mercury encounter from six DSN stations. Early in the flight the data was received from either DSS 12 or 14 at Goldstone DSCC and two overseas 26-m stations, DSS 62 in Spain and DSS 42 in Australia. About Jan. 1, 1974 data was received from the overseas 64-m stations (DSS 63 in Spain and DSS 43 in Australia). Throughout the remainder of the flight passes were obtained from both 26-m and 64-m stations.

The primary data type was two-way doppler (F2) taken at a nominal 60-s sample rate. This data was edited and compressed to a count time of 600 or 1200 s. The two overseas 26-m stations (DSSs 42 and 62) obtained near-Earth ranging data (MARKIA) for the first two months of the mission. This was selected at 600 or 1200 sec. The remaining stations had planetary ranging systems that produced one to three points per pass when active.

Throughout the flight, solutions were computed using three data sets: doppler only, doppler and range, and range only. Consistency among the solutions increased confidence in the data. Normally, the doppler and range solutions were the ones in which most confidence was placed.

2. Solution Sets

The frequency of OD solutions ranged from one per week during cruise periods to once every hour or two during launch and encounter periods. Each OD solution was in reality a large set of solutions consisting of batch filter runs estimating:

(1) Spacecraft state

(2) State + station locations

(3) State + solar pressure

(4) State + attitude control forces

(5) State + station locations + solar pressure

(6) Same as (e) + attitude control

(7) All parameters

and sequential filter runs duplicating all but (4) and (6). The attitude-control forces, i.e., spacecraft accelerations along the three spacecraft axes were used as stochastic parameters in all of the sequential filter runs. Parameters in (7) include all those mentioned plus planetary, Earth, and Moon masses and ephemerides depending on the mission phase.

The sequential filter was run with stochastic attitude-control acceleration a priori sigmas of 10^{-12} km/s^2 or 10^{-11} km/s^2. A batch size of one day and correlation time of from one to five days.

For orbit determination, the large accelerations over short time periods as in the TCMs and in the two events on January 28 and February 14 are best treated as instantaneous velocity changes. When such a velocity change is within a data arc used for an OD fit, the velocity changes tend to absorb errors, and no more information is gained than that from two OD fits, one before and one after the ΔV. For that reason OD fits were made only over data arcs where there were no sudden, large accelerations. Figure 166 shows the six time spans where OD fits were made: A. launch to TCM 1, B. TCM 1 to TCM 2, C. TCM 2 to January 28, D. January 28 to February 14, E. February 14 to TCM 3, and F. TCM 3 through Mercury encounter.

3. Orbit Determination Results

Table 40 lists the B-plane (see Fig. 167 for definition of B-plane) parameters for significant OD solutions through the first Mercury encounter. The following text gives a short description of the OD activities that led to the solutions shown in the table.

a. _Launch to TCM 1._ When the spacecraft is within the strong gravity field of the Earth, its orbit can be determined rather quickly compared to the time required in interplanetary space. One day after launch when tracking stations around the Earth had supplied tracking data, a reasonable OD was obtained. This fit was updated over the next few days and used to plan TCM 1 at launch plus 10 days.

Using doppler and range data the one-sigma error ellipse was about 400 km by 200 km. This is small compared to the TCM 1 execution one-sigma error of 1500 km. The batch filter and sequential filter performance was similar in this phase due to the strong near-Earth data and the short time span.

b. _TCM 1 to TCM 2._ This mission phase was the most critical for orbit determination. The accuracy of the orbit determined the parameters for TCM 2 which in turn determined the Venus delivery accuracy. Due to the geometry of the swingby trajectory there was a 1000 to 1 mapping of errors from Venus to Mercury. In other words, a 1-km miss at Venus mapped into a 1000-km miss at Mercury.

A time history of solutions in the Venus B plane is shown in Fig. 168 for batch filter solutions, and Fig. 169 for sequential filter solutions. Solutions for both long and short data arcs are shown for doppler only and doppler + range.

Table 39. Significant OD solutions

| Run ID | Param-eter set | Comments | B-plane | | | | Data | | |
			Planet	B·R	B·T	TCA	From	To	No. of Days
060006 Batch	a	Run used for TCM 1	Venus	-174	-51305	036 20:13:4.0	11/3	11/9	6
150004 Sequential	b	Run used for TCM 2	Venus	-5330	16552	036 17:00:19.8	11/14	1/2	49
210005 Sequential	b	Post TCM 2 (pre-gyro leak)	Venus	-5025	15188	036 17:01:52.0	1/21	1/29	7
260002/4 Batch/ Sequential	c	Near Venus	Venus	-5002.5	15179.2	036 17:01:49.5	1/29	2/11	13
260002/4 Batch/ Sequential	c	Near Venus	Mercury	4227	-12348	088 20:21:35.6	1/29	2/11	13
300009 Sequential	b	Run used for TCM 3	Mercury	4209	-12359	088 20:21:33.4	2/15	3/11	24
350003/5 Batch/ Sequential	c	Near Mercury	Mercury	491.2	3303	088 20:47:23.8	3/16	4/1	16

[a] State only

[b] State + solar pressure + station location

[c] State + planet GM, J2, and ephemeris

The long data arc is from TCM 1 (11/13) to the date shown on the abscissa. The short data arc is the 20 days preceding the date shown on the abscissa. All solutions shown include the spacecraft state, solar pressure parameters, and station locations. This solution set was chosen as most representative; other solution sets show similar behavior. Note that all of the fits with data up to 12/24 showed good agreement. The batch filter fits with data up to 1/2, however, show a wide scatter in B·R. One week later with data up to 1/10 the wide scatter is apparent in both B·R and B·T with the short arc doppler solution 800 km high in B·R. The sequential filter, on the other hand, with the exception of a short arc solution high in B·R, remained remarkably flat throughout the entire time period.

In addition to the scatter of solutions the data residuals showed a very small trend starting about January 4. The stochastic acceleration solution from the sequential filter and smoother showed a comparatively large (about 5×10^{-12} km/s^2) acceleration on January 4. Subsequent analysis of telemetered limit cycle data confirmed that there were unusual spacecraft forces for a 16-h period. Figure 170 shows a plot of the spacecraft accelerations along the Earth/spacecraft line of sight as determined by the sequential filter. The January 4 acceleration is the first large positive peak.

The performance of the sequential filter as shown in Fig. 169 and its ability to determine spacecraft accelerations was impressive. Its use gave a high degree of confidence to the solution used to define the parameters for TCM 2.

This figure was obtained by combining OD solutions from phases B through F, so the large acceleration of January 28 and February 14 do not show. Identifiable peaks are marked.

c. TCM 2 to January 28, 1974. After TCM 2 OD solutions were made every two days in order to get a rapid determination of the trajectory. Had TCM 2 not been successful there would still have been time to do another maneuver prior to Venus encounter. Here the batch and sequential filter gave similar results over the one week period. Figure 171a shows the solutions in the Venus B-plane for 3, 5, and 7 day arcs.

The actual and desired aim points are different due to incremental capabilities of the propulsion system. The actual flyby point is obtained from an OD solution using data before and after encounter. It is accurate to better than 1 km.

d. Near Venus. After the gas acceleration on January 28, short arc fits were made every two days. Figure 171b shows these solutions for
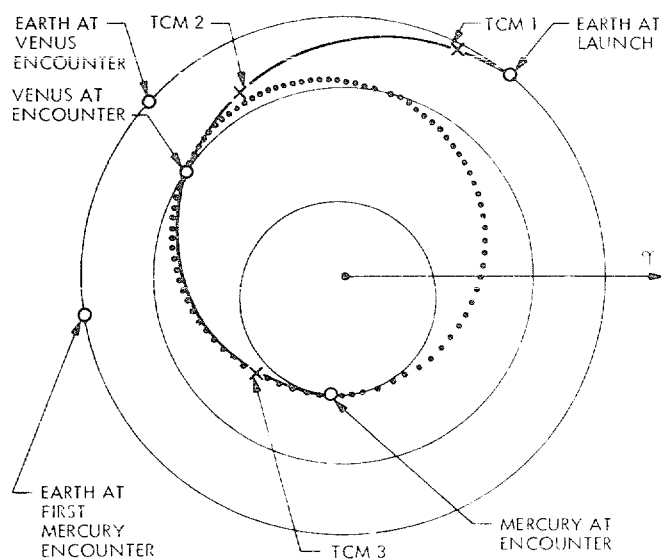
Fig. 165. Projection of trajectory into ecliptic plane
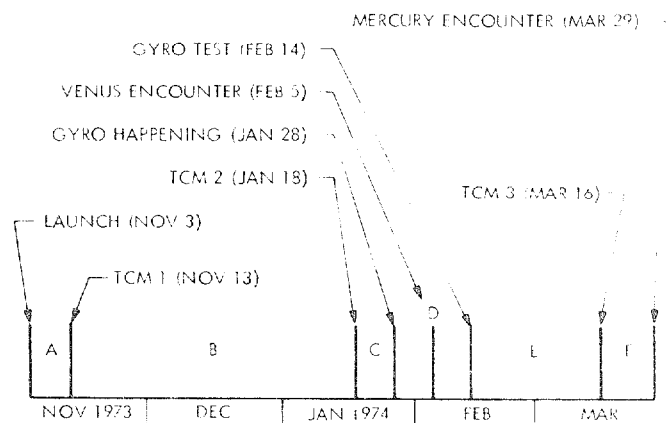
Fig. 166. Time spans during which orbit determinations were made
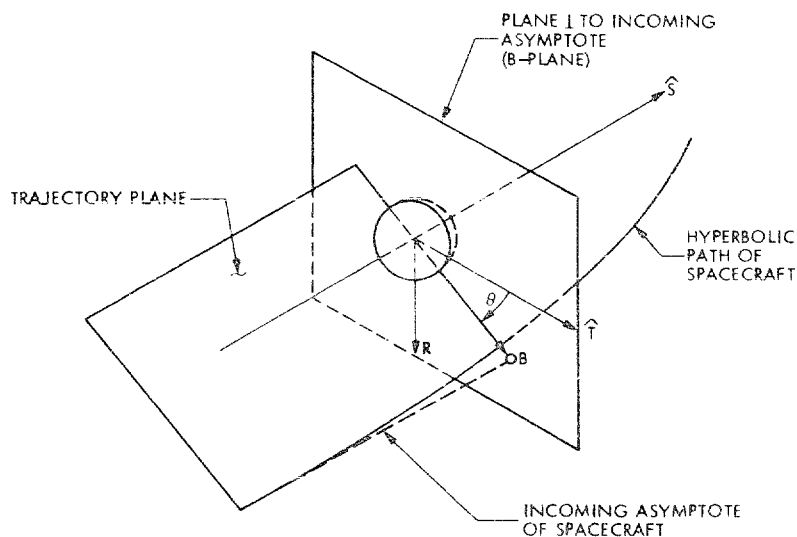
|B| MISS PARAMETER ($\bar{B} \perp \hat{S}$), DISTANCE IN B-PLANE FROM CENTER OF PLANET TO INCOMING ASYMPTOTE

S PARALLEL TO INCOMING ASYMPTOTE

T PARALLEL TO ECLIPTIC PLANE AND $\perp$ TO $\hat{S}$

R $\hat{S} \times \hat{T}$

θ ORIENTATION OF B WITH RESPECT TO T

Fig. 167. Definition of aiming plane
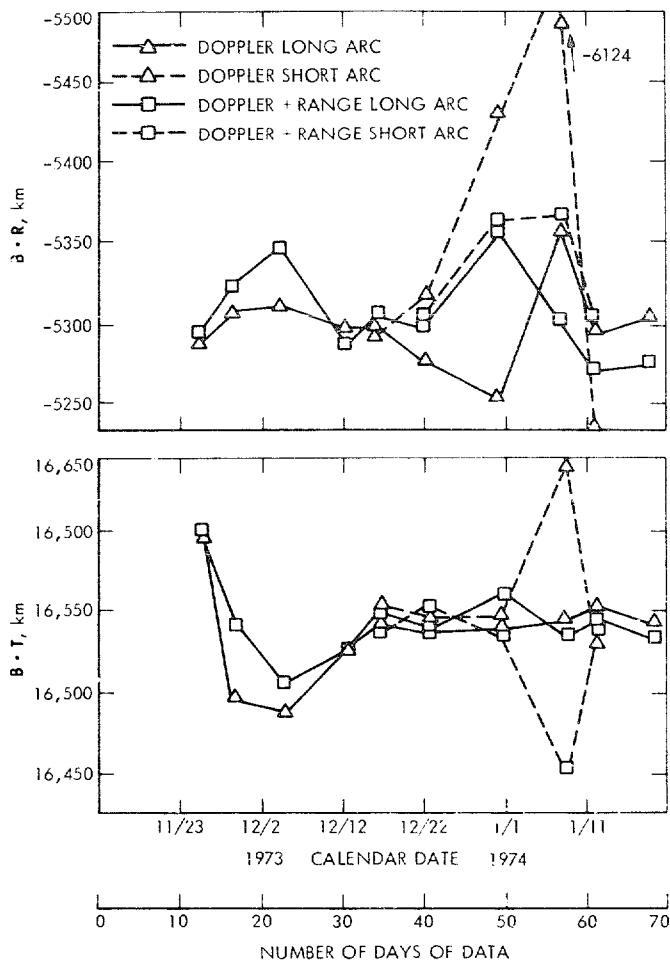
Fig. 168. Time history of solutions in the Venus B-plane — batch filter
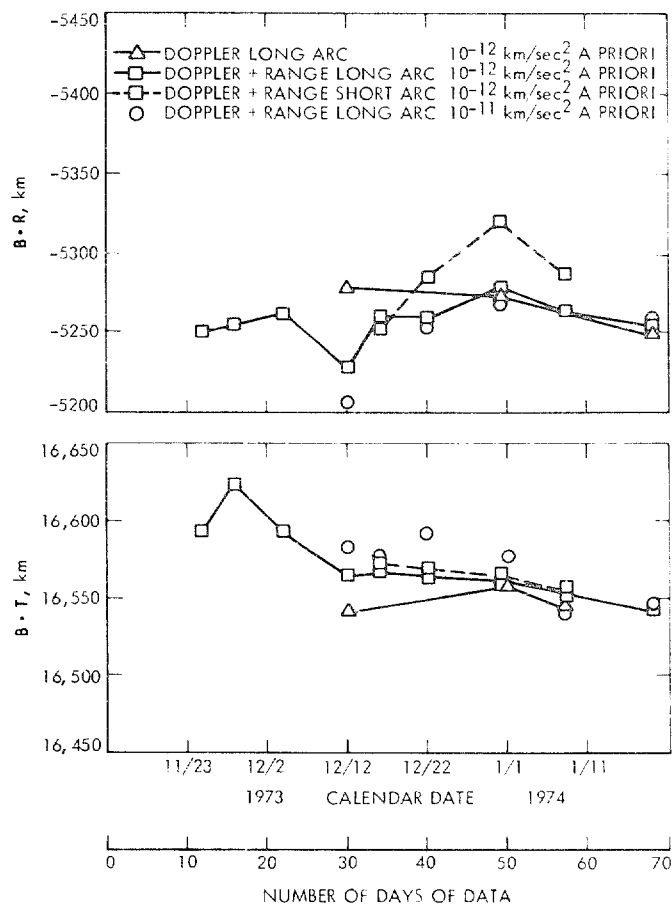
Fig. 169. Time history of solutions in the Venus B-plane — sequential filter
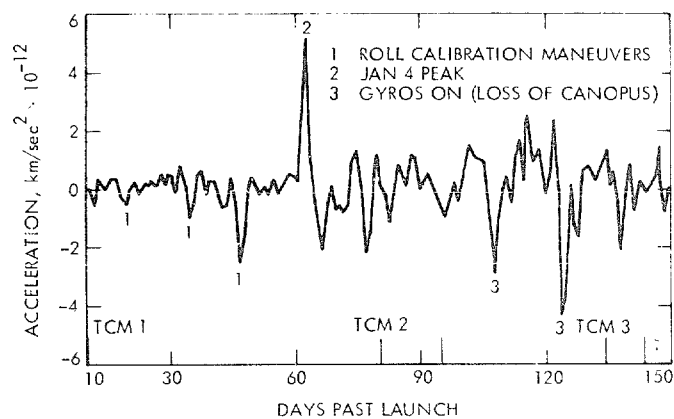
Fig. 170. Space accelerations along the line of sight

3, 5, and 7 days. Also shown is the actual trajectory point determined after the Venus flyby. By comparing these solutions with those of the previous week, it is seen that the January 28 acceleration moved the trajectory about 25 km in the B-plane. This number is consistent with that obtained by solving for the acceleration and analyzing the spacecraft telemetry giving gas usage and torques. Due to the large Venus gravity field experienced approaching and leaving the planet, the state of the spacecraft was determined very accurately (<1 km in the Venus B-plane). A 1-km error at Venus maps to a 1000-km error at Mercury.

e. **February 14 to TCM 3.** After the gyros were turned on in a testing mode on February 14, it was decided to not attempt a full maneuver where the gyros would be on for an hour or so. Instead a "sunline" maneuver, in which there are no turns and the gyros need only be on for the duration of the engine firing, was performed. The engine nozzle points toward the Sun on the spacecraft, so the thrust vector imparted to the spacecraft is along the Sun-spacecraft line, hence the name "sunline." Rather than three degrees of freedom, the sunline maneuver only has two, the magnitude of the thrust and the time the maneuver takes place. The trajectory was such that the desired aim point could be achieved with a TCM on March 16.

The orbit determination during this phase and the maneuver errors at TCM 3 determined the Mercury delivery accuracy. Again the sequential filter solutions showed more stability than the batch solutions. This is shown in Fig. 172 where the near-Venus and the later sequential filter solutions are seen to agree quite well.

f. **TCM 3 to Mercury.** The primary purpose of orbit determination during this phase was to accurately determine the trajectory so that the science instruments could be pointed accurately. As the spacecraft passed close to the planet, again the trajectory was determined very well with respect to Mercury (better than 2 km).

4. **Inflight Navigation Performance/Trajectory Correction Maneuvers**

a. **Trajectory Correction Maneuver (TCM) Strategy**

(1) **Preflight Planning.** The preflight maneuver accuracy studies had led to a plan to do two TCMs between Earth and Venus, two more between Venus and the first Mercury encounter and three between the first and second Mercury encounters. The propellant tank had been sized to guarantee a high probability of accomplishing the "baseline" mission, which ended after the first Mercury encounter.

(2) **Inflight Performance.** A great deal of flexibility was provided to allow a constructive interaction between the navigation strategy, the spacecraft capability and the scientific objectives. This proved invaluable when serious spacecraft anomalies threatened the success of the mission. The two TCMs between Earth and Venus were performed as planned, but a complete redesign of all subsequent TCMs was necessitated when the roll-gyro oscillation manifested itself shortly before the Venus encounter.

b. **Analysis of Results.** All of the encounter parameters given will be referenced to a standard set of encounter coordinates (Fig. 172). The coordinate system is centered at the planet and the B-plane, defined by the orthogonal $\hat{R}$ and $\hat{T}$ unit vectors, is normal to the incoming asymptotic unit velocity vector, $\hat{S}$. $\hat{T}$ is parallel to the ecliptic plane, and $\hat{R}$ is directed into the southern hemisphere. Flyby parameters will be specified by the time of closest approach and either a Cartesian set of B-plane parameters $(\overline{B} \cdot \hat{T}, \overline{B} \cdot \hat{R})$ or a polar set (B, θ), where B is the magnitude of $\overline{B}$ and θ is measured positive from $\hat{T}$ to $\hat{R}$.

(1) **TCM 1.** On November 14, 1973, ten days after launch, TCM 1 was performed. The purpose of TCM 1 was to remove the injection errors and a launch bias which had been intentionally designed into the trajectory in order to perform a propulsion system calibration. The Venus aim point for TCM 1 was chosen to obtain a nominal trajectory which satisfied the desired Mercury flyby conditions.[8] Figure 173 illustrates the pre-launch injection aim point, the uncorrected flyby point, and the aim point for TCM 1 in the Venus B-plane. The 1 σ and 3 σ predicted injection dispersion ellipses are also shown. Based on the three-dimensional error ellipsoids, the injection error corresponded to approximately a 5 σ miss (most of the error was in the Venus arrival time). The large injection error was attributed to off nominal performance of an accelerometer in the Centaur guidance unit.

Table 40 presents a summary of the B-plane conditions for all maneuvers on the baseline mission including the flybys at Venus and Mercury. The data for TCM 1 presents the Venus encounter conditions on the uncorrected launch trajectory (premaneuver nominal) and the predicted postmaneuver nominal flyby conditions, base on perfect execution of the commanded maneuver. The commanded maneuver differs from the ideal maneuver due to quantization errors in the two turns and the thrust duration. The mechanization of the spacecraft is such that the turns and thrust duration are controlled by a digital timer that restricts the turn angles and thrust duration to discrete values. In order to reduce the effect of the resulting maneuver error,

---

[8] The Venus flyby had the effect of reducing the heliocentric energy of the spacecraft, thus allowing a much lower launch energy in terms of a directly targeted mission. Further, since the scientific objectives were concentrated at Mercury, the targeting strategy for the pre-Venus maneuvers dictated that they be targeted directly to the desired Mercury flyby point thus allowing variations in the Venus flyby. These variations were dependent upon the actual trajectories achieved after injection and subsequent pre-Venus maneuvers.
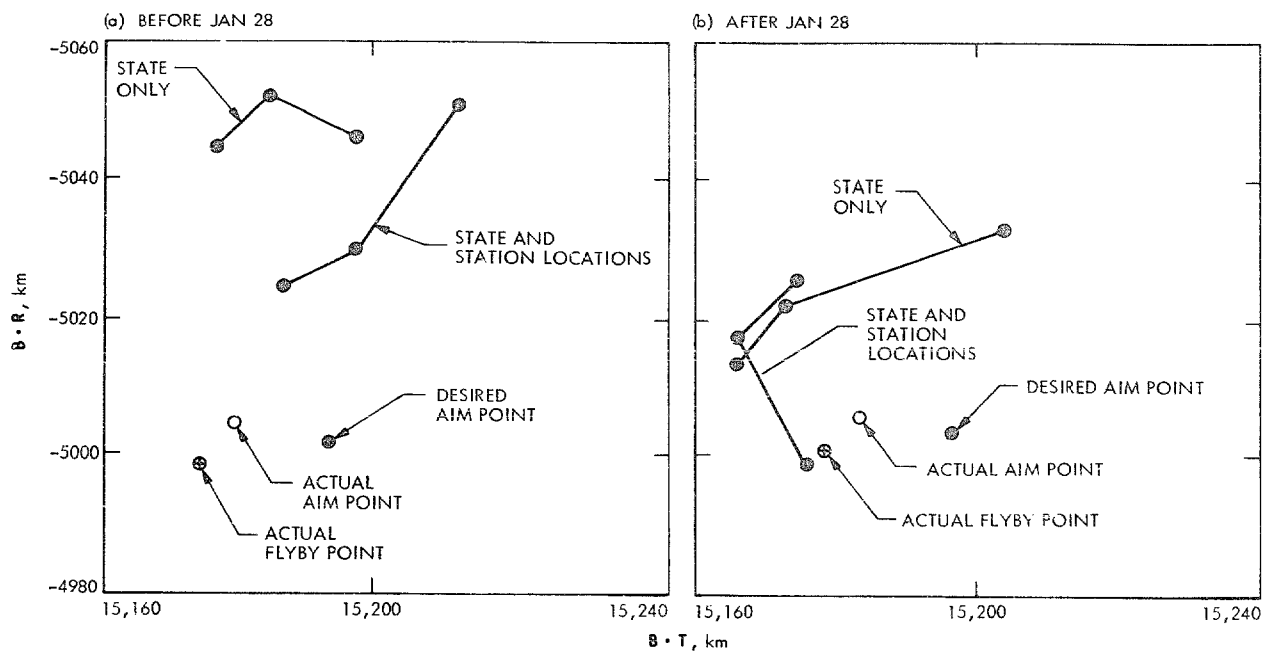
Fig. 171. Venus approach short arc solutions
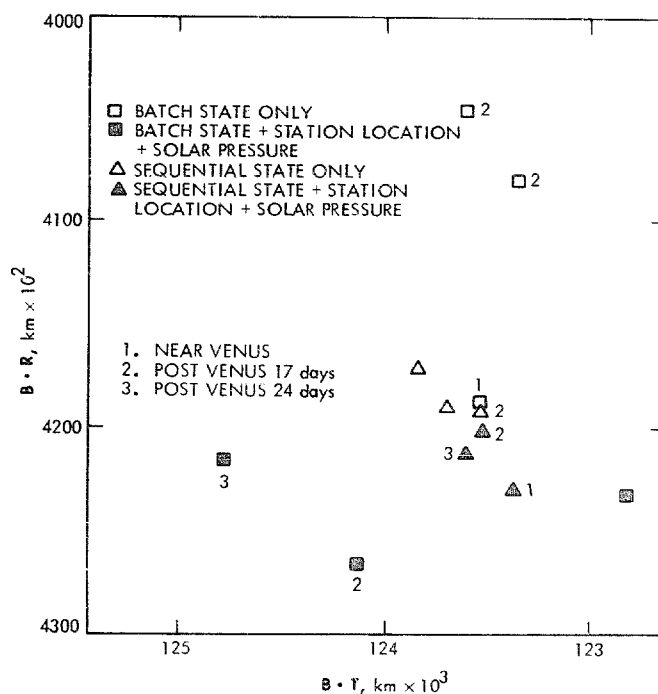
Fig. 172. Batch filter vs sequential filter
in the Mercury B-plane

Table 40. Trajectory correction maneuver and flyby summary

Baseline mission event	B-plane conditions	Venus Premaneuver[a]		Venus Postmaneuver[b]		Mercury Premaneuver		Mercury Postmaneuver	
		Nominal	Standard deviation[c]	Nominal	Standard deviation	Nominal	Standard deviation	Nominal	Standard deviation
TCM 1	$B \cdot T$	-51,305	340	15,317	1,010				
	$B \cdot R$	-180	225	-5,063	340				
	TCA	2/5/74 20:12:28	62	2/5/74 17:02:09	168				
TCM 2	$B \cdot T$	16,548	51	15,206	52			15,702	73,480
	$B \cdot R$	-5,329	76	-5,007	80			-2,189	24,270
	TCA	2/5/74 17:00:21	8.3	2/5/74 17:01:53	5.5			3/29/74 20:39:11	5,970
Flyby (Venus)	$B \cdot T$			15,179	0.07				
	$B \cdot R$			-5,002	0.2				
	TCA			2/5/74 17:01:49	0.01				
TCM 3	$B \cdot T$					-12,359	86	3,468	280
	$B \cdot R$					4,209	65	472	160
	TCA					3/29/74 20:20:48	27	3/29/74 20:46:44	30
Flyby (Mercury I)	$B \cdot T$							3,303	0.60
	$B \cdot R$							491	0.52
	TCA							3/29/74 20:46:49	0.04

[a]Represents nominal encounter conditions for the uncorrected trajectory at the time of the maneuver. Statistics contain uncertainties in orbit determination only.

[b]Represents targeting conditions for the maneuver. Statistics contain uncertainties in both orbit determination and maneuver execution.

Flybys represent post-maneuver conditions obtained from tracking data through planet encounter.

[c]Standard deviations on $B \cdot T$ and $B \cdot R$ in km.
Standard deviation on TCA in seconds.

values of the turns and thrust duration were chosen to minimize an error criterion. Typical criterion were errors in the miss at the forthcoming encounter and the projected ΔV at the next maneuver epoch.

Also presented on Table 40 are the standard deviations in the parameters describing the Venus encounter post-TCM 1. The premaneuver statistics reflect only the uncertainty in the orbit determination at the time of the maneuver while the post-maneuver a priori statistics include this uncertainty plus the statistical errors in the maneuver execution.

Table 41 presents a summary of the parameters (roll turn, pitch turn, and magnitude of the maneuver) for all maneuvers on the baseline mission. Quantities associated with the nominal parameters are, the computed values, the commanded values (which differ from the computed values by the quantization errors

previously mentioned), and the best estimate of the actual parameter.

The best estimate of the parameter was obtained using the Orbit Determination Program and estimating the maneuver parameters along with the orbit using tracking data on both sides of the maneuver. The fourth column of Table 41 lists the a priori standard deviations that were assigned to the various maneuver parameters based on system models and pre-flight testing. The fifth column relates the difference between the best estimate of the maneuver and the commanded maneuver in terms of the a priori standard deviations in the previous column. Column six gives a measure of the uncertainty in column 3. Table 40 indicates that the accuracy of TCM 1 was limited by execution errors. This prediction is verified in the discussion of TCM 2 results. Table 42 shows that a 1σ error was experienced in the magnitude of the velocity change. The pitch and roll turn errors are shown to be 0.3σ and 0.8σ.

Table 41. Trajectory correction maneuver parameter summary

Baseline mission event	Parameter[a]	Computed value	Commanded value	Best estimate of actual value	Maneuver execution standard deviation (A Priori)	Execution error (3-2) in standard deviations	Standard deviation in estimate of actual value
		(1)	(2)	(3)	(4)	(5)	(6)
TCM 1	Roll	48.998	49.017	49.512	0.624	0.79	0.12
	Pitch	127.54	127.552	127.697	0.471	0.31	0.06
	ΔV	7.786	7.778	7.919	0.123	1.15	0.01
TCM 2	Roll	46.17	46.17	47.95	0.653	2.79	0.02
	Pitch	34.78	34.71	35.17	0.471	1.00	0.01
	ΔV	1.363	1.369	1.376	0.024	0.30	0.0002
TCM 3	Yaw	0	0	0.056	0.370	0.15	0.005
	Pitch	0	0	0.254	0.370	0.70	0.007
	ΔV	17.825	17.831	17.702	0.290	0.40	0.006

[a] Roll and Pitch turns in degrees.

(2) TCM 2. TCM 2 was performed on Jan. 21, 1974, 15 days prior to Venus encounter. The purpose of this maneuver was to achieve an accurate flyby at Venus and thus minimize the magnitude of the post-Venus maneuvers. The aim point at Venus was the result of targeting directly to Mercury and thus the flyby parameters differed from both predicted pre-launch parameters and the targeted parameters at TCM 1.

In preflight planning, TCM 2 epoch was scheduled for 18 days prior to Venus encounter (E_V-18). During the mission, the E_V-18 maneuver had been computed to take advantage of the dynamics of the Venus flyby in order to both minimize the magnitude of the maneuver and to improve communications characteristics. In order to achieve these advantages, the magnitude of the pitch turn was increased with respect to the nominal maneuver. However, just prior to performing TCM 2 a problem occurred in the spacecraft electrical system. In order to reduce the stress placed on the electrical system, the decision was made to reduce the load placed on the spacecraft batteries during the maneuver which, in turn, dictated a reduction in the magnitude of the pitch turn. To allow time for a calculation and coordination of the nominal maneuver, with its reduced pitch turn, the maneuver was delayed 3 days. Since the predicted magnitude of TCM 2 was small and the sensitivity of TCM 2 to epoch over the three-day period was low, the delay had no significant effect on the ΔV requirements predicted for the remainder of the mission.

Table 40 presents a summary of the flyby conditions for TCM 2 at Venus and Mercury. The difference between the predicted Venus flyby post-TCM 1 and the pre-TCM 2 Venus flyby results from a combination of errors in the orbit determination, maneuver execution, and unmodeled forces along the connecting arc. Based on the statistics estimated at the time of TCM 2, this difference represents a 1.2 σ miss which

compared favorably with the best estimate of the maneuver errors from TCM 1 indicating only a small contribution due to the orbit determination and the unmodeled forces.

Table 41 presents a summary of the maneuver parameters for TCM 2. The best estimate of the maneuver was obtained using a weighted least-squares fit of various parameters during the maneuver. Examining the errors in the maneuver parameters, it may be seen that the ΔV and pitch errors were 1σ or less, but the roll error was significantly larger.

(3) Venus Flyby. The Venus flyby was one of the most critical phases of the mission in terms of the demand for precise navigation and the resulting impact on the ΔV requirements for post Venus maneuvers. Fundamentally, the gravity field of Venus provided a "retro maneuver" of about 1000 m/s in order to reduce the heliocentric energy of the outbound trajectory to the level required to achieve a Mercury encounter. The "execution errors" from this "maneuver" result primarily from B-plane errors at encounter which cause the direction of the outbound asymptote to deviate from the nominal. As was shown in Bibliographic Ref. 71, the ΔV required to correct this error dominated the ΔV requirements to achieve the first Mercury encounter.

Figure 174 shows the nominal aim point and the Venus flyby actually achieved. Also shown are the a priori post-TCM 2 dispersions about the nominal aim point. A comparison of the post TCM 2 predicted flyby point (Table 40) with the flyby point actually achieved shows that the B-plane error, which has the dominant effect on the magnitude of post Venus maneuvers, was 27 km. Based on the a priori dispersions, the total miss including time of flight, represented a 1.8 σ error. However, the B-plane error of 27 km reflects a 0.4 σ miss.

The post Venus maneuver required to correct this error was about 6 m/s as compared to the preflight predicted mean of 25 m/s.

(4) TCM 3. Premission planning called for two maneuvers on the Venus-Mercury leg. The first of these maneuvers was scheduled for Venus encounter plus 3 days and the second at Venus encounter plus 24 days. The first maneuver was designed to remove the velocity errors generated by dispersions in the Venus flyby, while the second maneuver corrected the execution errors from the first maneuver in order to provide the most accurate possible Mercury flyby. The epoch of the second maneuver was dictated by a spacecraft thermal constraint[9] which limited the periods during which the spacecraft could be oriented away from the nominal cruise attitude (Bibliographic Ref. 71). However, this strategy was extensively altered due to a serious spacecraft anomaly.

Seven days prior to Venus encounter, a roll maneuver was performed for the purpose of scientific instrument calibration. At the end of this maneuver, an anomaly occurred in the spacecraft attitude-control system which caused the attitude-control reaction jets in the roll axis to go into an oscillatory mode of rapid firing. This behavior was caused by a structural interaction of one of the higher vibratory modes of the solar panels with the roll gyro. The anomaly resulted in both a small velocity perturbation to the trajectory (due to the slight misalignment in the thruster pairs) and a significant reduction in the amount of available attitude control gas. Concern over a reoccurrence of the oscillatory behavior (which could result in a total depletion of the attitude control gas and hence loss of the spacecraft) dictated a complete review of the maneuver strategy and Mercury flyby requirements. The purpose of this review was to determine if maneuver strategies existed which would minimize any further significant attitude-control gas usage while achieving an acceptable Mercury flyby.

In the cruise attitude, the thrust vector of the spacecraft is directed toward the Sun. Thus, without a pitch turn, only radial velocity changes could be applied. While a restriction to radial maneuvers[10] would not yield a viable maneuver strategy in general, it became apparent immediately following the Venus flyby that, due to a fortuitous location of the uncorrected Mercury flyby point, radial maneuvers could be employed to achieve the desired Mercury encounter.

It should be noted that the velocity perturbation to the trajectory resulting from the attitude control system anomaly had a pronounced effect on the Venus flyby. In Bibliographic ref. 59 it is shown that estimates of the Venus flyby

point post-TCM 2 and prior to the anomaly were closer to the nominal B-plane aim point than the flyby actually achieved. However, the uncertainty on these estimates was on the order of the perturbation introduced by the anomaly. Therefore, absolute impact of the anomaly cannot be accurately assessed. However, the data does indicate that the ΔV imparted to the spacecraft due to the anomaly moved the flyby point at Venus in a direction favorable for performing radial maneuvers. Since radial maneuvers require that the spacecraft attitude be continuously maintained with the exhaust velocity vector pointed toward the Sun, maneuvers of this type came to be known as "sunline" maneuvers. The distinct advantage of sunline maneuvers are twofold. First, since they did not require reorientation of the spacecraft, the possibility of another period of high attitude-control gas usage was minimized. Second, they did not violate the spacecraft thermal constraint and thus could be executed any time during the Venus-Mercury cruise phase.

Figure 175 presents the uncorrected Mercury flyby and the directions of the Mercury B-plane changes produced by sunline maneuvers on various epochs. The epochs are measured from Venus encounter with the total Venus-Mercury leg taking 52 days. It should be pointed out that these corrections only control the flyby point in the B-plane and not the Mercury arrival time which was always later than the optimal time but was still within the acceptable window. As may be seen from Fig. 175, a maneuver 39 days after Venus encounter (March 16, 1974) yielded the desired B-plane change.

Science experiments at Venus encounter provided valuable insight into the viewing constraints for the various science instruments. This experience showed that the limits which had been placed on the aim zone at Mercury were too restrictive. In particular, it was possible to reduce the lower limit of the B-plane aim zone in B from 3380 to 3100 km. The prelaunch Mercury aim zone, the redefined aim zone and the post-TCM 3 a priori delivery dispersions are shown in Fig. 176. Given this new aim zone, the B-plane aim point for TCM 3 was chosen such that the probability of passing through the extended science zone was a maximum based on a priori dispersions.

Also shown in Fig. 176 is the "free return" contour and the prelaunch aim point at Mercury. This contour is the locus of points where the spacecraft heliocentric period after the flyby is twice Mercury's period. Thus a flyby which passes through this contour will return, without additional maneuvers, to the near vicinity of Mercury for a second encounter. As was shown in Bibliographic ref. 71, the ΔV gradient about

---

[9] The thermal constraint requires the spacecraft to remain in or near-cruise orientation if the solar intensity at the spacecraft is greater than three times the solar intensity at 1 AU. In this orientation, the rocket nozzle is pointed toward the Sun. For convenience, this constraint has been labeled the "3 suns" constraint and allows only radial velocity corrections during the periods when it is in effect.

[10] Radial maneuvers are restrictive due to the reduced set of flyby errors that can be corrected. The only controls available are the magnitude of the maneuver and the time of ignition.

this contour is very steep. Therefore, the decision to redefine the TCM 3 aim point, in order to maximize the science return from the Mercury flyby, caused the expected ΔV requirements for a second Mercury encounter to dramatically increase. However, studies were made to insure that the possibility of the second Mercury encounter had not been precluded. The impact of aim point redefinition on the maneuver strategy for the extended mission will be shown in the discussion of the second Mercury encounter.

Table 40 presents a summary of the encounter conditions for TCM 3 at Mercury. Based on a priori delivery dispersions at the time of TCM 2, the difference between the flyby point prior to TCM 3 and the predicted flyby point after TCM 2, represents a 1.2 σ error, including the error in arrival time (see Table 41). However, when only the B-plane errors are considered, the miss reduces to a 0.6 σ error.

Table 41 presents a summary of the maneuver parameters for TCM 3. The best estimate of the maneuver was obtained by a weighted least-squares fit, in the same fashion as for TCM 2. Table 41 shows that the execution errors from TCM 3 are smaller than those of the two previous maneuvers. However, due to the unique Sun orientation of the spacecraft during the maneuver, the pitch and yaw error were measured directly by the spacecraft's sun sensor, rather than being derived through a complex system simulation, with the result that an accurate estimate of the Mercury flyby point was available soon after the maneuver. Clearly, both the timeliness and accuracy of this estimate were very important since the 13 days remaining prior to Mercury encounter did not allow time for reconvergence of the orbit and calculation of a corrective maneuver. Table 40 indicates that the accuracy of TCM 3 was limited by execution errors. This prediction is verified in the discussion of the Mercury flyby.

As may be seen from Fig. 176, the post-maneuver estimate of the orbit passed through the extended aim zone and a final corrective maneuver was not considered.

(4) Mercury I Flyby. The encounter parameters for the Mercury I flyby are presented in Table 40. The flyby was within 168 km of the aim point and within 5 sec of the desired closest approach time. The difference between the aim point and the post-Mercury solution of the flyby point represents a 0.6 σ error. This result compares favorably with the best estimate of the maneuver as shown in Table 42 indicating only a small contribution from errors due to orbit determination and unmodeled forces.

c. Conclusions. The foregoing results have shown that the accuracy of the Mariner 10 navigation system met or exceeded all of the planetary delivery requirements. Further, the nominal ΔV required to achieve the first Mercury encounter allowed the continuation of the mission to a second Mercury encounter. It was also shown that the mission was flown with a spacecraft which experienced severe anomalies that directly impacted the ability to perform trajectory correction maneuvers. The success of the mission was the result of several factors. First, the project provided a

wide flexibility which promoted a constructive interaction between navigation strategy, spacecraft capability, and scientific objectives. This flexibility allowed for the continual development and evaluation of navigation strategies which adapted to the prevailing constraints and requirements. Second, even in the presence of anomalies, the spacecraft was proven to be a highly adaptive machine capable of meeting the stringent demands imposed by the maneuvers. It was also shown that in almost all cases the maneuvers were well within the performance specifications. Finally, all of the contributing error sources were accurately modeled and reported at realistic levels. The realistic estimation of the a priori statistics allowed resultant prediction to be used, not only in the selection of aim points, but also in decisions affecting overall navigation strategy.

E. NAVIGATION DEMONSTRATIONS

1. Radio Metric Demonstration

There were demonstrations of four different techniques during the flight: (1) dual-frequency S/X-band data used to calibrate the effect of charged particles on the radio metric data, (2) simultaneous doppler used to reduce the effect of unmodeled solar corona effects and unmodeled spacecraft acceleration, (3) simultaneous range used to enhance the measurement of declination when the spacecraft has low declination, and (4) the ramp ranging experiment where the range was deduced directly from doppler data. The results of each of these is described.

a. Dual-Frequency S/X-Band Data. Charged particles in the space plasma and ionosphere are one of the primary error sources in radio metric navigation. The ionosphere alone can produce errors of a few hundred kilometers in the target plane of Jupiter. Generally the effects of the space plasma are not as severe. However, if the radio signal passes close (~15 deg) to the Sun or is corrupted by a large space plasma event the navigation can be severely (100 km to 1000 km) degraded.

Attempts at calibrating charged particles began during Mariners 6 and 7. Techniques employing ionosonde, Faraday or differenced range vs. integrated doppler (DRVID) data have shown varying degrees of success but seldom anything startling. By far the most encouraging charged-particle calibration results were obtained from the S/X-band dual-frequency data obtained from Mariner 10. The spacecraft had the capability of receiving S-band doppler and range and returning to Deep Space Station 14 S-band and X-band doppler and range. Since the effect of the charged particles on the radio metric data is dispersive, the dual frequency data provides an ideal means of calibrating the charged particles.

The first portion of the Mariner 10 S/X-band demonstration consisted of determining the data quality of S/X-band calibrations by comparing them with Faraday rotation calibrations of the ionosphere. As illustrated in Fig. 177, Faraday rotation calibrations are obtained by monitoring a polarized signal transmitted from a stationary Earth satellite and then mapping the result to the spacecraft line-of-sight. Figure 178 contains a
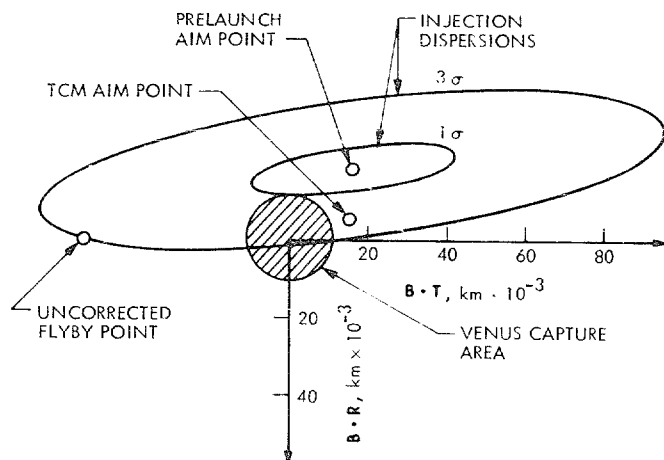
Fig. 173. Venus flyby conditions--TCM 1
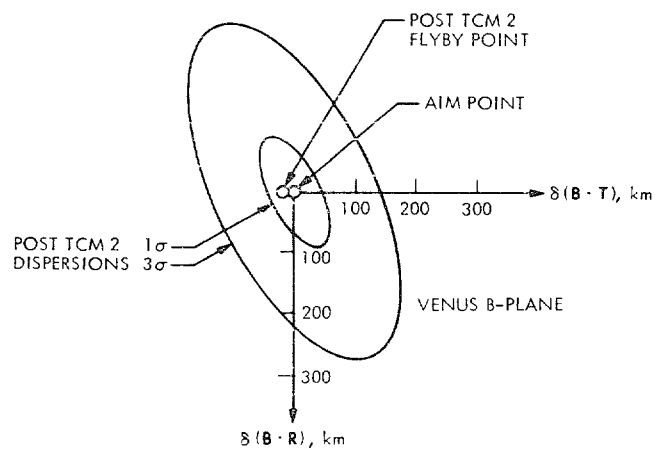
Fig. 174. Venus flyby
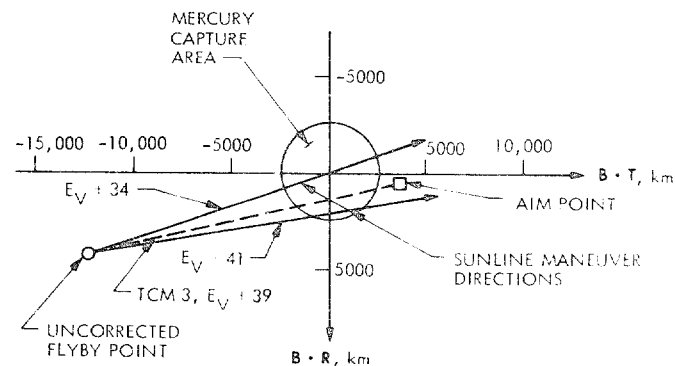
Fig. 175. Sunline maneuver capability in the Mercury B-plane
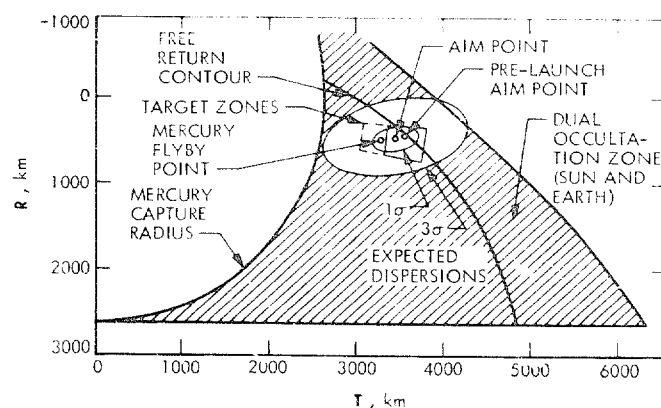
Fig. 176. TCM 3 trajectory and results in the Mercury B-plane
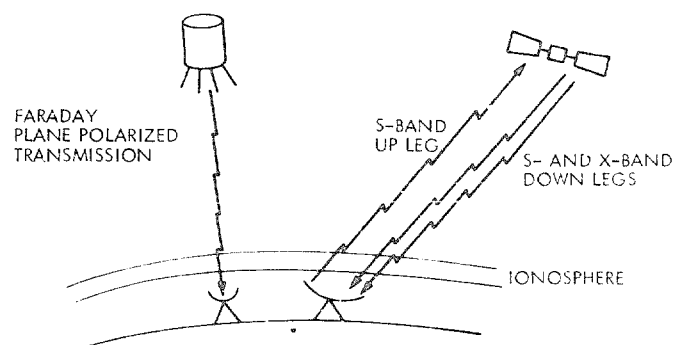
Fig. 177. Faraday rotation and S/X-band data configuration

comparison of S/X-band doppler and Faraday rotation calibrations for three tracking passes. The agreement during the first pass is very good, always within 10 cm. The agreement during the second pass is not nearly as good at low elevations. This difference is thought to be produced by deficiencies in the technique used to map the Faraday rotation data to the spacecraft line-of-sight. The dramatically different results displayed in the third pass were caused by a large space plasma event, which was detected by several different techniques. In general, the comparison of the S/X-band Faraday techniques showed the S/X-band calibrations to be accurate to approximately 30 cm, the estimated limit of the Faraday mapping. The high-frequency noise of the S/X-band data suggests that the calibrations may be good to a few centimeters.

The best way to demonstrate the effectiveness of a new data type is to include it in the orbit determination procedure and see how much it improves navigation capabilities. Unfortunately due to budget cutbacks, hardware problems, station conflicts with Pioneer 10 and other problems not nearly as much S/X-band data was obtained as was anticipated. However, due to the extraordinary efforts of some JPL telecommunication engineers and members of the Radio Science Team, enough S/X-band doppler data was obtained between the pre-Mercury maneuver and Mercury encounter to yield a calibrated orbit determination solution. Figure 179 shows uncalibrated and S/X-band calibrated B-plane solutions using six passes of data from DSS 14, taken between Mercury -13 days and Mercury -4 days. Also included in Fig. 179 is the current best estimate (CBE) of the actual trajectory based upon both pre- and postencounter data. Comparison of the solutions included in Fig. 179 shows that for the same set of data the S/X-band doppler calibrations reduces the error in the orbit determination solution from 600 km to 100 km. The solution using Faraday Rotation calibrations is approximately the same as the uncalibrated solution.

These pre-Mercury S/X-band results are very encouraging but by no means definitive. One of the limitations of the primary Mariner 10 mission to demonstrate new data types is that there was a maneuver a couple of weeks before both Venus and Mercury. Thus, the demonstrations were limited to short arcs shortly before encounters so that possible velocity errors which would produce large aim plane errors over a longer mapping time may not be particularly visible.

b. Simultaneous Doppler. The information contained in radio metric data comes from two sources, namely the spin of the Earth and the geocentric acceleration of the spacecraft. The geocentric acceleration can be a very powerful information source. However, generally the stronger the acceleration information the more the orbit determination solution may be degraded by unmodeled accelerations. As first discussed in Bibliographic ref. 56 this sensitivity to unmodeled accelerations can be almost entirely removed by differencing the data taken simultaneously from widely separated stations. The differencing removes the accelerations information (along with the sensitivity of unmodeled accelerations) but preserves information provided by the spin of the Earth.

The easiest method of obtaining simultaneous doppler is to use two-way and three-way data. The difficulty with this technique is that since the transmitted and received signals of three-way data employ different frequency standards, the three-way data will contain a bias which may vary. This bias must be solved for in the OD fit. This, in turn, degrades the solution somewhat.

Another method of obtaining simultaneous doppler from a spacecraft having a ranging transponder that does not have the bias in the three-way data is the Simultaneous Interference Tracking Technique (SITT) developed by Gordon Wood (Bibliographic Ref. 62). In principle, this technique should allow simultaneous doppler data to be taken from both stations that has the same quality as conventional two-way data. Doppler residuals obtained from Mariner 10 with DSSs 12 and 14 during the SITT demonstration shows that this technique is capable of providing simultaneous doppler data which is not subject to the typical frequency system errors.

Many orbit determination solutions using differenced doppler data were made during Mariner 10 operations. The effectiveness of differenced data to reduce the effect of moderate unmodeled accelerations is illustrated in Fig. 180. This figure shows the B-plane solutions using conventional and differenced data from Venus -13 days to Venus -3 days when the solar pressure model has been turned off. Turning off the solar pressure model introduces an unmodeled acceleration of approximately 10^{-10} km/sec^2 which is 30 times larger than Mariner 10 specifications. This unmodeled acceleration produces a 300-km aim plane error in the solution using conventional data. The solution using the differenced data is only 30 km away from the current best estimate of where the spacecraft actually went. Thus, the differenced data was an order of magnitude less sensitive than conventional data to moderate unmodeled accelerations as predicted by the accuracy analysis studies.

For the differenced data to be effective in eliminating the effects of small unmodeled accelerations usually experienced by Mariner class spacecraft (10^{-12} km/s^2) it will probably be necessary to have full S/X-band calibrations and either frequency systems based on hydrogen masers or SITT data.

Although the differenced data techniques were developed primarily to remove problems caused by unmodeled accelerations, experience gained during Mariner 10 also showed that it can be a very powerful method of reducing errors caused by the space plasma near superior conjunction. Figure 181 shows two-way, three-way and differenced doppler data taken four weeks (~12 deg) before superior conjunction. Usually the conventional doppler residuals would be around 5 mHz; however, the solar corona has already started to severely degrade the data. As shown in Fig. 181 the corruption of the two-way and three-way data is nearly common and is substantially removed in the differencing process. Figure 182 shows the daily standard deviation of the two-way and differenced doppler residuals. This figure shows that generally the differencing procedure reduces the noise introduced to the data by the solar corona by a factor of five.
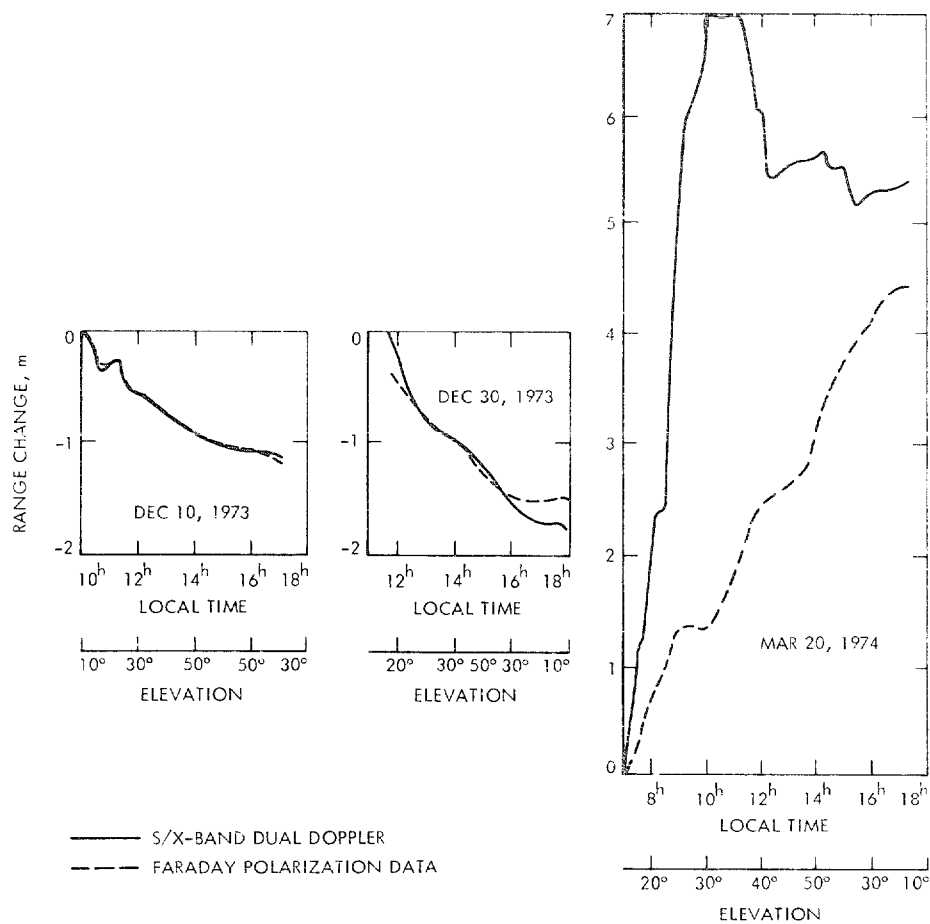
Fig. 178. Comparison of Faraday rotation and S/X-band
charged particle calibrations
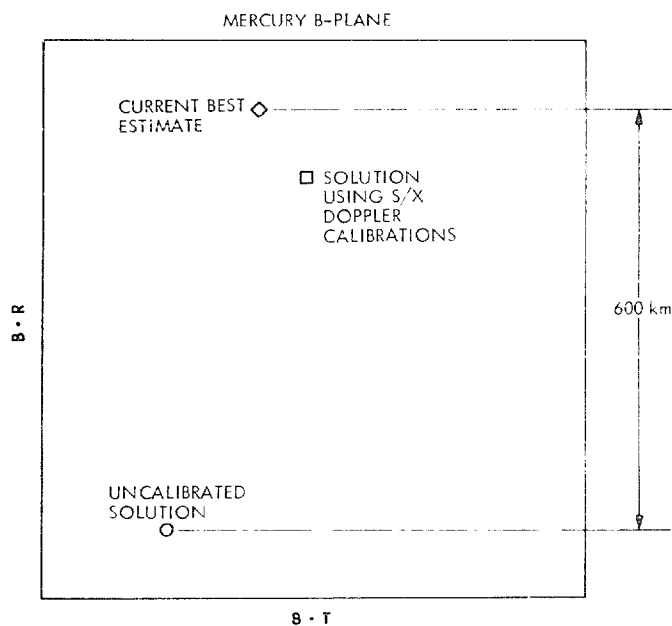
Fig. 179. Calibrated and uncalibrated solutions
using six passes between Mercury
minus 13 days and Mercury minus
4 days
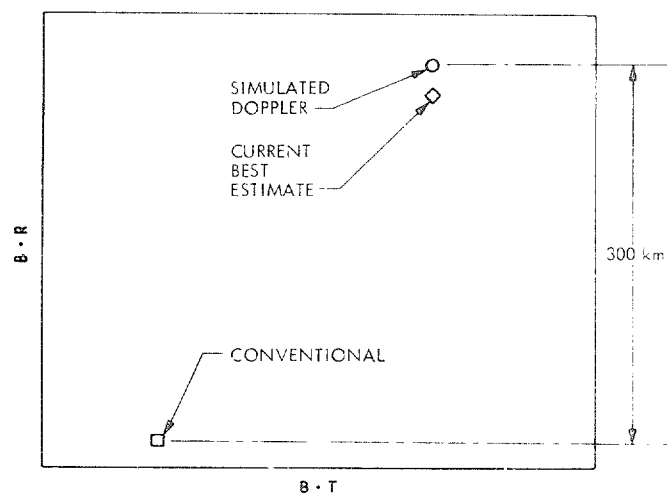
Fig. 180. Conventional and differenced data
solutions using data from Venus
minus 13 days to Venus minus
3 days with no solar pressure model

Unfortunately, the Australian stations were generally unavailable for tracking between the maneuvers one month before and one month after superior conjunction. The differenced data during this period consisted of one to three hours Spain-Goldstone tracking passes. Even with this limited amount of data, the long arc Mercury II solutions starting one month before superior conjunction and continuing for five to eight weeks, using the differenced data solutions, agreed with the conventional solutions to within a few hundred kilometers. Because of the large noise contained in the data around superior conjunction the short arc conventional data solutions (10 to 20 days) were generally quite unstable having a scatter of approximately 2000 km. However, the few short-arc differenced data solutions were much better having a scatter of about 400 km. The analysis of the superior conjunction data is continuing, but as has just been discussed, the preliminary results are very encouraging.

c. Simultaneous Range. Low-declination geometries present special problems for navigation based on conventional data. The problems arise because for short arcs the determination of the declination of the spacecraft is based upon a measure of the cosine of the declination. Several years ago (Bibliographic ref. 61) it was proposed that simultaneous range measurements from northern and southern hemisphere stations would provide a measure of the sine of the declination of the spacecraft and remove all the low declination problems. Figure 183 shows the principle behind this technique, using the simple example of two stations on the same longitude and equal but opposite latitudes viewing an infinitely distant spacecraft at meridian crossing. In practice the range measurements do not have to be taken simultaneously but may be separated by 30 to 45 minutes. For the simultaneous or near-simultaneous range technique to be effective, the measurements between stations have to be consistent to within a few meters.

Shortly before Venus encounter, experience with Goldstone and Australian range residuals, particularly those obtained from alternating range passes, indicated that the range measurements were consistent to within a few meters. Figure 184 shows Venus B-plane solutions, using doppler only, doppler and single-station range, single station range only, and nearly simultaneous range data taken between Venus -8 days and Venus -5 days. The current best estimate of the actual trajectory using pre- and post-Venus data is also shown. The doppler-only solution using 300 data points is in error by 120 km. The single-station range only solution is much worse having an error of over 500 km. Combining the doppler data with the single station range data reduces the error to only 30 km. An equally good solution is obtained by using 24 points of

nearly simultaneous range data. This result was extremely encouraging and shows that nearly simultaneous range data is not only capable of eliminating the low declination problem but may also provide highly accurate short-arc range-only solutions.

After Venus the range data quality from Station 43 seemed to degrade a bit and was not capable of supporting a nearly simultaneous range solution at Mercury.

d. Ramped Ranging Experiment. By using the DSN digitally controlled oscillator device, linear ramps can be imposed on the transmitted carrier frequency. The pattern on the carrier frequency received from the spacecraft is dependent on the round-trip light time, enabling measurement to be made of the topocentric distance from the station to the spacecraft. The advantage of this technique is that range measurements can be made to a spacecraft without a ranging transponder, e.g., Pioneers 10 and 11.

On Nov. 12, 1973, a ramp test was performed using DSS 14. The range obtained from this technique was compared directly to range measurements taken using the MARK IA system at DSSs 12 and 62. The results showed that the ramped doppler was sensitive to one-way range errors of about 1.5 km (Bibliographic ref. 65).

2. Optical Navigation Demonstration

Two opportunities were utilized to collect optical navigation data during the primary mission. The first was a series of pictures containing an overexposed Moon and a star in the field of view taken early in the mission. The second was a group of pictures looking back at Mercury and containing a star in the field of view. This series of pictures were taken following the Mercury encounter.

The results of these pictures were difficult to evaluate due to the fact that only a dozen or so independent exposures had been fit into the operational picture taking sequence. The associated orbital elements seemed to display a systematic bias which was not understood or accounted for originally.

After thorough analysis of the data and the method that was used to generate the orbit estimates, it became apparent that the light time effect was not being accounted for properly. The proper calculation of planetary aberration then reduced the biases by a factor of 3 to 4 and resultant accuracy of the demonstration was within 2% of the planet diameter, satisfying the accuracy goal required by the Mariner Jupiter Saturn Project.
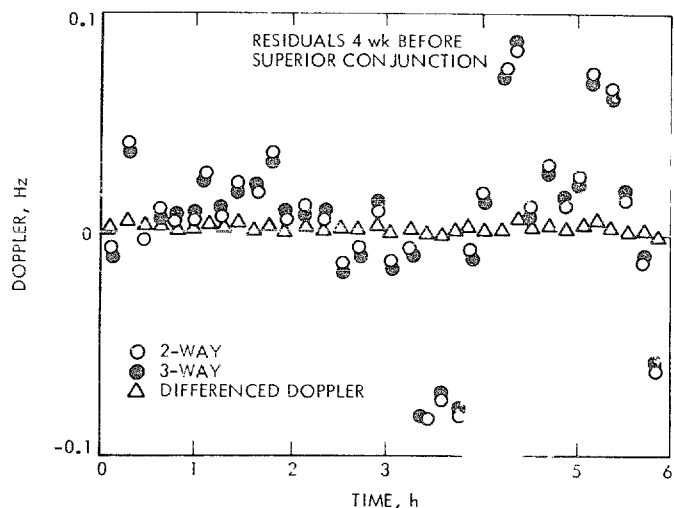
Fig. 181. Two-way, three-way, and differenced doppler 4 weeks before superior conjunction

$$\Delta\rho = \rho_2 - \rho_1 = z_B \sin \delta$$
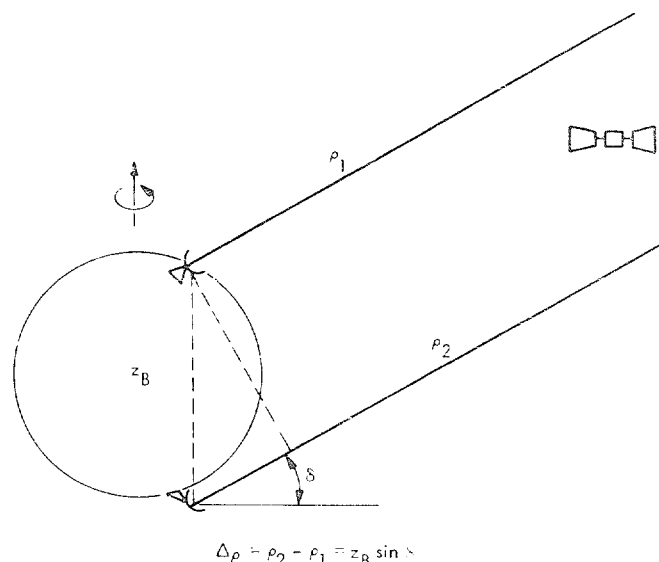
Fig. 183. Simultaneous range measurements
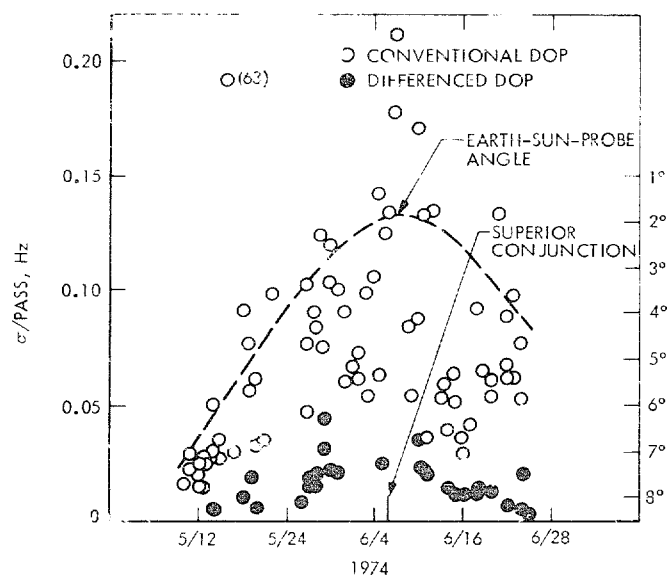
Fig. 182. Standard deviation per pass of two-way and differenced doppler residuals
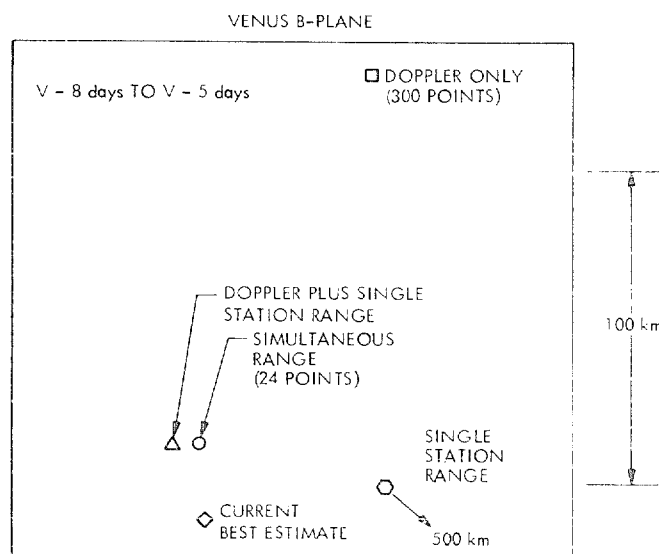
Fig. 184. Doppler only, doppler and single station range, single station range, and nearly simultaneous range solutions using data from Venus minus 8 days to Venus minus 5 days

A. NOVEMBER/DECEMBER 1973 MISSION SUPPORT

1. Planning Activities

a. NASA Support Plan. The NASA Support Plan (NSP) was revised and resubmitted for approval on October 25, 1973. Approval was completed on October 31, 1973, and the DSN published and distributed Revision 1 immediately thereafter. The MVM'73 primary mission extended to April 15, 1974. Support commitments for extended mission operations was documented in a NASA Support Plan scheduled for publication in April 1974.

b. DSN Operations Planning. During November and December 1973, emphasis was on proper execution of the previously published DSN Operations Plan for MVM'73. However, to accomplish this in the heavy support load environment, daily planning sessions with the Project were required to produce workable, detailed schedules and sequences of events. The Pioneer/Mariner 10 64-m subnet sharing plan was made more complex by the occurrence of Mariner 10 spacecraft problems resulting in numerous real-time changes to DSN schedules, sequences, and procedures.

2. Program Control

a. Status Reviews and Reports. Weekly status meetings with the Project continued throughout this reporting period. Subsequent to the successful completion of launch and near-Earth television operations, additional items pertinent to Mariner 10 cruise and encounter operations were added to the "Critical Lien List:" DSSs 43 and 63 planetary ranging, DSS 14 S/X-band, DSSs 43 and 63 high-rate video telemetry data handling, open-loop receiver/occultation recorder verification, 10 sample/s doppler capability, and recall capability for DSS radio metric original data records (ODRs).

3. Implementation Activities

Implementation was required to be completed by January 1, 1974 and is summarized in Table 43.

a. Telemetry and Command Data Subsystem (TCD). Previously reported problems regarding telemetry original data recording quality, except for time tag errors, were resolved prior to launch. A hardware solution for random occurrences of large timing errors in the timing distribution system/Telemetry and Command Processor (TCP) clock was not possible for MVM'73; therefore, operational procedures were designed to reduce or eliminate effects on data records. The Network Operations/Analysis Team checks timing accuracy of real-time telemetry blocks during each DSS prepass countdown. If timing errors were observed, front panel restarts were accomplished on TCD subsystem assemblies to reset the clock to the correct time. Checks were continued hourly during DSS tracks and the procedure was repeated as necessary.

Table 42. Postlaunch implementation and problems

Open implementation (I) and problems (P)	Location
Block IV S/X-band ranging/doppler (I)	DSS 14
Planetary ranging (I)	DSSs 43 and 63
10 sample/s doppler (I)	All DSSs
Radio metric original data record replay (I)	All DSSs
Open-loop analog recording (I/P)	DSSs 14 and 43
Standard analog recording validation and improvement (P)	All DSSs
Low-noise ultracone (I)	DSS 43
Third data decoder assembly (I)	DSS 61/63
Digital telemetry ODR time tag error (P)	All DSSs
Command Modulator Assembly (CMA) switch (I)	DSS 14

The third Data Decoder Assembly required to complete the DSSs 61 and 63 conjoint DSS three-string configuration was installed and checked out. Three strings are required at the conjoint 26- and 64-m DSS to accommodate (1) real-time recording of 117 kbits/s video, (2) real-time handling of 2450 bits/s nonimaging science, and (3) near-real-time, reduced-rate playback of video data via 28.5 kbits/s wideband communications circuits.

Digital recording of radio metric data in the DSS digital instrumentation subsystem (DIS) was initiated during the MVM'73 preparation period. However, the capability for posttrack recall/replay of these data was not developed in parallel. To achieve this capability in a timely manner, an overlay modification for an existing telemetry replay software program was prepared for delivery in January 1974, which involved replay of DIS recorder-produced digital tapes via the TCP/recorder requiring DIS/TCP tape deck compatibility. In the interim, radio metric data was recalled via low-speed punch recorder replay.

b. Tracking Data Handling Subsystem (TDH). Implementation of planetary ranging capabilities continued at DSSs 43 and 63 during this period; however, there was little productive

time due to Pioneer 10 encounter configuration freezes. In addition, installation kits were not complete in that a few required cables were not available. Consequently, the January 1, 1974 readiness date was not met. The impact of this late implementation on Project navigation was, at first, not significant since the DSN Mark IA Lunar Ranging Assembly was still providing good ranging data from 26-m DSSs. Mark IA support could have continued through late January 1974; however, on December 25, 1973, the spacecraft high-gain antenna experienced a problem that resulted in a significant loss in downlink signal performance. Since ranging from 26-m DSSs was no longer possible, priority action was taken to assure completion of planetary ranging checkout by January 15, 1974.

c. **Digital Instrumentation Subsystem (DIS).** Although the TDH subsystem was modified earlier to generate doppler data at a rate of 10 samples/s, the existing DIS software program could not handle this rate. This capability was required for radio science experiment support at planetary encounters, particularly at Mercury. Final checkout of the necessary software program update was made in January 1974.

d. **Antenna Microwave Subsystem.** Analysis of DSS 14 low-noise ultracone performance indicated that this capability would most likely permit sufficient RF link performance to support a data rate of 117 kbits/s at Mercury encounter. This would significantly increase the return from Mercury, since rather high resolution coverage of the entire planet area would be possible. Consequently, the decision was made to install a ultracone at DSS 43 to provide 117 kbits/s for use of the Mercury outgoing TV sequence. The cone had been shipped to Australia, and installation was planned in mid-January 1974.

e. **S/X-Band Equipment.** Installation of the R&D S/X-band equipment, except the Command Modulator Assembly switch, was completed at DSS 14 in late October 1973. However, completion of checkout and an operable status was not achieved by January 1, 1974, as planned due to a number of problems. Initial S/X-band checkout during November-December 1973 at DSS 14 was very difficult and at times impossible due to conflicts with the load, configuration control, and freeze imposed at the station for Pioneer 10 encounter. Some subsystem interface cable noise problems and faulty assembly modules further inhibited achievement of valid data. Most problems exhibited themselves in the X-band rather than S-band data in the form of frequent doppler cycle slips and offsets.

4. **Operations Summary**

Final DSN operational readiness tests were satisfactorily completed during the last week of October 1973, in preparation for Mariner 10 launch and near-Earth TV operations. Mariner 10 was launched on Nov. 3, 1973 as planned, and the DSN provided continuous coverage via a combination of 26-m and 64-m subnet deep space stations: DSSs 12, 42, 62, 14, 43, and 63. During November and December 1973, most coverage was provided by the 26-m subnet, with DSS 14

averaging about three passes per week. DSSs 43 and 63 tracks of Mariner 10 were nil due to higher priority support for Pioneer 10. DSS 44 was brought into use for Mariner 10 on a rush basis to avoid a 4-h gap in coverage on Dec. 3, 1973 due to Pioneer 10's use of both DSSs 42 and 43 during encounter closest approach.

DSN support for Mariner 10, including the high-activity Earth-Moon TV sequence and trajectory correction maneuver, was excellent. As expected in a continuous coverage operation, the DSN experienced problems and equipment failures; however, none had a significant impact on mission operations and data recovery.

B. **JANUARY AND FEBRUARY 1974 MISSION SUPPORT**

During January and February 1974, DSN preparations for the Mariner Venus/Mercury 1973 Venus encounter were completed, and the encounter was supported in a near flawless manner. In addition, the continuation of spacecraft problems required the Deep Space Network to respond with additional implementation and new operational techniques to facilitate achievement of mission objectives.

1. **Planning Activities**

During January 1974, DSN operations planning gave priority to preparations for the second trajectory correction maneuver (TCM) and for Venus encounter. However, in addition, a significant level of effort was required of the DSN Support Team to generate real-time operations plans in response to spacecraft problems. These problems and responses are discussed in Sect. 4, "Operations Summary."

Preparations for TCM No. 2 were well underway in early January 1974 for a mid-January burn. However, the occurrence of a spacecraft emergency on Jan. 8, 1974, involving spacecraft switch to the backup power chain, interrupted and delayed completion of the maneuver sequence. The TCM was rescheduled for Jan. 19, 1974 and then again slipped to Jan. 21, 1974 as additional spacecraft power constraints were factored in. These changes required the DSN to make corresponding adjustments to DSN schedules, sequences, and staffing. During one particular week, sixty-eight real-time schedule changes were required to realign network support for MVM'73, Pioneer 10 and 11, and radio science.

In parallel with TCM activities, the DSN planned a series of comprehensive Venus encounter readiness tests. These test procedures included Class I countdown exercises, appropriate portions of DSS system performance tests, critical requirements of the Venus encounter sequence of events, and use of the spacecraft as a data source. DSSs 14, 43, and 63 were scheduled for participation during the period of Jan. 17 to 30, 1974.

Following completion of TCM 2 activities, primary attention was again given to finalizing the sequence of events and configuration strategies for Venus encounter. However, this effort was complicated by the spacecraft roll gyro

oscillation-attitude gas consumption problem that occurred during the roll calibration maneuver on Jan. 28, 1974. In addition, a high level of effort went into the S/X-band radio science occultation portion of the sequence to assure feasibility of the demanding, rapid radio-frequency signal acquisition at exit occultation. Consequently, tweaking of the detailed DSN sequence continued until Venus encounter minus one day.

2. Program Control

Weekly status meetings with the Project continued throughout this reporting period. Open implementation items and problem areas were tracked until appropriate closures were accomplished. Weekly teletype status reports to NASA Headquarters and monthly inputs to the Project Management Report continued.

In late January 1974, the DSN conducted a Venus encounter readiness review to evaluate the final status of preparations and potential problem areas. The review and results of encounter readiness tests demonstrated that the DSN was in a high state of readiness for the critical operations.

3. Implementation Activities

a. Deep Space Stations. Implementation and engineering support were given by the deep space stations as follows.

(1) Antenna Microwave Subsystem. The listen-only low-noise ultracone was installed at DSS 43 without difficulty on the planned mid-January schedule. Excellent performance was demonstrated in follow-up tests. Tests continued through March 1974 to demonstrate adequate performance for reception of 117-kbits/s video data under expected marginal RF link conditions at Mercury encounter on Mar. 29, 1974.

By mid-February 1974, the spacecraft high-gain antenna problem had produced an RF down-link that was 6 dB less than normal and an antenna pattern which was nearly completely linear rather than circular. About 3 dB of this loss was attributed to cross-polarization between circular polarization of the DSS antenna and the now linear polarization of the spacecraft. In response to Project request and to meet Mercury TV experiment objectives, the DSN took emergency action in February to provide, ship, and install linear polarization equipment at each of the three 64-m DSSs, expecting to have it completed shortly before Mercury encounter.

(2) Telemetry and Command Data Subsystem. Accomplishment of capabilities in January 1974 for post-track recall of digitally recorded radio metric data marked the end of all required implementation in this subsystem. An existing Telemetry and Command Data Subsystem (TCD) software program was modified and integrated into the DSN to perform this function.

However, continuing engineering support was required to help analyze a problem observed in DSS 43's and 63's Original Data Records (ODRs) containing 117-kbits/s video data from Venus encounter. Essentially all of the video data were recorded on the ODR, but the data were not in the correct time-ordered sequence. "Old" and "new" data were interleaved in a repetitive pattern requiring special processing by the Mission Control and Computing Center (MCCC) to recover video frames. Special tests were planned and conducted at DSS 14 and CTA 21 to resolve this problem prior to Mercury encounter. However, the problem was observed only at the 117-kb/s rate, which would not have been used at Mercury encounter if the spacecraft antenna performance had remained 6 dB below normal.

(3) Tracking Data Handling Subsystem. Implementation of planetary ranging capabilities was completed at DSSs 43 and 63 in mid-January 1974 approximately two weeks later than planned. Although declared operational on the basis of successful system performance tests, DSS 63 ranging data exhibited a timing bias which made it difficult to use for navigation purposes. These capabilities came none too soon. Near simultaneous ranging data were required from DSSs 12, 14, 43, and 63 for critical orbit determination exercises to rapidly redetermine the orbit following perturbations from the gyro-attitude gas usage problem.

(4) Digital Instrumentation Subsystem. Update of the Digital Instrumentation Subsystem software program was completed and integrated into the DSS in January 1974 as planned. This update provided the required Venus encounter capability for real-time handling of 10 samples/s doppler data via high-speed data lines.

(5) Pre- and Post-Detection Recording Subsystem. Work continued on DSS 14's dedicated open-loop analog recording assemblies until two days prior to Venus encounter to achieve configuration and performance desired by radio science experimenters. Late modifications were required to adequately integrate both S- and X-band signals from the R&D Block IV receiver assemblies.

Also, quality checks of analog recording produced on the DSS standard analog recorder indicated improvements were needed to facilitate proper recording and recovery of telemetry data from this backup ODR. Tests at CTA 21 demonstrated that significant changes were required in channel assignments to achieve desired results. To avoid unacceptable risks of late configuration changes, this modification was only partially implemented prior to Venus encounter and then was completed thereafter.

(6) S/X-Band Equipment. X-band doppler cycle slips and offsets continued to be periodically observed. Interface cable replacements and assembly adjustments in January 1974 did, temporarily, eliminate these problems during the Venus encounter period. By mid-February 1974, the problems were back again. Therefore, the DSN initiated a special coordinated team effort between DSN engineering, operations, and Project radio science experimenters to troubleshoot and achieve required performance prior to Mercury encounter. Noise interference appears to be the major cause, but its source was unknown at that time.

In early January 1974, the Command Modulator Assembly switch required to provide Block IV exciter uplink capabilities was installed at

DSS 14 but failed to operate properly due to a wiring logic error. The switch was removed for rework. Since stability of the Block III exciter was sufficient to meet S/X-band requirements at Venus encounter, it was decided that the switch would be reinstalled during the week of Feb. 24, 1974 in preparation for Mercury encounter support. This installation was accomplished as planned. Post-installation tests and operational use demonstrated proper performance with the Block III configuration. However, due to interface signal errors, switch performance in the Block IV configuration was not acceptable.

b. DSN Ground Communications. Appropriate modifications and adjustments to the DSS 14/DSS 12 microwave link were initiated as a means of providing access to DSS 12's telemetry strings for backup to DSS 14's two-string configuration. The planned use of this microwave link was for transmission of 2450 bits/s telemetry data to DSS 12 in the event that DSS 14 should lose one string while supporting dual subcarrier operations.

The microwave link between DSS 63 and DSS 62 was reactivated and adjusted to support real-time transmission of low rate telemetry data from DSS 63 to DSS 62. This capability permitted continuation of the DSS 63 communications terminal relocation/reconfiguration without interrupting data flow to project users. This work was satisfactorily completed on Feb. 28, 1974.

4. Operations Summary

Following is a brief summary of DSN operations activities for January and February 1974. Primary attention was given to certain spacecraft problems which placed an unplanned, heavy load on the DSN in terms of revised plans, sequences, tests, schedules, and new implementation.

During this period, Mariner 10 coverage continued to be provided by a combination of 26- and 64-m subnet DSSs. In January 1974 Pioneer and Mariner equally shared the 64-m subnet. DSN readiness tests for Venus encounter were satisfactorily completed between January 17 and 30, 1974. Beginning Feb. 1, 1974, DSS 14, 43, and 63 configurations were frozen for Venus encounter operations. DSN support continued to be very satisfactory, with exceptional performance demonstrated during the critical Venus sequence and during a number of spacecraft problems.

The spacecraft high-gain antenna went through a number of fail-heal-fail cycles during this period. Degradation finally stabilized at a downlink loss of 6 dB and a linear polarization rather than circular. This problem made performance of the link marginal for 26-m subnet reception of 2450 bits/s telemetry at a bit error rate of 1 in 10^4 or less. Furthermore, even 22 kbits/s video data would have been marginal via a 64-m station at Mercury encounter. In response, the DSN performed frequent precision signal level measurements, conducted ellipticity measurements, and implemented linear polarization tracking capability in the 64-m subnet.

Spacecraft roll gyro oscillations caused periodic high usage of attitude-control gas. This perturbed the well-defined trajectory requiring rapid generation of additional amounts of accurate radio metric data in the DSN. In response, the DSN negotiated with the Pioneer Project for additional 64-m coverage for Mariner 10 and scheduled a series of near-simultaneous ranging acquisitions.

Spacecraft power problems were varied but were primarily observed by the DSN in the form of power-on resets (PORs). PORs were frequent during roll calibrations and gyro turn-ons. These cause the spacecraft to automatically switch, without warning, to a different data mode and to the interplex configuration. To minimize response time and data loss when PORs occurred, the DSN developed special procedures for subcarrier demodulator configurations, phasing, notch filter installation, and for analog record handling.

Flight and ground tests showed that the spacecraft auxiliary oscillator had a frequent one-half cycle offset when in the one-way mode. This instability would have masked Venus atmospheric effects on the RF signal severely degrading radio science occultation results. Proper auxiliary oscillator performance was obtained in the two-way mode but required use of the DSS 14 100-kW transmitter to gain adequate link performance. The two-way, 100-kW sequence had to be planned between Feb. 1, 1974 and Venus encounter on Feb. 5, 1974.

These problems caused delays of certain critical mission events such as trajectory correction maneuvers, calibrations, and spacecraft computer updates. DSN operations was hard pressed to accommodate these changes in plans, schedules, and ground command activities.

C. MARCH/APRIL MISSION SUPPORT

This section covers the period from March 1, 1974, through April 15, 1974. April 15, 1974, marked the end of the MVM'73 Project's primary mission and the beginning of the Mariner 10 Extended Mission Project. March 1974 proved to be the most dynamic and critical period of this rather eventful mission. DSN preparations for TCM 3 and for Mercury encounter were completed and support was provided in a near-flawless manner.

1. Planning Activities

During early March 1974, the DSN gave priority to preparations for TCM 3 and to development of the final sequence of events for Mercury encounter. TCM 3 was planned to occur over Deep Space Station (DSS) 14 on March 16, and the encounter TV sequence was planned around a 22.5 kbits/s rather than a 117.6-kbits/s data rate, because of the spacecraft antenna feed problem. However, two significant events during the first week of March required significant changes to these near-final arrangements.

On March 4, 1974, the spacecraft antenna problem corrected itself, thus reopening the possibility of real-time (117.6-kbits/s) TV operations at Mercury encounter. Further, on March 6, 1974, the spacecraft lost lock on Canopus, and gyros came on to provide attitude stability. However, the roll gyro began

oscillating, which resulted in high consumption of attitude-control gas. Gas usage effects on the orbit were such as to shift TCM 3 from the DSS 14 to the DSS 43 view period. Further orbit refinements again shifted the TCM to occur over DSS 63.

These problems and changes resulted in a heavy, unanticipated replanning load at a time when plans should have been in the final stage for the approaching encounter with Mercury. Revival of the 117-kbits/s TV sequence required development of special telecommunications link performance measurement tests, changes to planned DSS configurations, and schedule negotiations to accommodate Mariner 10 and Pioneer during encounter. Orbit uncertainties due to nongravitational forces necessitated development and execution of special procedures for generation of simultaneous doppler data and near-simultaneous ranging data to accurately redefine the orbit following TCM 3.

Furthermore, to preclude excessive gas consumption during any future loss-of-Canopus event, the spacecraft was placed into a "free-drift" mode using solar pressure on solar panels as an assist to attitude stabilization. In this mode, automatic gyro turn-on was inhibited. Consequently, loss of Canopus would result in the spacecraft's high-gain antenna drifting off the Earth line, and 64-m DSS support would be needed for reacquisition. Therefore, special agreements were negotiated with the Pioneer Project, and new DSN procedures were developed wherein one telemetry string at the 64-m stations would always be configured for immediate Mariner 10 support.

The introduction of these late but necessary changes shortly before the critical encounter period caused a great deal of DSN concern regarding the Network's ability to avoid operational errors which would be detrimental to the primary mission objectives. DSN Operations planners and advisors provided close support during this high-risk situation to help assure that required results were achieved.

2.   Program Control

On March 7, 1974, the DSN conducted a special review of various discrepancy areas in the Network, particularly those that represented continuing problems and those which had a potential to impact Mercury encounter support. The Discrepancy Report (DR) Review Board consisted of representatives from DSN Operations and Engineering. Following is a summary of the significant items discussed.

a.   Planetary Ranging. The recently implemented planetary ranging capability logged a number of discrepancies. Many of these problems were traceable to a lack of operational experience, which significantly improved with time. However, error dispersions continued to be larger than anticipated, and frequent biases and offsets were observed between and within station passes. DSS 63 exhibited a rather consistent 20-m bias. The consensus was that this ranging performance would meet Mariner 10 navigation requirements and that ranging assemblies should not be perturbed by any rework prior to end of the

mission. Recommended areas for on-going study included: (1) recalculate and verify the 64-m antenna Z-height, (2) check for timing errors as a possible cause, (3) resurvey the DSS 63 site location, and (4) evaluate calibration accuracies using the zero-delay device, and as a function of antenna angle position.

b.   DSS Command Subcarrier-Frequency and Bit-Rate Error Alarms. Alarms of this nature occurred periodically and accounted for a large percentage of open Discrepancy Reports in the system; 30 were open at the time of the review. It is important to note that these are alarms, not aborts. The DSN had experienced only one command abort for Mariner 10, which was due to an erroneous bit rate. Standard practice is to set the subcarrier-frequency alarm limit tighter than the Project abort limit; e.g., alarm at ±0.2 Hz, abort at ±0.3-Hz deviation. Analysis of station analog tape readouts disclosed that 80% of the bit-rate error alarms were false alarms resulting from bit-rate detection circuitry errors rather than actual bit-rate errors.

c.   Data Decoder Assembly. Although installation of new selector channels and other modifications significantly improved data decoder assembly (DDA) performance, problems continued throughout the Network. A number of discrepancies were grouped into two categories: DDA external and DDA internal.

(1)   DDA External. This category includes those events involving DDA halts and alarms. These problems are intermittent and are usually cleared in less than 10 min by DDA reinitialization or reload. Cause analysis had been difficult because of a lack of data. Deep Space Stations need to dump the DDA memory when a halt/alarm occurs in order to get useful trouble-shooting data; however, most projects are reluctant to approve an additional 15-20 min data outage while this is done. Post-review coordination with the MVM'73 Project resulted in an agreement and procedure for DDA memory dumps as required when critical data were not being handled.

(2)   DDA Internal. This category includes those discrepancies involving bit errors, improper data sequences, and timing errors. Telemetry data timing errors are now being worked around by special operational procedures involving front panel restarts when errors are observed. Of more concern is the mixing of data in the DDA through a linear combination of bits. This was observed on some of the Venus encounter digital original data records. All bits were recorded but were out of sequence in a systematic interleaving pattern. It was suggested that this was an initialization procedure problem. Actions were assigned for special testing to verify the specific cause and obtain a solution. Results of these tests are discussed in paragraph 3-a-(2).

The DSN Operations Status Review for Mercury encounter was conducted on March 21, 1974. The purpose was to evaluate the final status of encounter preparations and review potential problem areas. Subjects covered included: test and training, documentation updates, encounter time lines, occultation strategy, configurations, configuration freeze

plans, data shipment plans, staffing, and discrepancy report status. All items exhibited a satisfactory readiness posture for the start of encounter operations.

3.   Implementation Activities

    a.   Deep Space Stations. All major work on subsystems was completed prior to Venus encounter in February 1974; consequently, this section continues to diminish, reflecting only tasks to resolve problem areas.

    (1) Antenna Microwave Subsystem. DSN initiation of emergency implementation of linear polarization tracking capabilities in the 64-m subnet to match the changed polarization in the spacecraft due to high-gain antenna problems was continued as a contingency against future recurrences. This task, including performance verification tracking tests, was completed by mid-March 1974 as planned.

    (2) Telemetry and Command Data Subsystem. Return of the spacecraft telecommunications link to normal gain and polarity again made real-time 117.8-kbits/s TV data possible at Mercury encounter. Consequently, the previously reported problem in digital original data records of 117-kbits/s data was given priority attention. Special tests were conducted at DSS 14 and Compatibility Test Area (CTA 2i) to determine the cause of recorded data being out of sequence. As suspected, the problem was operationally induced and could be corrected by changes in operational procedures. To avoid having prepass countdown simulated data on the record delivered to Project, the original procedure called for loading of virgin tapes following countdown activities. This apparently left the DDA pointers out of phase with the high-density recorder tape position. The high-density cycle at 117 kbits/s resulted in a linear combination of bits in about 25% of the test cases. Reinitialization of the DDA following loading of new tapes was required to avoid this problem. Special operational instructions to this effect were issued to the stations. No further indications of the problem were observed in the Mercury encounter data.

    (3) S/X-Band Equipment. Improvement of the R&D S/X-band performance at DSS 14 was

effected by receiver control work, cable replacements, and other trouble-shooting analysis. Previously reported problems with the command modulator assembly switch were not completely resolved prior to Mercury encounter. Therefore, operations were continued in the Block III exciter rather than the desired Block IV exciter mode. This configuration was acceptable to the MVM'73 Project.

    b.   DSN Ground Communications. Per NASA request, the DSN coordinated the planning, configuration, test, and schedules for establishing a video circuit capability from JPL to Goddard Space Flight Center and NASA Headquarters. This service was employed for about 7 h during Mercury encounter to transmit real-time encounter TV and public information broadcasts to these NASA viewers.

4.   Operations Summary

    As planned, increasing use was made of the 64-m subnet during March-April 1974 for the trajectory correction maneuver and encounter support. However, Pioneer Project tracking requirements limited the configuration freeze for Mariner 10 to an 8-day period around encounter. Standard DSN encounter readiness tests were completed by mid-March 1974. However, special telecommunications link performance and S/X-band performance tests were continued until encounter day. DSN support continued to be satisfactory, with excellent performance demonstrated during the critical encounter sequence and during the occurrence of some additional spacecraft problems.

    On March 31 (GMT), at the start of an outgoing TV mosaic sequence, a spacecraft power subsystem problem occurred which resulted in large power dissipations in the spacecraft bus. One of the resulting effects was intermittent reduction of the X-band transponder output power by 27 dB and the development of sidebands on the carrier. A special effort was made at DSS 14 to detect sidebands and analyze their character.

    April 15, 1974, marked the end of the successful MVM'73 primary mission. An extended mission for a return to Mercury was approved.

IX. MISSION CONTROL AND COMPUTING CENTER (MCCC)

A. INTRODUCTION

The initial Mission Control and Computing Center Support Plan (MSP) was published July 1, 1971. The revised and final support document was published July 1, 1972 and approved by NASA Headquarters Nov. 15, 1972.

During the early mission planning phase, the functional requirement of the Mission Operations System were developed by the MOS Design Team of which MCCCC personnel were members. The functional requirements included software development, computer systems requirements, and Mission Support Area requirements.

B. SOFTWARE DEVELOPMENT

Software development included programs for command generation, planning and analysis, mission control, spacecraft analysis, science sequence recommendation, and navigation analysis.

The software provided means for entering commands into the MCCC system for transmission to the spacecraft, and also provided verification and confirmation visual displays.

The group of software programs provided the function of generating, handling, processing, and displaying data on a nonreal-time basis in support of Mission Operations.

Mission Control Software programs provided the necessary computations to support mission operations by generating command sequence, simulating spacecraft and science subsystem events, producing a sequence of events and providing scan platform pointing information.

The spacecraft analysis software was a set of programs which were utilized and controlled by cognizant analysts assigned to the spacecraft team. These programs provided relevant information to the spacecraft team to enable them to predict spacecraft performance, provided nonreal-time analysis and supported in-flight calibrations.

The Science Sequence Recommendation Software programs provided support in the development of science sequences for the various experiments. The programs were controlled by cognizant analysts assigned to the science team.

C. COMPUTER SYSTEMS SUPPORT

Figure 185 shows the MVM'73 Project computer commitments starting with the development phase in January 1972 and continuing through the end of the primary mission. The Project defined the critical, time-sensitive, and routine phases of the mission and the computer requirements associated with each of these phases.

D. MVM'73/PIONEER COHABITATION

Mariner/Pioneer cohabitation tests were conducted which demonstrated the capability of the 360/75 to support both Mariner and Pioneer mission requirements. There were only minor problems that occurred when COMGEN or SEG was running simultaneous with Pioneer data recall activity and when COMGEN or SEG was running simultaneous with PREDIX. These were problems that were worked by controlling the data processing activities.

E. MISSION SUPPORT AREA

The requirements as documented in the Mariner Venus/Mercury 1973 SIRD were based on using the Mariner Mars 1971 Mission Support Area (MSA) structural layout with only possible minor modifications.

A baseline drawing of the MSA, a matrix showing the operational voice communication capability per team position, and a TV switcher frame matrix showing the closed-circuit television display capability per team member position were distributed to the team chiefs for their approval, and after several iterations were approved.

Implementation was completed prior to start of testing. Minor changes were requested during the testing phase, and during the encounter phases. The MSA is shown in Fig. 186.

COMPUTER	DEVELOPMENT		INTEG	TRAIN.	FLIGHT	
	1972	1973			1974	
	J F M A M J J A S O N D	J F M A M J J A S C N D			J F M A M J J A S O N D	

The table below represents a Gantt-style chart with month columns J F M A M J J A S O N D across 1972, 1973, 1974.

COMPUTER	Schedule
360/75-A/B/C	
360/75-A/B/C	
360/75-A/B/C	
1108-B	
1108-A	
6050	
1230-A & 1219-A	
1230-B & 1219-B	JPL ◄═══ BOEING/KENT ═══► ETR
1218	
1230-C[a]	

▓▓▓ Priority for MVM '73 (250 hours per month, wall-clock time. Additional time as available.)

█▓█ Priority, 24 hours per day (IBM 360/75 shared with Pioneer Project.)

╲╲╲ Provided to MVM '73 (as available)

╱╱╱ Available as back-up for MVM '73

[a] Subject to approval for procurement.

Fig. 185. MCCC commitments

MISSION SUPPORT AREAS
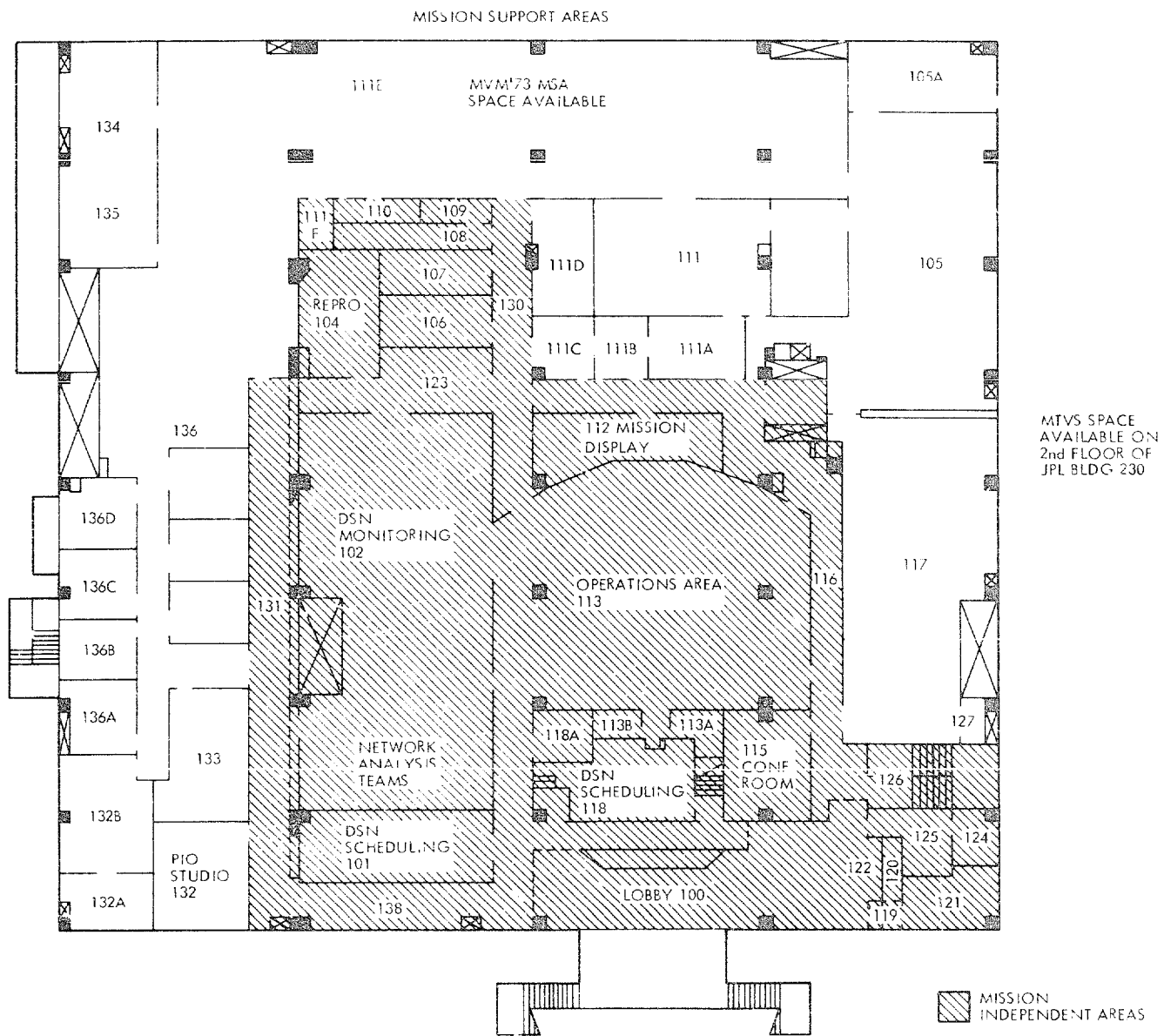
Fig. 186. Mission support area

A. MVM'73 PRIME MISSION SCIENCE DATA TEAM ACTIVITIES

The major activities for the Science Data Team during the mission portion of the flight of Mariner 10 were the following: validation and shipment of Experimenter Data Records (EDRs); production, validation and shipment of Supplementary Experimenter Data Records (SEDRs); development of utility programs and modification of existing data records production software to aid or make possible the production of valid SEDRs; and preparation of predicts data for and real-time support of the Venus and Mercury encounters.

B. EDR ACTIVITIES

These activities involve the receipt and logging of EDR magnetic tapes from the MTC; the running of EDRVAL to validate the contents of each tape; the coordination with MTC personnel for the reproduction, if possible, of EDRs with unrecoverable data content or invalid data gaps; the manufacture of individual tape logs describing EDR data content and the shipment of these data to the PIs. In addition to these activities, further processing of the magnetometer (EPIM) EDR received from the MTC must be accomplished. This tape contains not only all required EPIM data but a full complement of decommutated spacecraft engineering telemetry data as well. The tape must be input to the EDRGEN program which outputs the following three items: (1) a new EPIM EDR without the extraneous engineering data, (2) a Celestial Mechanics and Radio Science (CMRS) EDR consisting of CMRS engineering data only, and (3) a Scan Platform Telemetry (SPT) tape consisting of Guidance and Control engineering channels which is used in the production of SEDRs. During the extended mission period most (all but the Venus encounter and some Earth to Venus cruise) of the primary mission and all Mercury II EDRs were handled and shipped. This amounted to approximately 2400 EDRVAL and 850 EDRGEN computer runs and the shipment of 3178 EDRs.

C. SEDR ACTIVITIES

The production of SEDRs involves the accumulation of required input data and the processing of these inputs plus control information through several computer programs to obtain the desired outputs. The input data consists of spacecraft telemetry data, navigation data and command/event data files which are acquired throughout the mission based upon actual spacecraft history.

The following software is utilized to generate the input data: spacecraft telemetry data (EDRGEN), navigation data (DPTRAJ), and command/event data (COMGEN). Once the input data is accumulated, two methods of generating SEDRs are used. For CPT, PSE, MAG, and UVS (low scan platform activity periods) SEDRs, SPOP, FIP, RFMT and COPY are run to produce the desired product. These SEDRs all have the same data content and are generally referred to as PAFUVS SEDRs. TV, UVS (high scan platform activity periods) and IRR SEDRs are produced by running SPOP, LIBPOG, and RFMT. Once the SEDRs have been produced and validated, tape logs are prepared and the tapes shipped to the appropriate PI.

During the primary mission essentially no production SEDRs were produced due to the slow development of the data records portion of SPOP (processing mode) which derives limit cycle and scan platform parameters. However, during the transition period between primary and extended mission, a version of SPOP was delivered to the Science Data Team and was used to generate approximately 50% of the primary mission SEDRs. Production of the SEDRs was halted at this time to investigate some abnormal time differences between the navigation and spacecraft derived data that are merged together by RFMT to produce the PAFUVS SEDRs. The source of these time differences was traced to the fact that the navigation data was time tagged based on ephemeris time (ET), a time base system referenced back to the epoch of 1950.0, while the spacecraft data was referenced to GMT or universal time (UTC).

The time difference between these two systems (~45 sec) was contained within the navigation data, and a minor modification to RFMT was required to use this time difference to convert the ET to UTC so that proper merging of navigation and spacecraft data could be accomplished. While investigating this anomaly, two other errors related to timing were uncovered. First, the RFMT algorithm which converts navigation time (total seconds from the epoch of 1950.0) into units of year, day, hour, minute, second, and millisecond was incorrect, and all time tagging of navigation data in this manner was invalid. Second, inconsistent timing of spacecraft clock values on the SEDR was discovered and traced back to both the MTC and SPOP. The MTC based all of its engineering data time tagging upon spacecraft clock values (FDSC) and minor frame counter (SCI). During periods of spotty or invalid data the SCI was often incorrect and led to incorrect time tagging by the MTC resulting in minor frame time duplications and regressions. SPOP was programmed to receive and process data on a FDSC basis rather than a minor frame basis (4 minor frames/FDSC) and the time tagging of partial FDSCs (less than 4 minor frames) was often incorrect.

A decision was made at this point in time that all SEDRs produced to date should be reproduced after accomplishing modifications to RFMT to amend its timing problems and the development of a utility program designed to rectify MTC and SPOP timing problems. Utilizing this new utility program (STUFF) and the new version of RFMT, all primary mission SEDRs were produced and sent to the PIs. However, toward the end of this production phase, it became apparent that more serious problems in SPOP concerning scan platform pointing angles existed. An investigation in this area was conducted by the Science Data Team, and the result was that approximately 50% of the TV and UVS SEDRs that had been produced contained scan platform pointing errors. It was apparent that to correct these problems, a modification to SPOP would have to be made. Therefore, all known problems with SPOP were

tabulated and were systematically corrected and tested with Division 91 programming support.

A similar approach was then taken with the PAFUVS SEDR production portion of RFMT. The RFMT modification was undertaken due to the almost certainty of a Mercury III encounter in 1975 and the fact that the RFMT time algorithm for navigation data would not handle the year 1975. During the modifications of SPOP and RFMT, the utility program, STUFF, was expanded to include a representation for each FDSC of data. FDSCs in data gaps would be represented by four minor frames of filler data with correct time tags, while the missing portions of partial FDSCs would also be represented by correctly time-tagged filler data. This would insure that SPOP would not have to perform any time tagging during data gaps and for partial FDSCs. Utilizing the new program set, the SEDRs containing scan platform pointing errors (TV and UVS) were reproduced and all extended mission SEDRs were produced through Mercury II encounter. This same program set is expected to be adequate to produce all the SEDRs required for the Mercury III encounter.

D. REAL-TIME SUPPORT OF MISSION ACTIVITIES

The Science Data Team provided real-time support of the Venus and Mercury encounters. The activities in this area included checkout and verification of data links to provide real-time encounter data to PIs at remote sites, the scheduling of computer time for PI near real-time processing at JPL, the validation of quick-look EDRs received from the MTC and the generation of quick-look MAG EDRs as required. These services were also provided during other portions of the mission as required by the PIs. Other real-time or near real-time activities included the generation of daily science data logs and command logs, maintaining a list of significant spacecraft science events, and the generation of spacecraft clock value (FDSC) versus spacecraft event (SCE) time tables for the entire mission.

E. RECOMMENDATIONS

Flexibility should be built into noncritical mission software, e.g., the SEDR production program, in such a way that the programs involved can be updated and made available for production on a short turnaround basis without having to go through the bureaucracy of a mission build concept system.

The project should require maintenance support for interdivision software (software that is developed by one division and used by another), so that the user division will have an effective means of updating software as required during the mission.

Software users should be educated at least to the functional level as to the operation of his software tools and be able to absolutely verify the validity of the software execution by quickly analyzing the outputs.

XI. PROJECT RELIABILITY AND QUALITY ASSURANCE ACTIVITIES

A. INTRODUCTION

The Quality Assurance and Reliability Office for the MVM'73 Project was responsible for Reliability activities at the project level and Quality Assurance activities at the spacecraft system level. The greatest efforts for the project level activities were spent in getting consistent efforts applied by project personnel and division personnel in Design Review actions and failure reporting actions of Spacecraft, MOS, MCCC, and DSN system elements of the project.

B. MOS, MCCC, AND DSN SYSTEM RELIABILITY ACTIVITIES

1. Design Review

Mission Sequence Reviews were held starting at nine months prior to launch. These reviews brought together the elements of support to the project that represented the DSN, MOS, and MCCC. Action items were assigned from these reviews, answered or carried forward to the next review. All action items from the final review were answered by memo. Project MOS management reviewed and approved all action items. The Launch Readiness Review which reviewed the status of the spacecraft also reviewed the status of the launch vehicle, DSN, MCCC, and MOS elements of the project.

2. Failure Reporting

All major system elements of the project were required to have a failure reporting system. Provision was made to initiate failure reports among the several systems when a problem or failure in one system affected another system. In the earlier hardware phases of the project emphasis was placed upon launch vehicle and spacecraft failures reporting. After launch emphasis was changed to the DSN, GCF and MCCC reporting as well as spacecraft failure reporting.

3. Project Reliability and Quality Assurance Activities

Of particular interest was the Incident Surprise Anomaly (ISA) system of failure reporting that was initiated during spacecraft systems testing at Boeing and carried on through launch and the mission. The ISA system of failure reporting was an extension of the ISA procedure used on the MM'71 program. The procedure allowed for a simplified form of reporting that provided an umbrella for all failure reporting systems. The ISA system exposed all significant/critical problems that occurred in the spacecraft, DSN, MCCC, and GCF and provided a vehicle for project management and control of problems so identified. Following launch, 394 ISAs were written. Of these, 24 were marked critical. Of the 24, one was assigned to the MOS system, two to the MTC system, six to the MCCC system, and fifteen to the DSN system.

C. SPACECRAFT SYSTEM RELIABILITY ACTIVITIES

1. Reliability Assurance Program

The MVM'73 Spacecraft System Reliability program implementation was the responsibility of Boeing. The work unit which contained the implementation plan was 15-2-1. The JPL Reliability Program consisted of reliability tasks applicable to JPL GFE subsystems, reliability tasks applicable to science instruments and a control and monitoring function of the Boeing reliability efforts. The Boeing final report identifies reliability efforts, tasks, and responsibilities of Boeing. This report supplements the Boeing report and describes JPL responsibilities and activities.

JPL reliability efforts included the following:

(1) Development requirements for Spacecraft System Reliability contractor.

(2) Responsibility for and monitoring, and coordination of the Boeing Reliability effort as applied to the Spacecraft System.

(3) Participation in design reviews, FMECAs, design meetings, consent to ship, and consent to launch meetings.

(4) PFR control of GFE subsystems.

(5) FMECAs of GFE subsystems.

(6) Special parts review of GFE subsystems.

(7) Review of all NASA ALERTS for the project.

(8) Coordination of all PFR activities at JPL, including the review and approval of PFRs.

2. Recommendations

A System Failure Mode Effects and Criticality Analysis (FMECA) was performed by systems personnel at Boeing, but it was performed too late to be effective. It is recommended in future System FMECA studies that the work effort be more timely so as to support and impact system design decisions. Hardware safety was a concern from the beginning of the project. Initial guidance to Boeing was developed through Reliability efforts. JPL Project Management supported and emphasized a Safety program. Having the same Boeing manager responsible for both Reliability and Safety had beneficial results. Supported by the JPL Project Safety office, Tender Loving Care (TLC) of hardware received considerable attention on this project and was felt to be about as effective as the MM'69 or MM'71 projects. On future programs TLC should

begin early and be given much attention during the early phases of the program.

3. Spacecraft Design Review Program

Two series of design reviews were held on all spacecraft hardware. These two series of reviews were called Function Design Reviews (FDR) and Detail Design Review (DDR). The FDR schedule was accomplished in a 13-week period starting the middle of September 1971. A spacecraft system review was accomplished in the first week of the reviews. There were 15 major subsystem reviews, five nonimaging science instrument reviews and an X-band transmitter review. Most of these reviews were conducted by the System's contractor. All together, 255 action items were initiated from the FDR reviews. All Boeing-initiated action items were approved by Boeing and then reviewed and approved by JPL project and division management personnel prior to closure.

The DDR schedule was accomplished over a nine-month period starting December 1972. A systems review, 15 major subsystems reviews, one nonimaging science instrument review and an X-band transmitter subsystem review were held. In total there were 341 action items initiated from the DDR reviews. All action items were reviewed and approved by JPL project and division management personnel. The reviews contained the following elements: assignment of action items, TBC weekly status report of progress and the report of special problems, JPL review, and right to disapproval of the closure of any action item. The design review approach was felt to be rigorous and complete.

There were other spacecraft reviews which were conducted prior to launch. These included hardware reviews, spacecraft preshipment reviews, and a launch readiness review.

4. PFR Activities

Boeing was monitored very closely for adherence to PFR procedures. Timeliness of initiation, identification of significant failures and timely closeouts were all given special attention by JPL. In addition to the maintaining by Boeing of a tight control loop and management visibility to problems and failures, the JPL PFR Control Center also kept JPL Work Unit Managers and Project personnel informed of Boeing PFR activities and status.

The JPL PFR Center maintained responsibility for PFR distribution, filing, approval coordination and status reporting. A total of 1523 PFRs was processed within about two years (through launch). Timely and effective reporting of PFR status was made possible due to the implementation of a MARK IV system, a file management software program which was used for recording PFR data and for generating periodic standard reports and special reports.

5. PFR Data

Three different computer formats were chosen for this report to show PFR information. These three are as follows:

(1) PFRs initiated per month by subsystem from May 1972 through October 1973 (Table 43).

(2) Quantities of PFRs by failure cause per subsystem through October 1973 (Table 44).

(3) A subsystem summary report showing quantities of PFRs per subsystem by categories of PFRs, Support Equipment, Mission, risk, and safety (Table 45).

In addition to the above, a tabulation is included showing the PFRs written against the spacecraft during the mission. Thirty-nine problems were recorded in PFRs by early September of 1974. These are shown in a numerical PFR sequence in the chart. Also shown is a timeline (Fig. 34) chart of significant problems that developed on Mariner 10 spacecraft during flight through early September, 1974.

E. SPACECRAFT SYSTEM QUALITY ASSURANCE ACTIVITIES

The Quality Assurance Plan was developed around the requirements of NASA Document NHB 5300.4 1B. The negotiated differences to the NASA Document were identified in TBC's Implementation Plan 15-1-1. This contractually negotiated plan was the basis by which JPL QA monitored the TBC's quality control effort and efficiency.

The overall JPL Quality Assurance tasks supporting MVM'73 were as follows:

(1) Inspection and support for integrated circuit procurement for CC&S.

(2) QA support of JPL subsystem procurements.

(3) QA support of shipping effort from JPL to system contractor.

(4) Assist principal investigators upon request for QA support.

(5) Coordinate QA activities and requirements with MVM Project Office.

(6) Participate in review of all Project Documents for the inclusion of QA requirements.

(7) Review, negotiate, and approve Quality Assurance Plan of system contractor.

(8) Monitor/audit all quality activities to assure conformance to the approved Quality Assurance Plan.

(9) Establish and implement mandatory inspection points where deemed necessary for JPL inspection to ensure flight-quality hardware and spacecraft integrity.

(10) Represent JPL in all Material Board Actions.

(11) Implement the GFP Plan at the Boeing Company. Act as the control center for all GFP activity.

Table 43. Prelaunch PFR summary by month

Subsystem	Total PFRS	Pre-May	1972								1973									
			May	Jun	Jul	Aug	Sep	Oct	Nov	Dec	Jan	Feb	Mar	Apr	May	Jun	Jul	Aug	Sep	Oct
July 29, 1974																				
2000 Systems	30	0	0	1	0	1	0	0	5	2	5	3	1	1	6	2	2	0	2	0
2001 STRU	51	9	0	0	3	2	7	4	3	1	1	1	1	0	5	3	3	1	1	4
2002 RFS	231	26	34	45	39	9	10	2	15	4	3	6	0	1	4	12	2	14	3	2
2003 MDS	94	9	6	3	1	18	21	13	8	6	3	1	0	4	1	0	0	0	0	0
2004 Power	87	1	0	9	14	13	8	8	6	3	6	1	1	10	3	1	1	1	0	1
2005 CC&S	89	13	8	7	13	8	5	8	5	7	2	2	2	5	1	1	0	0	1	1
2006 FDS	179	1	0	0	10	37	30	33	7	7	0	3	5	8	8	6	3	0	5	4
2007 A/C	175	3	3	8	10	47	21	11	19	12	8	9	4	5	2	3	1	7	1	1
2008 Pyro	13	1	0	2	0	2	0	0	0	0	0	5	2	0	0	0	0	1	0	0
2009 Cabling	18	0	2	0	0	1	2	0	3	0	3	2	0	0	2	0	1	1	1	0
2010 Prop	67	1	2	3	14	13	1	8	12	1	0	2	3	1	2	0	1	2	0	1
2011 T/C	23	0	1	0	1	0	2	0	1	0	0	0	0	0	1	0	16	1	0	0
2012 Devices	21	3	0	1	2	3	5	2	0	1	0	0	1	0	1	0	0	0	2	0
2015 APS	34	1	2	1	2	0	3	5	2	1	5	5	2	3	1	1	0	0	0	0
2016 DSS	51	0	7	1	2	5	9	10	3	5	3	0	1	3	0	0	0	1	0	1
2017 SXA	19	0	0	0	0	4	1	3	2	1	1	1	0	0	1	0	0	4	1	0
2032 PSE	50	0	0	0	0	9	2	4	8	2	5	0	2	5	3	1	1	4	2	2
2033 CPT	32	0	0	0	0	2	0	2	1	0	3	1	0	11	2	0	3	7	0	0
2034 UVS	12	0	0	0	0	1	2	0	0	4	0	1	0	0	2	0	1	1	0	0
2035 MAG	39	2	1	0	0	1	4	2	0	7	6	2	3	3	2	2	0	1	2	1
2036 TVS	83	22	5	7	2	5	3	8	1	2	10	4	1	1	3	0	1	5	0	0
2037 XTX	23	0	0	1	3	4	4	5	0	0	2	0	1	0	2	0	1	0	0	0
2038 IRR	16	0	0	0	0	2	3	2	1	0	4	0	1	1	1	0	0	1	0	0
2500 ETE	86	0	1	1	10	7	13	8	13	6	12	5	1	1	4	2	1	1	0	0
	1,523	92	72	90	126	194	156	138	115	72	94	53	31	66	57	37	38	53	21	18

A team of JPL Quality Assurance Engineers and four Air Force Plant Representative Office (AFPRO) Quality Assurance Representatives were assigned in residence throughout the program to monitor and aid the program as necessary to assure the Project a quality spacecraft. Due to limited quantities of flight equipment, the primary concern throughout the program was the enforcement of hardware control and safety. There were significant problems with almost every spacecraft move from one area to another. Facility and control indoctrination would have been helpful prior to any spacecraft movement.

Table 44.   Prelaunch flight hardware PFRs

Subsystem	Total PFRs	A	D	H	M	P	S	T	W	X
2000 Systems	24	2	9				1	3	3	5
2001 STRU	46	4	26	2	3	1		1	2	7
2002 RFS	218	18	95	5	6	4	9	19	22	40
2003 MDS	79	2	26		2	6	10	4	20	9
2004 Power	80		24	4	9	4	5	7		27
2005 CC&S	78		16	4	4	12	2	10	12	18
2006 FDS	164	1	41	1	17	53	1	9	3	38
2007 A/C	155	7	21	7	3	6	7	55	12	37
2008 Pyro	7		2			1	2			2
2009 Cabling	17		9	1	3	3			1	
2010 Propellant	55		2		7	1	3	14		28
2011 T/C	23		8		1	1			1	12
2012 Devices	21	1	8	1	2			1	3	5
2015 APS	33	2	5	1	1			1	3	12
2016 DSS	49	3	12	2		4	2	3	11	14
2017 SXA	19	2	10	2			1		1	3
2032 PSE	42	1	11	2	2	1		9	9	7
2033 CPT	32		1	2	3	4			3	19
2034 UVS	12		2		2	1		1	2	4
2035 MAG	36	1	17	3	2	1	2	1	2	7
2036 TVS	77	1	24		8	9	1	11	6	17
2037 XTX	20		8			4	1		1	6
2038 IRR	15		1	1		4			4	5
	1,302	46	378	38	74	122	51	149	121	323

A	Adjustment	D	Design	H	Mishandling
M	Manufacture	P	Piece part	S	OSE failure
T	Operator error	W	Workmanship	X	Other

Table 45. PFRs subsystem summary report

Subsystem	Total PFRs	Flight hardware	Support equipment	Mission PFRs	Spacecraft risk factor[a]				Safety
					1	2	3	4	
2000 Systems	38	32	6	8	24	10	2	2	
2001 STRU	52	47	5	1	42	8	2		
2002 RFS	231	218	13		182	20	22	7	
2003 MDS	95	80	15	1	78	13	3	1	1
2004 Power	90	83	7	3	68	16	3		
2005 CC&S	89	78	11		60	16	6	7	
2006 FDS	180	165	15	1	126	19	33	2	
2007 A/C	181	161	20	6	169	9	3		2
2008 Pyro	13	7	6		10	3			
2009 Cabling	18	17	1		15	1	1		
2010 Propellant	68	56	12	1	61	5			1
2011 T/C	25	25		2	20	4		1	
2012 Devices	21	21			19	1	1		
2015 APS	34	33	1		18	9	5	2	
2016 DSS	53	51	2	2	32	12	9		
2017 SXA	20	20		1	12	4	3	1	
2032 PSE	53	45	8	3	51	2			
2033 CPT	32	32			28	3	1		
2034 UVS	13	13		1	9	2		2	1
2035 MAG	41	38	3	2	32	8		1	
2036 TVS	84	78	6	1	67	6	5	6	
2037 XTX	25	22	3	2	18	4	3		
2038 IRR	16	15	1		15	1			
2500 ETE	86		86		83		3		
	1,558	1,337	221	35	1,240	176	105	32	5

[a]1 = Known cause of failure with no risk.
2 = Unknown cause of failure with no risk.
3 = Known cause of failure with some risk.
4 = Unknown cause of failure with some risk.

XII. PROJECT FINANCIAL MANAGEMENT

A. PERSONNEL INDOCTRINATION

The most fundamental approach to cost control taken by the Project Management was to create a fixed-cost/variable-scope environment, to develop a cost-consciousness, and to inspire and sustain a strong motivation to meet the $98 million target. The orientation developed an understanding of the cost goals and the cost control plans and system. This orientation encompassed not only the Project Office personnel but all persons involved with the Project including the JPL Divisions, the System Contractor, the Scientists, the Program Office, and JPL and NASA Management.

B. BUDGET PLANNING

The Project Office delegated a measure of fiscal responsibility to the Flight Project Representatives with the understanding and agreement that budget emphasis was to be on cost-at-completion. Operating budgets were established with each organization after the scope and resources compatibility (equalization) were agreed upon.

A no-year funds approach was initiated by the Project. The planning for funds was the responsibility of the Project. The organizations were held at cost-at-completion, and budget surpluses at the end of fiscal years were allowed to remain in their budget. Although the Project required the Flight Project Representative (FPR) to track costs monthly and by fiscal year, the emphasis remained throughout on the estimated costs-at-completion.

C. MANAGEMENT METHOD OF COST CONTROL

The Project initiated a system and the formats for a monthly JPL Division Project Resources Review. The FPRs reported to the Project monthly on cost, schedules, and performance. This was done verbally, allowing for the airing out of problems and questions, and establishing good communications between the Project management and the FPRs. The FPRs' line management was encouraged to attend these monthly meetings, and it is felt that this participation enhanced the Lab-wide interest and involvement in the Project. During the Resource meeting, the FPRs presented and discussed viewgraphs. Copies of the viewgraphs, given to the Project Financial Manager, became a part of the Project historical records.

Tight control of the system contract was exercised by the Project and by the Procurement Division starting before award and throughout the life of the contract. Monthly reports by the Project Cost Analyst provided current details on contractor's performance. Major subcontracts were reviewed each month and the Project Cost Analyst issued monthly reports covering cost, funding, and highlights of current activities on all major subcontracts, with emphasis on existing or potential overruns. Plans of action were developed and implemented to avoid or to curb overruns.

D. SYSTEM CONTRACT

The system contract represented approximately 50% of the total cost ($98 million). The cost target could not have been met without the cooperation of a responsible and strongly motivated system contractor. Cost controls in this area began long before contract award and were evident in the processes of source selection, indoctrination and motivation, negotiation and contract structure.

1. Stability of Contract Target Cost

The final target cost for Part 2 was within one tenth of 1% of the original target, adjusted to include the Propulsion Subsystem (the result of a change in the make-or-buy plan):

	Thousands of dollars
Original target cost	$ 38,500
Propulsion subsystem	1,024
Total initial target cost	$ 39,524
Final target cost	39,572
Net increase in target cost	$ 51

The Project achieved this amazing stability through a vigilant awareness of the contractor's performance, the extensive use of tradeoff studies with the participation of the contractor, and a high degree of flexibility to implement changes. Specific examples of cost-saving decisions are listed below:

(1) Deleted the limit cycle compensator

    Estimated savings $ 700,000

(2) Deleted CC&S prototype

    Negotiated reduction $ 173,000

(3) Revised TCM/73-2 Test Program

    Negotiated reduction $ 139,000

(4) Eliminated engine thermal door

    Negotiated reduction $ 103,000

(5) Changed to power switching and equipment quantities

    Negotiated reduction $ 142,000

(6) Deleted one flight battery and various associated tests

    Negotiated reduction $ 58,000

Some of the above reductions were used either to offset the impact of increases in scope or to minimize incipient overruns in certain areas of the contract.

2. Monitoring of the System Contract

The flow of data from the contractor to the Project included performance measurement system reporting, estimates of funding requirements, weekly manpower reports, weekly major problems TWXs, monthly reports of management reserve usage, monthly overhead reports, daily update of schedule charts during critical stages of the contract.

a. Performance Measurement System (PMS). The system proved its worth by enabling the Project Cost Analyst to monitor the contractor cost activities very closely, to develop independent estimates at completion with reasonable accuracy, and to analyze Boeing's cost proposals for contractual changes with a solid background of current information.

3. Communication

The monthly progress review meetings, contractually required, were an excellent means of communication between the Project and the Contractor. From the standpoint of financial management, it provided updated information, it brought to the surface technical problems capable of affecting costs, and it opened the door for questions and comments that might not have been originated from reading only the written reports. Informal communication was excellent at all levels. The constructive use of the award fee briefings proved to be very effective.

E. INNOVATIONS

In addition to the many "firsts" achieved in space by Mariner 10, the MVM'73 Project also did some trailblazing in project management, as discussed below:

(1) The assignment to the Project of a Project Financial Manager from the Financial Management Division and a Cost Analyst from the Procurement Division, collocated with the Projects.

(2) The delegation of greater fiscal responsibility to the FPR.

(3) The use of computers to track budgets and actuals.

(4) The acceptance of a major subcontractor's own PMS to monitor and evaluate contract performance.

(5) The development of a contractual overhead ceiling based on indirect costs amounts rather than rates. (This ceiling was not invoked because Boeing experienced an underrun in direct costs.)

The Project initiated the use of business computers to provide current information on manpower usage and actual costs and to maintain a record of the changes in plan from the original basic plan to the latest update. Three computer reports were developed, admittedly too late to be of great use to this Project except for purposes of historical record-keeping. It should be recognized, however, that these reports could be used to considerable advantage by other JPL Projects. A brief description of these reports follows:

1. JPL Manpower Report (Equivalent Headcount)

Planned and actual staffing for prior fiscal years were reported, and plans and actuals by month for the current fiscal year. It provides both details (employee's name, job number) and summaries by system and by division.

2. Project Cost History

Actual costs and obligations were reflected at a reasonable level of detail for each job by cost element, including JPL manpower and subcontractor manpower (Categories A through D). Costs by month and cumulative (inception to date) with various intermediate subtotals (quarter, fiscal years) were shown.

3. Plan History

The original plan (as formalized through System for Resources Management (SRM) inputs) was recorded and each subsequent update in plan, by job and in summary. The variances between the latest plan and the plan immediately preceding were described and explained.

F. ESTIMATED FINAL COSTS

On November 27, 1974, the estimated costs at completion for the MVM'73 Project were $96,870,000 representing an underrun of $1,133,000 or 1.2% of the $98 million cost target.

Included in the above amounts are the subcontracted costs for the design, fabrication and testing of the spacecraft (one flight unit and one test model/spare) by the Boeing Aerospace Company, under JPL Contract No. 953000, as follows:

(In $1,000)	Part 1	Part 2	Total
Original contract costs	$3,287	$38,500	$41,787
Net amount of changes	353	1,072	1,425
Final contract costs	3,640	39,572	43,212
Estimated final actual costs	3,400	38,628	42,028
Estimated underrun	$ 240	$ 944	$ 1,184

The award fees associated with the costs shown above are as follows:

(In $1,000)	Part 1 8%	Part 2 15%	Total
Maximum award fee-basic contract	$263	$5,775	$6,038
Adjustment due to contract change	16	161	177
Adjusted maximum award fee	279	5,936	6,215
Fee awarded	256[1]	4,787[2]	5,043
Fee loss	$ 23	$1,149	$1,172

(1) Projected fee based on the estimated/actual number of level of effort hours through July 31, 1974. The fee awarded represents 7.53% of actual costs.

(2) The awarded fee includes in-flight performance fee, and represents 12.1% of target cost or 12.4% of estimated/actual costs.

G. ANALYSIS OF UNDERRUN, BOEING CONTRACT NO. 953000

(In thousands of dollars)

1. Part 1. Reason for underrun

	Direct cost	Cost through G&A[11]
Direct labor average rates lower than estimated	$ 110	$ 172
Unused level-of-effort (6,785 h)	60	94
Total underrun in labor	170	266
Underrun in travel and relocation	34	38
Variance in indirect cost:		
Underrun due to lower direct cost bases	100	(Included above)
Overrun due to higher rates (adverse effect of new overhead structure)	(64)	(64)
Net underrun		$ 240

[11] G&A - General and administrative overhead.

(In thousands of dollars)

2. Part 2. Summary of variances

	Direct cost	Cost through G&A
Overrun in manpower (63,000 h)	$ (88)	(1,047)
Underrun in average direct labor rates	769	1,165
Net underrun in labor	281	118
Overrun in subcontracts	(132)	(162)
Underrun in materials	340	417
Underrun in travel and other direct costs	184	211
Variance in indirect costs:		
Net overrun due to the above changes in direct cost bases	(89)	(Included above)
Underrun due to lower rates	360	360
Net underrun		$ 944

The Part 2 cost variances outlined above reflect the impact of many and complex events and situations, some of which were beyond the control of Boeing MVM'73 Management (e.g., union contracts, national wage controls, most indirect expense rates).

a. Overrun in Manpower: Major overruns occurred in Engineering Mechanics (particularly shop labor), CC&S, Reaction Control Assembly, Test and Operations. In some areas, such as CC&S, RCA, Tests and Operations, Boeing had underestimated the complexity of the effort. Some of the contributing factors to the manpower overruns were: designing problems, some false starts, poor handling of hardware, limited MVM'73 control over shop operations, extensive use of overtime for schedule recovery, over-optimism in the fruitfulness of technology transfer, inadequate planning for test requirements. There is no doubt, however, that very good management controls kept this overrun within bearable limits.

b. Underrun in Labor Costs: The 4% overrun in direct labor hours was completely offset by the lower-than-planned average direct labor rates. While Boeing should be credited for their efficient modulation of the skill mix, this contract also

benefited from the presidential wage controls implemented in late 1971. The resulting litigations with the engineering association (SPEEA) delayed all salary increases until early 1973, when a lump-sum retroactive adjustment was paid, totalling $700K through G&A. This created a spurious large underrun in labor costs for CY 1972. Another retroactive wage adjustment, to hourly workers, was paid in quarterly installments during CY 1974. In spite of these lump-sum adjustments, the average actual escalation in direct labor rates was lower than the projected escalation factor into the estimated rates in the original contract amounts.

c. Underrun in Subcontract. Overruns by Motorola and Texas Instruments were partially offset by an underrun by Electro Optical Systems. Strong cost incentives built into the subcontracts if not entirely successful in preventing overruns at least caused the subcontractors to absorb a share of them in the form of reduced fees (the reverse is true in the case of EOS). The total overrun amount excludes cost growth attributable to scope changes which were generally reflected in modifications to the JPL/Boeing contract.

d. Underrun in Materials and Purchased Equipment. The cause is undetermined but a probable contributing factor is that some material was government furnished (GFP) at no change in contractual cost for line item values of less than $5,000, in accordance with the terms of the contract.

e. Underrun in Travel. This reflects tight management control on actual travel.

f. Underrun due to Indirect Rates. Two events affected the actual indirect costs. On Jan. 1, 1973, the Boeing Company implemented a new overhead structure which increased the allocation of indirect costs to the MVM'73 Project. In anticipation of this change, a ceiling on the amount of indirect costs was provided in the contract. On an overall basis, the total indirect costs were underrun so this contractual protection did not need to be invoked.

g. Breakdown of Underrun by Area/Activity

(In $1,000)

Division/ Organization	Area/ Activity	Target	Actuals	Underrun (Overrun)
33	Telecommunications	$ 5,409	$ 5,402	$ 7
34	Guidance and Control, Power	10,162	9,852	310
35	Engineering Mechanics	8,628	9,053	(425)
36	Astrionics	3,192	3,362	(170)
38	Propulsion	734	585	149
29	Spacecraft System Integration	1,183	1,092	91
29/35	Environmental Requirements	2,086	1,534	552
29/35	Test and Operations	3,021	3,344	(323)
15	QA, Reliability, Safety	2,104	1,867	237
25	Program management	3,053	2,537	516
	Final Target (Contract value)	$39,572		
	Final Estimation/ Actual costs		$38,628	
	Net underrun			$ 944

The prime mission fiscal summary is given in Table 46.

Table 46. Prime mission — fiscal summary

	Costs (in thousands)					Man years					
	JPL	Boeing Part 1	Sub-total	Boeing Part 2	Total	Contractor	JPL	Boeing Part 1	Sub-total	Boeing Part 2	Total JPL and Boeing
Project Management											
Project Office, Control and Admin.	1068	399	1467		1467	0.1	19.5	15.6	35.1		35.1
Mission analysis and engineering	1110		1110		1110		20.7		20.7		20.7
Project division representatives	2320		2320		2320		48.5		48.5		48.5
Study	328		328		328		7.9		7.9		7.9
Total	4826	399	5225		5225	0.1	96.6	15.6	112.2		112.2
Project Science											
Science investigations											
Radio science team	520		520		520		5.9		5.9		5.9
Imaging team	650		650		650						
Data handling, analysis and records											
Library	244		244		244	7.3	4.2		4.2		4.2
IPL	864		864		864	5.4	8.7		8.7		8.7
Integration	1334	590	1924		1924	8.2	25.6	14.3	39.9		39.9
Instruments and data analysis											
Television	4208		4208		4208	6.0	34.0		34.0		34.0
Infrared radiometer	893		893		893						
Ultraviolet spectrometer	800		800		800						
Plasma science	1105		1105		1105						
Charged particle telescope	606		606		606						
Magnetometer	670		670		670						
Science manager	200		200		200		4.0		4.0		4.0
Total	12094	590	12684		12684	26.9	82.4	14.3	96.7		96.7
Spacecraft											
Management	568		568	2818	3386		9.9		9.9	105.0	114.9
QA and reliability	615		615	1684	2299	17.9	11.1		11.1	57.9	69.0
System design, analysis and support											
System interface design	388		388	107	495		8.9		8.9	3.0	11.9
System design and analysis	2662	694	3356	5187	8543	2.9	53.5	11.9	65.4	136.7	202.1
Env. requirements and test support	3584		3584	1736	5320	6.8	22.3		22.3	52.6	74.9
Hardware and subsystems											
Radio, antennas and support equipment (SE)	431	67	498	3617	4115		9.5	4.8	14.3	25.1	39.

Table 46. Prime mission — fiscal summary (contd)

	Costs (in thousands)					Man years					
	JPL	Boeing Part 1	Sub-total	Boeing Part 2	Total	Contractor	JPL	Boeing Part 1	Sub-total	Boeing Part 2	Total JPL and Boeing
Mod/Demod and SE	210		210	1649	1859		4.7		4.7	8.5	13.
35-W amplifier TWTA	464		464		464		0.8		0.8		
Power	460		460	3301	3761		10.4		10.4	20.7	31.
Spacecraft control	1050		1050	4824	5874		19.8		19.8	118.0	137.
Support equipment — power and spacecraft control	166		166	1726	1892		3.6		3.6	36.1	39.
Engineering mechanics	691	208	899	4728	5627		10.7	13.5	24.2	149.9	174.
CC&S and SE	677		677	1573	2250	0.9	8.2		8.2	53.5	61.
FDS and SE	5182		5182		5182	3.5	18.6		18.6		18.
DSS and SE	117		117	1790	1907		3.0		3.0	6.6	9.
Pyrotechnics and SE	315	27	342		342	0.7	7.9	1.2	9.1		9.
Propulsion and SE	1872	93	1965	586	2551	1.4	15.5	6.8	22.3	17.1	39.
Total	19452	1089	20541	35326	55867	34.1	218.4	38.2	256.6	790.7	1047.
System Test and Operations	4027	214	4241	3302	7543	39.5	31.6	25.4	57.0	87.6	144.
Mission Operations System											
Management, planning, design and development	2959	441	3400		3400	7.8	41.6	26.4	68.0		68.
Flight operation and training	2239	667	2906		2906		39.0	6.8	45.8		45.
Total	5198	1108	6306		6306	7.8	80.6	33.2	113.8		113.
Project subtotal	45597	3400	48997	38628	87625	108.4	509.6	126.7	636.3	878.3	1514.
Boeing fee		254	254	4934	5138						
JPL burden on Boeing		353	353	4212	4565						
Total MVM'73 Project	45597	4007	49604	47774	97378	108.4	509.6	126.7	636.3	878.3	1514.

BIBLIOGRAPHY

General

1. Ashlock, J., "MVM DSS Motor Voltage Analysis," IOM 3632-74-096 MVM'73, Oct. 31, 1974 (JPL internal document).

2. Becker, R. A., "Division 35 Applied Mechanics Report on Performance of Mariner 10, Launch Through Launch plus 30 Days," IOM 3533MVM-74-041, Jan. 10, 1974 (JPL internal document).

3. Becker, R. A., "Mariner 10 Temperature Control Performance, Launch plus 30 Days Through Launch plus 70 Days," IOM 3533MVM-74-042, Jan. 24, 1974 (JPL internal document).

4. Becker, R. A., "Mariner 10 Temperature Control Performance, Launch plus 70 Days Through Launch plus 110 Days," IOM 3533MVM-74-044, March 22, 1974 (JPL internal document).

5. Becker, R. A., "Mariner 10 Temperature Control Performance, Launch plus 110 Days Through 165 Days," IOM 3533MVM-74-046, June 18, 1974 (JPL internal document).

6. Bourke, R. D., and Beerer, J. G., "Mariner Mission to Venus and Mercury in 1973," Astronautics and Aeronautics, January 1971, pp. 52-59.

7. Bullock, G., "MVM'73 Tape Recorder Failure," IOM 3631-74-224 MVM'73, Dec. 6, 1974 (JPL internal document).

8. Bullock, G., "DSS Anomalous Behavior," IOM 3621-74-186 MVM'73, Aug. 21, 1974 (JPL internal document).

9. Christensen, C. S., "Solar Pressure Model for MVM'73," Tech. Memo 391-240, Oct. 28, 1971 (JPL internal document).

10. Christensen, C. S., and Reinbold, S. J., "Navigation of the Mariner 10 Spacecraft to Venus and Mercury," AIAA Paper No. 74-844, AIAA Mechanics and Control of Flight Conference, Anaheim, Calif., August 1974.

11. Cowley, R. T., "Propulsion System Performance During TCM 2 and TCM 3," IOM MVM73-74-838, May 6, 1974 (JPL internal document).

12. Evanchuck, V. L., "Radio Frequency Subsystem, Launch plus 13 Days to plus 107 Days," IOM 3396-74-037, Feb. 26, 1974 (JPL internal document).

13. Evanchuck, V. L., "Telecom MVM In-Flight Problem Summaries," IOM 3396-74-132, July 8, 1974 (JPL internal document).

14. Frewing, K., "Revised Description of MVM'73 TV Heater Failure," IOM 292-74-F19, July 19, 1974 (JPL internal document).

15. Georgevic, R. M., "Mathematical Formulation of the Solar Pressure and Torques on the Components of a Spacecraft," Technical Memorandum 44-494, Jet Propulsion Laboratory, Pasadena, Calif., Oct. 1, 1971.

16. Hardman, J. M., "Results and Conclusions from MVM73 High Gain Antenna Calibrations No. 1, 2 and 3," IOM 343-5-74-029 Jan. 14, 1974 (JPL internal document).

17. Hooke, A., "Summary of the MVM'73 POR Problem, IOM 3645-74-110, July 15, 1974 (JPL internal document).

18. Hooke, A., "Mariner 10 Tape Recorder Failure," IOM 3645-74-164 MVM'73, Sept. 5, 1974 (JPL internal document).

19. Just, W., "CC&S Investigation of the In-Flight Power Chain Switchover," IOM 3611-74-086, Feb. 28, 1974 (JPL internal document).

20. Leising, C. J., and Cowley, R. T., "Propulsion System Performance During TCM-1," IOM MVM73-73-831, Jan. 18, 1974 (JPL internal document).

21. Lord, D., "CC&S Investigation of In-Flight FDS Power on Reset," IOM 3611-73-424 MVM'73, Dec. 4, 1973 (JPL internal document).

22. Lord, D., "CC&S Investigation of In-Flight FDS Power on Reset," IOM 3611-73-443 MVM'73, Dec. 13, 1974.

23. Lord, D., "CC&S Investigation of the In-Flight Power Chain Switchover," IOM 3611-74-090 MVM'73, March 4, 1974 (JPL internal document).

24. Lord, D., "CC&S Investigation of the Gyro Oscillation Problem," IOM 3611-75-019 MVM'73, Jan. 17, 1975 (JPL internal document).

25. Lord, D., "CC&S Investigation of the 'Day 90 Power Problem' and the CC&S Not Issuing 'TWT High Power' Command," IOM 3611-75-020 MVM'73, Jan. 17, 1975 (JPL internal document).

26. McKinley, E. L., et al., "Mariner Venus/Mercury Navigation Strategy," AAS/AIAA Astrodynamics Conference, Vail, Colorado, July 1973.

27. Messner, A., "CC&S Memory Readout," IOM MVM-2-247, Nov. 20, 1973 (JPL internal document).

28. Schumacher, L. L., "MVM73 Pitch Axis Disturbance Torque Observations," IOM 344-7-LLS, Feb. 7, 1974 (JPL internal document).

29. Schumacher, L. L., "MVM73 Scan Engineering Tests Summary," IOM 344-7-LLS, April 12, 1974, (JPL internal document).

30. Schumacher, L. L., "MVM73 Launch Performance Summary," IOM 344-7-LLS, May 7, 1974 (JPL internal document).

31. Schumacher, L. L., "A Hybrid Roll Axis Ground Control Mode When Disturbance Torque Exceeds Solar Panel Control Torque," IOM 344-7-LLS, March 18, 1974 (JPL internal document).

32. Schumacher, L. L., "MMV In-Flight Problem Summaries," IOM 344-7-LLS, July 8, 1974 (JPL internal document).

33. Shirley, D. L., "Mariner 10 Mission Analysis: Application of a Black Art," AIAA Paper No. 75-53, 13th Aerospace Sciences Meeting, Pasadena, Calif., Jan. 20-22, 1975.

34. Swenson, D. H., "Summary of In-Flight PSE Problems," IOM DHS: 296-74-379, July 10, 1974 (JPL internal document).

Constants

35. Khatib, A. R., Christensen, C. S. and Newhall, X. X., "DPTRAJ/ODP MVM'73 Mission Parameters Lockfile," IOM 392.4-911, June 4, 1973 (JPL internal document).

Effects of Nongravitational Forces (Preflight)

36. Christensen, C. S., "Mariner Venus/Mercury Final SRD for DPODP," IOM 391.3-275, March 10, 1972 (describes sequential filter formulation), (JPL internal document).

37. Curkendall, D. W., et al., "Mariner '73 Venus Encounter Orbit Determination Study Report," Tech. Memo 391-200, June 4, 1971 (JPL internal document).

38. PD 615-128, "Final Orbit Determination Strategy and Accuracy, MVM'73", Sept. 15, 1973 (JPL internal document).

Ephemeris

39. Keesey, M. S. W., "Venus and Mercury Ephemeris Uncertainties," EM 391-507, Oct. 26, 1973 (JPL internal document).

40. Standish, E. M., and Keesey, M. S. W., "Development Ephemeris 84--Announcement," IOM 391.4-553, Aug. 22, 1973 (JPL internal document).

41. Standish, E. M., "MIT-JPL Ephemeris Comparison; Part II," IOM 391.4-565, Sept. 28, 1973 (JPL internal document).

Flight Operations

42. Christensen, C. S., and Reinbold, S. J., "Navigation of the Mariner 10 Spacecraft to Venus and Mercury," presented at the AIAA Mechanics and Control of Flight Conference, Anaheim, Calif., Aug. 5-9, 1974.

43. Pease, G.E., "Mariner 10 Anomalous Attitude Control Gas Use History," EM 391-647, May 14, 1975. (JPL internal document).

44. "MVM'73 DRVID and Its Use in the Orbit Determination Process," IOM 391-3-789, April 1974 (JPL internal document).

45. "Ionospheric Charged-Particle Influences on Mercury B-Plane Coordinate Estimates (Report 4, March 16 to March 24, 1974)," IOM 391.3-787, April 5, 1974 (JPL internal document).

46. "Actual Corruption of the MVM'73 B-Plane Coordinate Estimates: Ionospheric Charged-Particle Influences on Goldstone DSN Tracking Data (Report 3, Jan. 21 to Feb. 5, 1974), IOM 391.3-775, Feb. 22, 1974 (JPL internal document).

47. "S/X Dispersive Doppler Demonstration--Report 1," IOM 391.3-772, Feb. 1, 1974.

48. "Actual Corruption of the MVM'73 B-Plane Coordinate Estimates: Ionospheric Charged-Particle Influences on Goldstone DSN Tracking Data (Report 2, Dec. 20, 1973)," IOM 391.3-770, Jan. 29, 1974 (JPL internal document).

Inflight Results

49. Barton, J. R., "Power Chain Transfer, Mariner 10," IOM 342-74-B-236, July 9, 1974 (JPL internal document).

50. Barton, J. R., "90-Day Anomaly, Mariner 10," IOM 342-74-B-237, July 10, 1974 (JPL internal document).

51. Barton, J. R., "Solar Panel Current Anomaly," IOM 342-74-B-240, July 11, 1974 (JPL internal document).

52. Barton, J. R., "Power Chain Switchover Analysis, Mariner 10," Engineering Memo 342-257, June 24, 1974 (JPL internal document).

53. Barton, J. R., "Solar Panel Current Anomaly (PFR 5027)," Engineering Memo 342-272, Oct. 18, 1974 (JPL internal document).

54. Barton, J. R., "Power Subsystem Cruise Analysis," Engineering Memo 342-245, Nov. 21, 1974 (JPL internal document).

55. Jones, J. B., "MVM'73 Trajectory Correction Maneuver Number 1," IOM 392.6-630, March 26, 1974 (JPL internal document).

56. Jones, J. B., "TCM 1 Reconstruction," IOM 392.6-606, March 25, 1974 (JPL internal document).

57. Horiuchi, H. H., "MVM'73 APS Flight Performance--A Brief Summary," IOM 344-6-HHH, May 8, 1974 (JPL internal document).

58. Jones, J. B., "MVM'73 Trajectory Correction Maneuver Number 2," IOM 392.6-631, March 27, 1974 (JPL internal document).

59. Jones, J. B., "Preliminary TCM 2 Accuracy Evaluation," IOM 392.6-636, April 10, 1974 (JPL internal document).

60. Liu, A. S., and Pease, G. E., "Preliminary Estimates of Range Measurements to a Spacecraft By Means of Ground Digitally Controlled Oscillators," AIAA Paper 74-830, AIAA Mechanics and Control of Flight Conference, Anaheim, Calif., Aug. 5--9, 1974.

61. Ondrasik, V. J., and Rourke, K. H., "Applications to Quasi-VLBI Tracking Data Types to the Zero Declination and Process Noise Problems," AIAA/AAS Paper 71-399, AIAA/AAS Astrodynamics Specialists Conference, Fort Lauderdale, Fla., Aug. 17--19, 1971.

62. Wood, G. E., "Acquisition of Simultaneous Tracking Data From Planetary Spacecraft by Interference Techniques," IOM 3396-73-025, January 1973 (JPL internal document).

63. "MVM'73 Trajectory Correction Maneuver Number 3," IOM 392.6-680, July 18, 1974 (JPL internal document).

64. "TCM 3 Accuracy Evaluation," IOM 392.6-681, July 19, 1974 (JPL internal document).

65. Science, Vol. 185, No. 4146, July 12, 1974.

Occultation Time Uncertainties

66. Christensen, C. S., "Earth Occultation Time Uncertainty for a Planetary Flyby," IOM 391.3-795, May 22, 1974 (JPL internal document).

67. Christensen, C. S., "Uncertainty of Mercury Occultation Time," IOM 391.8-69, July 23, 1973 (JPL internal document).

68. Pease, G. E., "Venus Doppler Dispersions and Occultation Time Uncertainties," IOM 391.8-77, Aug. 20, 1973 (JPL internal document).

Preflight Preparation

69. Ellis, J. M., "S/C Constraints and Idiosyncracies," Boeing Memo 2-1083-SSE-854, Jan. 15, 1973.

70. McKinley, E. L., "Mariner Venus Mercury 1973 Midcourse Velocity Requirements and Delivery Accuracy," JPL Quarterly Technical Review, Vol. 1, No. 4, Jet Propulsion Laboratory, Pasadena, Calif., January 1972.

71. "Preliminary Maneuver Strategy and Accuracy Document," PD 615-56 (JPL internal document).

72. "Mariner Venus/Mercury 1973 Final Maneuver Analysis," Project Document 615-134, Oct. 1, 1973 (JPL internal document).

Station Locations

73. Rourke, K. H., and Mottinger, N. A., "LS 41-Final Pre-Venus M-10 Station Location Update," IOM 391.8-147, Jan. 15, 1974 (JPL internal document).

74. Mottinger, N. A., "Station Location Set 39," EM 391-525, Oct. 16, 1973 (JPL internal document).